The Institute of Paper Chemistry

Appleton, Wisconsin

Doctor's Dissertation

Retention Dynamics for Small Particles on Cylindrical Fibers

David A. Dyer

June, 1977

RETENTION DYNAMICS FOR SMALL PARTICLES ON CYLINDRICAL FIBERS

A thesis submitted by

David A. Dyer

B.S. 1971, The University of Maine

M.S. 1974, Lawrence University

in partial fulfillment of the requirements
of The Institute of Paper Chemistry
for the degree of Doctor of Philosophy
from Lawrence University,
Appleton, Wisconsin

June, 1977

to Judi ...

for your patience and understanding

TABLE OF CONTENTS

ABSTRACT

The mechanisms controlling the retention of small particles within a fibrous porous medium are of basic importance to many processes within the paper industry. Therefore, a better understanding of the retention process could prove to be of economic and environmental value. This thesis was proposed to clarify some questions related to the process of particle collection.

The objective of the thesis was an investigation into the relative importance of hydrodynamic and colloidal forces thought to exist within a retention system. Such forces were assumed to affect the transport mechanisms of inertial impaction, flow-line interception, and diffusion. In addition, the effects of molecular attractive forces and double-layer interaction were studied. Each was evaluated by investigating which type of interaction produced the greatest change in retention. In this way relevant data could be obtained concerning how particulate matter is removed from a flow stream by a fiber assemblage.

The objective has been accomplished through the construction of a mathematical model, developed to predict retention occurring in a simplified flow system. The model is based on the equivalent unit cell approach and a set of particle motion equations, which describe a particle's trajectory through this cell. The unit cell is composed of two concentric cylinders, the inner one represents the fiber, while the outer one is called the fluid envelope, with a radius dependent on system porosity. Creeping motion equations are the basis for a description of flow through the cell. Two equations were derived which describe the particle's trajectory; these equations can be modified to investigate, separately, each of the forces mentioned above. Determination of trajectories in this manner permitted the calculation of a collection efficiency representing the amount of particulate matter retained by a single fiber.

An experimental program was performed to provide data for a comparison with model predictions. A simplified permeation procedure was followed in which titanium dioxide particles were retained in a pad of synthetic fibers. By adjusting system variables of the experiment to conform to those utilized in the model, an adequate comparison between theory and experiment was realized.

Calculations indicate that the inclusion of molecular attractive forces in the model is necessary for any appreciable retention. Double-layer repulsion was also found important, but it could be controlled by modifying the ionic suspension conditions. Inertial impaction was found negligible and diffusion only slightly affected overall retention. From both the model and experiment, it was shown that retention decreases with increasing porosity and with increasing bulk velocity. The model has also predicted that retention will decrease as particle size decreases.

INTRODUCTION

There are many processes within the paper industry which are dependent for success on a phenomenon known as retention. In the most general terms, the concept of retention can be defined as any process in which small particles are removed from a suspending medium and collected by a solid substrate. As is evident from the title of this investigation, the particles observed here were small in size and spherical in shape, while the solid substrate was composed of an assemblage of fibers, each characterized by a circular cross section. The suspending medium employed was water. Specifically, the study was concerned with the movement of particles entrained in the fluid as they approached a much larger fiber. If system conditions were favorable, the particles were effectively removed from the flow stream by colliding with the fiber and being retained by it.

Application of this retention process is by no means limited to the paper industry. Many industries are concerned with the removal of particulate matter from liquid or air streams. Any system utilizing a porous medium filter would be related to this process. These applications are even more numerous than they are varied. Examples of aerosol retention (removal of particles from an air stream) would include situations ranging from the removal of bacteria by a surgeon's mask to the large quantities of dirt and dust removed by a typical fiber filter employed on any large-scale industrial air conditioning unit. The air filter on any automobile depends on retention to remove both liquid droplets and solid particles from the air supplied to the combustion chambers. If the suspending medium is a fluid, the opportunities for use of retention concepts are just as plentiful. Innumerable industrial operations require that water be filtered of impurities before being used. A significant amount of this purification is now accomplished by utilizing some form of porous medium filter, generally composed of granular or fibrous material. The list of

retention applications could go on and on, but suffice it to say that retention is important for a wide variety of operations. The particular one studied in this investigation, however, is of special interest to the paper industry.

IMPORTANCE OF RETENTION IN THE PAPER INDUSTRY

Considering only the paper industry, there are many instances where retention is important. Logically, the most obvious and, in the minds of some, the most important, is the effect of retention on the formation of the paper sheet. As the dilute suspension of fiber, fines, and pigment is laid down on the forming wire, various forces, hydrodynamic, molecular, and colloidal in nature, govern what material will be retained in the sheet and what will be passed through the wire during drainage. Retention is influenced by all types of force. This investigation has been involved with a study of these forces and how they affect the interaction between a particle and fiber; specifically, how the motion of an entrained particle is altered by this interaction.

Such an interaction has far reaching effects that carry over to the finished product. Inorganic particulate matter in a paper machine furnish can be composed of either natural or synthetic materials, generally clay, titanium dioxide, or silicates. Incorporation of these so-called fillers into the paper sheet imparts to it many useful properties. The correct filler, in the proper amount, will improve paper smoothness, brightness, opacity, ink receptivity or porosity. With the wrong quantity of filler, each of these parameters can be adversely affected, producing a worthless product. Thus the right amount of retention is of great economic benefit to anyone producing a filled sheet of paper.

Again, correct formation of a filled sheet is only one application where retention is important within the paper mill. Any use of a porous medium filter, employed on either a liquid or gaseous stream, would be controlled by retention

phenomena. As with almost any industrial process, improvements in, or increased efficiencies of, retention processes are possible, and in many cases necessary.

Necessary is the key word in the previous statement. In the area of paper or board formation, poor retention means that the unretained materials are eventually found in the waste stream of the mill, and in past years, this meant the sewer. Recently, government regulations have necessitated a drastic reduction of these waste streams which would have reentered the environment unchanged. Within several years, the requirement will be that the dumping of any waste material to the environment is prohibited; this concept is more generally known as zero discharge. There are several ways in which the industry is trying to comply with this law. The most widely used method is the waste treatment plant, where suspended solids and organic materials are removed from the waste streams. Improved retention within the mill would have the effect of reducing the load on these systems. This improvement would also be of economic value since filler pigments are generally quite expensive, thus if the amount lost within the mill decreases, the cost of producing the product would also decrease. Another method for reducing waste loads involves recycling the white water. This means the suspension removed from the furnish through the wire is returned to the papermaking system to be reused. If retention is poor, particulate matter will accumulate within this closed loop. This could lead to adverse effects on the paper qualities mentioned above. Also, the particulate material could be harmful to equipment due to its abrasive nature. Of particular concern would be the effect on pumps, shower heads, cleaners, etc. In addition, premature plugging of felts might be a consequence of this buildup, requiring their replacement sooner than should be necessary. These problems can theoretically be solved by increased first pass retention during formation, thus initially retaining as much of the particulates as possible.

The above discussion has shown that good retention is an important concern of the paper industry for both environmental and economic reasons. However, the improvement of retention will be a difficult task because, to accomplish this, the question of how retention occurs will have to be answered. There has been considerable research done in past years aimed at this answer but it is evident that there remains much to do. Good qualitative and quantitative information must be produced which shows exactly what happens to a particle as it approaches a fiber. Answers must be found to show which forces govern whether a particle will collide with, and be retained by, a fiber, or whether it remains suspended in the fluid flow. This investigation was initiated for the purpose of answering some of the questions surrounding this important process.

RETENTION MECHANISMS

One of the most important aspects of understanding retention is the visualization of how a particle, flowing in a fluid near a much larger fiber, moves close enough to that fiber to impact on its surface and be retained. For this reason, a brief review pertaining to some so-called retention mechanisms is in order. In much of the literature concerning this aspect of the retention process, there have been several mechanisms mentioned repeatedly as influencing the movement of a particle suspended in a flow stream (1-4). The first of these is inertial impaction (Fig. 1). When a fluid stream approaches a circular, cylindrical fiber, the streamlines (solid lines) curve around the fiber. If a particle is suspended in this flow and its density is equal to that of the fluid, then it might follow the flow. If the particle possesses a density greater than the fluid, then because of its inertia, it will resist any acceleration away from the fiber and its path (dashed line) will cross the streamlines. This action serves to increase the probability of collision. This mechanism is of

great importance to aerosol retention applications because of the large density variation between particle and fluid.

Flow line or direct interception (Fig. 2) represents the movement of a particle considered to possess a density similar to the fluid. In this case, the particle will continue to follow the flow of the streamlines; however, it will collide with the fiber if it passes within a distance less than its radius, $d/2$, from the fiber's surface.

When a particle is suspended in a fluid, it is constantly colliding with the fluid molecules. If the particle is small enough, these collisions will cause it to undergo a random displacement that is called Brownian motion or diffusion. This movement could mean that a particle, initially outside the range for interception, could be displaced into a position close enough to the fiber for interception to occur (Fig. 3). Of course, since this is a random process, the reverse action is also possible and the particle could be displaced from a path which would have led to collision.

There are several other possible collection mechanisms mentioned in the literature, but these are thought to be negligible in the type of retention system under investigation in this thesis. These mechanisms would include sieving, settling, and thermal diffusion.

All of the mechanisms discussed above are physical processes. In addition, there are several physiochemical considerations which would also influence the collision between a particle and fiber. These might affect retention by themselves or act to bring a particle into a position where its movement would be controlled by another mechanism. There exist between any two particles of matter, whatever their size and chemical composition, both attractive and repulsive forces. These forces exist between atoms, molecules or groups of

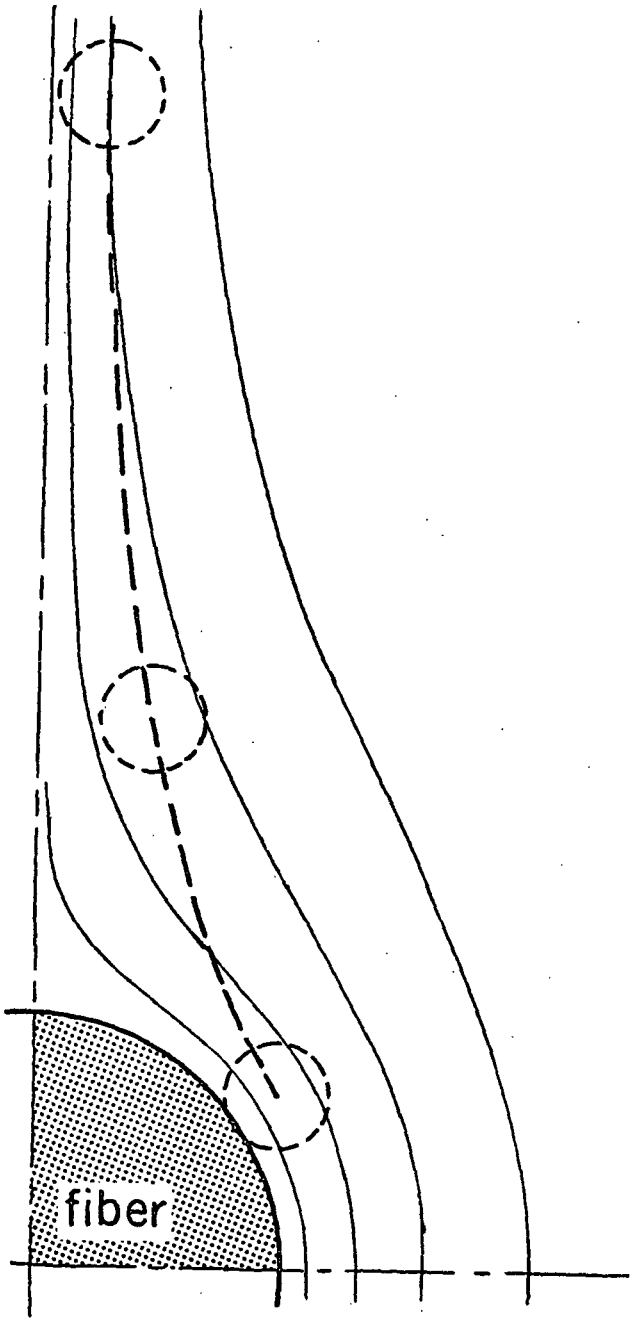

Figure 1. Schematic of Collection Caused by Inertial Impaction

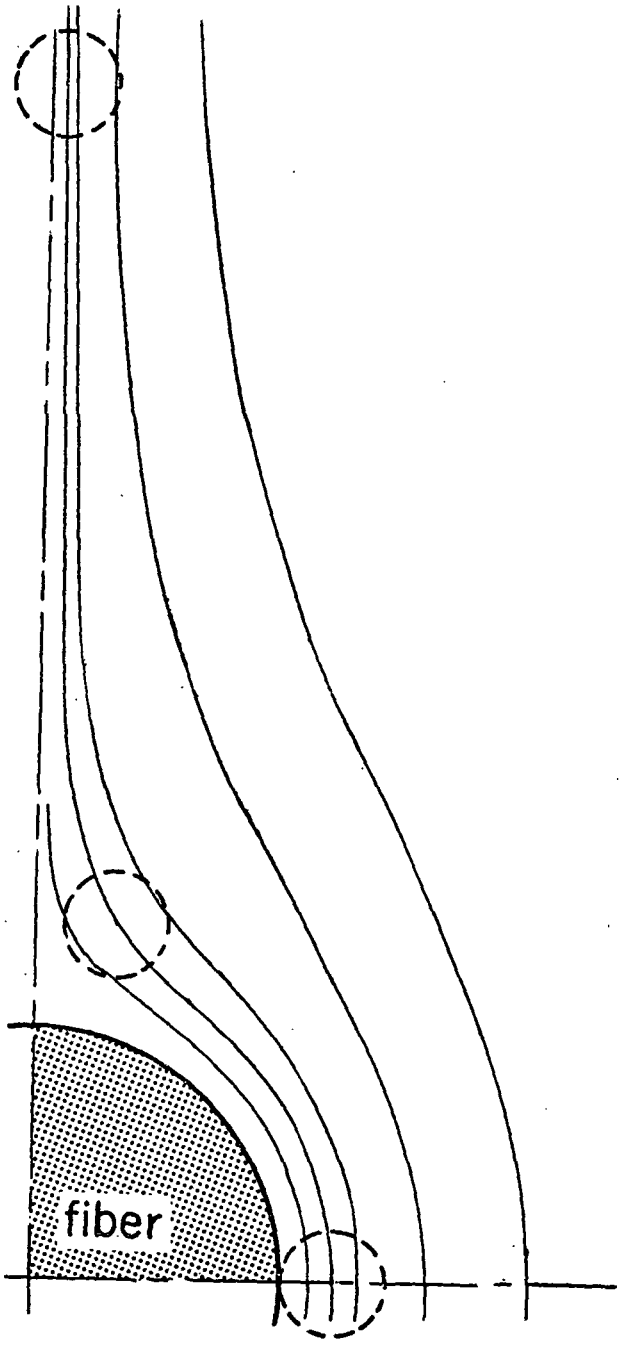

Figure 2. Schematic of Collection Caused by Flow Line Interception

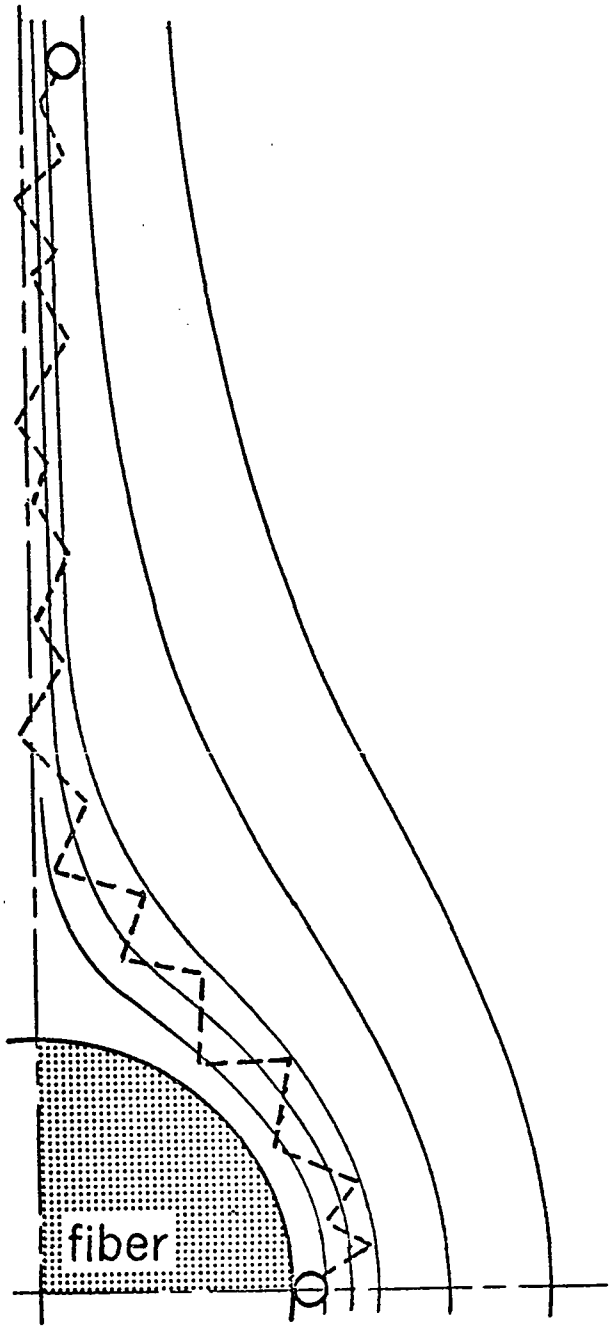

Figure 3. Schematic of Collection Caused by Diffusion or Brownian Motion

molecules and, therefore, would be included in the interaction potential between a particle and fiber in the retention process (5). These forces can generally be grouped in terms of primary or secondary valence effects. The primary effects are those which cause atoms to join and form molecules or chemical compounds. They are more conventionally known as ionic, covalent, or metallic bonds. The secondary effects occur after the primary effects have been satisfied; for example, these can be thought of as forces causing the liquefaction or solidification of the inert gases or the physical adsorption of molecules to solid surfaces when no chemical bonds are formed.

The attractive forces present during the interaction of a particle and fiber, assuming no electrostatic attraction, are caused by these secondary valence effects, and are generally combined into a single term known as the Van der Waals force (5-7). In general, this force arises from an attraction between induced dipoles formed within separate molecules of the interacting materials; therefore, it is present in any system and independent of the physical or chemical environment. The magnitude of the force is dependent on separation distance, and decreases rapidly as this distance increases. If this force is dominant in a particle-fiber system, it could lead to a collision between the particle and fiber, thus becoming an important factor in the retention of the particle.

The repulsive force that can arise in a particle-fiber system is commonly known as the double-layer force. This force originates when the solid material is dispersed in a liquid. The solid assumes a surface charge through direct ionization of surface groups or by preferential adsorption of a particular ion present in the suspending medium. Surface charge induces the formation of a diffuse layer of opposite charge, composed of counterions, which extends from the solid's surface out into the suspending medium. This mobile layer of charge

is the double layer. If two interacting bodies have double layers of like charge, a repulsive force is exerted as the two approach one another. This charge is diffuse, therefore its effect drops off dramatically with increasing separation distance. If such a repulsive barrier is present between a particle and fiber, it must be overcome before the particle can reach a point where the attractive forces dominate and a collision with the fiber is possible. If the repulsion is sufficiently strong, the particle cannot get close enough to the fiber for collision. This double-layer charge is sensitive to the ionic environment of the medium. Thus, modification of this environment through the addition of electrolytes can alter this effect, and in some cases reverse the sign of the charge.

From this information, it has been well established that retention is dependent on a balance between the attractive and repulsive forces present in a particle-fiber system. Their importance cannot be overstated. A more detailed presentation of these force effects will be made in a later section.

THESIS OBJECTIVES

The previous discussion has been presented in an attempt to show that retention is a very important concept in the paper industry, while at the same time, it is very complex and not well understood. This thesis was initiated to answer some of the questions pertaining to how retention occurs and what might be done to improve its effectiveness. As proposed, the thesis would be concerned with an investigation of the relative importance of various forces, hydrodynamic, molecular, and colloidal, exerting influence in the retention process. This necessitated the determination of individual force effects on the interaction between a particle and fiber, and to discern how they affect the overall retention obtained with such a system. Once this was established, then suggestions would be made as to how retention might be improved or made more efficient.

The thesis was concerned primarily with the construction of a mathematical model to simulate retention occurring in a system composed of particles and fibers. The model was set up to predict retention efficiencies obtained from a highly idealized system. Since this was the first attempt to look at such a system in this manner, it was felt ideal conditions had to be assumed and employed as a first approximation in a scheme to produce a simulation of an actual industrial process. These conditions were that a spherical particle of finite size was mathematically observed during its approach and interaction with an infinitely long fiber of circular cross section. The fiber was assumed to have a smooth surface and its diameter was assumed to be approximately one-hundred times larger than that of the particle. By monitoring the movement of the particle as it flowed around the fiber and was affected by various physical and physiochemical forces, a retention efficiency could be calculated and correlated to various system parameters.

It was felt that there should be some experimental data generated to compare with the model, only to show, however, that the simulation technique was on the right track in predicting retention values. A program was designed to study retention within a porous mat of uniform fibers by utilizing a standard permeation technique. The materials and system conditions employed in the experimentation were as close as possible to the model values to insure a favorable comparison. For this reason, a synthetic fiber of circular cross section, particles very nearly spherical in shape, and highly purified water were used. From the degree of particulate material retained by the mat of fibers, a retention efficiency could be calculated and compared to the model predictions.

One of the main goals of this thesis was the establishment of an accurate, and fairly simple, working model of the retention process for use in future

work. It was realized that a single thesis is not sufficient to complete a study of this very complex process. A significant amount of work remains to be done before the model discussed here will accurately simulate an industrial application of the retention process. However, this thesis has shown that such a model is feasible and can quite accurately predict the degree of retention present in a simplified flow system.

ORGANIZATION OF THE THESIS

The work accomplished in connection with this thesis is presented in two major sections. In the first, the theoretical program is discussed. This includes the development of the mathematical model and the results that have been obtained from it. Also presented in this section is a brief, historical review of retention theory and any applicable modeling work performed in the areas of filtration, permeation, or retention. The second section deals with a discussion of the experimental program: the materials utilized, procedures followed, and the results obtained. This section also contains a summary of other research pertinent to the program.

The final sections of this manuscript present a comparison of the theoretical predictions and experimental determinations of retention efficiency. Reasons for any differences in these values will be discussed. In addition, some suggestions are made concerning future refinements of the model to improve the accuracy of its predictions and its applicability to more complex retention systems.

THEORETICAL PROGRAM

BACKGROUND

Realization of the importance of the retention process has been the incentive for much research in this area. Advances in understanding this complicated process have been reported for a considerable number of years. However, only recently has it been possible to use this basic knowledge in conjunction with new, sophisticated procedures and equipment, thereby providing significant contributions to the theories governing retention. In much of the previous work concerning the collection of small particles within a porous medium, the mechanisms proposed as controlling this process have been based on the conservation of mass. Due to this procedure, the accumulation of particulate matter was considered proportional to the mass flow rate of particles through the medium. That is, most of the information gained was based on changes in particle concentrations. The fraction retained by the medium has been traditionally reported by a parameter called the collection coefficient. In most cases, this concept has substituted for a description of the system dynamics but has been limited to overall characteristics of the process. Recently, there have been several more rigorous approaches to the problem of defining retention mechanisms. The increased power of the digital computer has been most influential in this area, since the retention process can now be represented in a much more specific form. This has led to the construction of mathematical models for simulating various retention systems. Such a model is mathematically exact, and a good model will closely approximate the process. High-speed computers have made it feasible to study the behavior of good models.

Before a description of any of these models is presented, some background information should be provided. This information represents significant research

efforts in the areas of aerosol and water filtration. Most of the modeling work accomplished in past years, including the present investigation, is based on this work. In general, the research described below has been based on either granular or fibrous porous media. Many developments in retention theory obtained through the years can be applied to either form of filter material.

AEROSOL FILTRATION

The term aerosol filtration can be defined as the removal of solid particles or liquid droplets from a gas by means of a porous medium filter. This process is more rigorous than the common air cleaning connotation which imposes less exacting demands on removal, but remains adequate for most industrial applications. Air cleaning systems make use of scrubbers, cyclones, sedimentation tanks, packed granular beds, etc., but most are inefficient at removing particles less than 1 μm in diameter. However, air filtration has been refined to the extent where 95% of suspended material less than 1 μm in size can be removed from any substantial air flow. Historically, the development of air filters has been progressing for more than 2000 years. Roman industries and mines were well organized and problems encountered due to dust were recognized; therefore, the use of cloth to cover the nose and mouth became one of the first applications of air filtration (2). Much of the development work in air filter design and composition since that time has dealt with aids to respiration; one of the most obvious has been the improvement in gas masks for industrial and military use. Most of this type of work has been concerned with fiber filters commonly composed of cotton, wood, or asbestos fiber. In recent years, the demand for efficient filters has grown, not only for the protection of life, but also for keeping sophisticated electronic and biological equipment free from dirt and dust. The advent of nuclear energy meant that new demands had to be placed on fiber filters; for example, filters had to be designed for the

removal of radioactive particles from high temperature air streams before they were dispersed into the atmosphere.

From the long history of aerosol filtration, and its varied use in today's society, there is sufficient information available to provide a valid description of this process. An interesting and complete review of this subject has been presented by Davies (2). This report traces the theoretical development of air filters from their inception to some highly sophisticated, modern techniques for filter analysis and design. The mechanisms of particle inertia, interception, and Brownian motion were discussed in terms of their contributions to the mechanical efficiency of the filter. These mechanisms were also shown to be affected by gravitation, temperature, and pressure. Consideration was also given to the effects of electric charges on collectors and on particulate matter. These charges would relate to the surface forces which are thought to exist in an aerosol filtration system.

Davies devoted much of his discussion to the various applications of fibrous filters. This was with good reason since most aerosol filtration research has been accomplished by assuming this type of collecting material (3,8-11). However, there has been some work done in the area pertaining to collection by spherical collectors (4) and membrane filters (12,13). Membrane filters deal with the collection of particles within an open pore of an otherwise solid structure. These are used primarily for sampling and size analysis of aerosols.

Even though this thesis has dealt with the removal of particulate matter from a liquid flow stream by the action of fibrous collectors, some of the retention theory presented in connection with aerosol filtration studies has direct relationships to the liquid system. Chen (3) presented an overview of retention concepts concerning the collection of submicron particles by a

fibrous medium. He stated that the design of these filters should be based on practical considerations dealing with the efficiency of particle collection and the pressure drop resulting from this collection. It was mentioned that a good fiber filter is characterized by a high porosity and interfiber distances that are large compared to particle size. Because of this, the mechanisms by which collection occurs and the flow pattern around individual fibers are of fundamental importance. Work was presented indicating that collection can occur by interception, inertia, Brownian motion (diffusion), gravity, and electrical attraction. However, this review largely ignored the electrical effects. Of particular interest was a description of the contribution to collection made possible by Brownian motion. The discussion pertaining to diffusion coefficients and random walk theory was thought to be directly applicable to the present study. Conclusions based on all of the gathered information were that, for aerosol collection, excluding electrical effects, inertial impaction was important at high fluid velocities, while diffusion appeared to be the controlling factor at low velocities.

Lundgren and Whitby (8) studied the effect of particle electrostatic charge on collection by a fibrous filter. The results of the study provided a relationship between a collection efficiency of submicron particles and an image force-drag force parameter. The flow rates observed were quite low, all converted to Reynolds numbers below one based on the particle. The authors stated that if the particles were charged, the resulting image force was the dominant mechanism behind collection, becoming more influencial than inertia or interception. Another interesting point mentioned within this investigation was the definition of collection efficiency used in obtaining the results. A single fiber efficiency was defined as the ratio of the flow stream area from which all particles were removed to the projected area of the fiber. This

meant that the concentration of particles had to be uniform across the flow stream. This definition had been used to represent collection or retention efficiency in many studies concerned with aerosol filtration.

Wong, et al. (11) presented the results of a quantitative investigation dealing with the inertial impaction mechanism of aerosol collection by a fibrous medium. Also discussed was their derivation and utilization of a collection efficiency parameter similar to that mentioned above. The results of this work indicated that diffusion, electrostatic attraction, and gravitation effects were negligible. It was shown that the efficiency increased with increasing velocity; this is consistent with the theory based on the effect of inertia. Since the particle would be moving faster, it would possess greater momentum, and therefore would follow a more direct path to the collector's surface.

There have been several other studies presented in the literature that are beneficial to the understanding of aerosol retention in fibrous, porous media. For example, Friedlander (9) studied the effect of diffusion on small particles as they approached the surface of a cylinder or sphere. His theoretical results compared favorably with experimental data acquired from other aerosol filtration studies. Finally, George and Pohlein (4) investigated the movement of a particle around a spherical collector, as it was affected by all of the physical transport mechanisms as well as an electrostatic force. A Coulombic type of interaction potential was assumed to exist between the particle and collector, and it was concluded that this was the dominant force leading to collection. The collection efficiency utilized in this work was similar in definition to that mentioned above. If the electrostatic attraction is strong enough, the authors showed that efficiency, by their definition, could be greater than one.

WATER FILTRATION

As with aerosol filtration, the concept of removing particulate matter from liquid streams has been practiced for a considerable amount of time. For example, charcoal has been employed for centuries to purify the water used in a variety of applications. There are, however, some basic differences between the theories governing water and aerosol filtration. One difference is that the densities of water and particle are much closer than those between air and the same particle, meaning that particle inertia would not be as important a factor in promoting collection when the fluid is water. For this reason, the contribution of inertia to the overall retention rate is often neglected in liquid flow systems. Secondly, the dispersion of colloidal particles in water generally gives rise to surface charges; the effect of these charges on a particle approaching a collector has to be accounted for. The differences between aerosol and water filtration mentioned here imply that, because the influence of interception is minor for small particles, some types of attractive force must be present in a water filtration system which would cause a significant amount of retention.

There has been considerable work performed in the area of water filtration; most has dealt with applications to deep bed filtration employing a granular porous medium. An example of this type of system would be a sand filter. However, there have been some studies concerning the utilization of fibrous porous media for water filtration applications. Some pertinent work involving both forms of collection media will be discussed here. Yao, et al. (14) presented a conceptual model for deep bed filtration of small colloidal particles and how this process would relate to waste water treatment. They viewed the collection process as being similar to coagulation. Two distinct steps were visualized as occurring. The first step involved the transport of the particle

to the vicinity of the solid-liquid interface of the filter grain. It was stated that this occurs predominantly through the mechanisms of diffusion for smaller particles and by interception or settling for larger ones. The second step was considered to be the actual attachment of the particle to the collector. The authors, however, reasoned that for significant retention, the system would have to be destabilized by the addition of chemicals or polymers. No attempt was made to investigate molecular or surface forces present in the system.

In a recent series of articles, Spielman and various coworkers (15-17) presented comprehensive theoretical and experimental studies dealing with particle collection on various types of filter media, employing many of the physical and physiochemical forces thought to exist in such a system. In the first of this series (15), a theoretical observation was made of a small particle in motion, approaching a much larger collector. Equations were developed which described the particle's motion as affected by the hydrodynamic and London-Van der Waals forces. In this paper, only minor consideration was given to diffusion and the double-layer force was neglected. Numerical solution of these equations (16) led to predictions of particle capture from suspensions flowing around variously shaped collectors. These solutions included only the effects of hydrodynamic, gravitational, and Van der Waals forces, as again, non-Brownian particles were assumed and the double-layer interaction was omitted. Experimental data for comparison to these predictions was made possible (17) by a study involving the collection of latex particles in beds of glass beads. Since these particles were generally larger than 1 μm, diffusion was neglected in the analysis. Also, double-layer repulsion was found negligible compared to other effects. Agreement of experimental and theoretical values was within a factor of two when Van der Waals force, gravity, and hydrodynamic forces were considered. The experiments did confirm that collection increased with

increasing particle size, decreasing velocity, and increasing ionic strength of the particle suspension. This last observation would seem to mean that double-layer repulsion could be an important factor in the degree of collection obtained if suspension conditions were adjusted correctly. Finally, no attempt was made to obtain experimental verification of the theory dealing with collection by cylindrical collectors.

Goren and O'Neill (18) discussed a method for the estimation of the hydrodynamic force effect exerted on a small particle moving slowly around a much larger spherical or cylindrical collector, particularly when the particle was very close to the obstacle. While these authors investigated only the hydrodynamic forces in this system, several observations were made which were thought important to the present investigation. In this work, it was assumed that because of the large difference in size between the particle and collector, the flow field past the collector would be essentially undisturbed by a particle except in the immediate vicinity of that particle. Also mentioned was the hypothesis that at distances of separation greater than several particle radii, the particle does not deviate from the fluid streamlines. The results of a rigorous mathematical examination of the hydrodynamic forces were presented by these authors. This led to the conclusion that for a small value of the ratio of particle to collector diameters, the particle will move undisturbed in the fluid flow pattern at separation distances greater than two or three particle radii. They concluded that at smaller distances, the particle's motion may be adequately described as being similar to that of a particle moving near a flat plate. This observation permits easier application of expressions representing molecular or surface forces to equations describing the particle-collector interaction.

MATHEMATICAL MODELING OF FILTRATION

A primary objective of the present investigation was the development of a mathematical model which would predict retention or collection efficiencies for a system composed of small spherical particles flowing slowly around a transverse array of much larger circular cylinders. In general, a mathematical model of this type is characterized by several intricate equations. Solution of these equations provides a description of the motion of a particle, or its trajectory, as it approaches a collector. The effects of various force terms applied to the system are represented by their influence on the particle's trajectory. The literature was reviewed for any similar work in which modeling techniques were applied to filtration systems. Several studies were found which have some relevance to this type of system. Those of particular interest are summarized below.

An investigation performed by Chen (3) has been mentioned previously. Actually, various portions of this work can be regarded as a type of model for aerosol filtration. All of the mechanisms involved in filtration, including inertia, interception, diffusion, sedimentation, and electrostatic interactions were represented by mathematical expressions. Proper arrangement of these expressions and their subsequent numerical solution provide collection efficiencies for certain system conditions. Results obtained by this author indicate that efficiency increases as porosity decreases and at low velocities (low Reynolds numbers) the efficiency increases as the particle diameter decreases.

Spielman and Cukor (19) presented a model for the flow of non-Brownian particles (diameters greater than 1 μm) within a bed of spherical collectors. The objective of this work was to show how these particles are influenced by colloidal forces. In other work by Spielman, as mentioned above, double-layer

interaction had been neglected. However, this model includes an investigation of the combined effects of double-layer repulsion and Van der Waals attraction. Such a combination of forces means that there exists a potential energy of interaction distribution with the basic shape as shown in Fig. 4. The particle must possess sufficient kinetic energy to overcome the energy barrier, leading to collision with the fiber. Most of the results discussed for this model were concerned with changes in the magnitudes of these force effects and their subsequent influence on collection efficiency. Of particular interest was the prediction of a decrease in efficiency with an increase in the double-layer strength. Some correlation was attempted between these predictions and experimental data obtained with spherical collectors.

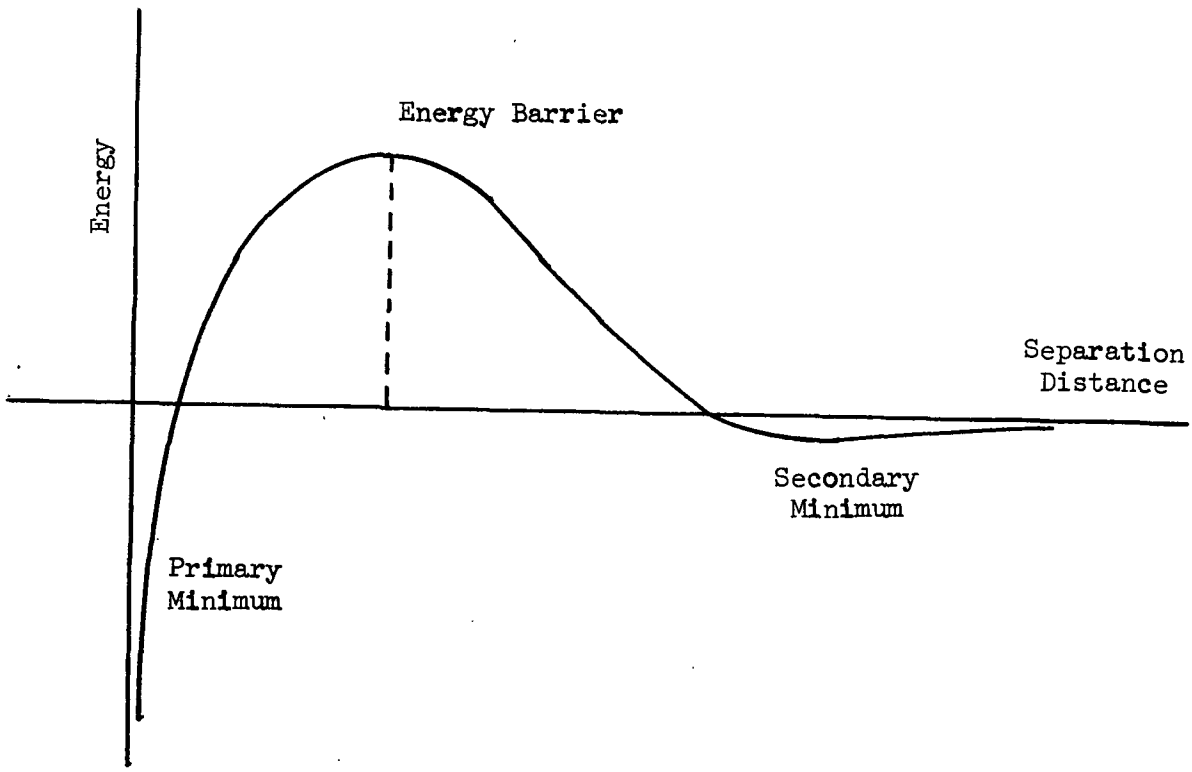

Figure 4. Pictorial Representation of the Interaction Energy Versus Separation Distance for a Combination of Double-layer Repulsion and Van der Waals Attraction

Wnek, et al. (20) described a method for establishing a force balance on a colloidal particle approaching a collector, resulting in a set of differential equations describing the particle's trajectory. The system conditions utilized with this model have a direct relationship to deep bed filtration. The particle was assumed to be transported to the collector by the mechanisms of interception, diffusion, and sedimentation. The surface forces arising from interactions of the double layers and Van der Waals attraction were assumed to exist in this system. Collision due to inertia was neglected. The authors stated that at very small separation distances the motion of the particle toward the collector is retarded. This is due to the fact that the rate of drainage between the solid bodies becomes infinitesmally small as the distance decreases, meaning that collision could not occur if there were no attractive forces present. Since the Van der Waals force increases rapidly as the separation distance becomes small, this drainage effect is overcome and collision can occur. It was also recognized in this study that effects of the surface and molecular forces on particle motion were additive, thus permitting the independent investigation of each force.

A sophisticated model with direct relevance to deep bed filtration through uniform spheres has been reported in a series of articles by Payatakes, et al. (7,21-25). This model of granular porous media has been of interest due to the utilization of the unit cell technique. This concept means that the porous medium can be assumed equivalent to an assemblage of independent units of simple geometry. Ideally, calculated flow patterns around or through this single unit can be adequately related to those actually existing within the assemblage. The unit cell applied by these authors (7,21) is representative of the channel formed between two spherical collectors embedded within a granular filter. This orientation permits the study of the effect exerted by neighboring collectors

on the motion of a particle as it moves through the cell. The particles selected for the model were large enough to neglect Brownian motion (greater than 1 μm in diameter). However, other forces such as hydrodynamic drag, dispersion, and double layer were all considered present in this filtration system (7,23,24). Also included in this investigation was the effect of a retardation factor applied to Van der Waals interaction. This correction factor originates from the lag time of attraction, which is constrained by the finite speed of electromagnetic radiation. This effect significantly decreases the attractive force potential as separation distance increases. The authors have calculated particle trajectories by numerical integration of particle motion equations; from these trajectories indicating capture, an efficiency of collection was calculated and compared to experimental data obtained from similar systems. Results of this model predicted that the double-layer repulsive force was significant in affecting particle collection. It was also shown theoretically that there was a layer of fluid immediately surrounding the collector in which Van der Waals attraction dominated this double-layer effect. Other results obtained by this model included a decrease in collection with increasing velocity and, for particles less than 1 μm, a decrease in collection with an increase in particle size.

As is evident from the material summarized above, there has been some sophisticated work performed in the area of model development pertaining to filtration applications. However, none has been observed which directly applies to the scope of the model constructed in the present investigation. Some are similar, but generally do not incorporate all forces thought necessary to show how a particle moves in relation to a cylindrical collector. Furthermore, the sizes and shapes of the interacting bodies are generally quite different from those modeled in this thesis.

FORCE EXPRESSIONS APPLICABLE TO THE MODEL

In order to obtain accurate equations for simulating particle movement near a much larger fiber, the effects of hydrodynamic forces, diffusion, Van der Waals attraction, and double-layer interaction all had to be taken into account. This meant that mathematical expressions for these forces had to be derived, or modified from those found in the literature. A detailed description of each force expression used in the model will be provided in later sections; however, it was thought that a summary of their development, as found in the literature, would be appropriate at this point.

Diffusion

Particle transport due to diffusion is actually the result of a series of random displacements imposed on the particle by collisions between it and molecules of the fluid. It has been shown by various authors (3,14,25) that diffusion of a finite particle can be characterized by Einstein's diffusion coefficient:

$$\mathscr{D} = \frac{kT}{3\pi\mu d} \tag{1}$$

where d = particle diameter, cm

k = Boltzmann's constant, 1.380×10^{-16} erg/degree

T = absolute temperature, °K

μ = fluid viscosity, poise

$\mathscr{D}$ = diffusion coefficient, sq cm/sec

This diffusion coefficient can be used to calculate an average value of displacement in a certain direction, $\bar{x}$, occurring with a certain specified time interval, Δt, by the random walk theory (1,3):

$$\bar{x} = (4/\pi \mathscr{D} \Delta t)^{\frac{1}{2}} \tag{2}$$

This term makes it possible to estimate the consequences of diffusion by adding a displacement of this magnitude to particle motion, where the displacement is taken in a random direction at times separated by a small time increment, Δt.

Van der Waals Attractive Forces

The study of Van der Waals attractive forces has been the basis of much research for a considerable amount of time (26,27). Considering a single atom, fluctuations in charge distribution are caused by orbiting electrons, this action polarizes neighboring atoms to the point where unlike charges would face one another, therefore, producing an attractive force. These interactions are called dispersion forces and are considered additive among separate atoms. For this reason, they can be applied accurately to the interaction between colloidal particles. The exact nature and resultant effects of these forces in colloidal systems continues to be of great interest (28-30).

To study the influence of Van der Waals forces within the system under investigation, an expression had to be found which represents this interaction as it occurs between a spherical particle and a flat infinite plate. A suitable expression was found (7,31) and with slight modifications has been applied to the present system in the following form:

$$F_{VdW} = -\frac{2H}{3}\frac{a_p^3}{\delta^2(2a_p + \delta)^2}\alpha \qquad (3)$$

where F_{VdW} = Van der Waals force, dynes

a_p = particle radius, cm

H = Hamaker constant, ergs

α = retardation correction factor, $0 < \alpha < 1$

δ = separation distance, cm

This force is dependent on particle size and separation distance. The retardation correction factor, α, is a function of separation distance, and approaches zero as the distance becomes larger. This is due to the fact that an interaction between molecules separated by a distance greater than the wavelength of electron oscillation (generally on the order of 10^{-5} cm) is delayed, thus causing a decrease in the magnitude of the force. Many investigations have ignored this force correction by assuming it to be negligible; however, as will be shown later, this is a questionable practice.

Double-Layer Interaction

Theoretical analyses of the double layers surrounding colloidal particles have been provided by Verwey and Overbeek (32) and Hogg, et al. (33). The equations proposed by these authors describing the interaction between two spheres have been simplified (7,19) to simulate that occurring between a sphere and a flat plate. The form of this equation, as used in this thesis, is as follows:

$$F_{DL} = \varepsilon_d \, a_p \kappa \left\{ \zeta_1 \, \zeta_2 \, \frac{e^{-\kappa\delta}}{(1 + e^{-\kappa\delta}} - \tfrac{1}{2} (\zeta_1 - \zeta_2)^2 \, \frac{e^{-2\kappa\delta}}{(1 - e^{-2\kappa\delta}} \right\} \qquad (4)$$

where F_{DL} = double-layer force, dynes

a_p = particle radius, cm

δ = separation distance, cm

ε_d = dielectric constant for water

ζ_1, ζ_2 = zeta potentials for particle and collector, volts

κ = Debye-Huckel reciprocal length, $(8\pi e'^2 z^2 c/\varepsilon_d kT)^{\frac{1}{2}}$, cm^{-1}

c = concentration of ions in suspension, number/cm^3

e' = electronic charge

k = Boltzmann's constant

$\underline{T}$ = absolute temperature, °K

$\underline{z}$ = valence of ions in suspension

This equation has been found adequate for zeta potentials less than 60 mv and values of κa_p larger than 10. It should be pointed out that it is not valid for separation distances less than 50 A. This is due to the fact that when δ approaches zero, the force becomes an infinitely strong attraction. However, this breakdown causes no major problems since at these small separation distances, the Van der Waals force would be dominant.

DEVELOPMENT OF THE MODEL

The model constructed during this investigation has been set up to simulate a system where a dilute suspension of small, spherical particles was flowing through an assemblage of circular, cylindrical fibers. Basically, there have been three separate force terms examined independently with the model, all assumed to be influencing the interaction between a particle and fiber. These forces were the hydrodynamic drag force, the attractive or replusive forces arising from surface charges, and the molecular attractive forces. It was decided that Brownian motion also should be examined as being a possible mechanism of particle transport. The effect of inertia on particle movement has been shown negligible since the fluid medium considered was water and the particle suspension was visualized as flowing at a very low rate. These assumptions led to the development of a model for the investigation of the relative importance of the forces mentioned in a simulated retention system.

The basis for the model has been the derivation of particle trajectory equations which describe the motion of a particle as it flows around a fiber, or collides with it. Various system parameters have been investigated to show how they relate to particle movement; these have included porosity, approach

velocity of the particle suspension, particle size, and the ionic environment of the suspending medium. Solution of these equations has provided a means of calculating collection efficiencies which has been the values used for correlating all of the results. This section will provide material relating to the derivation of these equations, the solution, and a review of how the results are reported.

DESCRIPTION OF THE BASIC FLUID FLOW EQUATIONS

Theoretical analysis of all fluid flow problems must begin with the two basic equations describing isothermal systems. These equations express the fundamental laws concerning the conservation of mass and the conservation of momentum, and are known as the equations of continuity and motion (34,35).

The equation of continuity is obtained by applying a mass balance around a small, stationary volume element with fluid flowing through it. This equation can be expressed as:

$$\frac{\partial \rho}{\partial t} = - \nabla \cdot (\rho \vec{v}) \tag{5}$$

where ρ is the local density of the fluid and $\vec{v}$ is the local mass average fluid velocity. The equation states that an increase in density within the volume element equals mass accumulation per unit volume. Since water is the fluid under consideration in this investigation, and since water can be assumed incompressible, its density remains constant. Therefore, the continuity equation can be simplified to:

$$\nabla \cdot \vec{v} = 0. \tag{6}$$

The equation of motion is found by applying a momentum balance around a small volume element moving with the fluid. It states that this element is

accelerated due to forces acting on it, in essence, a statement of Newton's Second Law. The equation can be written as:

$$\rho \frac{D\vec{v}}{Dt} = - \nabla p - [\nabla \cdot \tau] + \rho\vec{g} \qquad (7)$$

The left-hand side is a description of the mass per unit volume multiplied by acceleration, while the right-hand side separates the pressure, viscous, and gravitational forces exerted on the fluid element.

Within an isothermal, Newtonian system, the viscosity of the fluid, μ, will remain constant. When combined with the assumption of constant density, the motion equation can be simplified to:

$$\rho \frac{D\vec{v}}{Dt} = - \nabla p + \mu\nabla^2\vec{v} + \rho\vec{g} \qquad (8)$$

This is the well-known Navier-Stokes equation.

The flow rates observed in this study will be quite small. Thus the inertial terms, $\rho[(\partial\underline{\vec{v}}/\partial\underline{t}) + \underline{\vec{v}} \cdot \nabla\underline{\vec{v}}]$, in the Navier-Stokes equation can be modified or omitted as compared to the viscous terms, $\mu\nabla^2\underline{\vec{v}}$ and the pressure term. If the flow is steady, the first of these inertial parameters is zero; if the second is neglected as well as gravity, then Equation (8) assumes the form of the creeping motion equation:

$$\mu(\nabla^2\vec{v}) \doteq \nabla p \qquad (9)$$

The flow model is based on this creeping motion equation in conjunction with the simplified continuity equation. For reasons that will be apparent shortly, the fluid and particle motion equations will be expressed in terms of circular cylindrical coordinates. The form in which the model is presented also suggests that only two dimensions need be considered. Thus Equations (6) and (9) can be written for the creeping motion regime in the following general form:

$$\frac{\partial v_r}{\partial r} + \frac{v_r}{r} + \frac{1}{r}\frac{\partial v_\theta}{\partial \theta} = 0 \tag{10}$$

$$\frac{\partial p}{\partial r} = \mu\left(\nabla^2 v_r - \frac{v_r}{r^2} - \frac{2}{r^2}\frac{\partial v_\theta}{\partial \theta}\right) \tag{11}$$

$$\frac{1}{r}\frac{\partial p}{\partial \theta} = \mu\left(\nabla^2 v_\theta - \frac{v_\theta}{r^2} + \frac{2}{r^2}\frac{\partial v_r}{\partial \theta}\right) \tag{12}$$

In these equations, v_r and v_θ are the velocity components of fluid flow in the r- and θ-directions, respectively.

DESCRIPTION OF THE UNIT CELL

The mathematical model was designed to monitor flow around a transverse parallel array of circular fibers, with the flow moving in a direction perpendicular to the fiber axis. Theoretically, it is possible to remove a single fiber from an assemblage and describe it and the space about it in such a manner that it may be thought of as an average of all other fibers in that assemblage. Each fiber within this assemblage can be considered to have an environment similar to the one being observed. In other words, a physical system is replaced with an equivalent arrangement based on a single collector. It has been established (7,36,37) that observation of such a collector can lead to accurate results in terms of the entire filter as well as greatly simplifying the mathematics. This assumption is the basis for the unit cell model. The unit cell described below has been the one employed in the present model, and was obtained through some modification of a cell used by Happel (38).

The unit cell utilized in this investigation is shown schematically in Fig. 5. The cell can be visualized as consisting of two concentric cylinders. The inner cylinder, of radius A, represents the solid fiber, while the outer cylinder, with a radius of B, has been called the fluid envelope, and is

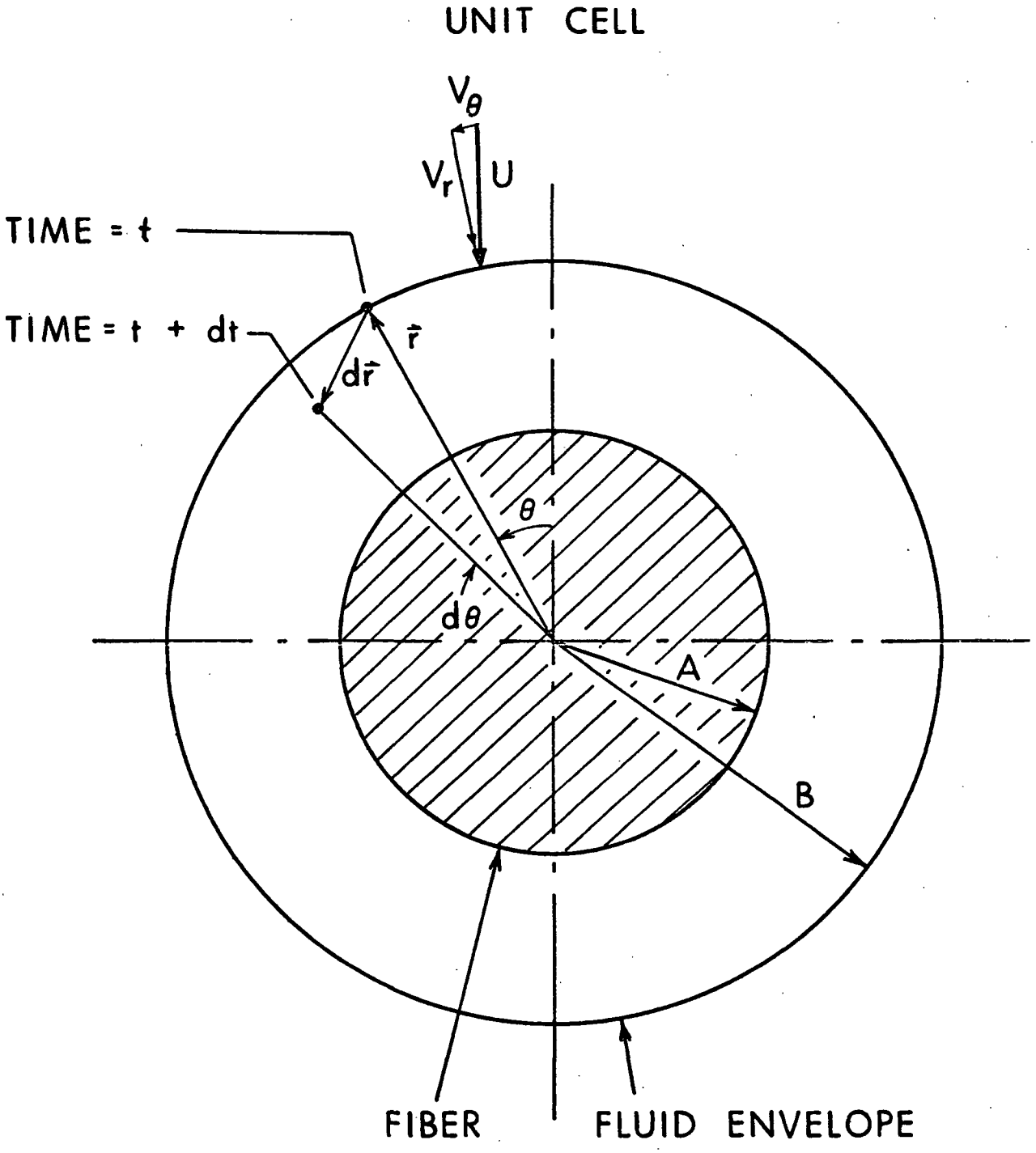

Figure 5. Schematic Diagram of the Unit Cell Which is the Basis of the Flow Model

characterized by a free surface. The porosity is found by the ratio of the fluid area to the total area within the boundary of the cell. At any point within the fluid annulus, the fiber is said to affect the motion of the fluid and any entrained particles during the period of time the suspension is within the cell. It should be emphasized again that the fiber environment described here is considered an average of all fiber environments within the assemblage.

At this point, a couple of assumptions should be mentioned which are directly associated with this unit cell. The first of these is that the usual no-slip condition is assumed to exist at the fiber surface. This means that the fluid velocity at the surface, in both the r- and θ-directions, is zero. This creates a velocity gradient within the annulus of the cell. The second assumption pertains to the fluid envelope. Since this imaginary boundary is described as a free surface, it can be stated that the friction or shear stress at the boundary is zero.

Other observations made in relation to the unit cell include the fact that the fluid approach velocity, U, may be expressed in terms of its components. The terms v_r and v_θ are the same components of velocity that appeared in the creeping motion equations. The pathway that an element of fluid takes as it moves through the cell can be monitored if these velocity components are locally known. For example, at a time t, a fluid element would be situated within the fluid envelope. At some increment of time later, $t + dt$, the same element will have arrived at a new position by moving a distance $\vec{dr}$, through an angle, $d\theta$. Integration of the velocity component equations over a specified time step, dt, will yield these distance and direction values.

GENERAL STREAM FUNCTION

For various classes of fluid flow problems, the differential equations describing fluid motion can be rearranged to make their solution easier. Considering a fluid of constant density and viscosity, the creeping motion equations can be transformed by means of the stream function, ψ. In this way, the fluid velocity components can be defined in the following manner:

$$v_r = \frac{1}{r}\frac{\partial \psi}{\partial \theta} \quad ; \quad v_\theta = -\frac{\partial \psi}{\partial r} \tag{13}$$

By this definition, the continuity equation is automatically satisfied. These statements permit the two components of the motion equation to be combined, by eliminating the terms involving pressure. This results in a fourth order, scalar equation in terms of ψ:

$$\nabla^4 \psi = \nabla^2(\nabla^2 \psi) = 0 \tag{14}$$

For details of this transformation, the reader is referred to Happel and Brenner (35). The physical significance of the stream function is that lines of constant ψ are the streamlines of fluid motion around the circular fiber. These would be the actual paths that fluid molecules follow in their orbit of the fiber.

Equation (14) is called a biharmonic equation, and a general solution to this equation is readily available. There are many solutions possible. However, the particular solution fitting the flow system under study has the form:

$$\psi = \sin\theta[Cr^3 + Dr + E/r + F\, r \ln r] \tag{15}$$

where C, D, E, and F are integration constants. The complete derivation of this equation is provided in Appendix I.

BOUNDARY CONDITIONS AND THE SPECIFIC STREAM FUNCTION

For a specific solution to Equation (15) which would represent the flow system depicted in Fig. 5, four boundary conditions have to be defined in order to calculate the four integration constants. The boundary conditions utilized were provided through the assumptions made during the description of the unit cell. First, it was stated that a no-slip condition exists at the surface of the fiber, therefore, the velocity components at the surface are zero. Secondly, at the fluid envelope, the fluid possesses a finite velocity and, as mentioned, the shear stress at this point would be zero. Thus the boundary conditions were identified as being the following:

$$\text{at} \quad r = A \qquad v_r = 0 \tag{16}$$

$$v_\theta = 0 \tag{17}$$

$$\text{at} \quad r = B \qquad v_r = -U \cos\theta \tag{18}$$

$$\tau_{r\theta} = \mu\left(\frac{1}{r}\frac{\partial v_r}{\partial \theta} + \frac{\partial v_\theta}{\partial r} - \frac{v_\theta}{r}\right) = 0 \tag{19}$$

Applying these four expressions to Equation (15) permits the derivation of the specific stream function for slow flow around a circular fiber within the unit cell:

$$\psi = \frac{U \sin\theta}{f(\varepsilon)}\left\{\frac{(1-\varepsilon)^2 r^3}{A^2} - \frac{A^2}{r} - 2[1 + (1-\varepsilon)^2]\, r \ln\frac{r}{A}(1-\varepsilon)^{\frac{1}{2}} - r\, f(\varepsilon)\right\} \tag{20}$$

where ε = porosity, $(1 - A^2/B^2)$ (21)

$$f(\varepsilon) = (1-\varepsilon)^2 - 1 + 2[1 + (1-\varepsilon)^2] \ln (1-\varepsilon)^{-\frac{1}{2}} \tag{22}$$

As shown in Equation (20), the value for ψ is dependent on the fiber radius, A, the fluid approach velocity, U, and the porosity, ε. A detailed description of the procedure followed for obtaining this equation is given in Appendix II.

FLUID VELOCITY COMPONENTS

The components of fluid velocity at any point within the annulus of the unit cell can be found by applying Equation (13) to the stream function. Once this is completed, the following expressions are obtained (see Appendix III):

$$v_r = \frac{U \cos \theta}{f(\varepsilon)} \left\{ (1 - \varepsilon)^2 \frac{r^2}{A^2} - \frac{A^2}{r^2} - 2[1 + (1 - \varepsilon)^2] \ln \frac{r}{A} (1 - \varepsilon)^{\frac{1}{2}} - f(\varepsilon) \right\} \tag{23}$$

$$v_\theta = \frac{-U \sin \theta}{f(\varepsilon)} \left\{ 3(1 - \varepsilon)^2 \frac{r^2}{A^2} + \frac{A^2}{r^2} - 2[1 + (1 - \varepsilon)^2] \left[\ln \frac{r}{A} (1 - \varepsilon)^{\frac{1}{2}} + 1 \right] - f(\varepsilon) \right\} \tag{24}$$

By integration of these velocity equations in accordance with either one of the Equations (13), the streamlines of fluid flowing through the unit cell can be traced.

DERIVATION OF PARTICLE MOTION EQUATIONS

The next step in the model development was to examine the effect of the flow pattern on a small, spherical particle entering the unit cell suspended in the fluid. As a particle moves through a stationary fluid, there is a resistance to flow exerted on it by the fluid. This is known as the drag force. Within the creeping motion regime, the magnitude of this force is given by Stokes' Law:

$$F = 3\pi\mu d\, V \qquad (25)$$

This force is shown to be dependent on the viscosity, particle size, and the velocity, V, with which the particle is moving. If a particle is suspended in a moving fluid and is simultaneously subjected to other effects, then the drag force is dependent on both fluid and particle velocity. Thus the velocity term in Equation (25) would assume the form of a relative velocity and Stokes' Law can be rewritten as:

$$\vec{F} = -\, 3\pi\mu d\, (\vec{v} - \frac{\vec{dr}}{dt}) \qquad (26)$$

In this equation, $\vec{v}$ is the fluid velocity vector, while $\vec{dr}/dt$ refers to the particle velocity. The negative sign implies only that the force is exerted in a direction opposite to the motion. The velocity vectors in this equation can be broken down into their unit vector components:

$$\vec{v} = v_r \vec{i} + v_\theta \vec{j} \qquad (27)$$

$$\vec{dr} = dr\, \vec{i} + r\, d\theta\, \vec{j} \qquad (28)$$

Particle motion can be described by Newton's Second Law:

$$\vec{P} = \frac{d}{dt} (m \frac{\vec{dr}}{dt}) \qquad (29)$$

where m is the particle mass. This equation states that force equals the rate of change in momentum.

Since $\vec{P}$ is a force vector, and if it is assumed at this point that drag is the only force acting on the particle, then Equations (26) and (29) can be set equal. Once this is done, and the $\vec{i}$ and $\vec{j}$ components are separated, the result can be written as two, second order, nonlinear differential equations.

These describe the movement of a particle through the unit cell in terms of its radial and angular components:

$$\frac{d^2r}{dt^2} = K_1 \left(v_r - \frac{dr}{dt}\right) + r \left(\frac{d\theta}{dt}\right)^2 \tag{30}$$

$$\frac{d^2\theta}{dt^2} = K_1 \left(\frac{v_\theta}{r} - \frac{d\theta}{dt}\right) - \frac{2}{r}\frac{dr}{dt}\frac{d\theta}{dt} \tag{31}$$

where $K_1 = 18\mu A/d^2\rho_p U$

ρ_p = particle density, gm/cm^3

The derivation of these nondimensional equations is presented in Appendix IV. Integration of the equations will yield the trajectory of a particle as it travels around the fiber, influenced only by the drag force and inertia. It should be mentioned at this point that the motion equations have been derived under the assumption that the particle is pointlike but not massless and does not rotate as it follows a trajectory. Therefore, possible effects caused by such a rotation and drift have been neglected.

APPLICATION OF ADDITIONAL FORCE EXPRESSIONS TO THE TRAJECTORY EQUATIONS

Since Equations (30) and (31) reflect only the effect of drag and inertia on particle motion, a means of incorporating other expressions representing surface and molecular forces have to be derived. The method employed for accomplishing this was to add the appropriate force expressions to the corresponding component equation. This practice has been employed by several investigators in previous studies (7,19,20). In addition, it has been proposed for the model developed here that the interaction between the particle and fiber can be approximated accurately by the interaction which would exist between a small sphere and a flat, infinite plate. This has been a common practice in modeling

work for a variety of reasons. The difference in size between the two bodies is large, generally on the order of two orders of magnitude. Since the interaction distances involved with either the surface forces or dispersion forces are very small, approximating the fiber as a flat plate causes no major problems; that is, the effect caused by the curvature of the fiber would be negligible at these distances. In addition, the equations which describe these forces are greatly simplified by assuming this sphere-flat plate approach.

Van der Waals Unretarded Force

Application of the unretarded molecular forces to the model has been accomplished by utilizing Equation (3). These forces are attractive and are assumed additive between individual molecules of two colloidal particles. The interaction can be considered a body-centered force, meaning that the effect of the interaction lies on a line connecting the centers of the solid bodies. Therefore, such a radially directed force need only be added to the radial component of particle motion, Equation (30). Also, in order to make Equation (3) consistent with the trajectory equation, it had to be converted into a nondimensional form. This was accomplished by dividing the force expression by the mass of the particle and an acceleration term based on the appropriate nondimensional variables (see Appendix V). Once completed, Equation (30) assumed the following form:

$$\frac{d^2r}{dt^2} = K_1 \left(v_r - \frac{dr}{dt}\right) + r \left(\frac{d\theta}{dt}\right)^2 - \frac{2H}{3\,U^2\,m\,\delta^2(2a_p + \delta)^2} \frac{a_p^3}{} \qquad (32)$$

where H is the Hamaker constant and m is particle mass.

The Hamaker constant is an important factor in this equation. The value of the constant is known to be dependent on the nature and number of atoms in the interacting materials. Therefore, an accurate value of this constant had to be

found for use in the model which would correctly reflect materials used in obtaining experimental data for comparison with the model predictions. Visser (39) and Gregory (40) have reviewed the importance of this parameter and have presented methods for its calculation in relation to a wide variety of compounds. In this calculation, the suspending medium between the two solids also had to be considered. As will be discussed later, the experimental portion of this thesis employed titanium dioxide as the particulate matter, nylon as the fiber component, and water as the suspending medium. From the Hamaker constants for each of the pure substances, the value of the constant reflecting an interaction between them was calculated. The value obtained was 3.2×10^{-13} ergs. This value was consistent with other reported values corresponding to similar systems, all of which were within the range of 10^{-12} to 10^{-13} ergs.

Van der Waals Retardation Correction Factor

For separation distances between a particle and fiber greater than a few hundred Angstroms, the magnitude of Van der Waals dispersion forces will be reduced due to the physical restraint of a finite velocity for electromagnetic radiation. This reduction of force has been quantitatively summarized in the form of a retardation correction factor, α. This factor can be visualized as a continuously decreasing function of separation distance, meaning that when this distance is zero, $\alpha = 1$, and at an infinite separation, $\alpha = 0$. This factor is also a function of particle radius, a_p, and the wavelength of electron oscillation, λ_e, which is generally considered to be about 10^{-5} cm. Correction of Van der Waals forces should be accomplished in this manner if separation distance is greater than λ_e.

There is little literature available which presents the derivation for an expression of the correction factor existing between a sphere and cylinder. However, there has been some work done concerning this retarded interaction

occurring between a sphere and flat plate. Clayfield and Lumb (41) presented a mathematical derivation of an expression for α as it would exist in such a system. These authors started with the interaction between individual atoms and assumed these were not affected by neighboring atoms. A similar expression for α has been used in the present model. Theoretically, there are three separate conditions, based on the magnitude of separation distance, which provide for three different expressions of this factor (7,41). In the present work, only one has been used; this represents the condition where all atoms of the particle are at a distance greater than about 500 A from the fiber surface. Inside this region, the unretarded Van der Waals force would be adequate for describing the attraction between the particle and fiber. The expression obtained for α is quite long and cumbersome. Suffice it to say that this expression is dependent on particle size and separation distance; it is also in a form that is easily programmed for calculation on a computer. Figure 6 is given to show how the value of α is related to separation distance. As is evident, the inclusion of the correction term into the Van der Waals force expression is important because of its large influence on the magnitude of the force. This figure shows that a small increase in separation distance can cause a significant decrease in attraction. A derivation of the expression used for α in the trajectory equations is provided in Appendix V.

Double-Layer Force

A suitable expression for the double-layer interaction between a sphere and flat plate was presented as Equation (4). This term was given as a force; as with the Van der Waals force expression, it had to be converted into a nondimensional form through division by mass and acceleration before inclusion into the trajectory equations. This led to the following equation for a double-layer interaction:

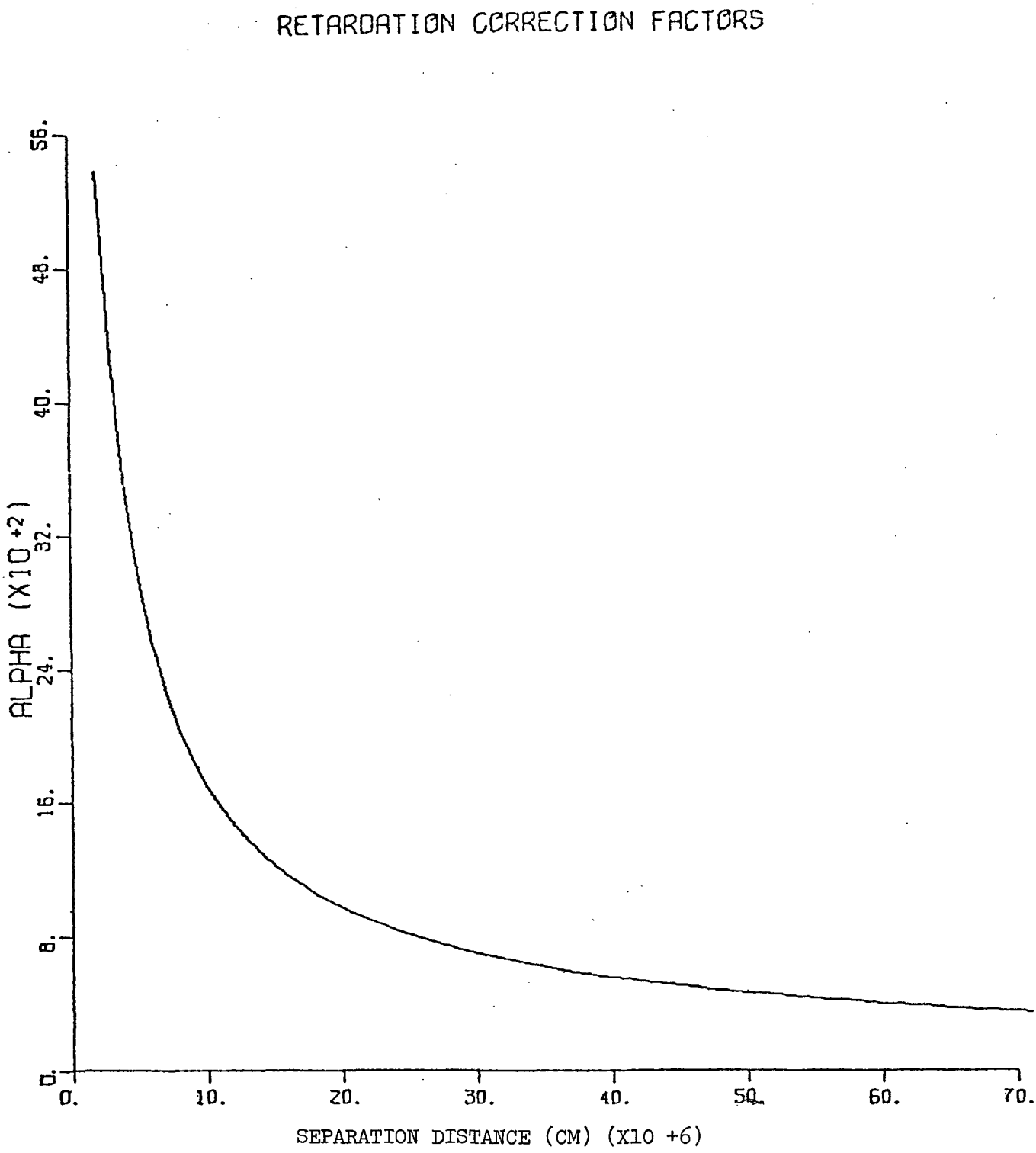

Figure 6. Plot Showing the Magnitude of the Retardation Correction Factor, α, as a Function of Separation

$$F_{DL} = \frac{\varepsilon_d \kappa\, a_p\, A^2}{(300)^2\, m\, U^2} \left\{ \zeta_1\, \zeta_2\, \frac{e^{-\kappa\delta A}}{1 + e^{-\kappa\delta A}} - \tfrac{1}{2} (\zeta_1 - \zeta_2)^2\, \frac{e^{-2\kappa\delta A}}{1 - e^{-2\kappa\delta A}} \right\} \qquad (33)$$

The factor 1/300 arises from the fact that the dimensions of Equation (4) are actually in volts. These units can be converted to statvolts by this factor. The statvolt is a measure of potential in the cgs absolute electrostatic system and can be converted into force units. Notice that Equation (33) would be applicable to either a repulsive or attractive double-layer interaction due to the fact that the potential would be positive or negative as determined by the signs of the zeta potentials, ζ_1 and ζ_2.

With an argument similar to that presented in connection with Van der Waals attraction, this double-layer interaction can be considered a body-centered force. Therefore, the expression need only be added to the radial component of particle motion. For this reason, the addition of Van der Waals and double-layer force terms to the trajectory equations means that Equations (30) and (31) would become the following:

$$\frac{d^2r}{dt^2} = K_1 \left(v_r - \frac{dr}{dt}\right) + r \left(\frac{d\theta}{dt}\right)^2 - F_{VdW} \cdot \alpha + F_{DL} \qquad (34)$$

$$\frac{d^2\theta}{dt^2} = K_1 \left(\frac{v_\theta}{r} - \frac{d\theta}{dt}\right) - \frac{2}{r} \frac{dr}{dt} \frac{d\theta}{dt} \qquad (35)$$

These equations represent the final form of the trajectory equations utilized in the model.

Diffusion

The effect of Brownian motion or diffusion on the trajectory of a particle traveling around a fiber was explored only for a limited number of system conditions. The main purpose behind this portion of the investigation was an attempt to show the power of the diffusion process in a system such as the one

being modeled. Some authors have stated that diffusion might be the controlling mechanism of particle collision (1,3), or if not controlling, quite important.

The distance and direction of particle motion due to diffusion can be considered as a random movement. This means that the random walk theory can be applied, and the displacement over a specified length of time, in a certain direction, can be calculated by Equation (2). With this model, the effect of diffusion was monitored by first taking a known position of the particle ($\underline{r}$,θ) and stating that within a certain time interval, the particle will move to a new position as dictated by the trajectory equations. This new position can then be modified as required by the diffusion equations, by moving a specified distance in a random direction. Through the calculation of the same trajectory a great many times, a statistical view of the diffusion effect was obtained. Further discussion pertaining to this effect will be presented in a later section.

SOLUTION OF THE TRAJECTORY EQUATIONS

The complete particle trajectory equations given above are quite complicated and are not easily integrated. In order to obtain a numerical solution for these equations, the digital computer was a necessity. It was realized very early in the investigation that a straightforward, easily mechanized and accurate method of numerical integration had to be selected in order to perform these calculations effectively. For these reasons, an algorithm of the Runge-Kutta method (42,43) was chosen and employed in a computer program written to solve the motion equations. The advantage of the Runge-Kutta method is that it is quite accurate, and will respond to small perturbations in the solution scheme that might otherwise go unnoticed. Also, this method is easy to program and is self-starting. The biggest disadvantage is probably the necessity for

using a small time step and the resulting large number of iterations required for each trajectory. This had the effect of increasing, significantly, the amount of computer time needed for the solution of a single trajectory. As it was necessary to calculate a large number of trajectories, this became a major handicap. However, it was felt that accuracy was more important than speed in this investigation, mainly because this has been the initial attempt at modeling the proposed system. It was assumed that once the model has been standardized and verified, faster methods of integration can be attempted to see if they would adversely affect the accuracy obtained with the present model. For example, it would be interesting to make an attempt to solve these equations using an analogue computer. A sufficiently large computer of this type could probably perform the integrations much quicker than the digital computer. However, there would be a substantial loss of accuracy with this machine.

The computer program written to integrate the particle trajectory equations utilizes two, parallel subroutines for similar treatment of each equation. A FORTRAN IV listing of the program used for the model is provided in Appendix VI. A block diagram of the mainline program is given in Fig. 7. As is evident, the diagram does not go into the fine details of the calculations for either the mainline program or the subroutines. It is sufficient to realize that the subroutines, called NEWR and NEWTH, represent the radial and angular component equations, respectively. Both of these subroutines employ the same numerical integration scheme, but NEWR is more complicated due to the fact that Equation (34) is more involved then Equation (35). A block diagram of NEWR is given in Fig. 8. This shows that the integration scheme based on the Runge-Kutta method involves the calculation of four correction factors based on four different values of position and velocity. These values are then used to update the particle's position and velocity after one complete iteration. Also evident

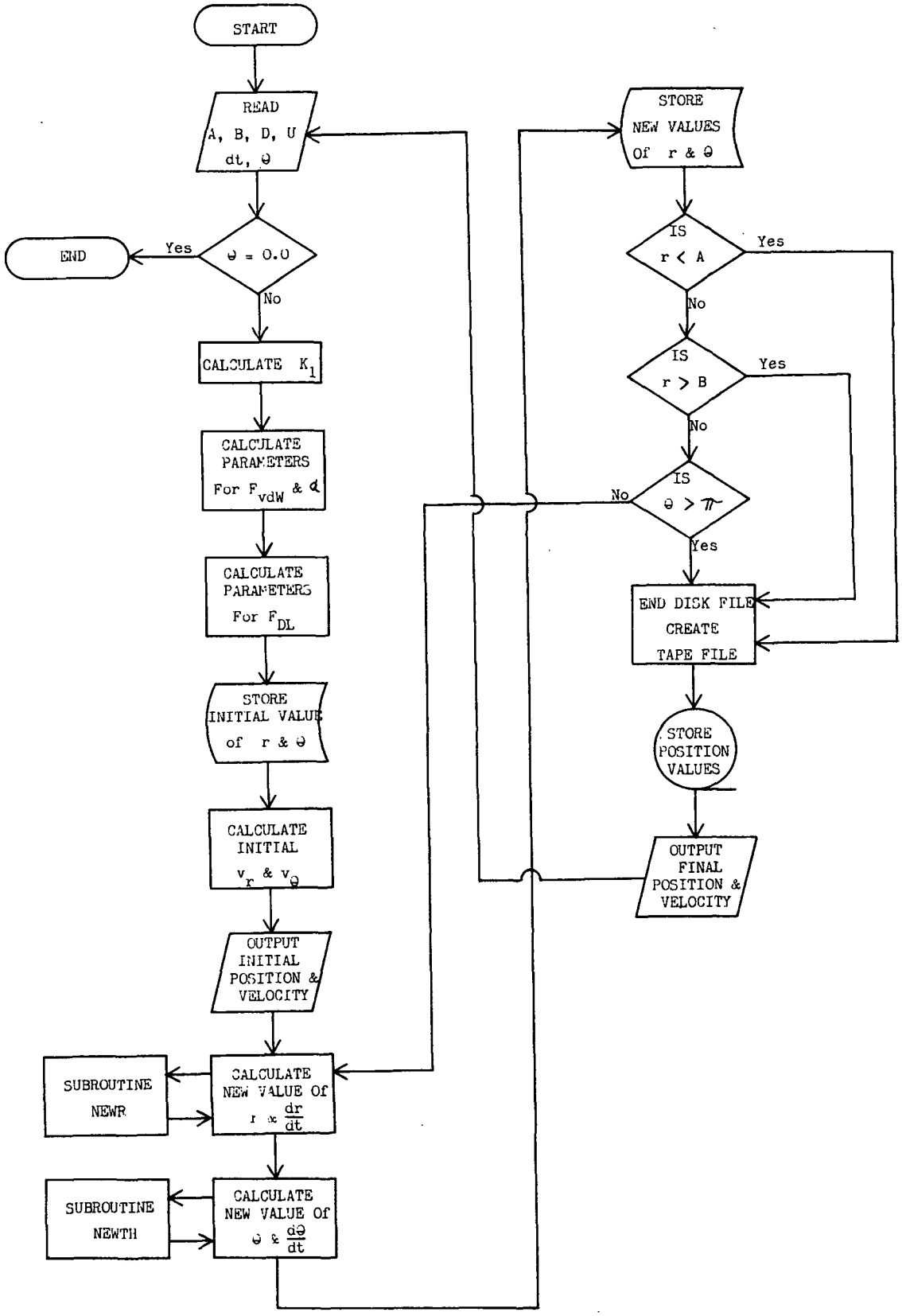

Figure 7. Block Diagram of the Mainline Program for Calculation of Particle Trajectories

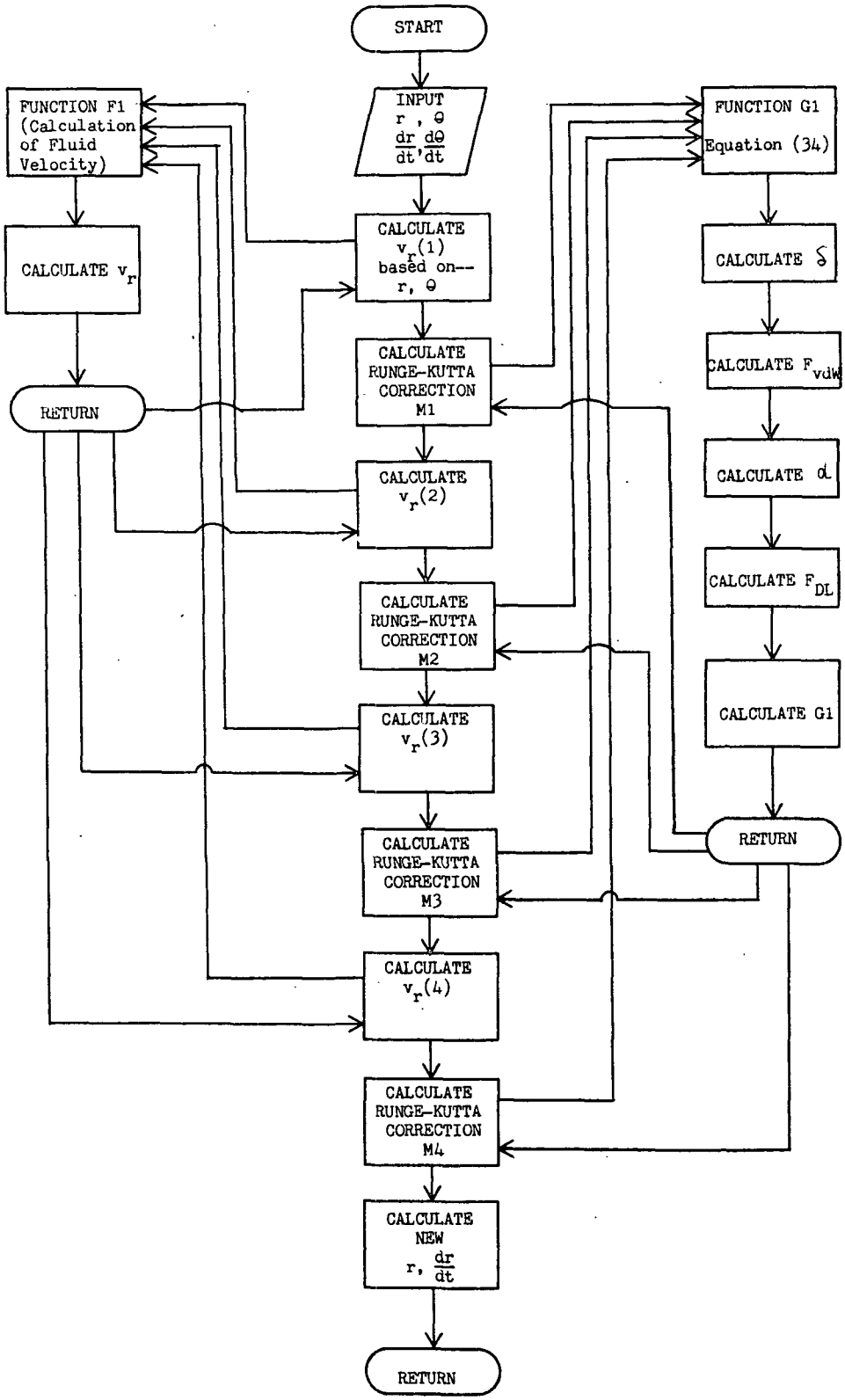

Figure 8. Block Diagram of Subroutine NEWR, Used for the Calculation of New Radial Position and Velocity Components

from this diagram is the fact that each force expression is calculated separately and then applied to the motion equation. In this subroutine, the trajectory equation has been labeled G1. The second subroutine, NEWTH, is identical in construction to NEWR. However, it is somewhat less complicated as most of the force terms do not influence the angular component of particle motion. Notice that these diagrams omit diffusion in their description of the programming scheme. The addition of this effect will be explained in detail later.

One of the most important variables in the programming scheme has been the time step used for each iteration of the equations. It was known that the step size would govern the accuracy of the integration method; however, it was also discovered that the equations were very sensitive to this variable, and the calculations necessitated that a sufficiently small step be used in order to stabilize the equations. For most of the trajectories obtained with this program, a time step, dt of 10^{-4} dimensionless time units was used. This value is equivalent to 10^{-7} seconds. It was found that this time step was not suitable for all particle sizes employed in the modeling sequence. Generally, the smaller the particle size, the smaller the time increment had to be in order to keep the program stable. Naturally, the smaller time increment increased required computer time. For example, if the increment was decreased to 10^{-5} units, the time required for the trajectory calculation would increase by a factor of 10. This is the reason that most of the predictions obtained have been for particle sizes greater than or equal to 0.5 μm. Smaller sizes required the smaller time step.

The results of the calculations performed by the computer program were, for each trajectory, a series of r- and θ-coordinates representing the position of the particle after each iteration step. These were obtained in the following manner. When calculating a trajectory, the initial particle position was

assumed to be on the fluid envelope. Thus the initial r-value was determined from the system porosity. The initial θ-value was selected by the operator, and was the means of categorizing trajectories for a particular set of system conditions. At the initial point, the velocity of the particle was assumed to be equal to the velocity of the fluid in which it was flowing. Once the initial position was selected, the velocities were calculated from Equations (23) and (24). These values were then fed into the integration scheme controlled by the Runge-Kutta method and new values of particle position and velocity were calculated. The new values would represent the status of the particle after one time increment. Subsequently, these newly calculated values would serve as the input data for the next integration step and another set of components would be generated. Continuing this procedure thousands of times served to create the series of position values which traced the trajectory of the particle's center.

The easiest method of distinguishing between, and the analysis of, these particle trajectories was found to be a pictoral representation based on a modified diagram of the unit cell (Fig. 5). The plots constructed for this purpose have been drawn by the computer. A FORTRAN IV listing of this program is provided in Appendix VII. Figure 9 depicts the particle trajectories calculated with the described programming sequence, where the trajectories were considered to be represented by Equations (30) and (31). This means that these trajectories show only the effect of inertia on the particle's motion. The initial positions of the trajectories were values of θ equal to 0.01, 0.1, 0.3, and 0.5 radians, respectively, measured from the vertical axis of the fiber (see Fig. 5). The porosity assumed for the system was 0.75, the particle diameter was set at 0.5 μm, fiber diameter at 20 μm approach velocity at 1.0 cm/sec, and the time step used was 10^{-4} time units. It is important to note that none of the particles was shown to collide with the fiber.

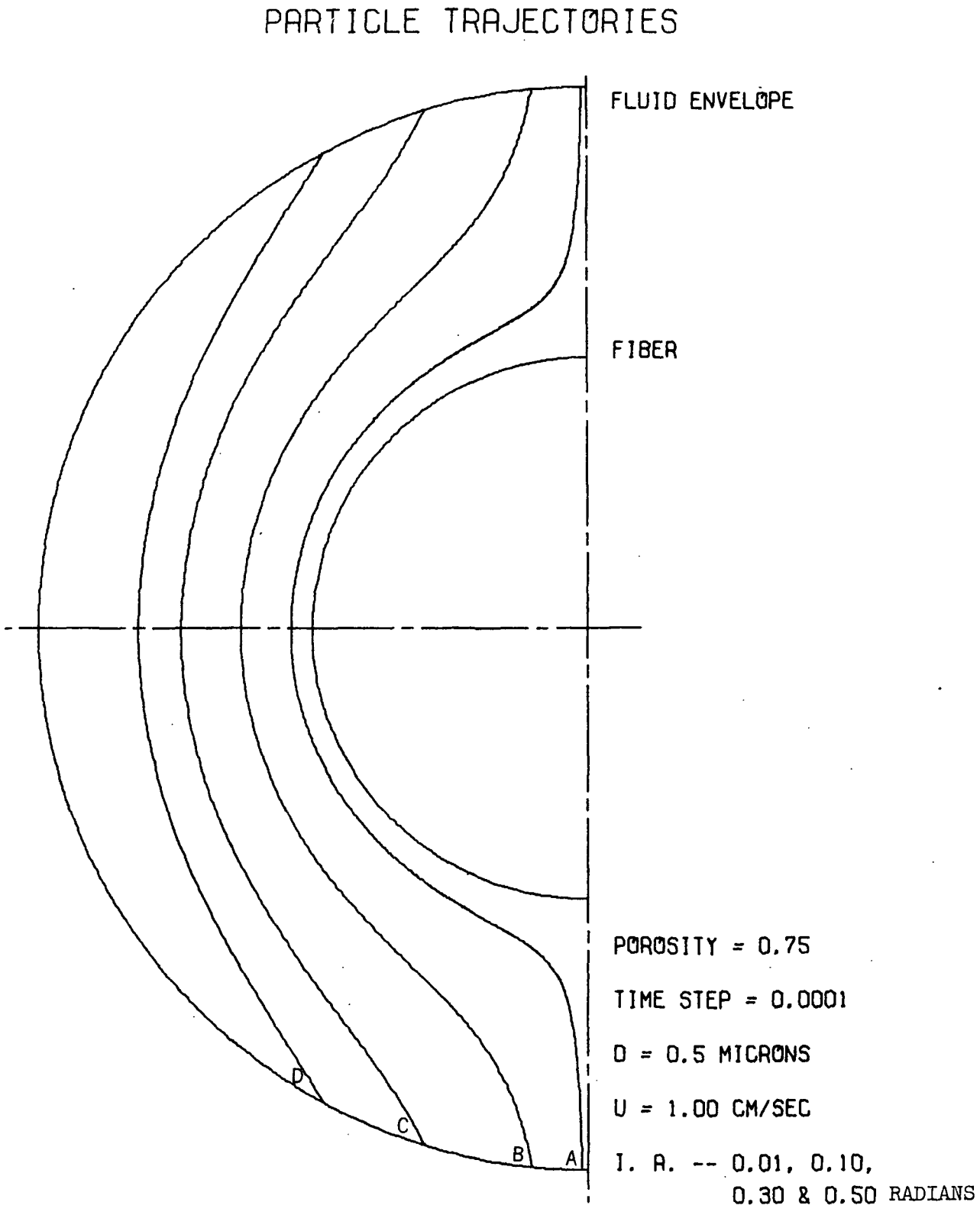

Figure 9. Plot of Several Particle Trajectories Showing the Influence of Inertia on Particle Motion

Figure 10 is given to provide some idea as to the overall effect of inertia on particle movement. This figure represents the fluid streamlines surrounding the fiber. These streamlines were obtained by integration of the fluid velocity components given by Equations (23) and (24). Applicable initial conditions and system parameters were identical to those given above. A comparison of Fig. 9 and 10 show no difference between the streamlines and particle trajectories. The conclusion is that inertia, under the conditions employed, exerts a negligible effect on the particle motion.

The preceding example was given to provide the reader with an understanding of how the theoretical results were obtained and organized. A complete discussion of these results, especially those calculated after the inclusion of other force expressions, is presented in the next section.

RESULTS AND DISCUSSION

DEFINITION OF COLLECTION EFFICIENCY

The mathematical model has been developed in a way which permits the calculation of a collection efficiency, defined as a means for predicting the amount of retention occurring within the simulated system. There are actually many different bases from which this efficiency can be determined, and one of these was arbitrarily chosen for this investigation. This particular form of collection efficiency is based on an area ratio, and it is explained in detail below.

Figure 11 has been provided as an aid in understanding the definition of collection efficiency as applied in this thesis; the figure is based on the unit cell described previously and is not to scale. The heavy line represents the limiting trajectory, which is a unique pathway dependent upon the system conditions assumed for the trial. The limiting trajectory is characterized

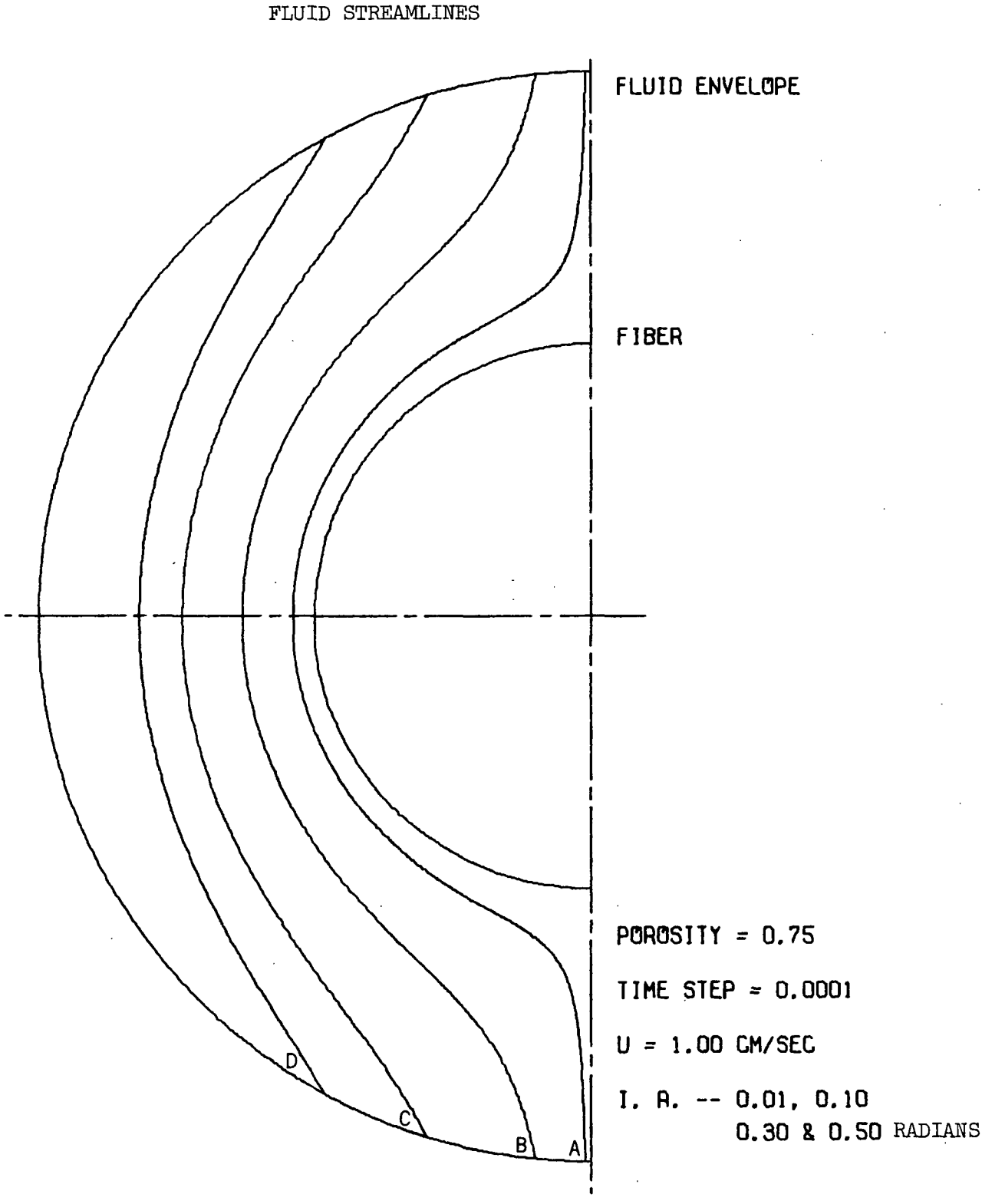

Figure 10. Plot of the Streamlines of Fluid Flow Surrounding a Fiber at a Porosity of 0.75

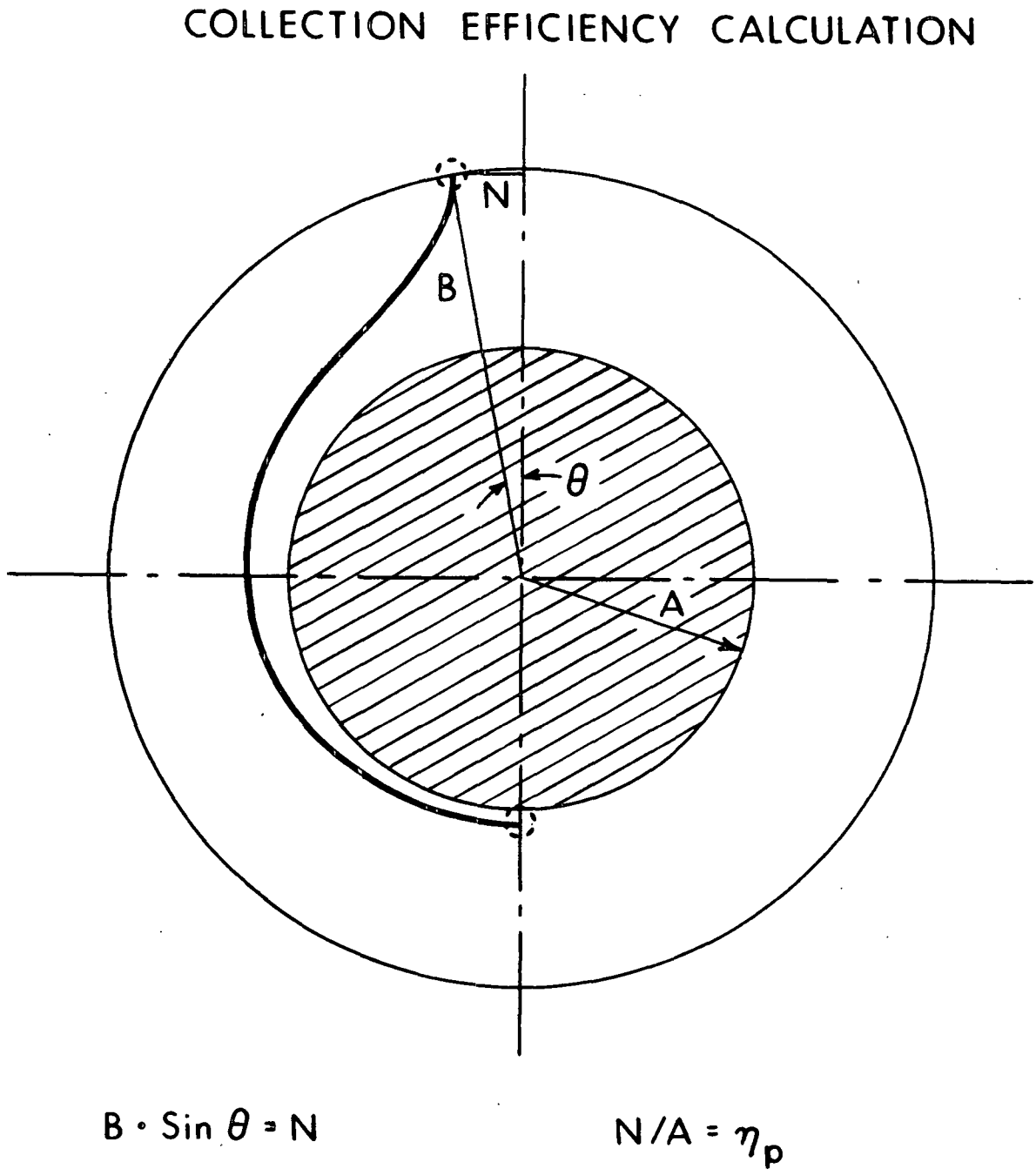

Figure 11. Pictorial Representation for the Calculation of Collection Efficiency. The Heavy Line Depicts the Limiting Trajectory for this System; the Efficiency, η_p, is Given by N/A

by the fact that the point of impaction on the fiber for a particle following this path is located at the downstream axis of the unit cell. Therefore, a particle entering the unit cell through the fluid envelope at an initial angle less than θ will impact on the fiber. Particles entering with an initial angle greater than θ will travel completely around the fiber without colliding. Thus the collection efficiency for this model has been defined as the ratio of the area of flow from which particles are removed to the projected area of the fiber.

To find the initial coordinates for the limiting trajectory, a trial and error procedure was used. This method required the selection of a point on the fluid envelope, calculating the particle trajectory based on this initial position and determining whether or not the trajectory leads to particle impaction. By repeating this procedure, the range of the limiting trajectory was narrowed. This method was unrealistic for obtaining the actual limiting trajectory because of the time required for this type of approach. However, it was possible to evaluate the initial point of this pathway to within a range of 0.0001 radians. As is shown later, this procedure provided an efficiency which was accurate to within a value of ±0.0002. The equations necessary for calculating the efficiency once the limiting trajectory was identified are given in Fig. 11. The predicted collection efficiency, η_p, has been evaluated by the ratio $\underline{N}/\underline{A}$. Further discussion concerning collection efficiency theory is provided in Appendix VIII.

When the definition of the collection efficiency was formulated, consideration was given to the planned experimental program. One goal of this investigation was a comparison of collection efficiencies calculated from theoretical and experimental data to be used as a method for determining the accuracy of the model. Therefore, calculation of efficiencies within the two programs had

to be similar in order to provide for a fair comparison. It will be shown in a later section that the collection efficiency just defined is comparable to one employed in the experimental program.

EFFECT ON INDIVIDUAL FORCE TERMS ON THE PARTICLE-FIBER INTERACTION

It was mentioned previously that the fluid and particle would be moving at different velocities due to the inertia of the particle. Figure 9 has shown that density differences between the particle and fluid are not sufficient to cause the particle to deviate from its streamline. Thus interception became the only mechanism available by which a particle would collide with a fiber. The collection efficiency calculated for such a system would be very small.

Effect of Van der Waals Unretarded Force

To obtain some degree of retention in a system similar to that presented in Fig. 9, other forces had to be incorporated into the model. The first force included was representative of unretarded Van der Waals forces. This was accomplished by utilizing Equation (32) as the particle motion equation, in place of Equation (30). Figure 12 is given to illustrate the effect of this force term on the trajectories. This attractive force can cause the particle to deviate from its streamline and collide with the surface of the fiber (Trajectory A). In this figure, the initial angle for each curve is 0.01 radians. Trajectory B is identical to Trajectory A in Fig. 9. The only difference between the two trajectories given in Fig. 12 is that Curve A made use of the influence of Van der Waals unretarded forces.

The collection efficiency for a particular set of system conditions was calculated by a trial and error method, aimed at converging on the limiting trajectory. An example of such a procedure is depicted in Fig. 13. Trajectories

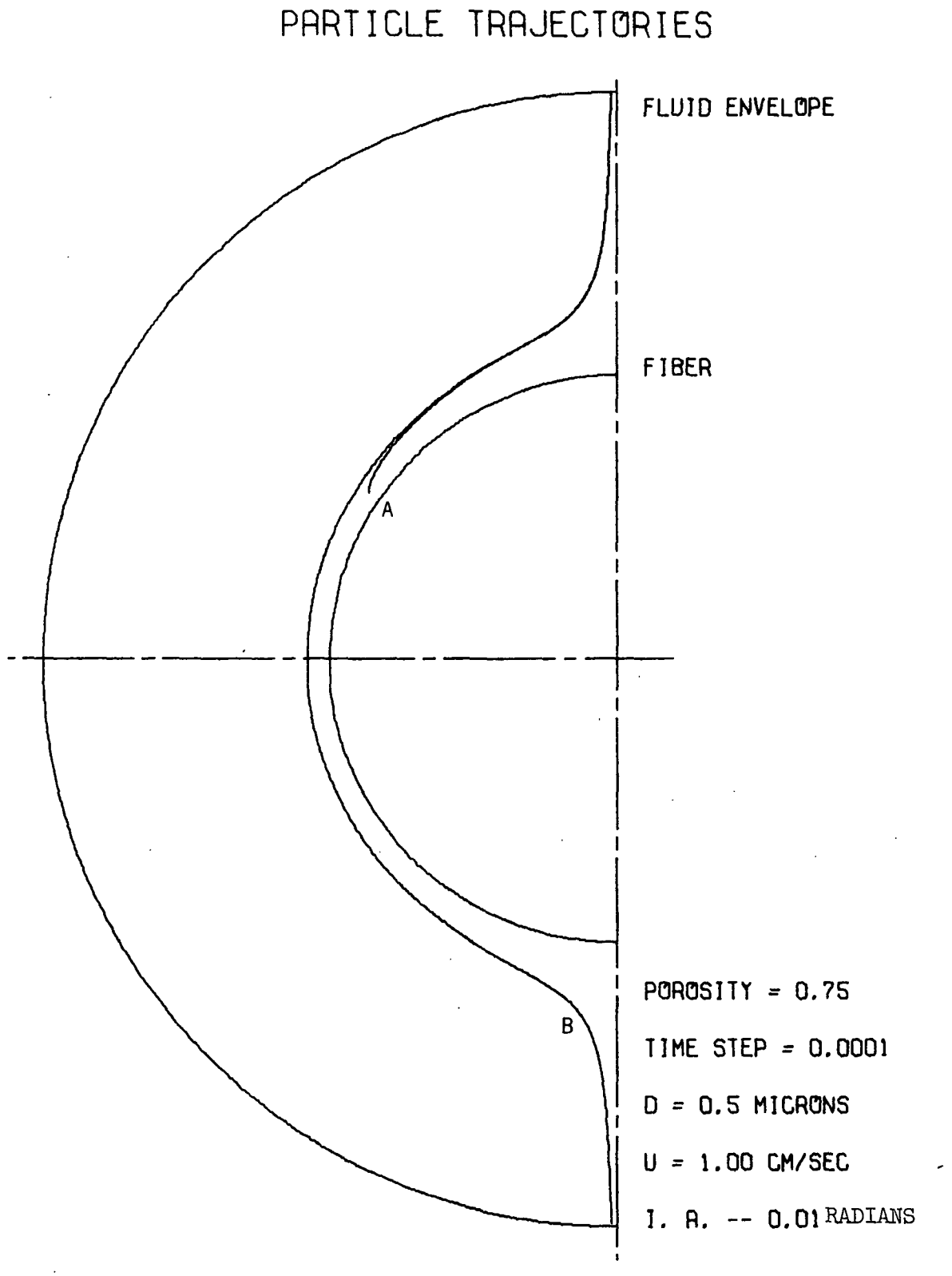

Figure 12. Plot of the Unit Cell Representing the Inclusion of Van der Waals Unretarded Force into the Motion Equations. Trajectory A Takes this Force into Account, While Trajectory B Shows the Effect of Drag and Inertia in Causing a Particle to Follow the Streamline

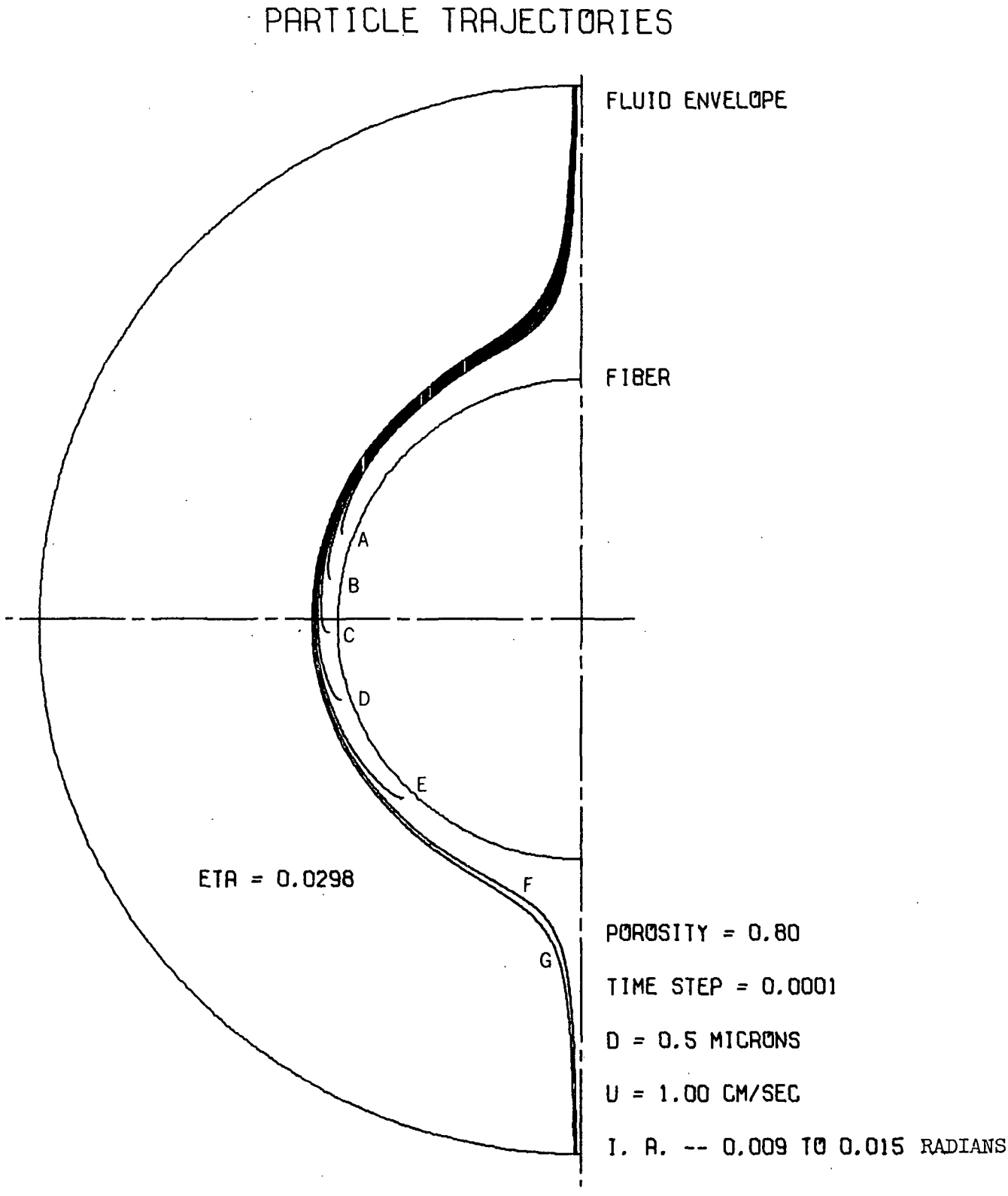

Figure 13. Plot Representing the Calculation of Cellection Efficiency, ETA. The Limiting Trajectory Lies Between Curves E and F, Meaning Its Initial Position is Denoted by an Angle Between 0.013 and 0.014 Radians

A through G originate at the fluid envelope with initial angles of θ = 0.009 to 0.015 radians. Trajectories A through E indicate particle impaction and capture by the fiber, while particles following Trajectories F and G were shown to miss the fiber and remain entrained in the fluid. To obtain the efficiency for this system, calculations for η_p were made (see Fig. 11) based on initial angles for Curves E and F. These two angles define points which bracket the initial position of the limiting trajectory in this system. The reported value of collection efficiency for this example was found by calculating η_p for each of the two trajectories mentioned and taking the average. This procedure resulted in a value of efficiency as given on the figure, ETA = 0.0298.

As mentioned in a previous section, the Hamaker constant, H, included in the Van der Waals force expression is thought to be an important factor in controlling the magnitude of the attractive force. Most investigators have reported the value of this constant as being in the range of 10^{-12} to 10^{-13} ergs when calculated for a particle-fiber system such as the one being modeled. However, there are values available which fall outside this range. A series of computer trials were made to investigate the effects of H on particle trajectories. Abnormally high and low values of H were used for these trials and were found in the literature as 3.5×10^{-11} ergs (44) and 3.0×10^{-14} ergs (45). Figure 14 shows particle trajectories calculated with these varying values of Hamaker constant; Trajectory A was found by using H = 3.5×10^{-11} ergs and Trajectory C with 3.0×10^{-14} ergs. Trajectory B utilized the value of H which had been calculated for, and based on, the solid and liquid components simulated by the model; this value of H was found to be 3.2×10^{-13} ergs. The results indicate that a change in the Hamaker constant can alter particle trajectories significantly. This also means that collection efficiencies would be highly dependent on H. Correct data for efficiency calculation, therefore, depends on a reliable value for the Hamaker constant. All other

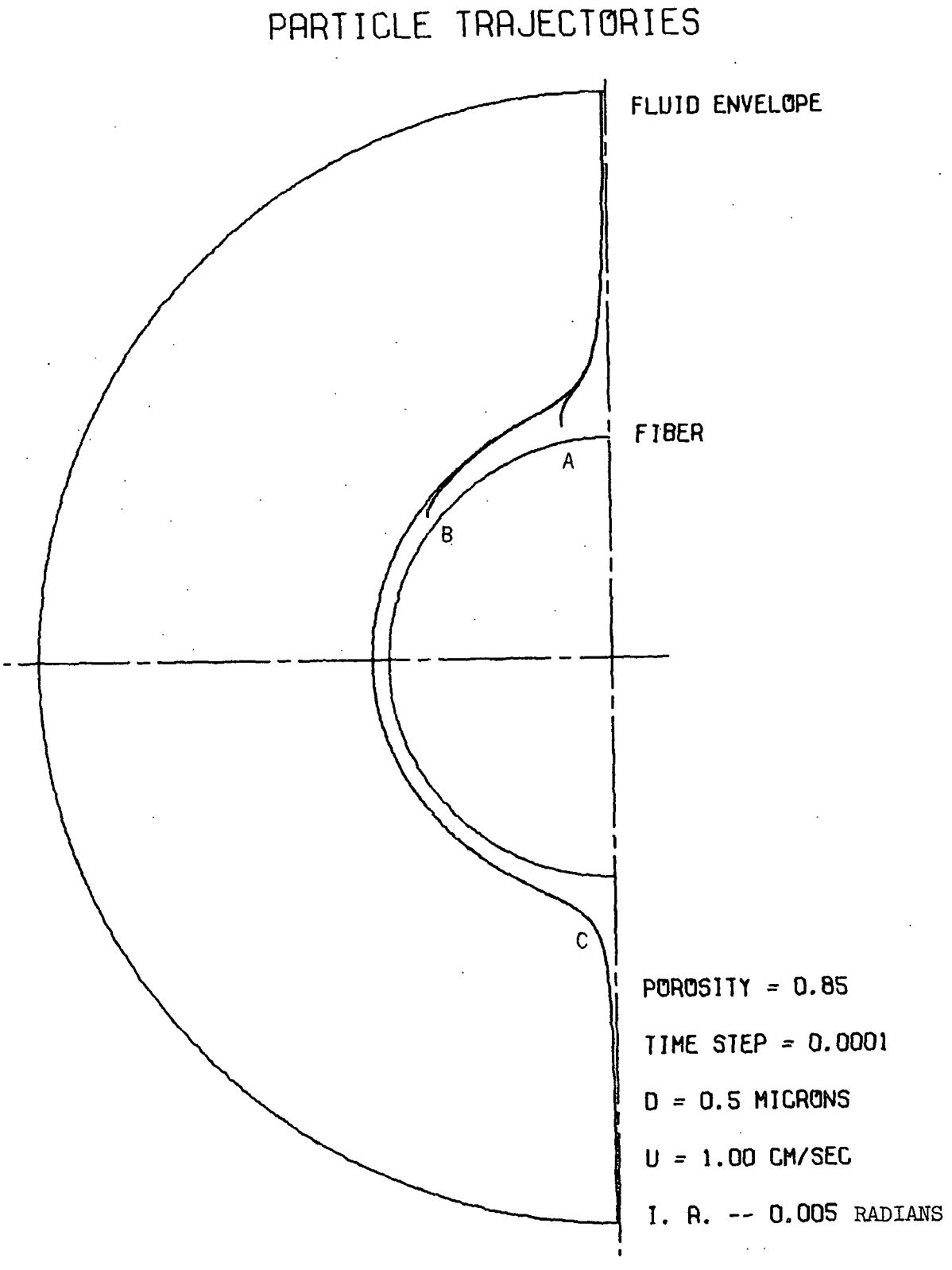

Figure 14. Plot Showing the Effect of Varying Hamaker Constant Values on Particle Trajectories. Curves A, B, and C are Calculated Using Values of H Equal to 3.5×10^{-11}, 3.2×10^{-13}, and 3.0×10^{-14} Ergs

particle trajectories calculated for the model employed the value of 3.2 x 10^{-13} ergs for this constant. Since this has been based on actual system materials, it was felt that it was probably the best available value.

Inclusion of Van der Waals Retarded Force

The retardation correction factor, α, as applied to Van der Waals force, was shown in Fig. 6 to exert a large effect on the magnitude of the molecular attraction existing between a particle and fiber. Table I offers a comparison between collection efficiencies predicted by the model, indicating differences between retarded and unretarded force effects. All of these values were based on a particle diameter of 0.5 μm and an approach velocity of 1.0 cm/sec. Application of the retardation factor to the force expression and, therefore, to the motion equations is shown to decrease the calculated efficiency values greatly. This effect is realized since the function of α is to decrease the attractive molecular dispersion forces. The decrease in efficiency is on the order of 60% for all of the examples given.

TABLE I

COMPARISON OF UNRETARDED AND RETARDED VAN DER WAALS FORCES AS THEY AFFECT COLLECTION EFFICIENCY

	Efficiency, η_p	
Porosity	Unretarded	Retarded
0.75	0.035	0.0149
0.80	0.0298	0.0122
0.85	0.0246	0.0100

Inclusion of the Double-Layer Force

Equation (33) was presented as an expression for estimating the magnitude of the double-layer interaction between a small sphere and a much larger fiber. This interaction, whether attractive or repulsive, is caused by surface charges

on the solid components, arising when these solids are immersed in water. These surface charges can be represented by zeta potentials, ζ_1 and ζ_2, of the particle and fiber, respectively. The computer trials for investigating this interaction utilized zeta potential values appropriate for a nylon fiber-titanium dioxide system. Titanium dioxide has been studied extensively, and is generally considered to assume a zeta potential of about -25 mv when dispersed in water (46). Nylon has not been as well characterized, but material was found (47) indicating a zeta potential of approximately -15 mv. Since both components have the same sign, the interaction between a nylon fiber and a TiO_2 particle would be repulsive in nature. Another variable in the double-layer expression which is dependent on suspension conditions is κ, the Debye-Huckel reciprocal length. This term is considered a measure of the double-layer thickness, that is, the larger the value of κ, the smaller the distance the double layer extends into the suspension from the solid-liquid interface. The value of κ is dependent on the ionic conditions of the dispersion, including the ionic concentration and the valence of these ions. For example, the addition of two moles of $CaCl_2$ to 100 liters of water would yield a value of κ on the order of 9×10^6 cm^{-1}. Decreasing the concentration or valence of the electrolyte in suspension would decrease the value of κ, thus increasing double-layer thickness and, consequently, the repulsive forces.

The application of this double-layer force to the motion equation resulted in Equation (34). Initial computer trials incorporating this modified motion equation assumed that the double layers surrounding the solid components were highly collapsed. The values for zeta potentials and κ mentioned above were used in these trials, and interesting results were obtained. Equation (34) states that particle motion is considered to be controlled by a series of attractive and repulsive forces, corresponding to negative and positive components

of acceleration, respectively. Both force expressions, Van der Waals and double layer, have been shown to be functions of the distance separating a fiber and particle; therefore, it is possible that there would be a specific value of this distance where attractive and repulsive forces would be equal. At this point, the particle would be unable to move toward or away from the fiber, unless affected by another type of force or some form of mechanical action. The model has predicted that this balance occurs and the results show how a particle travelling around a fiber would become locked in a pathway characterized by a constant separation distance.

Therefore, in an ideal case, most particles will become entrained in a trajectory at a fixed distance from the fiber's surface and will not impact on the fiber. This would mean a substantial decrease in retention. In a real system, this balance probably would not occur because of the many perturbations existing in such a system which would influence both particle motion and force strength. There is another consideration that must be accounted for when the particle is very close to the fiber. It was stated in a previous section that the expression utilized for a double-layer interaction was invalid, or would break down as the value for separation distance approached zero. This fact should cause no major problems in the theory governing the model since, at a small separation distance, the Van der Waals forces would become dominant and cause particle capture.

To present an example of the separation distances at which a force balance might occur, some of the model predictions are given here. By using the values mentioned above for zeta potentials and κ, a significant number of particle trajectories were calculated utilizing Equations (34) and (35). For a basis of comparison with other results, the same conditions and initial positions were used in trajectory calculations for systems influenced by Van der Waals forces only. It was predicted that some of the particles following these new

trajectories would become locked in a path at a separation distance of 0.003. This is a dimensionless value and would translate into 3×10^{-6} cm, or roughly one-tenth of the particle's diameter. This value can be considered well within the range where variation in particle shape, fiber roughness, or flow patterns would lead to collision with the fiber. This assumption led to the observation that collection efficiencies would not change due to the inclusion of the double-layer force into the flow model, under the conditions specified. Trajectories calculated with and without this force were essentially the same. The conclusion was that if the double layer is present in a collapsed state, it exerts little effect on predicted retention values.

The model was also used to predict collection efficiencies when the value of κ was based on a monovalent electrolyte. The results indicated that the same type of force balance occurred, but at a larger value of separation distance, equal to 0.006. Again, this is a very small distance, and it could be assumed that most particles would collide with the fiber when this separation was attained. However, it is possible that, because of the greater separation, some of the particles might be effectively hindered from impaction. This would be reflected as a decrease in efficiency. The decrease would be consistent with theory since the lower valency of the electrolyte would permit an increased double-layer thickness and, therefore, an increased repulsive effect. From these observations, it was felt that calculation of a particle trajectory including a double-layer term based on no additions of electrolytes or pH controlling chemicals, would indicate negligible retention. In such a system, the only electrolyte present would be a minute amount of dispersing agent transferred into the suspension with the TiO_2 stock solution. Trajectories were calculated for these conditions and the separation distance at the force balance was approximately 0.13 to 0.41, depending on the valence value assumed for the

electrolyte. This distance would be great enough to prevent most particles from colliding with the fiber. Therefore, retention under these conditions would be virtually nonexistent.

Application of Diffusion

Much has been discussed in previous sections of this thesis concerning the importance of diffusion in the retention process. This mechanism was the final addition incorporated into the model. Diffusion, or Brownian motion, has been considered a random process, therefore, any meaningful results obtained from its application to the model would be statistical in nature. That is, its effect on a single particle trajectory would have to be calculated many times in order to formulate an accurate description of its contribution to retention. Diffusion has been considered as a transport mechanism rather than a force; therefore, an expression for its effect on particle motion was not included in the trajectory equations. Rather, individual coordinates representing the position of a particle on its trajectory were modified according to the diffusion effect after they were calculated. These modified values were then used in the motion equation to calculate the particle's next position.

Relevent expressions available for the calculation of diffusional motion were presented as Equations (1) and (2). In the model, the time step utilized for the solution of the trajectory equations has been employed as the time variable necessary for calculating the displacement caused by diffusion, $\bar{x}$. This procedure yields a value of $\bar{x}$ which is on the order of 10^{-8} cm, meaning that displacement within a single time step represents approximately one-thousandth of a particle diameter. At first, this seems to be a negligible value, but considering the large number of iterations needed to calculate a single trajectory, the effect of diffusion applied in this manner could be significant.

Figure 15 is provided to show how the diffusion mechanism has been incorporated into the model. The appropriate computer subroutines utilized are listed in Appendix IX. A single integration step in the solution of the motion equations would indicate particle movement from Point A to Point B along the particle's trajectory. The coordinates of the particle would change from $(\underline{r},\theta)$ to $(\underline{r}',\theta')$. If diffusion is truly a random process, then the displacement caused by it can occur with equal probability in any direction. If the displacement is applied to the newly calculated particle position (Point B), the particle can be moved to any point on a circle, with radius $\overline{\underline{x}}$, surrounding this position. For simplicity, the computer program was modified to consider only four directions in which the particle could be displaced; these are shown in the figure as being perpendicular to one another, and parallel to the x- and y-axes. The direction of the displacement was randomly chosen by the computer through a random number generator; the magnitude of this random number designated the direction of movement for each iteration of the trajectory equations. Thus, the particle's position after diffusion is considered to be denoted by any of the four points shown. These would be the coordinates used for the next iteration step and the entire procedure would be repeated. Because this is a random process, it was felt that any conclusion based on the influence of diffusion would have to be related to a significant number of trajectories, each calculated from the same initial point. This would provide a statistical view of the diffusion effect. Calculations were performed on trajectories which were known to be very nearly equal to the limiting trajectories for their individual systems. It was felt that this would indicate whether or not diffusion could drastically alter values of collection efficiency.

The limited results obtained reflecting the effect of diffusion in retention systems indicate that collection efficiency is decreased slightly when

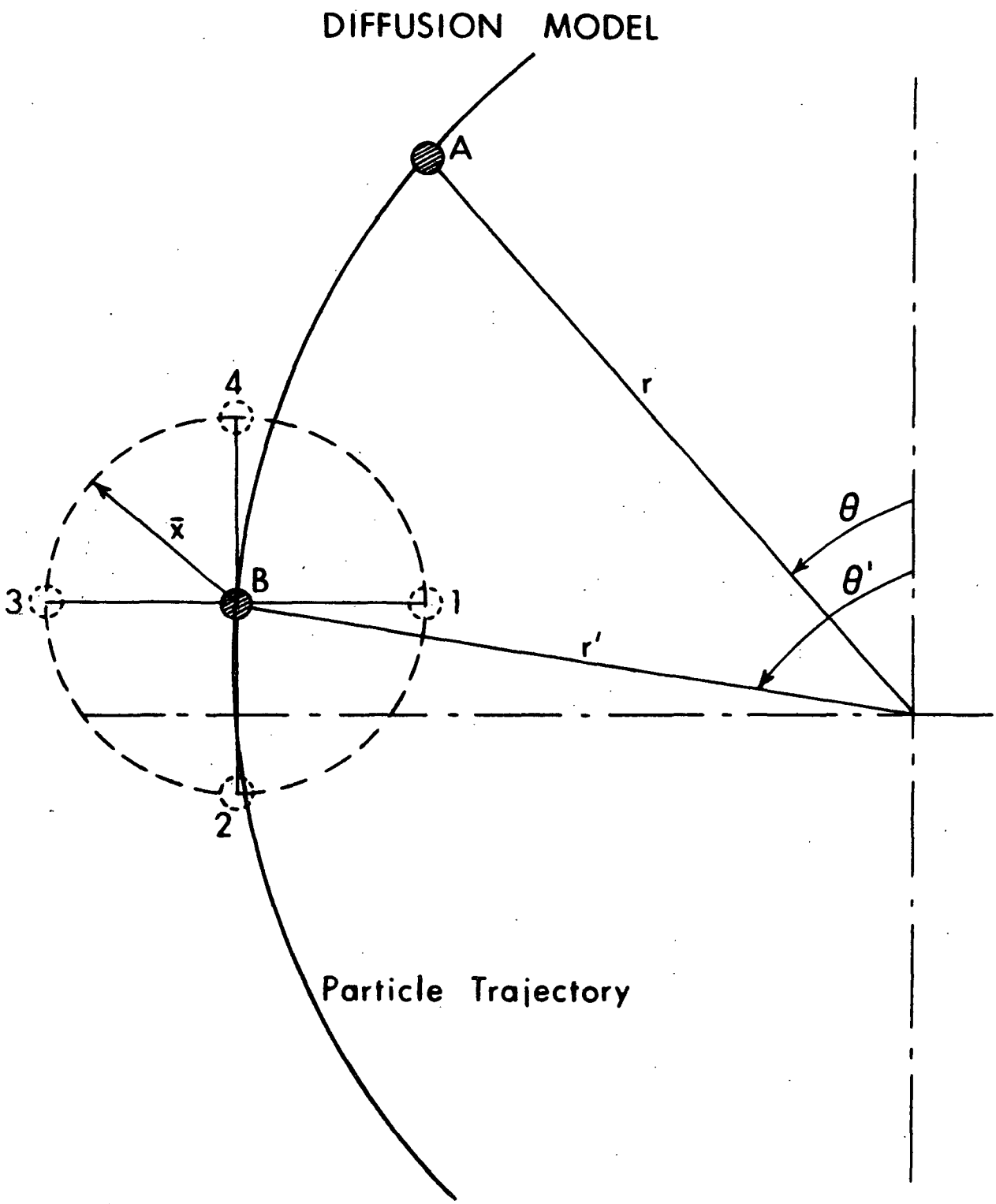

Figure 15. Pictorial Representation of the Method Used for Applying the Concept of Diffusion to the Model. Diffusion Will Cause a Particle to be Displaced from Point B to Some Position of the Circle Characterized by a Radius of $\bar{x}$

diffusion is considered. The magnitude of this decrease in efficiency is less than 0.0002, or approximately a 1 to 2% change. The reason for the decrease can be seen in Fig. 15. If a particle trajectory curves around a fiber in the direction indicated, it is evident that a greater area of the dashed circle, with radius $\bar{x}$, will lie "outside" the trajectory, or at a greater distance from the fiber. Since it is theorized that all points on this circle have an equal probability of representing the particle's position, there would appear to be a slight tendency for the particle to drift away from the fiber, thus leading to a decrease in efficiency. Considering only the four possible positions used in the model, the probability is greater, for this particular location on the trajectory, that the particle will move away from the fiber. If the theory governing diffusion is correct as applied to the model, the effect of this random motion in a real system would also reflect a reduction in collection efficiency, to the extent that the consideration of a single cell is adequate.

The remainder of results presented in this section will not include the diffusion parameter. Time did not permit the calculation of the great number of trajectories necessary for this. However, the effect of diffusion on particle motion has been shown to be small in comparison to the overall influence of interparticle forces; therefore, its omission should cause no problems in the analysis of other results.

By way of summarizing individual force effects on particle motion and retention, it has been shown that obtaining a significant collection efficiency is dependent on the inclusion of Van der Waals forces in the computing scheme. This attractive force must be present to simulate deviation of a particle from its streamline and subsequent impaction on the fiber.

EFFECT OF SYSTEM VARIABLES ON COLLECTION EFFICIENCY

Table II provides a brief summary of some collection efficiencies calculated with the model. All of the values were obtained by solving Equations (34) and (35), assuming the double layers surrounding the solid components were collapsed.

TABLE II

PREDICED COLLECTION EFFICIENCIES

Porosity	Velocity (cm/sec)	Particle Size d = 1.0 μm	d = 0.5 μm	d = 0.3 μm
0.75	0.78	0.0286	0.0159	
	1.00	0.0270	0.0149	0.0103
	1.17	0.0262	0.0143	
	1.50	0.0252	0.013	
0.80	0.78	0.0231	0.0131	
	1.00	0.0220	0.0122	
	1.17	0.0215	0.0118	
	1.50	0.0202	0.010	
0.85	0.78	0.0187	0.012	
	1.00	0.0177	0.0100	0.0068
	1.17	0.0172	0.0095	
	1.50	0.0162	0.0089	0.0064

Within the range of conditions appearing in Table II, the collection efficiency is accurately represented by the regression model:

$$\eta_r = b_0 + b_1\varepsilon + b_2U + b_3d + b_4\varepsilon U + b_5\varepsilon d + b_6Ud + b_7\varepsilon^2 + b_8U^2 + b_9d^2 \quad (36)$$

where

i	b_i	σ_i
1	-0.309691	0.0900924
2	-0.0102113 sec/cm	0.00253081
3	0.0957688 cm^{-1}	0.00437517

i	b_i	σ_i
4	0.0	
5	$-0.0952418\ cm^{-1}$	0.00543676
6	0.0	
7	0.195115	0.0561644
8	$0.00276022\ (sec/cm)^2$	0.00108855
9	0.0	
0	0.132688	

The coefficients (b_i) indicate what change will occur in the collection efficiency when a system variable is modified. The formula reproduces the completed values, as indicated by $R^2 = 0.99$.

It is interesting to note that the presence of a nonzero coefficient, b_5, indicates a joint dependence of collection efficiency on porosity and particle size. This lack of independence is shown in Table III, where efficiencies were calculated by Equation (36) utilizing the average of velocities given in Table II. The model may be used to fill in the missing calculations in Table II for the particle size of 0.3 μm.

TABLE III

COLLECTION EFFICIENCIES CALCULATED FROM THE REGRESSION EQUATION

(U = 1.1125 cm/sec)

Particle Size	Porosity		
	0.75	0.80	0.85
1.0 μm	0.0265	0.0214	0.0173
0.5 μm	0.0144	0.0117	0.0099

Effect of Porosity

The values of efficiency presented in Table II indicate that retention decreases as porosity increases. The porosity as defined and calculated in the model is assumed equal to the relative areas of fluid to solid within the unit cell, or the area available to suspension flow. The efficiency values reflect the fact that for a 6% decrease in porosity, the collection efficiency decreases approximately 20%. This is uniform over the entire range of porosities investigated.

This effect can be explained by noting that at a decreased porosity, the flow area is reduced, therefore, more particles will follow trajectories that travel closer to the fiber surface. A larger number of particles will be influenced sooner and to a greater degree by Van der Waals attractive forces, meaning that they will have an increased opportunity to be attracted to the fiber and retained by it. The resultant effect would be an increase in collection efficiency.

Effect of Approach Velocity

As stated previously, the model assumes a particle enters the unit cell with a velocity equal to that of the bulk suspension. Within the cell, the particle is affected by hydrodynamic, molecular, and colloidal forces which cause a change in its velocity. Again, all of the velocities investigated were characterized by Reynolds numbers below one. The model has predicted that as approach velocity increased, the collection efficiency decreased. This decrease is consistent for all velocity and porosity values used.

Figure 16 is provided to show how a change in velocity will affect particle trajectories and collection efficiency. Curves A, B, C, and D represent trajectories calculated with velocities of 0.78, 1.00, 1.17, and 1.50 cm/sec,

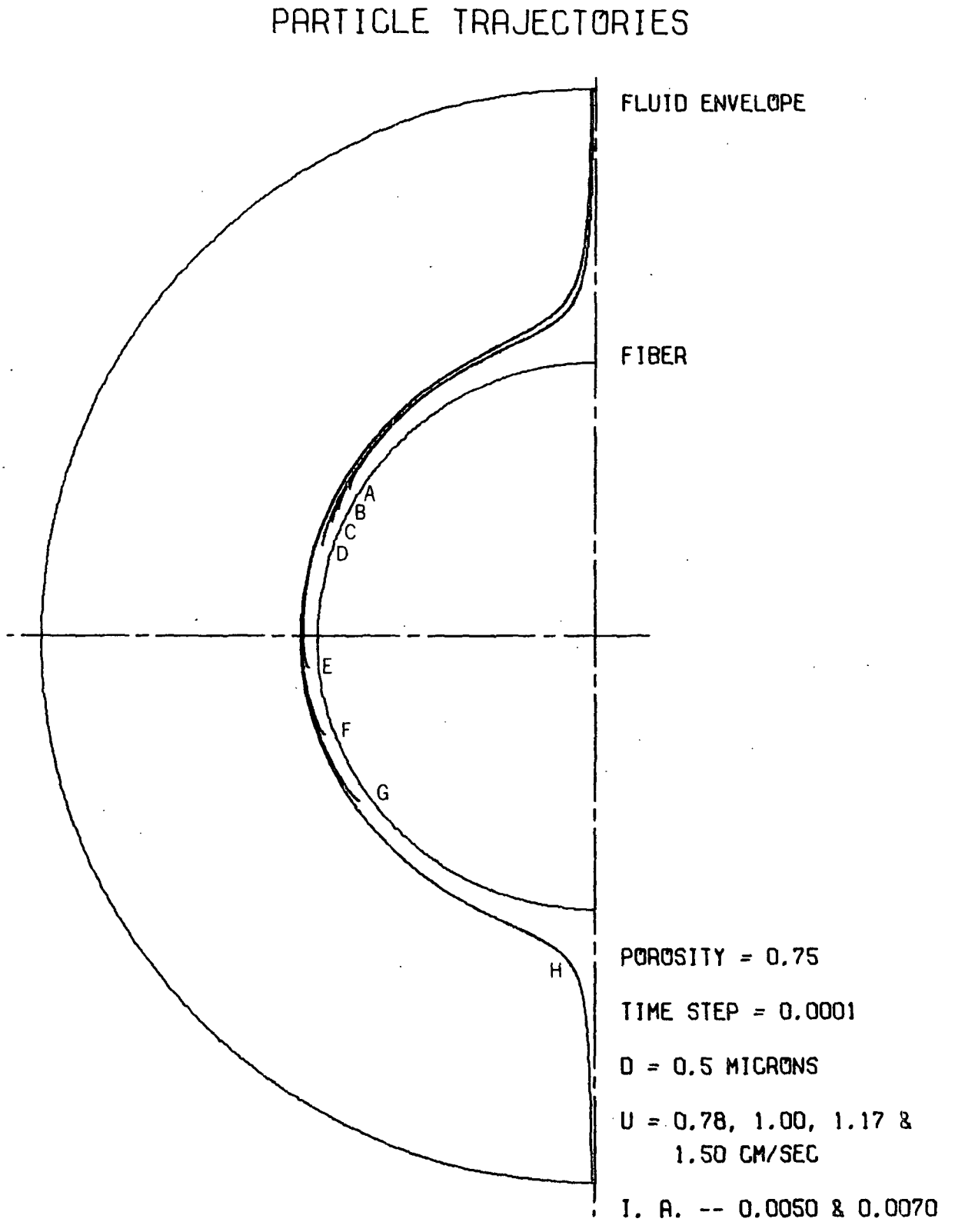

Figure 16. Plot Showing the Effect of Varying Approach Velocity on Particle Trajectories. Results Indicate the Lower the Velocity, the Greater the Amount of Retention

respectively, all initial positions at the fluid envelope were $\theta = 0.0050$ radians. Curves E, F, G, and H represent the same velocities for trajectories starting at $\theta = 0.0070$ radians. As shown, a change in velocity can significantly alter a particle trajectory. The reason for this is related to the time available for the particle to be influenced by the various forces present in the system. The faster the particle moves through the unit cell, the shorter its exposure to the attractive forces. This would lead to a reduction in the number of particles retained and a decrease in efficiency.

Effect of Particle Size

One of the more important aspects of particle retention as applied to any real system would be the effect of particle size on the amount of solids retained. A final observation available from Table II is that an increase in particle size can be related to an increase in collection efficiency. Most efficiency values calculated with the model have been based on a particle size of 0.5 μm or larger. However, some calculations were made representing smaller particles, which were assumed to be 0.3 μm in diameter. This value was chosen because the particle size of titanium dioxide as used in most filling operations in a paper mill is approximately of this magnitude. Calculations for this small particle were limited since a smaller time step was necessary to stabilize the integration procedure under these conditions. The reduced time step meant that the computer program would run an order of magnitude slower in calculating a single trajectory. This was a very inefficient use of available computer time, and necessitated a reduction in the range of system conditions investigated.

Figure 17 represents the change occurring in a trajectory if the particle size is altered. Curves A, B, and C reflect particle diameters of 1.0, 0.5, and 0.3 μm, all with an initial angle of $\theta = 0.0050$ radians. This shows quite

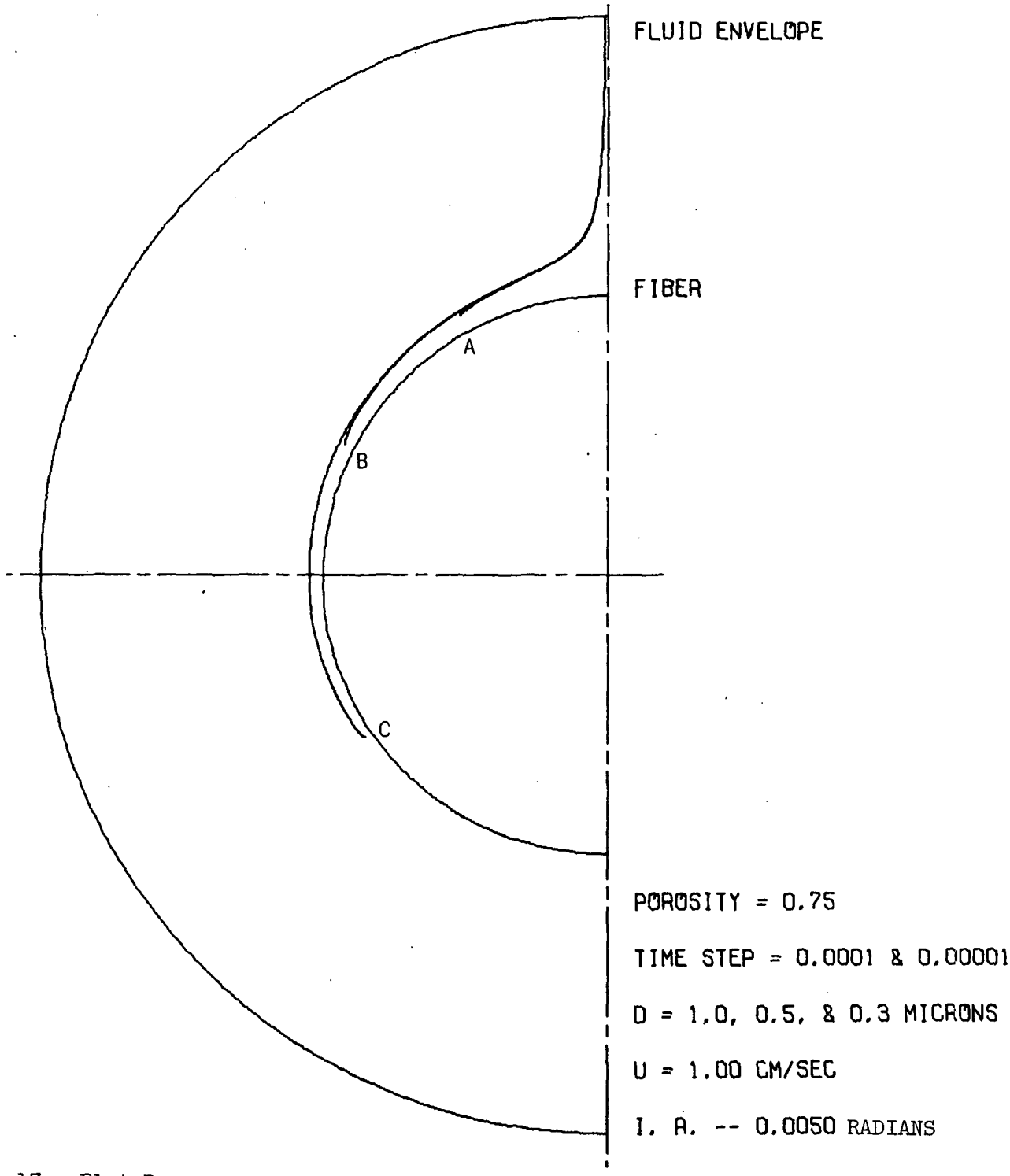

Figure 17. Plot Representing the Effect of Particle Size on the Trajectories. Curve A was Calculated for $\underline{d}$ = 1.0 μm, Curve B for 0.5 μm, and Curve C for 0.3 μm

clearly how efficiency decreases with decreasing particle size. An explanation for this change can be based on the effect of Van der Waals attractive forces. Equation (32) indicates that the magnitude of the attraction is directly proportional to the cube of particle radius, meaning an increase in size would cause a large increase in attraction. The attractive force has been described as occurring between individual molecules of the interacting solids. Therefore, the larger the solid body, the more molecules are involved in the interaction, and the greater the force. Increasing the force would lead to an increased number of particles impacting on the fiber surface, and a resulting increase in efficiency.

The trajectories and collection efficiencies reported in this section represent only a small percentage of the total number calculated with the model. An inclusive list of all trajectories is given in Appendix X. The system conditions are provided for each one, and an indication was made concerning whether or not the particle was retained. All of the trajectories listed in this table are available on computer tape for future reference.

EXPERIMENTAL PROGRAM

BACKGROUND

The previous sections of this thesis have dealt with the theoretical phase of the investigation into retention processes. The mathematical model was constructed for the prediction of retention efficiencies existing within a simplified system composed of small, spherical particles and fibers of circular cross section. After the model had been developed and was working in what appeared to be a logical manner, a question remained regarding its applicability and accuracy. That is, were the calculated retention efficiencies adequate for describing such values obtained from a real retention system. This led to the development of an experimental program, designed to provide collection efficiencies to be used for a comparison with the predicted values. The goal was to show that the model was performing well enough to provide a good first approximation for efficiency within such a system. An exact agreement between experimental and theoretical values was not expected; however, it was felt that a good model would yield relevant values, and a comparison well within an order of magnitude should be realized.

The experimental phase of this thesis was designed as a straightforward, permeation procedure for measuring the retention obtained after a dilute suspension of particles had been passed through a preformed pad of synthetic fibers. Subsequent to the permeation operation, the pad was sectioned into layers and each layer was analyzed for the amount of accumulated particulate matter. This data provided a profile for the distribution of retained particles through pad thickness, and permitted the calculation of a collection efficiency for comparison to a predicted value obtained from the model.

There were several assumptions made during the theoretical program which directly relate to the physical appearance of the solid components being modeled. Specifically, the particles were considered small in size and spherical in shape; the fibers were assumed to possess a circular cross section and a very large length to diameter ratio. Therefore, the particulate and fibrous materials used in the experimental program had to match these conditions as closely as possible. Thus, titanium dioxide was employed as the particulate component, while a synthetic fiber, nylon, was used in the construction of the pad. An additional reason for using nylon in this work was that this type of fiber was known to have a very smooth surface as compared to other forms of synthetic fibers. The effect of surface roughness on the fluid flow pattern around the fiber was not considered in the model; therefore, the fiber used during experimentation had to be smooth in order to provide for a good comparison. A more detailed description of materials utilized in the experimental phase of this thesis will be provided in a later section.

PREVIOUS STUDIES CONCERNING FILTRATION AND RETENTION

As mentioned previously, there have been a significant number of experimental investigations conducted in the areas of aerosol and water filtration. Many of these were designed to produce comparison data in conjunction with theoretical models. A great deal of the theory behind the procedures for such experimental programs, as outlined in these studies, has proved beneficial in the design of a program for this thesis.

The present investigation has a strong relationship with the paper industry, in particular, concerning the process of filler retention with a bed of fibers. Since the materials to be used here were titanium dioxide and nylon fiber, the literature was reviewed for any pertinent filtration studies performed utilizing

these materials. It was found that there has been a fair amount of work in this area of filtration, all concerned with the retention of titanium dioxide within a fiber pad. This pigment has been studied extensively because the individual particles are small, nearly spherical in shape, and are chemically stable when dispersed in water. All of the investigations outlined below have dealt with retention studies utilizing this pigment in conjunction with either wood pulp or synthetic fibers.

Johnson (1) performed an experimental investigation concerned with the removal of titanium dioxide particles from a dilute suspension flowing through a bed of nylon fibers. Of importance in this work were discussions relating the effects of fluid velocity, fiber diameter, and pad porosity on the amount of particles retained within the pad. An analysis of the flow system involved in this study and considerations of assumptions made to simplify it led the author to the conclusion that there were four transport mechanisms which could influence the relative movement of a particle and fiber and lead to a collision. These were inertial impaction, flow line interception, Brownian motion, and settling. The experimental procedure consisted of passing a dilute suspension of the particles through a preformed bed of nylon fibers at a constant rate and analyzing for the amount of titanium dioxide retained by the pad. The porosity of the pad was held constant during the procedure by compressing it with a permeable piston. Also, the concentration of the particle suspension was held constant through agitation. A final assumption in this work was that once a particle collided with and became retained by a fiber, it was not removed by any applied force or shear stress.

The means for reporting results within this investigation was in the familiar form of a collection efficiency. The fiber pad was considered as a network of cylindrical collectors, all possessing an identical effective fiber

collection efficiency. This efficiency value was derived from a material balance around a single fiber layer, which was then integrated over the entire pad thickness. For a compressed pad of constant porosity, this theory states that efficiency would be constant through pad thickness.

The main conclusion formed as a result of this study was that, of the four transport mechanisms mentioned above, only Brownian motion appeared significant in causing a particle to move across streamlines toward collision with the fiber. It was also shown that the degree of retention within the pad was highly dependent on the ionic conditions of the suspension. For example, it was found that with pH above 7.0 and with a low concentration of ions in the suspension, essentially no retention occurred. However, there was no attempt in this study to quantify these effects as part of a double-layer interaction. Also, the only reference made concerning the effect of molecular forces was that these were probably the main forces holding a particle to the fiber after collision. The role of these forces in affecting retention mechanisms was not explored.

Han (48) offered an analysis of Johnson's experimental data in connection with an investigation of particle collection in fiber mats. The conclusion was reached that retention is controlled by Brownian diffusion and a theoretical approach to the concepts governing this diffusional retention was described. This diffusion idea was described in the following way:

> "If solid boundaries or objects are placed in a field of flow, the particles will also collide with the solids primarily due to diffusion if the particle inertia is negligible. The frequency of collision may be determined from the particle concentration and diffusivity, the geometry of the solids, and the flow pattern. On collision they may adhere to or bounce off the solid surfaces. Whether attachment or detachment will result depends on the forces operating at the site of collision.

> In the absence of repulsive forces, the particles tend to agglomerate with each other or adhere to a solid surface when they come into close proximity where the Van der Waals-London forces are operating."

The author went on to mention that the addition of electrolytes to the suspension would cause repulsive forces which would tend to stabilize the particle suspension. This meant that retention was shown to be dependent on a balance between the attractive and repulsive forces present in a particle-fiber system.

An experimental investigation was described which employed Dacron fibers and titanium dioxide; the results were compared with the nylon-TiO_2 system used by Johnson. This program consisted of a filtration procedure where both fibers and particles were retained from a single suspension. There were differences in retention rates noted between the two systems; however, diffusion still appeared to be the controlling mechanism for particle transport. These variations meant that the effect of identical ionic conditions differs for each particle-fiber system. This substantiated the conclusions that retention was dependent on the surface conditions of the particles and fibers. Thus adhesion forces were seen as a dominant factor in particle retention once the particle had been transported, by diffusion, to a position near the fiber where these forces operate.

The studies mentioned above were concerned with fiber pads composed of synthetic materials. There also has been considerable work done in applying retention concepts to wood pulp fibers. Miller (6) investigated the retention of titanium dioxide particles on bleached sulfite pulp fibers. This was a constant-rate filtration study where both particle attachment and removal were considered.

A major problem encountered when studying systems composed of wood pulp is the varying shape of the individual fibers. In most general terms, this type of fiber can be assumed elliptical in cross section; however, the surface is neither smooth nor regular. Also, these fibers are compressible, meaning their shape can change during a filtration experiment. Due to these considerations, it would be very difficult to obtain an accurate description of the flow patterns surrounding these fibers. Within a sample of pulp fibers, individual physical dimensions differ markedly unless great care is taken to separate various fiber classifications (i.e., earlywood or latewood). These differences would affect both the compressibility of the fibers as well as their hydrodynamic properties (49). A final characteristic of wood pulp which would affect their performance in capturing and retaining suspended particles would be the presence of microfibrils on their surface. These are hairlike fiber filaments projecting from the surface and are thought to affect the flow pattern around the fiber. Miller observed that particle collection was more pronounced at these fibrils than on the relatively flat surface of the fiber, even though some retention was evident on the surface. Of course, a build-up of particulate matter on the fibrils would further alter fluid flow around the fiber.

This investigation included experimentation designed to permit the visual observation of particle attachment and removal processes. This resulted in the conclusion that the majority of particles, once attached, are not subject to removal. Those that were removed were shown to be the resultant effect of a break in the fiber itself such as the loss of a fibril. This meant that if the ionic conditions of the suspension were suitable, the surface forces holding the particle to the fiber were sufficiently strong to prevent removal. This substantiates the hypothesis that at contact, or very close approach, the Van der Waals-London forces would dominate any repulsive forces present or the

shear forces induced by fluid flow. Therefore, with favorable colloidal conditions, the retention process can be considered irreversible. However, an unfavorable ionic environment would reintroduce strong repulsive forces which, in turn, would initiate removal.

An interesting conclusion of this work was that the concept of collection efficiency based on separate probabilities for collision and adhesion was inadequate to describe the retention obtained in a wood pulp-TiO_2 system. A proposal was mentioned (50) for combining molecular, colloidal, and hydrodynamic variables into a single kinetic equation which would adequately describe particle motion. This procedure was thought to be a better way of describing the attachment process in a particle-fiber system such as the one studied. This concept was, in essence, the origin for the formulation of the motion equations derived previously for detailing flow around fibers as visualized in the present thesis.

Williams and Swanson (51) reported on the results obtained from an experimental filtration system, in which they measured retention of titanium dioxide particles on bleached, kraft pulp fibers. They developed an empirical form of a retention equation originally used for incompressible fiber pads and applied it to the compressible wood pulp system. These authors stressed the importance of colloidal forces between particles and fibers, and stated that these forces were the controlling factor in the amount of retention obtained. It was pointed out in this study that a large proportion of the retention could be occurring before the filtration process was initiated. Within a suspension containing both fiber and particulate material, the same colloidal forces inducing retention during mat formation will cause an agglomeration of particles and fibers in the bulk suspension. If one is interested in only the retention occurring during formation, then this prefiltration coagulation must be considered.

The obvious procedure for eliminating this problem would be to form the pad prior to filtration of the particle suspension.

From the above discussion concerning various filtration studies, it can be concluded that utilization of wood pulp fibers in such a system introduces numerous problems in the analysis of applicable retention processes. The compressible nature of these fibers, their irregular shape and size, and the presence of surface irregularities make determinations of flow patterns and investigations of surface forces difficult, if not impossible. For these reasons, it was decided that a synthetic fiber should be used in the experimental program for the present thesis. This was also necessary because the model has been developed to simulate retention occurring on a well defined fiber, as well as uniform coverage of the entire fiber surface. It is hoped that further improvements and refinements of the model will lead to the simulation of particle flow around and collision with irregular fibers such as those found in wood pulp. The type of fiber used in this study was nylon, identical to that employed by Johnson. Many of the procedures set forth in the investigations mentioned above have been modified for use in the present experimental program. Such procedures, along with a description of the entire experimental system will be presented below.

APPARATUS

A piping diagram of the apparatus used for pad formation and particle suspension permeation is shown in Fig. 18. In this system, freshly distilled water is pumped from a large storage tank (A) through a millipore filter (I) to a 30 gallon, Teflon lined mixing tank (B). Both fiber and particle suspensions were made up in this smaller tank. Each suspension was gravity fed to the forming tube (C) where the pad was formed and, subsequently, the particles

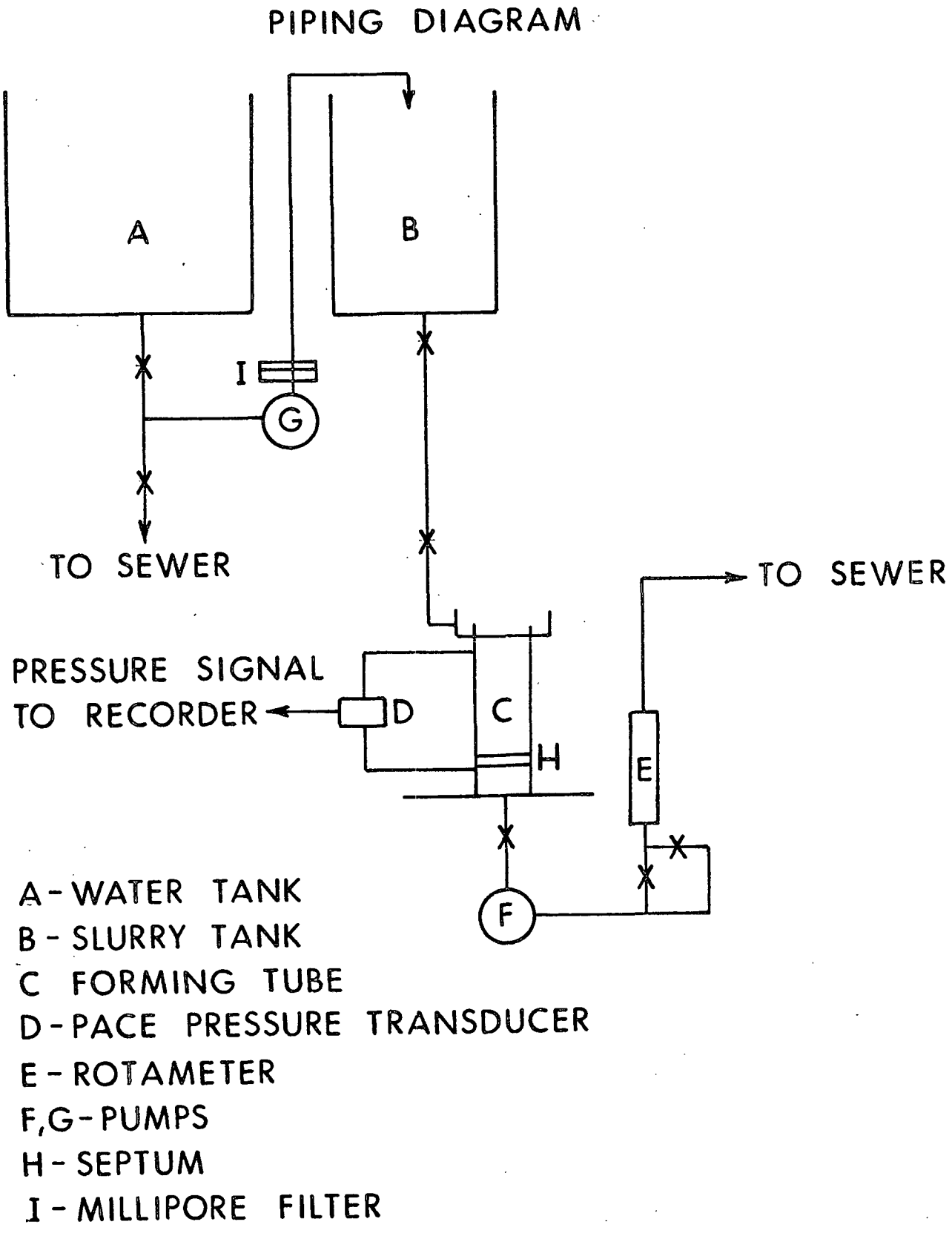

Figure 18. Schematic Diagram of the Experimental Apparatus Used for Pad Formation and Particle Permeation

filtered from their suspension. The filtrate was pumped from the bottom of the tube at differing flow rates by a variable speed, gear pump (F). It was then passed through a rotameter (E) for measurement and control of the flow rate.

The flow tube was constructed of Lucite, with an inside diameter of 3 inches and wall thickness of 1/4 inch. Thus the area available for flow within the tube was 45.6 sq cm. The septum (H) was composed of a 35-mesh stainless steel screen. The backing plate, or support for the wire, was made from stainless steel plate, 1/2-inch thick. This plate was drilled with 1/4-inch holes on 5/16-inch centers in an equilateral triangle pattern. In addition, smaller diameter holes were drilled in the plate where this pattern did not come close to the edge of the area available to flow. All of these holes were countersunk to insure a minimum of plate area perpendicular to the flow field, such areas would cause unwanted channelling and provide places where particles might settle out of the suspension.

The base of the flow tube was constructed of brass, with the same cross-sectional area as the flow tube. This was an original design built to hold the septum and septum support, while at the same time provide a strong, rigid coupling with the Lucite flow tube.

This system was also fitted with pressure taps which allowed for continuous measurement of the pressure drop across the pad. The pressure change was sensed by a Pace pressure transducer, and the resulting electronic signal was recorded.

The formation of the synthetic fiber pad can be accomplished with the equipment shown in Fig. 18. For the permeation portion of the procedure, in which the particle suspension is pumped through the pad, the fiber assemblage must be compressed to a calculated thickness in order to achieve the desired porosity. To accomplish this, a permeable piston is placed in the flow tube

and a hydraulic ram is used to force the piston down against the pad. The piston is then locked into place and remains steady for the entire permeation run. The degree of compression obtained is sufficient to prevent any flow distortion within the pad. The permeable piston is constructed of 1/2-inch stainless steel plate and it is drilled in a manner identical to the septum support described above. The downstream face of the piston is covered by a 35-mesh stainless wire to prevent any fibers from being forced up into the holes.

It is important to note that all surfaces which contact the flow stream prior to and including the septum support are constructed of stainless steel or plastic. Also, the water tanks are stainless or lined with Teflon and the feed lines are polyethylene or Tygon. The system is constructed in this way to prohibit unwanted ions from entering the flow stream, thus upsetting ionic conditions. Other studies (1) have used brass for the piston and septum, and it was feared that some ions, such as copper, could have become incorporated into the flow. It was stated that the base of the tube was brass, but this is of no concern as the filtrate is not recycled.

Figure 19 is a photograph of the assembled flow tube in operation, during the permeation portion of the experimentation. The dilute titanium dioxide suspension was being introduced to the tube (A) through the gravity feed line and controlled by the check valve (B). The ram and piston assembly (C) was in place to compress the pad which has been preformed on the septum (D). The recording device for the pressure drop was also operating (E).

Once the permeation is complete, the tube can be uncoupled at its base and the pad removed. Figure 20 shows a compressed pad ready to be taken from the assembly for further analysis. The details of the permeable piston (A)

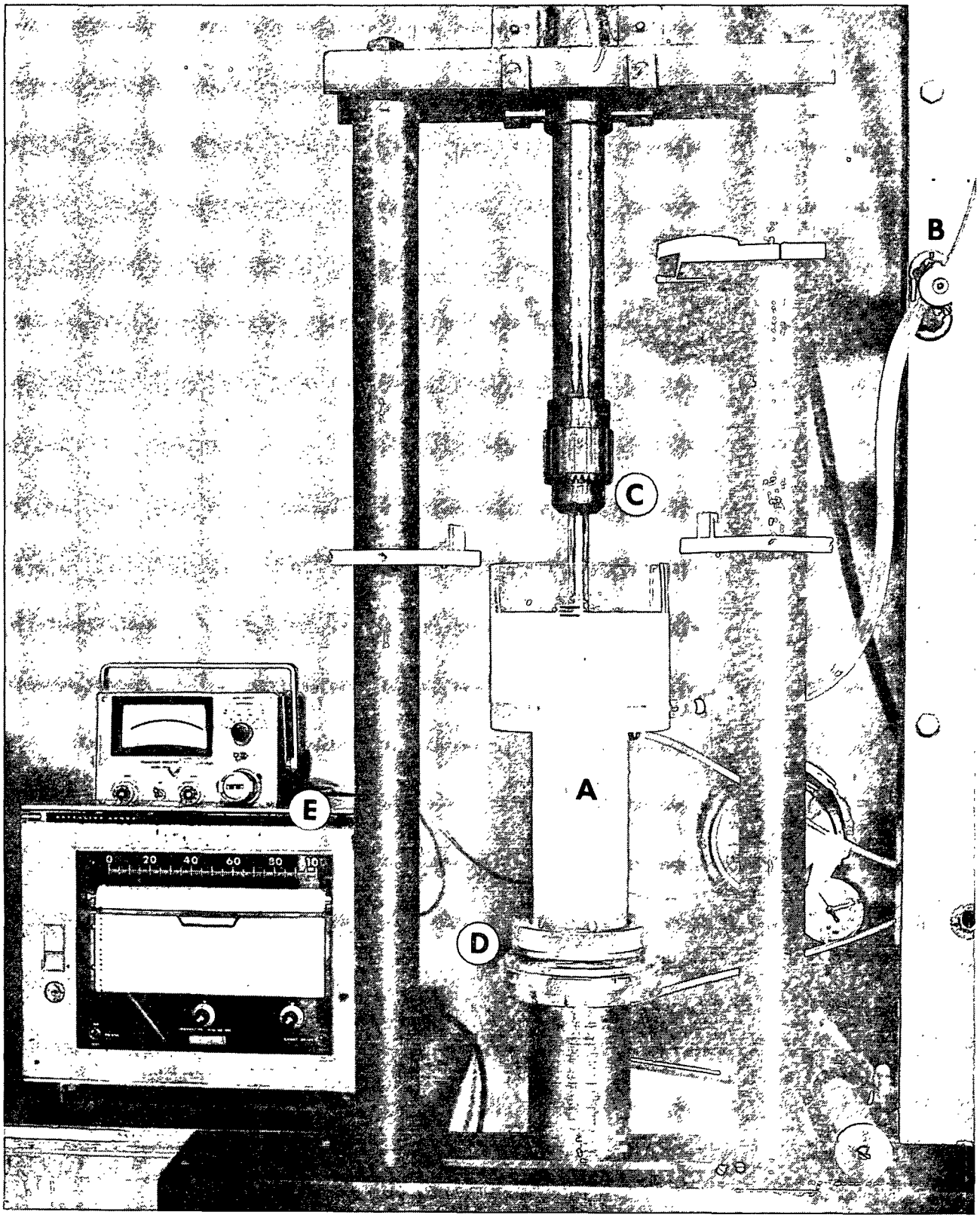

Figure 19. Photograph of Flow Tube Assembly Taken During the Permeation Procedure

are quite evident in this photograph. By releasing the pressure on the piston, and removing the retaining ring (B), the pad and septum support can be lifted from the assembly with very little disruption to the pad structure.

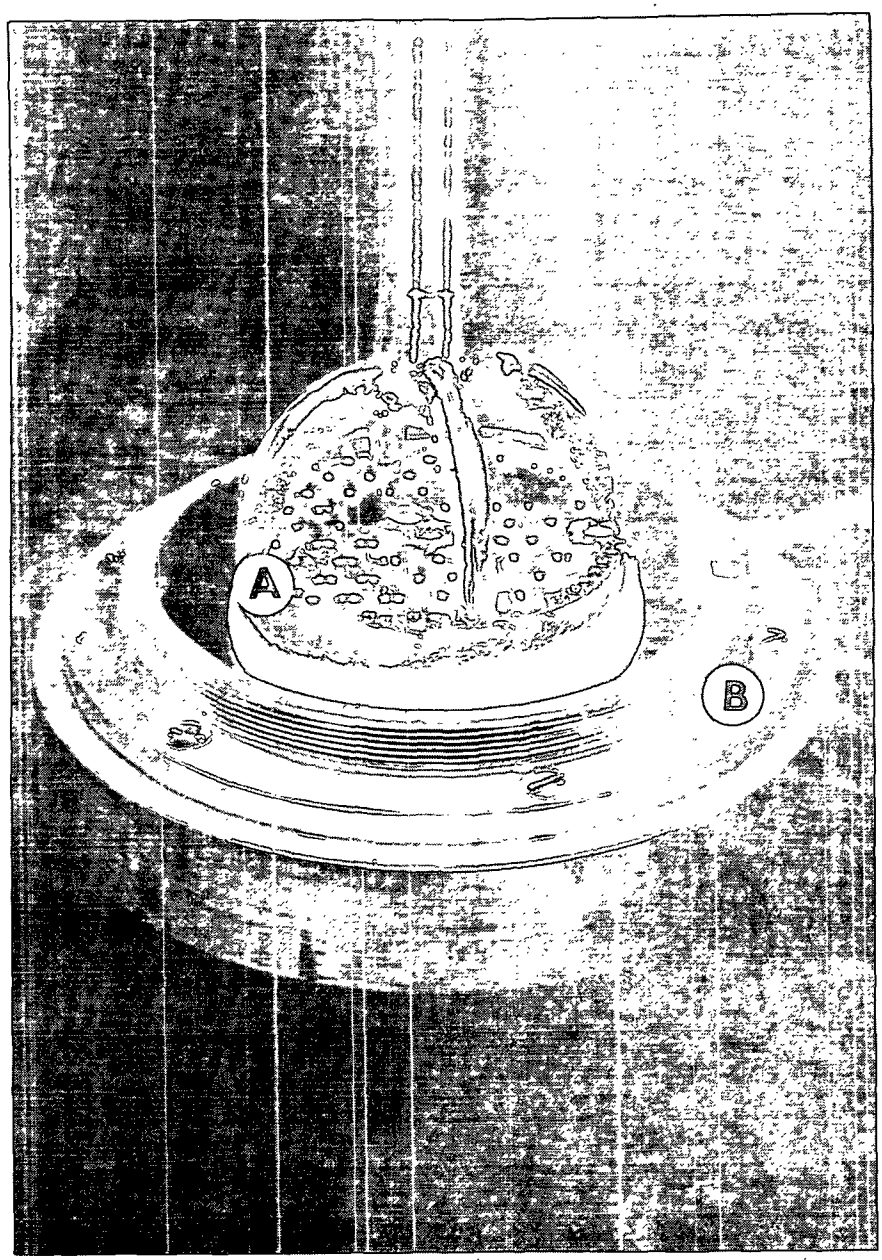

Figure 20. Photograph of a Compressed Pad

MATERIALS

WATER

Since separate fiber and particle suspensions had to be made, about 200 liters of water were necessary for each experimental run. Previous investigation (1) revealed that water quality was an important factor in retention studies because high pH values or the presence of any ions in the water would adversely affect the colloidal conditions necessary for obtaining retention. The water used in this study was always freshly distilled and was not allowed to remain in the storage tank for any appreciable time before use. Prior to distillation, the water was filtered twice and deionized. The resulting water was found to have a pH of approximately 7.0 and measurements on the zeta meter indicated that it possessed a conductivity of less than 2 μmhos/cm. The water quality remained fairly constant throughout the experimental program, helping to insure reproducible results.

A problem arose early in the experimental program which might be of importance to other research activities. The tubing originally used to transfer water from the still to the storage tank was made of Tygon. It was found that if the water was fairly warm and remained that way for several hours, some of the plasticizer used in constructing the tubing leached out and was deposited in the tank. This material appeared as an oily substance. The particular chemical involved was identified through isolation of the oily residue and IR spectroscopy. The tubing was replaced by polyethylene, and no further problems were encountered. The important point is that Tygon tubing might not always be the best material to use, even for transporting water.

FIBER

Some of the fiber qualities needed for this study have been mentioned previously. These included the necessity of utilizing a fiber characterized by a smooth surface and a circular cross section. The requirements were necessary due to the assumptions made when constructing the model. Other factors that were taken into consideration when searching for an appropriate fiber included the idea that the fibers should be easy to disperse in water and that they should be nonswelling when dispersed. For these reasons, a nylon fiber, manufactured by E. I. du Pont de Nemours & Co. was chosen. This was one of the fibers investigated by Johnson (1) in his experimentation.

The fiber used was 3 denier, or had a diameter of approximately 20 μm. Its length was 1/4 inch. Since the fibers were opaque, they did contain some titanium dioxide. The amount of pigment, or ash, in a sample of fiber was first investigated by Johnson. This was reproduced in the present study, and was found to be about 0.3%.

Figure 21 is a scanning electron micrograph of the fibers utilized in this investigation, it is clear that they are characterized by a smooth surface. The difference between synthetic fibers such as these and natural wood pulp fibers is startling, especially after observing photographs of pulp fibers such as those in Miller's thesis (6). Figure 22 is presented to show that the nylon fibers possess a circular cross section. This figure also predicts some variation in fiber size; however, due to the preparation techniques used in producing the photographs, some of the fibers may have been cut on an angle, thus making them appear larger in cross section than they really are.

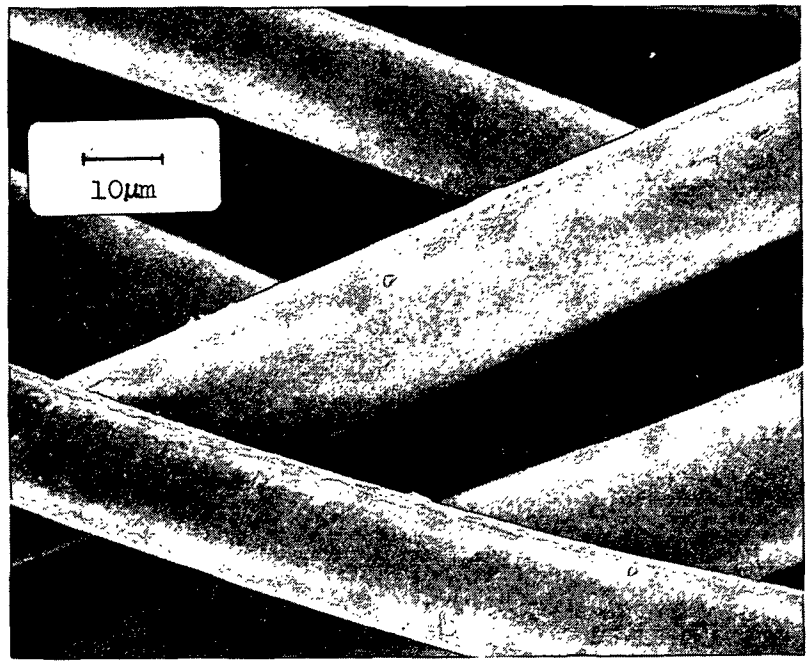

Figure 21. Scanning Electron Micrograph of the Nylon Fibers Depicting the Very Smooth Surface

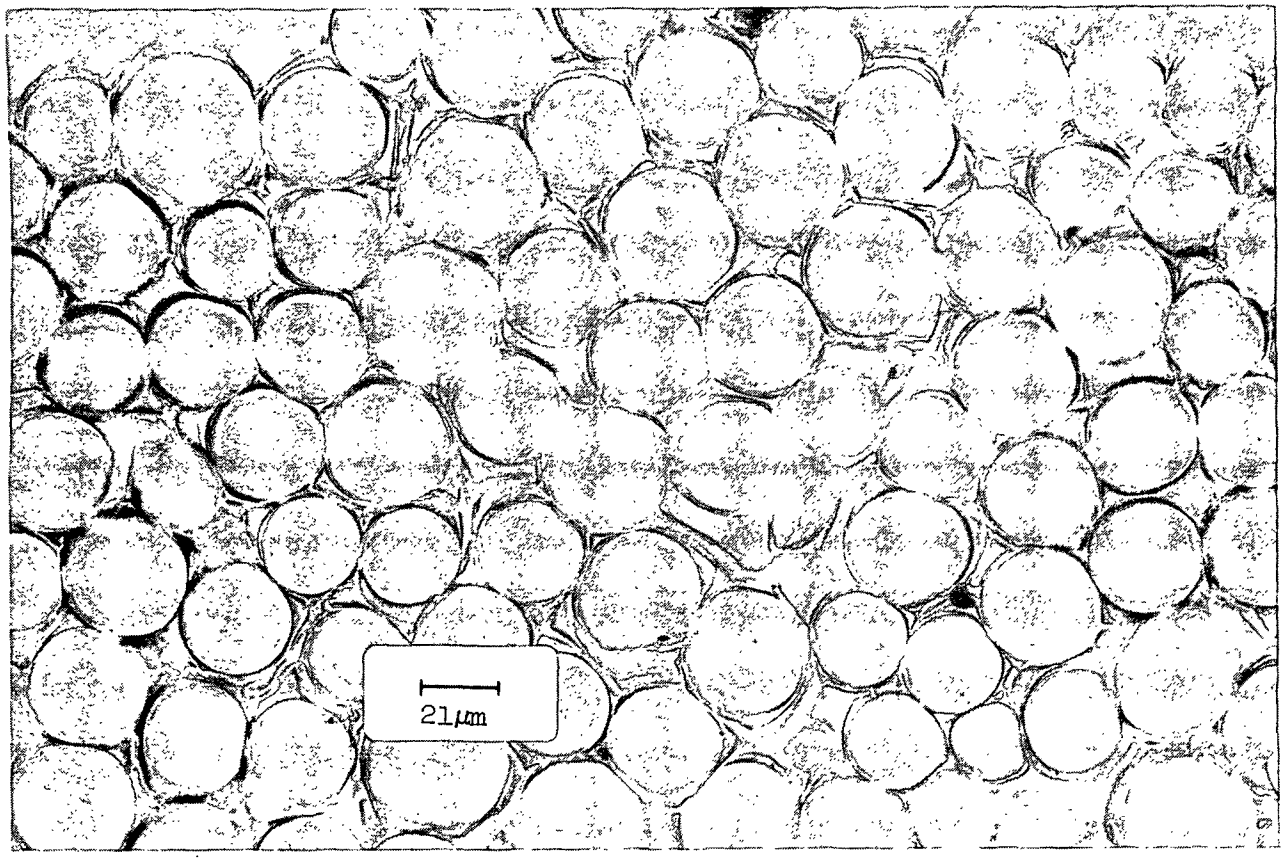

Figure 22. Micrograph of a Fiber Bundle in Cross Section, Individual Fibers are Shown to be Circular

TITANIUM DIOXIDE PARTICLES

Titanium dioxide was chosen as the particle component in this study for a variety of reasons. First of all, it has direct relevence to the retention processes involved with papermaking. Also, there is significant literature available concerning applications of TiO_2 to similar experimental techniques. The individual titanium dioxide particles are fairly uniform in size and nearly spherical in shape. A dispersion of these particles can be stabilized easily by the addition of a very small amount of dispersing agent.

A commercial grade of titanium dioxide (Titanox RA50) was chosen. A stable dispersion of these particles was made at 70% solids concentration by employing Calgon as a dispersing agent. The exact procedure followed in mixing this dispersion is provided in Appendix XI. The suspension was then diluted to 30% solids and the removal of any large agglomerates was achieved by settling. It was stored in a continually rotating container to prevent any further settling. Throughout the experimental program, the solids content was periodically verified to insure that no appreciable agglomeration and settling were occurring. The quantity of dispersion used in preparing the desired suspension concentrations for permeation was determined from the solids content of this stock solution.

To identify the actual size and shape of the titanium dioxide particles, a small sample of a very dilute suspension was dried and placed in the scanning electron microscope. The result is shown in Fig. 23. When the suspension dried, coagulation occurred, thus the particles are not presented as individuals. However, this figure does serve to show that the particles are nearly spherical, and do appear to have a small size range. A particle size distribution was obtained by actually measuring a large number of particles from this and other

micrographs. The distribution curve is presented in Fig. 24. This diagram shows quite clearly that the vast majority of individual particles have diameters between 0.2 and 0.3 μm.

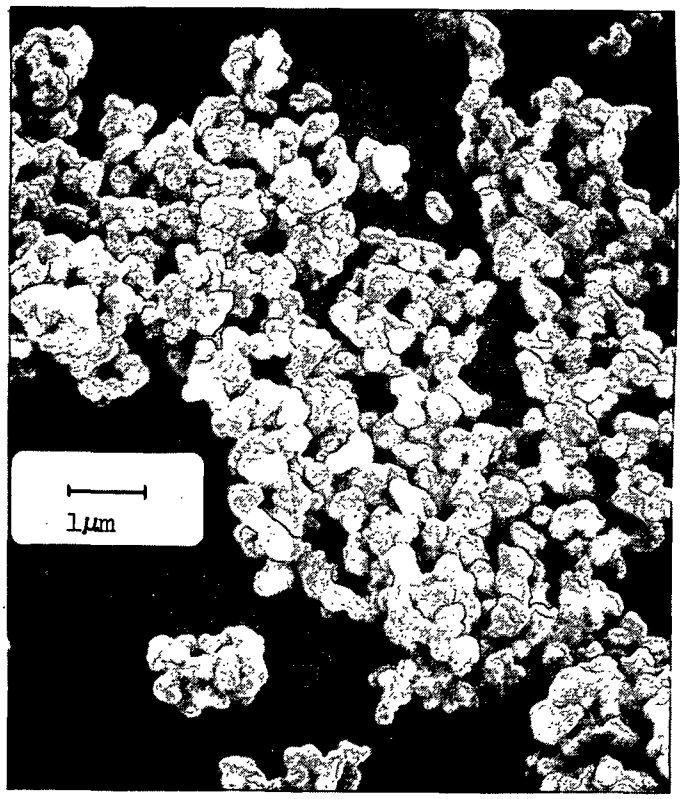

Figure 23. Scanning Electron Micrograph of Titanium Dixoide Particles

ELECTROLYTES

It has been theorized that the ionic environment plays a large role in determining the retention of small particles in fibrous media; therefore, some standard chemical compounds had to be selected as a means of altering the chemical environment existing in the particle and fiber suspensions. In order to obtain any significant retention, an acidic pH has to be maintained in the suspension (1,6,51); hydrochloric acid was used for this purpose. Also, the addition of electrolytes into a suspension will act to collapse the double

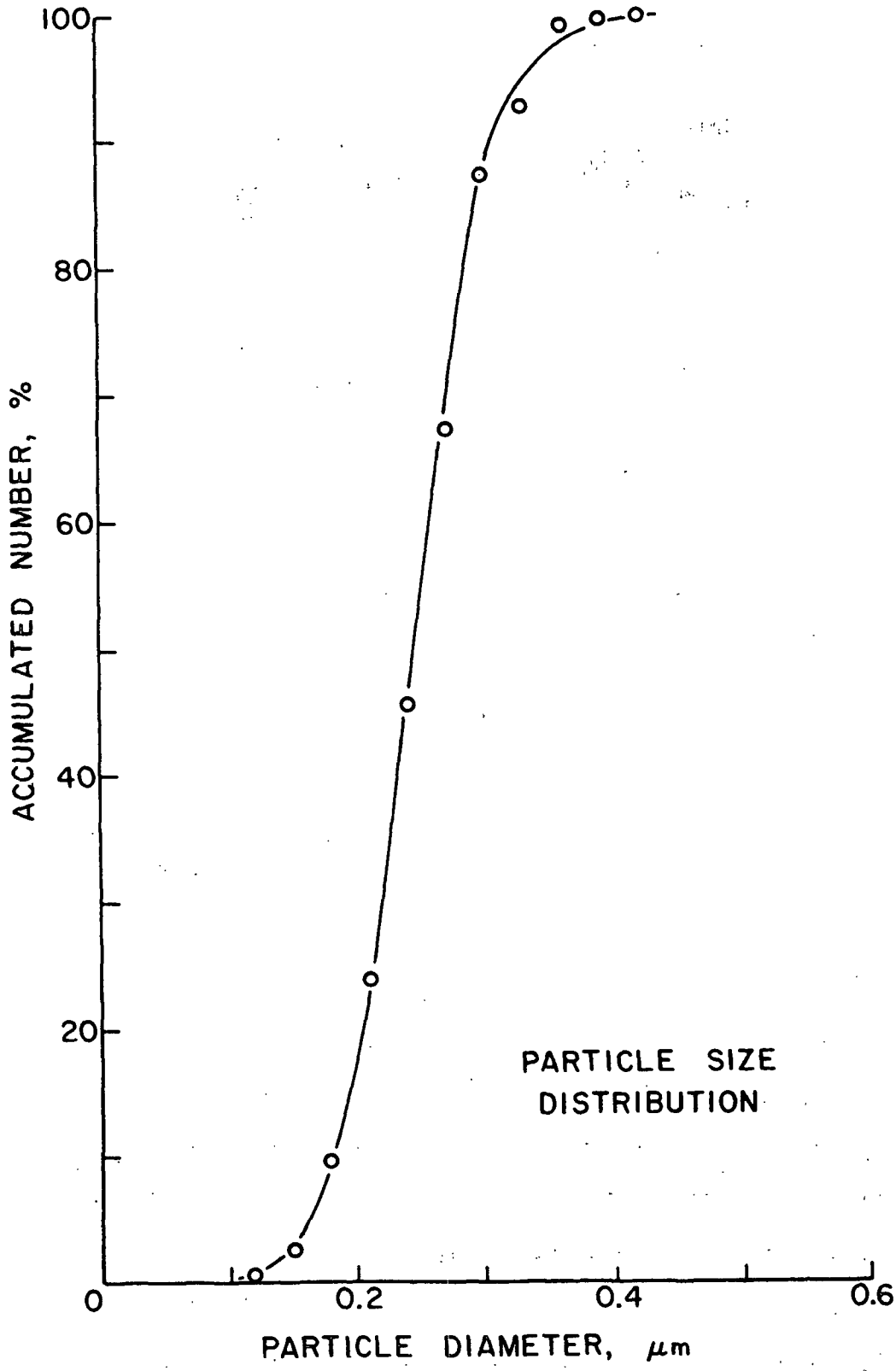

Figure 24. Distribution Curve Related to the Range of Particle Sizes Present in a Sample of Titanium Dioxide

layers surrounding the dispersed solids; in this case, such action would reduce the repulsive force between a particle and fiber. The electrolyte used in this investigation was a monovalent salt, ammonium chloride.

EXPERIMENTAL PROCEDURES

PAD FORMATION

Approximately 10 g of oven-dried, nylon fibers were transferred to a filter flask containing 1 liter of boiling water. The fibers were deaerated in vacuo. They were then added to 100 liters of freshly distilled water in the mix tank. The pH was adjusted to the desired level and 2 moles of ammonium chloride were added to insure a good dispersion. A slow agitator was employed to keep a uniform consistency throughout the suspension during formation.

The flow tube and septum were cleaned and assembled. The piston was inserted and, when resting on the septum, a zero reading was taken on a cathetometer; this was used in a subsequent step for accurately measuring pad thickness. The piston was removed and water was introduced into the tube from below the septum in order to remove any air bubbles trapped under the wire screen. The entire tube was filled with water in this manner.

The next step was the formation of the pad, accomplished by pumping the suspension through the tube and filtering the fibers at the septum. This was done at a low superficial velocity, generally set at 1.0 cm/sec, to insure that most of the fibers in the pad would be oriented in the x-y plane. This meant that when the particle suspension was allowed to permeate the pad, the flow would be approximately perpendicular to the fiber axes. When the mix tank was empty, the filtration process was halted before any air could be drawn into the pad.

of fibers between layers. Secondly, because the fibers are nylon, there is no interfiber bonding. Generally, 10 layers of sufficient weight could be obtained from a single pad. These layers were weighed and dried overnight in an oven set at 105°C.

The dried layers were weighed and placed in a muffle furnace for ashing. The ashing procedure was slow, the temperature was raised in small steps to prevent any loss of ash during the decomposition of the nylon. The initial temperature was set at 450°F. It was raised 100°F each hour until the temperature reached 850°F. After being held at this value for 1 hour, it was raised to 900°F for an hour and then 1200°F for 2 hours. The ash samples were removed from the oven at the end of this 8 hour period, cooled, and weighed.

In this investigation, it was felt that the weight of the ash would be a sufficient indication of the amount of TiO_2 retained by each particular layer of the pad in question. If this weight were corrected for the amount of ash in the nylon itself, then the remainder of the ash should be from the retained pigment. The only other compound that could be present in the ash would be traces of the salt added for the adjustment of ionic conditions in the particle suspension. However, the salt used here, ammonium chloride, sublimes at 644°F, therefore, it should not survive the ashing procedure. Thus the gravimetric method is applicable if there is enough ash present to be weighed accurately. There is an analytical procedure available which will determine titanium dioxide content by colorimetry. This procedure is discussed completely in Miller's thesis (6). This procedure was run several times in this work and a good comparison between it and the gravimetric method was obtained.

RESULTS AND DISCUSSION

Before a detailed explanation of the results is presented, Fig. 25 is given to show that there is significant retention occurring in this system. These scanning electron micrographs represent a sample of fibers removed from an inside layer of one of the pads. The photographs are all of the same sample, but at different magnifications. As is evident, there has been collection of the titanium dioxide on the surface of the nylon fibers. The micrographs have not been presented as a quantitative measure of retention, since the samples had been dried and subjected to some jostling before the photographs were taken. Thus, some of the particles initially retained may have been removed from the surfaces. This could be an explanation for apparent variations in coverage of the particles as shown in the figure. It is also interesting to note that the particles tend to become attached to other particles, thus building up in layers. In this case, the retained particles may be altering the flow patterns around the fiber which could cause an increased frequency of collision in this area of the fiber surface.

DEFINITION OF EFFECTIVE FIBER COLLECTION EFFICIENCY

There is probably no experimental procedure available which would allow an accurate determination of the amount of particles retained by a single fiber embedded within a fiber pad. The method employed for calculating collection efficiency within the system used in this thesis has been to relate entrance and exit particle concentrations to an empirical definition of collection by a single fiber. A derivation of such an efficiency was first proposed by Wong (11) and is summarized below.

In essence, this efficiency can be defined as the ratio of the area of suspension flow from which all particles are removed through collision with the

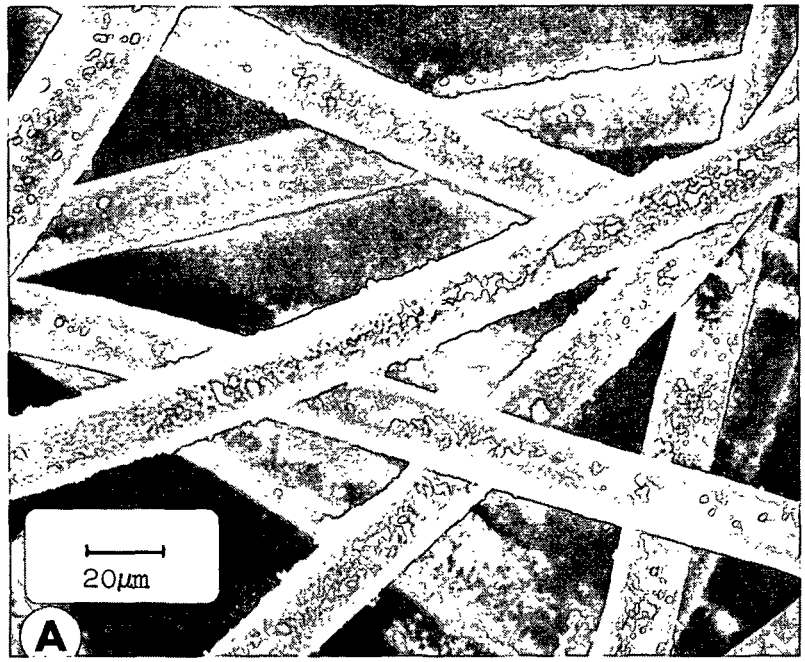

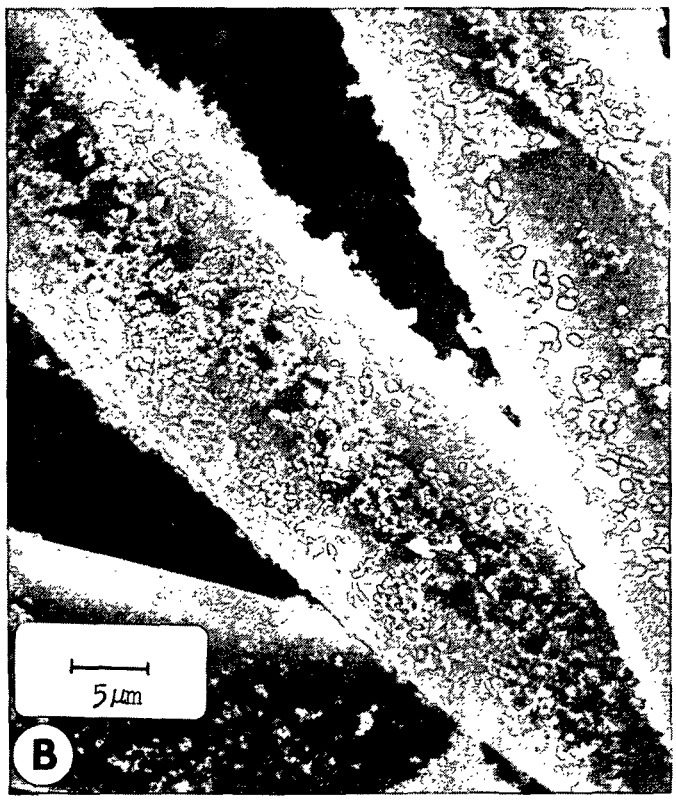

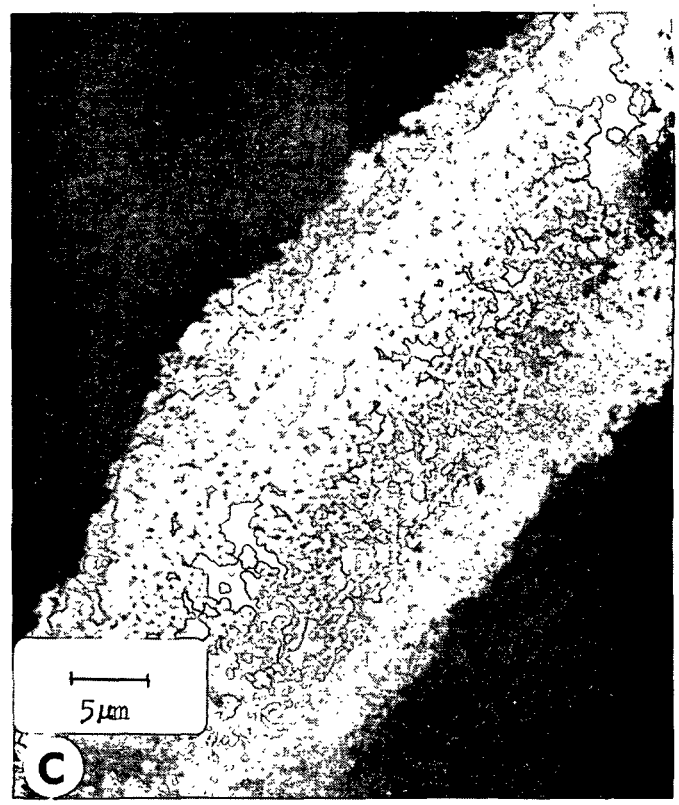

Figure 25. Scanning Electron Micrographs Showing Retained Titanium Dioxide Particles on the Surface on Nylon Fibers

fiber, to the cross-sectional area of the fiber projected perpendicular to the flow stream. This can be visualized by observing Fig. 11 which was used in the discussion of the definition of the theoretical collection efficiency used with the model. The area of the flow stream affected can be seen as being equal to 2N times the length of the fiber, while the projected area of the fiber would be 2A times its length. The ratio of these values would be N/A. This is equal to the predicted collection efficiency value. From this discussion, it can be seen that the definition of the theoretical and experimental collection efficiencies are comparable.

To translate this definition of efficiency into mathematical form, the following derivation is presented. This concept of collection is dependent on the assumption that the fiber pad is uniform throughout its thickness, h. The projected area of fiber perpendicular to flow direction in a section of the pad, dh, would be $(L\ A_f\ dh)(D_f)$, where L is the total length of fiber per unit volume, A_f is the area of the pad exposed to flow, and D_f is the fiber diameter. The fraction of incoming particles within the projected fiber area would be:

$$\mathscr{F} = \frac{(L\ A_f\ dh)(D_f)}{A_f} \tag{37}$$

If η_e represents the fraction of these particles, $\mathscr{F}$, that are collected, then:

$$-\frac{dC}{C} = \mathscr{F}\eta_e = \frac{(L\ A_f\ dh)(D_f)}{A_f}\eta_e = L\ D_f\ dh\ \eta_e \tag{38}$$

where C is the number of particles per unit volume in the bulk suspension and dC is the number of particles removed by the layer dh. The fiber volume within the layer is:

$$(1 - \varepsilon) = (L)(\pi D_f^2/4) \tag{39}$$

Therefore, Equation (38) becomes:

$$-\frac{dC}{C} = \eta_e \, 4(1 - \varepsilon)dh/\pi D_f \tag{40}$$

Integrating this equation over the thickness of the layer and the particle concentrations entering, $\underline{C_o}$, and exiting, $\underline{C_h}$, one obtains the following equation for $\underline{\eta_e}$:

$$\eta_e = \frac{D_f \pi}{4(1 - \varepsilon)h} \ln (C_o/C_h) \tag{41}$$

By assuming a monodisperse distribution of particle size and the occurrence of no fractionation during filtration, the equation for efficiency can be rewritten to reflect particle mass rather than concentration:

$$\eta_e = \frac{D_f \pi}{4(1 - \varepsilon)h} \ln (M_o/M_h) \tag{42}$$

where $\underline{M_o}$ = particle mass entering the pad per unit volume of suspension

$\underline{M_h}$ = particle mass exiting the pad

$\underline{M_{mat}}$ = particle mass retained, $\underline{M_o} - \underline{M_h}$

The derivation presented above relies on the fact that the porosity, and therefore fiber volume, of the pad remains constant through its thickness. This condition is realized if the pad is compressed while at the same time, the individual fibers are rigid enough not to deform. These concepts are valid in the experimental system used. Therefore, the porosity will be constant through pad thickness, and the collection efficiency will also be uniform throughout. The experimental results obtained from the investigation substantiate this theory and will be presented shortly.

RETAINED TITANIUM DIOXIDE DISTRIBUTION THROUGH THE PAD

There are many methods available for presenting the results of the permeation procedure. For this study, it was thought that a graphical representation, showing the distribution of retained titanium dioxide through the thickness of the pad would be appropriate. It should be remembered that the amount of ash obtained from each pad layer has been assumed equal to the amount of pigment retained by that layer, after a small correction is made for the ash content of the fiber.

Figure 26 depicts the ash distribution in comparison to the nylon fiber distribution, both given as a function of the overall pad weight for a typical experimental run. This particular pad (Run No. 14) was composed of about 7.7 g of nylon fiber and was compressed to a porosity of 0.75. A particle suspension, initially containing 1.4 g of titanium dioxide was passed through the pad at 1.00 cm/sec. The pad was then sectioned into 11 layers for ashing. Each of the curves in the figure is based on the total weight of the nylon or ash in the pad. The individual data points represent separate layers, with the top layer on the left and bottom layer on the right. At the bottom, of course, 100% of both the nylon and ash have been accounted for. As an example to clarify this plot, consider the third layer. This set of two data points indicates that after 25% of the nylon had been stripped away, approximately 35% of the total ash in the pad had been removed. In other words, this amount of retained pigment has been shown to exist in the top three layers of the pad.

Theory states that collection efficiency is constant through pad thickness if porosity is constant. If this were followed exactly in the system depicted, the two lines for ash and nylon distribution would coincide. In actuality, the plot shows that there is slightly more pigment retained in the top several

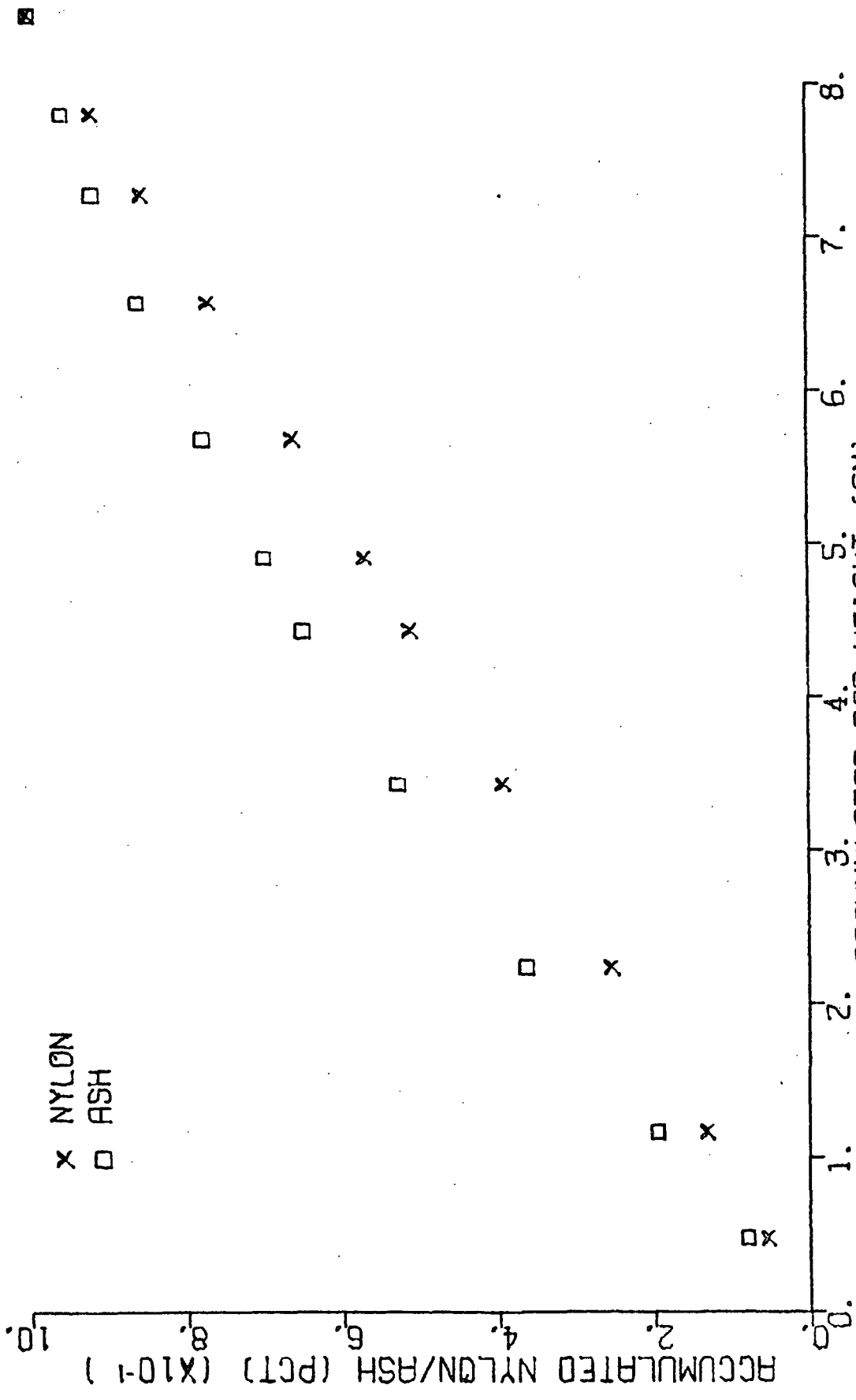

Figure 26. Diagram of Nylon and Ash Distribution Through the Thickness of the Pad

layers of the pad. This could be explained by the fact that the collection occurring in the upper portion of the pad reduces the concentration of particles reaching the lower layers, thus reducing the amount of particulates available for retention. However, it is felt that the difference in collection shown in Fig. 26, although noticeable, is not overwhelming. In reality, the changes in efficiency values involved are not that large. Summarizing, the results depicted here indicate that retention is slightly greater at the top of the pad than at the bottom.

This observation is substantiated in Fig. 27. This plot has been provided to show the distribution of accumulated ash weight as related to overall pad weight for the same run as described above. Again the data points represent each layer analyzed. The plot shows a relatively uniform ash concentration through pad thickness, with a slight, but constant decrease as the pad becomes thicker. This is the same trend shown in the previous figure. In addition to the decrease in particle concentration through the pad as mentioned above, the increased retention within the upper layers of the pad could be caused by flow perturbations created by previously retained particles. Figure 25 showed that at certain areas on the fiber surface, the particles build up in thick layers, probably caused by attractive forces between particles. However, it still remains to be seen how the variation shown here is reflected in the actual value of collection efficiency calculated for this typical run.

In addition, Fig. 27 shows that, in the entire pad, approximately 9% of its dry weight is due to retained titanium dioxide. Other calculations performed for this particular run indicate that about 51% of the pigment fed to the pad was retained by it. Of course, this value would vary from system to system, but it well represents the fact that a significant amount of retention is occurring.

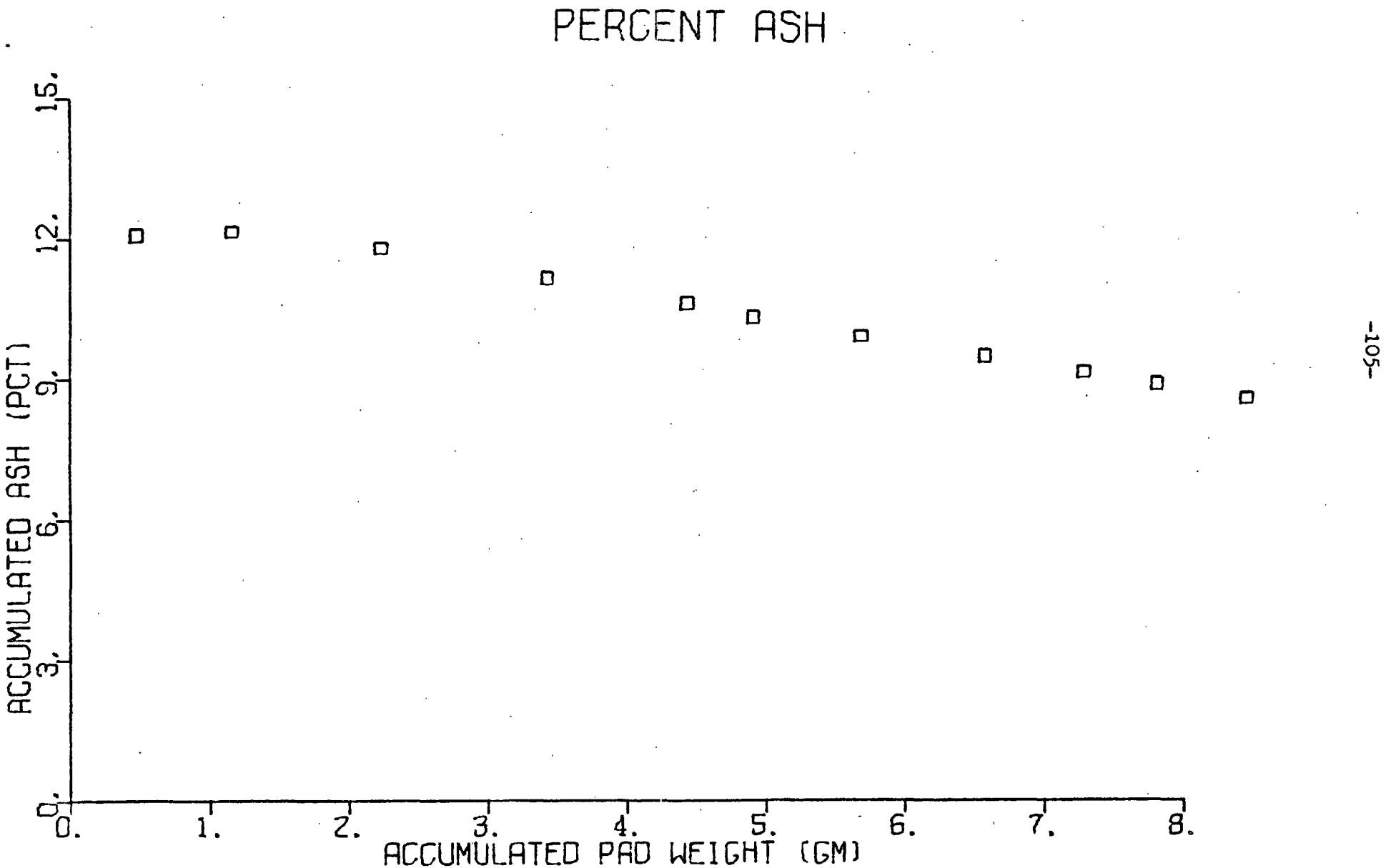

Figure 27. Ash Content of Individual Pad Layers

The mathematics involved in the calculation of the effective fiber collection efficiency, η_e, was provided in the previous section. The value of η_e was shown to be [see Equation (42)] a function of entrance and exit particle mass flux, fiber diameter, and pad dimensions. If the collection efficiency is constant through pad thickness, a plot of $\ln(M_o/M_h)$ vs. h should yield a straight line which passes through the origin. The value of η_e could then be calculated from the slope of this line. Since it was impractical to attempt a measurement of each layer's thickness, and since the porosity of the pad was known, h was known to be proportional to the accumulated pad weight, M. A plot of the logarithm term vs. M would also yield a straight line from which the efficiency could be calculated.

Figure 28 is a plot constructed in this manner for the same run as described above. As can be seen from the regression line (correlation coefficient - 0.999), the data do fall on a straight line. From the slope, a value of $\eta_e = 0.007$ was calculated. This straight line correlation indicates that collection efficiency is constant through pad thickness.

All calculations for the results depicted in Fig. 26-28 were performed by the computer; the diagrams were drawn by the computer. A FORTRAN IV listing of the program written to perform these tasks is presented in Appendix XII. Also, the results, both in tabular and graphical form, for other pertinent experimental runs are provided in Appendix XIII. It is interesting to note that all of the runs have exhibited results similar to those described here. That is, all of the diagrams were of the same form, again substantiating the fact that, in the type of system used, collection efficiency is constant through pad thickness.

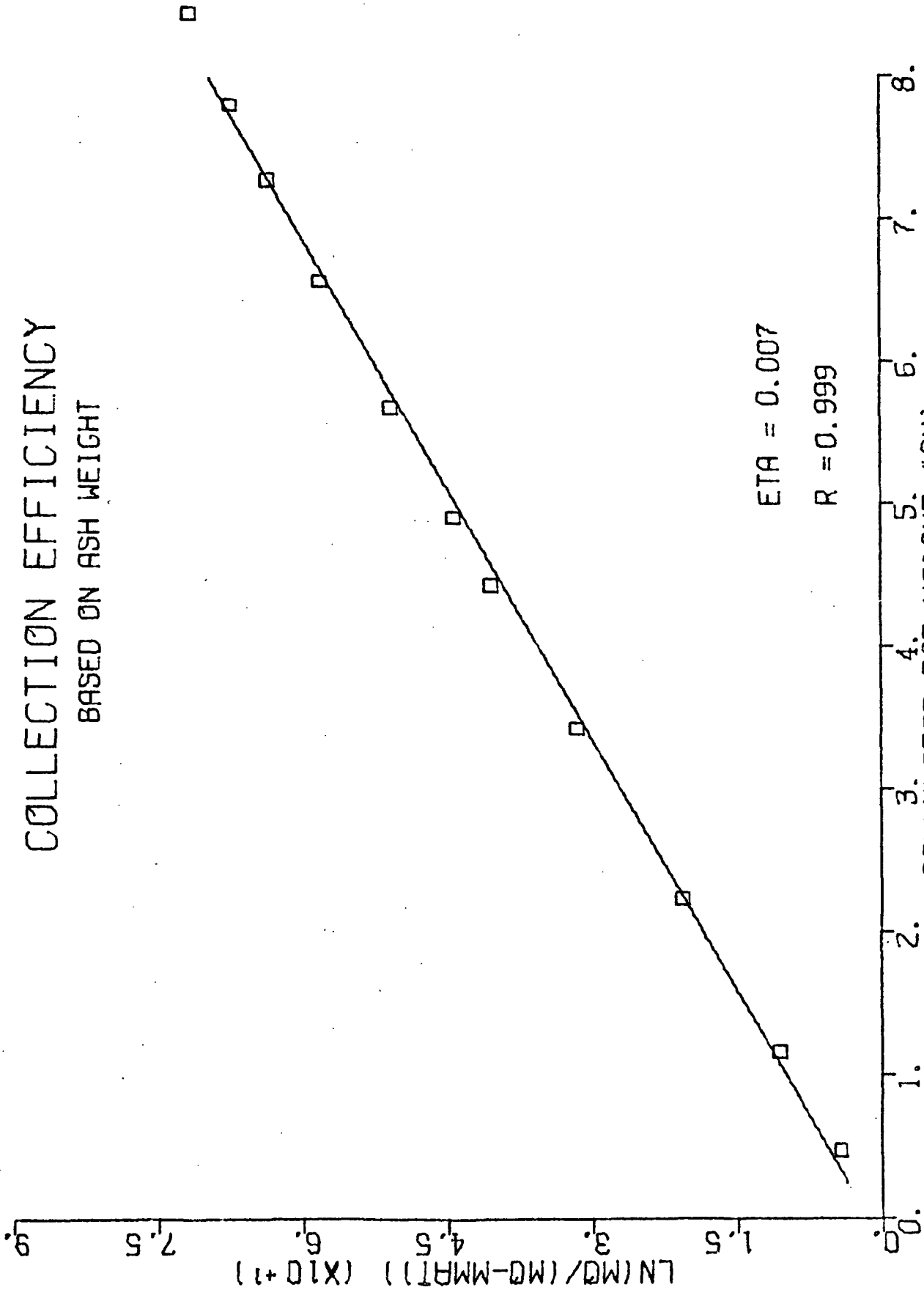

Figure 28. Diagram Used for the Calculation of Collection Efficiency, Using the Slope of Line, η_e = 0.007

EFFECT OF SYSTEM CONDITIONS ON EFFICIENCY

Table IV gives some of the values for effective fiber collection efficiency calculated from the experimental runs. With the particular system used for these runs, there were three main system variables which could be related adequately to variations in efficiency. These were porosity, approach velocity of the particle suspension, and the ionic characteristics of this suspension.

TABLE IV

EFFECTIVE FIBER COLLECTION EFFICIENCIES

Porosity	Velocity (cm/sec)	Ionic Conditions of Suspension	Efficiency (η_e)
0.85	1.50	Salt/acid	0.0045
0.75	1.50	Salt/acid	0.0052
	1.00	Salt/acid	0.0070
	1.00	Acid	0.0059
	1.00	None	0.0008

Effect of Porosity

The porosity of a fiber pad can be defined as the void volume of that pad, or the areas within the pad available for fluid flow. Accurate values of porosity were obtained for this system by careful measurement of pad thickness during permeation; by knowing pad area and fiber density, the porosity can be calculated utilizing this thickness value. From the results presented in Table IV, it has been shown that the collection efficiency of a pad decreased as porosity increased. This can be explained by the fact that as porosity decreases, the void volume within the pad decreases, effectively placing a greater number of particles in a smaller volume. This would mean that an increased number of particles would be in a position close enough to the fiber's surface to be

affected by particle transport mechanisms and surface attractive forces which would lead to collision and retention. Thus an increased number of particles would be retained.

Effect of Approach Velocity

The approach velocity of the particle suspension was controlled by the magnitude of its flow rate through the pad during permeation. All of the flow rates observed represented Reynolds numbers based on the fiber diameter below one. From the tabulated values, it is apparent that collection efficiency decreases as the velocity increases. At an increased velocity, the particles in suspension would have less time in their paths through the pad to be influenced by any of the forces present in the system. This would mean that particles which would be affected, and probably retained, if sufficient exposure to these forces was available, would pass through uncollected, thereby decreasing the efficiency.

Effect of Suspension Ionic Conditions

Many previous studies have indicated that the ionic conditions of the particle suspension are very important in determining the amount of retention possible with a given set of operating variables. In the nylon-TiO_2 system utilized in this study, it was thought that both solid components would assume a negative surface charge when immersed in water. Thus, the addition of an acid such as HCl would reduce this charge through the adsorption of hydrogen ions. Also, the double layers surrounding the solid components could be collapsed by the addition of an electrolyte. Therefore, several of the trials made with differing ionic conditions are listed among the tabulated values. As indicated, omission of the salt from the suspension causes a slight decrease in collection efficiency. This is due to the fact that the repulsive double layers between particle and fiber would be stronger, permitting fewer particles

to reach the fiber's surface. A much more drastic influence on efficiency is noted when no additions are made to the suspension. This would mean that repulsive potentials between the solids are unchecked, indicating that the repulsive force would dominate the attractive molecular forces, and would permit no significant retention. These observations could mean that the presence of hydrogen ions in this system is more beneficial to retention than the presence of the electrolyte. Thus retention in a system such as the one used here can be considered to be dependent on the pH of the particle suspension.

CONCLUSIONS

The objective of this thesis has been to develop a mathematical model for simulating a retention process involving the collection of small, spherical particles on fibers of circular cross section. In addition, an experimental program was completed which provided data on collection efficiencies to be used in a comparison with similar values predicted by the model. This comparison was made to determine the applicability of the model; that is, to show whether the model can predict efficiencies close to those actually obtained from a real retention system. This manuscript has presented, separately, the development and results of the model, followed by the procedures and results from the experimentation. This section summarizes the comparison between these two systems, and presents evidence pertaining to the relevance of the model.

Table V provides a comparison between the theoretical, η_p, and experimental, η_e, collection efficiencies obtained from this study. The values indicate that, generally, agreement between the two efficiency values is quite good. This supports a conclusion that the model is appropriate and is within range for predicting a good first approximation of retention occurring in a real system. It is important to note that all of the trends shown in the table, or expressed in previous sections, reflecting the effect of various system parameters on efficiency are the same for both the theoretical and experimental programs. These include the facts that efficiency decreases with increasing porosity, and it decreases with increasing velocity. It has also been shown that some favorable comparisons could be made between the two phases of work representing a decrease in retention with a decreasing ionic concentration in the suspension. Results have indicated that retention is negligible when no additions were made for control of suspension conditions.

TABLE V

COMPARISON OF THEORETICAL AND EXPERIMENTAL COLLECTION EFFICIENCIES

Porosity	Velocity	Ionic Conditions of Suspension	Efficiency η_e	Efficiency η_p (d = 0.3 μm)
0.85	1.50	Salt/acid	0.0045	0.0064
	1.00	Salt/acid	0.0069	0.0068
0.75	1.50	Salt/acid	0.0052	0.0093
	1.00	Salt/acid	0.0070	0.0103
	1.00	None	0.0008	Negligible

The difference between the two values of efficiency is fairly consistent, indicating that, in general, the experimental values are slightly lower than the predicted ones. There are many possible explanations for this occurrence. The most obvious one would be that, in the experimental system, there could be some removal of particles which had been attached to a fiber. The removal of particles was checked on several occasions; after permeation was complete, a volume of clean water, conditioned to comparable ionic concentrations was passed through the pad at a low flow rate. Some removal was observed, but it was not more than approximately 10% of the particulate matter initially retained. This is not sufficient to explain the variations between most of the values given in Table V; however, it does not account for particles which were lost during the permeation procedure itself. Of course, the model did not account for particle removal.

Overprediction could be caused by an increased boundary layer on the downstream side of the fiber. The creeping motion equations are valid only when the Reynolds number vanishes. The equations are linear in this case, therefore, there is symmetry of flow around the upstream and downstream faces

of the fiber; the boundary layer surrounding the fiber would be symmetrical. Even at Reynolds numbers less than one, this symmetry is lost. The result would be a larger boundary layer on the downstream side. If this is the case, then fewer particles than predicted would be able to cross this layer and collide with the fiber. Neglecting this effect would lead to an overprediction of collection efficiency.

Another reason for the difference in efficiency values could be related to the effect of particle size on efficiency. The model predicted that efficiency decreased significantly with a decrease in particle size. The predicted values in Table V were calculated for a particle diameter of 0.3 μm. However, the particle size distribution for the titanium dioxide sample used in the experiments (Fig. 24) shows that there could be a large population of particles with a diameter less than this value. If the model were to account for smaller particles, the predicted efficiency would decrease, thus bringing it closer to the appropriate experimental value.

A final consideration to be noted here would be the effect of flow perturbations within the fiber mat. The flow rate of the particle suspension through the pad was kept quite low, however, some irregularities in flow patterns could develop due to varying fiber orientations. Although it is unlikely, there could be some channeling of the flow through the pad, caused by the holes in the permeable piston. A combination of these effects might decrease the efficiency of particle retention.

Considering all of the factors involved, the conclusion had been reached that the model performs adequately and can be considered to yield relevant predictions of the retention occurring in a relatively simple system. Just as important is the ability of the model to predict various trends in collection

efficiency caused by variations in system parameters. It was also concluded that the objectives of the thesis have been satisfied, in that the results indicate the Van der Waals force is the most important factor in the modeled retention process. If this is not considered, retention is negligible. Of course, this is predicated on the fact that suspension conditions are such that the double layers surrounding the solid components are collapsed. If these double layers are active, then their repulsive effect will dominate the attractive forces, and retention will not occur. The effect of diffusion in this system is less clear. It has been shown that diffusion will transport particles and affect retention to a greater extent than either inertial impaction or interception. However, the results also indicate that diffusion would tend to move a particle away from the fiber, causing a decrease in the amount retained.

SUGGESTIONS FOR FUTURE WORK

The work performed during this thesis has presented a sound basis for future work. The ultimate goal of further investigations in this area would be closer simulation of retention processes applicable to the paper industry, specifically, the retention of pigment materials in the paper sheet. The ability to predict retention efficiencies for such systems would permit the study of new equipment or chemical additives before their inclusion into the process, and thus be of economic value.

To get to this stage, the present model would require sufficient refinements to allow the investigation of many system variables which were not considered in this study. One area for refinement would be in predicting the suspension conditions needed for maximum retention. Further investigation into effects of a wide range of electrolytes could be made. This would lead the way for the study of the effect on retention caused by suspension additions involving polymeric retention or drainage aids, a practice common in today's paper mill. The end result of this might involve the prediction of the optimum amounts of these polymers necessary for maximum retention.

For a complete study of chemical effects on retention, further investigation of the double-layer interaction and the addition of a Coulombic type force expression to the model would be anticipated. Most chemical additives used today are polyionic and can be either positively or negatively charged. Force effects caused by such additions would be very important in the interaction between a particle and fiber.

Possibilities exist for utilizing the model in further investigations concerning the effects on retention caused by changes in system variables related to the physical characteristics of the materials used and the process itself.

The influence of various fiber sizes and shapes on retention could be quantified. For example, it would be interesting to show how an elliptical fiber would change the flow patterns and, therefore, retention efficiencies. An aid for future study in this area could be a recent investigation into fluid flow around fibers with an elliptical cross section (52). Other model refinements in this area would lead to observations relating the effects on retention of increased flow rates. Major problems in this area would be discovered in obtaining the basic flow equations describing fluid and particle motion through an assemblage of fibers. Motion equations outside of the creeping motion regime would be very complex and, in some cases, simplified forms of such equations are nonexistent. However, progress might be made in this area which would permit incorporation of higher velocities into the model.

The experimental system utilized for this study is a fairly straightforward and an easily understood system. Flow rates, ionic concentration, and pad dimensions (i.e., porosity) are easy to manipulate and provide for investigations over a wide range of system conditions. Most of the model refinements mentioned above can and should be compared to experimental data obtained from this type of system. Adequate values of retention efficiencies for natural fibers also could be obtained from similar equipment. However, if such fibers contained any significant amount of ash, some analysis procedure for titanium dioxide would have to be used, possibly similar to that used by Miller (6). This would be necessary because it would be impossible to rely on a constant fiber ash content when studying natural fibers.

The work performed in this study has been related to two separate disciplines, applied mathematics and physicochemistry. Ultimately, it would be beneficial to be able to link these together in some basic manner. It might be possible to get the mathematical model and the experimentation into agreement

to the point where constants in the force expressions could be correlated to some physical condition of the system, one of the most obvious being pH. This would mean that by knowing the pH of a system the model could be precisely defined, and alternately, experimental conditions could be obtained from model parameters. This would yield a very flexible and useful model.

In conclusion, it is felt that this investigation has been a first step toward an improved understanding of the retention process. Within the paper industry, this process is, and will be, of great economic and environmental interest; a mathematical model could be a powerful tool in gaining new and important information concerning this complex process.

LIST OF SYMBOLS

A = Fiber radius

A_f = Area of fiber pad exposed to flow

a_p = Particle radius

B = Fluid envelope radius

b_i $(i=1,9)$ = Coefficients calculated for regression equations

C, D, E, F = Integration constants

C = Number of particles per unit volume in bulk suspension

C_h = Particle concentration exiting fiber layer

C_o = Particle concentration entering fiber layer

c = Ion concentration

D_f = Fiber diameter

$\mathscr{D}$ = Einstein's diffusion coefficient

d = Particle diameter

$\bar{dr}$ = Temporary distance and direction of particle motion

e' = Electronic charge

F_{DL} = Double-layer force

F_{VdW} = Van der Waals force

$\vec{F}$ = Drag force vector

$\mathscr{f}$ = Ratios of projected fiber area to pad area

$f(\varepsilon)$ = Function dependent on system porosity

g = Acceleration due to gravity

$g(\varepsilon)$ = Function dependent on system porosity

H = Hamaker constant

h = Pad thickness

$\vec{i}$, $\vec{j}$ = Unit vectors

K_1 = Coefficient in particle motion equations

k = Boltzmann's constant

L = Total length of fiber per unit volume

M = Accumulated pad weight

M_h = Particle mass exiting pad

M_{mat} = Particle mass retained, $M_o - M_h$

M_o = Particle mass entering pad

m = Particle mass

N = Distance value used for calculation of predicted collection efficiency

n = Exponents of the biharmonic equation

$\vec{P}$ = Force vector, rate of change of momentum

p = Pressure

R = Correlation coefficient

r = Radial position component

r^* = Nondimensional particle distance

T = Absolute temperature

t = Time

t^* = Nondimensional time variable

U = Fluid approach velocity

V = Particle velocity in a stationary fluid

v_r = Radial component of fluid velocity

v_r^* = Nondimensional radial fluid velocity

v_θ = Angular component of fluid velocity

v_θ^* = Nondimensional angular fluid velocity

$\vec{v}$ = Local mass average fluid velocity

$\vec{x}$ = Average displacement due to diffusion

z = Valence of ions

α = Retardation correction factor

Γ_{VdW}^{ret} = Retarded Van der Waals potential between two atoms

δ = Separation distance between particle and fiber

ε = Porosity

ε_d = Dielectric constant of water

ζ_1, ζ_2 = Zeta potentials for particle and fiber

η_e = Experimental collection efficiency

η_p = Predicted collection efficiency

η_p' = Alternate value of predicted collection efficiency

η_r = Collection efficiency obtained from regression model

θ = Angular position component

κ = Debye-Huckel reciprocal length

λ_e = Wavelength of electron oscillation

μ = Fluid viscosity

ρ = Fluid density

ρ_p = Particle density

σ = Standard deviation

τ = Fluid stress

$\tau_{r,\theta}$ = Shear stress at the fluid envelope

ψ = Stream function

ACKNOWLEDGMENTS

My sincere appreciation is extended to the members of my Thesis Advisory Committee: Dr. Richard W. Nelson, Chairman, Mr. Nai L. Chang, and Dr. Robert A. Stratton, for their continued advice and support. Special thanks are due to Mr. Heribert Meyer and Dr. Dale G. Williams who are former chairman and committee member, respectively. I am especially grateful to Mr. Meyer who, after his retirement, continued to express interest in the work and offered much guidance to me.

I would like to acknowledge every individual within the Institute community who aided in the completion of this thesis. Special appreciation is offered to John J. Bachhuber and John O. Church for their assistance and advice concerning the computer programs, to Bruce D. Andrews for sharing his vast experience relating to filtration and permeation processes, and to Delores Managan for her expert typing of the manuscript.

LITERATURE CITED

1. Johnson, R. C. A Study of Particle Retention in Relation to the Structure of a Fibrous Mat. Doctoral Dissertation. Appleton, Wisconsin, The Institute of Paper Chemistry, 1962.

2. Davies, C. N. Air Filtration. London and New York, Academic Press, 1973.

3. Chen, C. Y., Chem. Revs. 55(3):595-623(1955).

4. George, H. F. and Poehlein, G. W., Envir. Sci. Tech. 8(1):46-9(1974).

5. Swanson, J. W., unpublished work, 1973.

6. Miller, J. R., Jr. An Investigation of the Retention of Titanium Dioxide on Wood Pulp Fibers. Doctoral Dissertation. Appleton, Wisconsin, The Institute of Paper Chemistry, 1972.

7. Payatakes, A. A New Model for Granular Porous Media. Application to Filtration Through Packed Beds. Doctoral Dissertation. Syracuse, New York, Syracuse University, 1973.

8. Lundgren, D. A. and Whitby, K. T., I.&E.C. Process Design and Development 4(4):345-9(1969).

9. Friedlander, S. K., J. Coll. Inter. Sci. 23:157-64(1967).

10. Kirsch, A. A. and Fuchs, N. A., Ann. Occup. Hyg. 10:23-30(1967).

11. Wong, J. B., Ranz, W. B., and Johnstone, H. F., J. Appl. Phys. 27(2):161-9 (1956).

12. Smith, T. N. and Philips, C. R., Envir. Sci. Tech. 9(6):564-8(1975).

13. Smith, T. N., Philips, C. R., and Melo, O. T., Envir. Sci. Tech. 10(3): 274-7(1976).

14. Yao, K.-M., Habibian, M. T., and O'Melia, C. R., Envir. Sci. Tech. 5(11): 1105-12(1971).

15. Spielman, L. A. and Goren, S. L., Envir. Sci. Tech. 4(2):135-40(1970).

16. Spielman, L. A. and Fitzpatrick, J. A., J. Coll. Inter. Sci. 42(3):607-23 (1973).

17. Fitzpatrick, J. A. and Spielman, L. A., J. Coll. Inter. Sci. 43(2):350-69 (1973).

18. Goren, S. L. and O'Neill, M. E., Chem. Eng. Sic. 26:325-38(1971).

19. Spielman, L. A. and Cukor, P. M., J. Coll. Inter. Sci. 43(1):51-65(1973).

20. Wnek, W. J., Gidaspow, D., and Wasan, D. T., Chem. Eng. Sic. 30:1035-47 (1975).

21. Payatakes, A. C., Tien, C., and Turian, R. M., AIChE Journal 19(1):58-67 (1973).

22. Payatakes, A. C., Tien, C., and Turian, R. M., AIChE Journal 19(1):67-76 (1973).

23. Payatakes, A. C., Tien, C., and Turian, R. M., AIChE Journal 20(5):889-900 (1974).

24. Payatakes, A. C., Tien, C., and Turian, R. M., AIChE Journal 20(5):900-5 (1974).

25. Ruckenstein, E. and Prieve, D. C., J. Chem. Soc. Faraday Trans. II 69(10): 1522-36(1973).

26. Hamaker, H. C., Recueil des Travaux Chimiques des Pays-Bas 55:1015-26 (1936).

27. Lifshitz, E. M., Sov. Physics JETP 2:73(1956).

28. Fowkes, F. M., Ind. Eng. Chem. 56(12):40-52(1964).

29. Winterton, R. H. S., Contemp. Phys. 11(6):559-74(1970).

30. Israelachvili, J. N., Contemp. Phys. 15(2):159-78(1974).

31. Rosenfeld, J. I. and Wasan, D. T., J. Coll. Inter. Sci. 47(1):27-31(1974).

32. Verwey, E. J. W. and Overbeek, J. Th. G. Theory of the Stability of Lyophobic Colloids. Amsterdam and New York, Elsevier Publishing Company, 1948.

33. Hogg, H., Healy, T. W., and Fuerstenau, D. W., Trans. Faraday Soc. 62:1638-51 (1966).

34. Bird, R. B., Stewart, W. E., and Lightfoot, E. N. Transport Phenomena. New York, London, and Sydney, John Wiley & Sons, Inc., 1960.

35. Happel, J. and Brenner, H. Low Reynolds Number Hydrodynamics. New Jersey, Prentice-Hall, Inc., 1965.

36. Harrop, J. A. and Stenhouse, J. I. T., Chem. Eng. Sci. 24:1475-81(1969).

37. Rajagopalan, R. Stochastic Modeling and Experimental Analysis of Particle Transport in Water Filtration. Doctoral Dissertation. Syracuse, New York, Syracuse University, 1974.

38. Happel, J., AIChE Journal 5(2):174-7(1959).

39. Visser, J., Adv. Coll. Inter. Sci. 3:331-63(1972).

40. Gregory, J., Adv. Coll. Inter. Sci. 2:396-417(1969).

41. Clayfield, E. J. and Lumb, E. C., J. Coll. Inter. Sci. 37(2):382-9(1971).

42. Collatz, L. The Numerical Treatment of Differential Equations. Berlin, Springer-Verlag, 1960.

43. Nelson, R. W., personal communication, 1975.

44. Webb, J. T. An Investigation of Electric-Double-Layer Concepts and Colloidal Stability of Titanium Dioxide Suspensions. Doctoral Dissertation. Appleton, Wisconsin, The Institute of Paper Chemistry, 1971.

45. Richmond, P., J. Chem. Soc. Faraday Trans. II 70(10):1650-9(1974).

46. Stratton, R. A., personal communication, 1977.

47. Neale, S. M. and Peters, R. H., Trans. Faraday Soc. 42:478-87(1946).

48. Han, S. T., Tappi 47(12):782-7(1964).

49. Binotto, A. P. Correlation of Certain Morphological and Hydrodynamic Aspects of Loblolly Pine Bleached Kraft Pulp. Doctoral Dissertation. Appleton, Wisconsin, The Institute of Paper Chemistry, 1977.

50. Meyer, H., unpublished work, 1969.

51. Williams, D. G. and Swanson, J. W., Tappi 49(4):147-51(1966).

52. Brown, G. R. Creeping Flow of Fluids Through Assemblages of Elliptic Cylinders and its Application to the Permeability of Fiber Mats. Doctoral Dissertation. Appleton, Wisconsin, The Institute of Paper Chemistry, 1975.

APPENDIX I

DERIVATION OF THE GENERAL STREAM FUNCTION

The biharmonic equation was given in the following form:

$$\nabla^2(\nabla^2\psi) = \nabla^4\psi = 0, \tag{I-1}$$

where the Laplacian operator for cylindrical coordinates is defined as:

$$\nabla^2 = \frac{\partial^2}{\partial r^2} + \frac{1}{r}\frac{\partial}{\partial r} + \frac{1}{r^2}\frac{\partial^2}{\partial \theta^2} \tag{I-2}$$

The stream function can be written as $\psi = \underline{R}(r)\Theta(\theta)$, and from the boundary conditions associated with this system, it can be shown that $\Theta(\theta) = \sin\theta$. Therefore Equation (I-2) can be written as:

$$\nabla^2\psi = R''\Theta + \frac{1}{r}R'\Theta + \frac{1}{r^2}R\Theta'' \tag{I-3}$$

By considering the definition of velocity components presented in Equations (13), the solution of Equation (I-1) must be of the form:

$$r^n \sin\theta = R(r)\Theta(\theta) \tag{I-4}$$

Equation (I-3) can be rewritten:

$$\begin{aligned}\nabla^2\psi &= n(n-1)r^{n-2}\sin\theta + n(r^{n-2})\sin\theta - r^{n-2}\sin\theta \\ &= [n(n-1) + n - 1]\, r^{n-2}\sin\theta \\ &= (n^2 - 1)\, r^{n-2}\sin\theta \end{aligned} \tag{I-5}$$

Following the same procedure, it is shown that:

$$\nabla^4\psi = (n^2-1)\left[(n-2)(n-3)r^{n-4}\sin\theta + \frac{1}{r}(n-2)\, r^{n-3}\sin\theta - \frac{1}{r^2}r^{n-2}\sin\theta\right] = 0 \tag{I-6}$$

The factor $\underline{r}^{n-4}$ sin θ is common to all three terms and there remains:

$$(n^2-1)(n^2 - 4n + 3) = 0 \qquad \text{(I-7)}$$

Thus the exponents in the trial solution, Equation (I-4), are $\underline{n} = \pm 1, 1, 3$. From this equation, the stream function can be considered to exist in the following form:

$$\psi = [Cr^3 + Dr + \frac{E}{r} + Fr \ln r] \sin \theta, \qquad \text{(I-8)}$$

where $\underline{C}$, $\underline{D}$, $\underline{E}$, and $\underline{F}$ are integration constants. The logarithmic term in the brackets arises from the fact that there are repeating roots involved in obtaining the solution of Equation (I-7).

APPENDIX II

DERIVATION OF THE SPECIFIC STREAM FUNCTION APPLICABLE TO THE FLOW SYSTEM USED

The general form of the stream function was presented as Equation (I-8). The purpose of the present discussion will be to calculate the four integration constants listed in this equation. To accomplish this, four boundary conditions must be utilized. These were provided earlier as Equations (16) through (19). These conditions define fluid flow around a stationary cylinder of circular cross section based on the concept of the unit cell as pictured in Fig. 5. The boundary conditions are:

at $r = A$ (fiber radius)

$$v_r = \frac{1}{r}\frac{\partial \psi}{\partial \theta} = 0 \qquad \text{(II-1)}$$

$$v_\theta = -\frac{\partial \psi}{\partial r} = 0 \qquad \text{(II-2)}$$

at $r = B$ (fluid envelope radius)

$$v_r = -U \cos \theta \qquad \text{(II-3)}$$

$$\frac{\partial v_\theta}{\partial r} + \frac{1}{r}\frac{\partial v_r}{\partial \theta} - \frac{v_\theta}{r} = 0 \qquad \text{(II-4)}$$

By applying these boundary conditions to the stream function, ψ, the following expressions can be obtained:

$$v_r = \cos \theta \left[Cr^2 + D + E/r^2 + F \ln r\right]_{r=A} = 0 \qquad \text{(II-5)}$$

$$v_\theta = -\sin \theta \left[3Cr^2 + D - E/r^2 + F(\ln r + 1)\right]_{r=A} = 0 \qquad \text{(II-6)}$$

$$v_r = \cos \theta \left[Cr^2 + D + E/r^2 + F \ln r\right]_{r=B} = -U \cos \theta \qquad \text{(II-7)}$$

$$\frac{\partial v_\theta}{\partial r} = -\theta \left[6Cr + 2E/r^3 + F/r\right]_{r=B} \qquad \text{(II-8)}$$

$$\frac{1}{r}\frac{\partial v_r}{\partial \theta} = -\sin\theta\left[Cr + D/r + E/r^3 + \frac{F}{r}\ln r\right]_{r=B} \qquad \text{(II-9)}$$

$$-\frac{v_\theta}{r} = \sin\theta\left[3Cr + D/r - E/r^3 + \frac{F}{r}(\ln r + 1)\right]_{r=B} \qquad \text{(II-10)}$$

By use of these last three expressions, Equation (II-4) becomes:

$$\left[6Cr + 2E/r^3 + F/r + Cr + D/r + E/r^3 + \frac{F}{r}\ln r - 3Cr - D/r + E/r^3 - \frac{F}{r}\ln r - F/r\right]_{r=B}\sin\theta = 0 \qquad \text{(II-11)}$$

$$-\sin\theta\left[4Cr + 4E/r^3\right]_{r=B} = 0 \qquad \text{(II-12)}$$

Inserting the proper values of r into these expressions yields four equations that can be solved simultaneously to obtain the four values representing the integration constants:

$$C A^2 + D + E/A^2 + F \ln A = 0 \qquad \text{(II-13)}$$

$$3C A^2 + D - E/A^2 + F(\ln A + 1) = 0 \qquad \text{(II-14)}$$

$$C B^2 + D + E/B^2 + F \ln B = -U \qquad \text{(II-15)}$$

$$4C B + 4E/B^3 = 0 \qquad \text{(II-16)}$$

Simplifying Equation (II-16) provides:

$$C = -E/B^4 \qquad \text{(II-17)}$$

Substituting the value for C into (II-13), (II-14) and (II-15) gives:

$$-E A^2/B^4 + D + E/A^2 + F \ln A = 0 \qquad \text{(II-18)}$$

$$-3E A^2/B^4 + D - E/A^2 + F(\ln A + 1) = 0 \qquad \text{(II-19)}$$

$$-E/B^2 + D + E/B^2 + F \ln B = -U \qquad \text{(II-20)}$$

Combining Equations (II-18) and (II-19):

$$- 2E \frac{A^2}{B^2} - 2 \frac{E}{A^2} + F = 0, \qquad \text{(II-21)}$$

therefore,

$$F = 2E \left(\frac{A^4 + B^4}{A^2 B^2} \right) \qquad \text{(II-22)}$$

Equation (II-20) can then be written as:

$$- E/B^2 + D + E/B^2 + 2E \left(\frac{A^4 + B^4}{A^2 B^4} \right) \ln B = -U \qquad \text{(II-23)}$$

$$D = - 2E \left(\frac{A^4 + B^4}{A^2 B^4} \right) \ln B - U \qquad \text{(II-24)}$$

By inserting the values calculated for C, D, and F into Equation (II-18), an expression for E can be obtained:

$$- E \frac{A^2}{B^4} - 2E \left(\frac{A^4 + B^4}{A^2 B^4} \right) \ln B - U + E/A^2 + 2E \left(\frac{A^4 + B^4}{A^2 B^4} \right) \ln A = 0 \qquad \text{(II-25)}$$

$$E - \frac{A^2}{B^4} - \left(\frac{A^4 + B^4}{A^2 B^4} \right) \ln B^2 + 1/A^2 + \left(\frac{A^4 + B^4}{A^2 B^4} \right) \ln A^2 = U \qquad \text{(II-26)}$$

$$E - \frac{A^2}{B^4} + 1/A^2 + \left(\frac{A^4 + B^4}{A^2 B^4} \right) \ln \left(\frac{A^2}{B^2} \right) = U \qquad \text{(II-27)}$$

$$E = \frac{U}{- \frac{A^2}{B^4} + 1/A^2 + \left(\frac{A^4 + B^4}{A^2 B^4} \right) \ln \left(\frac{A^2}{B^2} \right)} \qquad \text{(II-28)}$$

If g(ε) is set equal to the denominator of this equation, then E becomes:

$$E = U/g(\varepsilon) \qquad \text{(II-29)}$$

Using this value, the other constants can be calculated as:

$$C = - \frac{U}{B^4 \, g(\varepsilon)} \tag{II-30}$$

$$D = - 2U/g(\varepsilon) \left(\frac{A^4 + B^4}{A^2 \; B^4} \right) \ln B - U \tag{II-31}$$

$$F = 2U/g(\varepsilon) \left(\frac{A^4 + B^4}{A^2 \; B^4} \right) \tag{II-32}$$

Substituting Equations (II-30) through (II-32) into the stream function equation yields the following:

$$\psi = \sin \theta \left\{ - r^3 \frac{U}{B^4 \, g(\varepsilon)} - r \frac{U}{g(\varepsilon)} \left(\frac{A^4 + B^4}{A^2 \; B^4} \right) \ln B^2 + \frac{U}{r \, g(\varepsilon)} - r \, U \right.$$
$$\left. + r \ln r \frac{2U}{g(\varepsilon)} \left(\frac{A^4 + B^4}{A^2 \; B^4} \right) \right\} \tag{II-33}$$

$$\psi = \frac{U \sin \theta}{g(\varepsilon)} \left\{ - \frac{r^3}{B^4} + 1/r \; r \left(\frac{A^4 + B^4}{A^2 \; B^4} \right) (\ln r^2 - \ln B^2) - r \, g(\varepsilon) \right\} \tag{II-34}$$

Let $$f(\varepsilon) = - A^2 \, g(\varepsilon) = \frac{A^4}{B^4} - 1 - \left(\frac{A^4 + B^4}{B^4} \right) \ln \left(\frac{A}{B} \right)^2$$

If the porosity, ε, equals $(\underline{B}^2 - \underline{A}^2)/\underline{B}^2$, then

$$(1 - \varepsilon) = \frac{A^2}{B^2} \tag{II-35}$$

Thus $$f(\varepsilon) = (1 - \varepsilon)^2 - 1 + 2(1 + (1 - \varepsilon)^2) \ln (1 - \varepsilon)^{-\frac{1}{2}} \tag{II-36}$$

The stream function then assumes the form:

$$\psi = \frac{U \sin \theta}{f(\varepsilon)} (-A^2) \left\{ - \frac{r^3}{B^4} + r \left(\frac{A^4 + B^4}{A^2 \; B^4} \right) (\ln r^2 - \ln B^2) - r \frac{f(\varepsilon)}{-A^2} \right\} \tag{II-37}$$

$$\psi - \frac{U \sin\theta}{f(\varepsilon)} \left\{ \frac{A^4 r^3}{B^4 A^2} - \frac{A^2}{r} - 2(1 + (1 - \varepsilon)^2)\, r \ln \left(\frac{A}{B}\frac{r}{A}\right) - r\, f(\varepsilon) \right\} \qquad \text{(II-38)}$$

$$\psi = \frac{U \sin\theta}{f(\varepsilon)} \left\{ (1 - \varepsilon)^2 \frac{r^3}{A^2} - \frac{A^2}{r} - 2(1 + (1 - \varepsilon)^2)\, r \ln \left((1 - \varepsilon)^{\frac{1}{2}} \frac{r}{A} \right) - r\, f(\varepsilon) \right\} \qquad \text{(II-39)}$$

APPENDIX III

DERIVATION OF FLUID VELOCITY EQUATIONS

From the expression representing the specific stream function, ψ, the fluid velocity components can be obtained through Equations (13):

$$v_r = \frac{1}{r}\frac{\partial \psi}{\partial \theta} = \frac{U \cos \theta}{f(\varepsilon)}\left\{(1-\varepsilon)^2 \frac{r^2}{A^2} - \frac{A^2}{r^2} - 2(1+(1-\varepsilon)^2) \ln \frac{r}{A}(1-\varepsilon)^{\frac{1}{2}} - f(\varepsilon)\right\} \qquad \text{(III-1)}$$

$$v_\theta = -\frac{\partial \psi}{\partial r} = \frac{-U \sin \theta}{f(\varepsilon)}\left\{3(1-\varepsilon)^2 \frac{r^2}{A^2} + \frac{A^2}{r^2} - 2(1+(1-\varepsilon)^2)\left[\ln \frac{r}{A}(1-\varepsilon)^{\frac{1}{2}} + 1\right] - f(\varepsilon)\right\} \qquad \text{(III-2)}$$

Equations (III-1) and (III-2) provide the values for fluid velocity at any position within the fluid annulus of the unit cell. They are applicable to a system in which the solid cylinder is stationary, and the fluid is flowing around it in a direction perpendicular to its length.

The procedure that has been followed in deriving the stream function and the velocity components can be used to obtain similar expressions for a system in which the fiber is flowing through a stationary fluid. This can be found in work performed by Happel (38).

APPENDIX IV

DERIVATION OF PARTICLE MOTION EQUATIONS

After the equations representing fluid flow around the cylinder had been developed, the motion of a small spherical particle suspended in this flow had to be described. Within any regime of motion, there is a resistance to flow exerted on this particle by the fluid; under creeping flow conditions this drag force is generally presented in the form of Stokes' law:

$$F = 3\pi\mu d\, V \tag{IV-1}$$

This equation describes the drag force encountered by a particle moving with a velocity, $\underline{V}$, in a stationary fluid. As mentioned previously, if the fluid is also in motion, the particle will move at a different velocity and in a different direction than the fluid, and the drag force becomes:

$$\vec{F} = -\, 3\pi\mu d\, (\vec{v} - \frac{\vec{dr}}{dt}) \tag{IV-2}$$

Particle motion can be represented by Newton's Second law:

$$\vec{P} = \frac{d}{dt}\,(m\,\frac{\vec{dr}}{dt}), \tag{IV-3}$$

where $\vec{P}$ is a force vector, $\underline{m}$ is the particle mass, and $\underline{\vec{dr}/dt}$ is the velocity vector of the particle. This equation can be restated as follows. Since:

$$\vec{dr} = dr\,\vec{i} + r\,d\theta\,\vec{j} \tag{IV-4}$$

The force vector assumes the following form:

$$\vec{P} = \frac{d}{dt}\,(m\,\frac{dr}{dt}\,\vec{i} + mr\,\frac{d\theta}{dt}\,\vec{j}) \tag{IV-5}$$

$$\vec{P} = m\,\frac{d^2r}{dt^2}\,\vec{i} + mr\,\frac{d^2\theta}{dt^2}\,\vec{j} + m\,\frac{dr}{dt}\,\frac{d\theta}{dt}\,\vec{j} + m\,\frac{dr}{dt}\,\frac{d\theta}{dt}\,\vec{j} - mr\,(\frac{d\theta}{dt})^2\,\vec{i} \tag{IV-6}$$

If it is assumed at this point that drag is the only force affecting particle motion, and since:

$$\vec{v} = v_r \vec{i} + v_\theta \vec{j}, \tag{IV-7}$$

Equation (IV-2) becomes:

$$F = -3\pi\mu d \left[(v_r \vec{i} + v_\theta \vec{j}) - \left(\frac{dr}{dt}\vec{i} + r\frac{d\theta}{dt}\vec{j}\right)\right] \tag{IV-8}$$

Combining Equations (IV-6) and (IV-8) and separating the unit vector components, the following is obtained:

$$\left\{ m\frac{d^2r}{dt^2} - 3\pi\mu d\, v_r + 3\pi\mu d\frac{dr}{dt} - mr\left(\frac{d\theta}{dt}\right)^2 \right\}\vec{i} = \left\{ -mr\frac{d^2\theta}{dt^2} - 2m\frac{dr}{dt}\frac{d\theta}{dt} + 3\pi\mu d\, v_\theta - 3\pi\mu d\frac{d\theta}{dt} \right\}\vec{j} \tag{IV-9}$$

This equation has meaning only if both sides are zero. Therefore, two second-order differential equations result. They are:

$$\frac{d^2r}{dt^2} = \frac{3\pi\mu d}{m}\left(v_r - \frac{dr}{dt}\right) + r\left(\frac{d\theta}{dt}\right)^2 \tag{IV-10}$$

$$\frac{d^2\theta}{dt^2} = \frac{3\pi\mu d}{m}\left(\frac{v_\theta}{r} - \frac{d\theta}{dt}\right) - \frac{2}{r}\frac{dr}{dt}\frac{d\theta}{dt} \tag{IV-11}$$

Integration of these equations provides the pathway that a particle would follow as it travels around a fiber.

To simplify the calculations and the analysis of the results, Equations (IV-10) and (IV-11) were transformed into a nondimensional form. This was accomplished through the use of the following nondimensional variables:

$$r^* = \frac{r}{A}, \qquad t^* = t\frac{U}{A}, \qquad v_{r^*} = \frac{v_r}{U}, \qquad v_{\theta^*} = \frac{v_\theta}{U}, \tag{IV-12}$$

where A is the fiber radius and U is the fluid approach velocity. Inserting the variables into Equation (IV-10), the result is:

$$\frac{d^2r^*A}{dt^{*2}(A/U)^2} = \frac{3\pi\mu d}{m}\left(v_{r^*}\,U - \frac{dr^*}{dt^*}\frac{A}{(A/U)} + r^*\,A\left(\frac{d\theta}{dt^*}\right)^2 (U/A)^2\right), \qquad \text{(IV-13)}$$

which can be simplified to:

$$\frac{d^2r^*}{dt^{*2}} = \frac{3\pi\mu d\,A}{mU}\left(v_{r^*} - \frac{dr^*}{dt^*}\right) + r^*\left(\frac{d\theta}{dt^*}\right)^2 \qquad \text{(IV-14)}$$

The first term on the right-hand side of this equation can be modified by defining the particle mass as $d^3\pi\rho_p/6$. Thus the coefficient would become $(18\mu A)/(d^2\rho_p U)$, and Equation (IV-14) can be rewritten as:

$$\frac{d^2r^*}{dt^{*2}} = \frac{18\mu A}{d^2\rho_p U}\left(v_{r^*} - \frac{dr^*}{dt^*}\right) + r^*\left(\frac{d\theta}{dt^*}\right)^2 \qquad \text{(IV-15)}$$

In the same way, Equation (IV-11) can be restated as follows:

$$\frac{d^2\theta}{dt^{*2}} = \frac{18\mu A}{d^2\rho_p U}\left(v_{\theta^*} - \frac{d\theta}{dt^*}\right) - \frac{2}{r^*}\frac{dr^*}{dt^*}\frac{d\theta}{dt^*} \qquad \text{(IV-16)}$$

These two motion equations are identical to Equations (30) and (31) presented previously. The asterisks have been omitted for simplicity.

APPENDIX V

DERIVATION OF VAN DER WAALS AND DOUBLE-LAYER FORCE EXPRESSIONS

The purpose of this appendix is to describe the methods used to obtain the expressions for Van der Waals forces and the double-layer interaction as employed in the motion equations.

UNRETARDED VAN DER WAALS FORCE

The expression for Van der Waals unretarded force was presented as Equation (3):

$$F_{VdW} = -\frac{2H}{3}\frac{a_p^3}{\delta^2(2a_p + \delta)^2} \qquad (V\text{-}1)$$

By utilizing the nondimensional variables given in Appendix IV, it can be shown that this expression must be multiplied by $(\underline{A}/\underline{mU^2})$ when added to the radial component trajectory equation. Thus the term to be included in the motion equation has the form:

$$F_{VdW} = -\frac{2H}{3\,U^2\,m}\,\frac{a_p^3}{\delta^2(2a_p + \delta)^2} \qquad (V\text{-}2)$$

The result is provided as Equation (32).

RETARDATION CORRECTION FACTOR

It was mentioned previously that the magnitude of Van der Waals force is reduced by the retardation correction factor, α, which takes into consideration the distance of separation between the interacting bodies. Assuming a sphere-flat plate system, previous investigators (7,41) have presented methods for obtaining an expression for this parameter. The following description is similar to these. Two assumptions must be made at this point. First, it is

assumed that the energy potential between each pair of atoms in the solid bodies is unaffected by neighboring atoms. Secondly, these potentials are assumed additive. Figure 29 is a schematic diagram showing the variables involved with this type of interaction. Ideally, there are three separate expressions possible for α, depending on the magnitude of separation distance. In the present study, only one of these was considered, this represented the situation where all atoms of the sphere were at a distance greater than $3\lambda_e/2\pi = 480$ A from the flat surface. It was felt that further refinement for smaller distances would not be relevant in view of such complications as fiber roughness. Thus the potential between two atoms can be obtained by integrating the following equation:

$$\Gamma_{VdW}^{ret} = -2H \int_0^{2a_p} dx\, x(2a_p - x) \int_0^{\infty} db \int_0^{\infty} dl\, 1 \left(\frac{2.45\,\lambda_e}{2\pi\, r^7} - \frac{2.04\,\lambda_e^2}{4\,\pi^2\, r^8} \right) \tag{V-3}$$

$$r = \sqrt{(x + b + \delta)^2 + l^2} \tag{V-4}$$

Upon integration, this expression assumes the form:

$$\Gamma_{VdW}^{ret} = -H \left\{ \frac{2.45\,\lambda_e}{60\pi} \left[\frac{2}{(2a_p + \delta)} - \frac{(2a_p + \delta)}{(2a_p + \delta)^2} + \frac{a_p}{\delta^2} - \frac{1}{\delta} \right] - \right.$$

$$\left. \frac{2.04\,\lambda_e^2}{720\,\pi^2} \left[\frac{2a_p}{\delta^3} - \frac{1}{\delta^2} + \frac{2}{(2a_p + \delta)^2} - \frac{\delta}{(2a_p + \delta)^3} \right] \right\} \tag{V-5}$$

The Van der Waals retarded force can be obtained from this potential expression by applying the following:

$$F_{VdW}^{ret} = \frac{d\Gamma_{VdW}^{ret}}{d\,\delta} \tag{V-6}$$

The result of this derivation is:

$$F_{VdW}^{ret} = \left\{ -\frac{2H}{3} \frac{a_p^3}{\delta^2(2a_p + \delta)^2} \right\} \frac{1}{a_p^3} \left\{ 0.1225 \frac{\lambda e}{2\pi} \left[\frac{(2a_p - \delta)(2a_p + \delta)^2}{\delta} + \frac{(4a_p + \delta)\delta^2}{(2a_p + \delta)} \right] - 0.034 \left(\frac{\lambda_e}{2\pi}\right)^2 \left[\frac{(3a_p - \delta)(2a_p + \delta)^2}{\delta^2} + \frac{(5a_p + \delta)\delta^2}{(2a_p + \delta)^2} \right] \right\} \quad \text{(V-7)}$$

The first term within brackets is the expression for the unretarded force. Therefore, the remainder of the equation is representative of α.

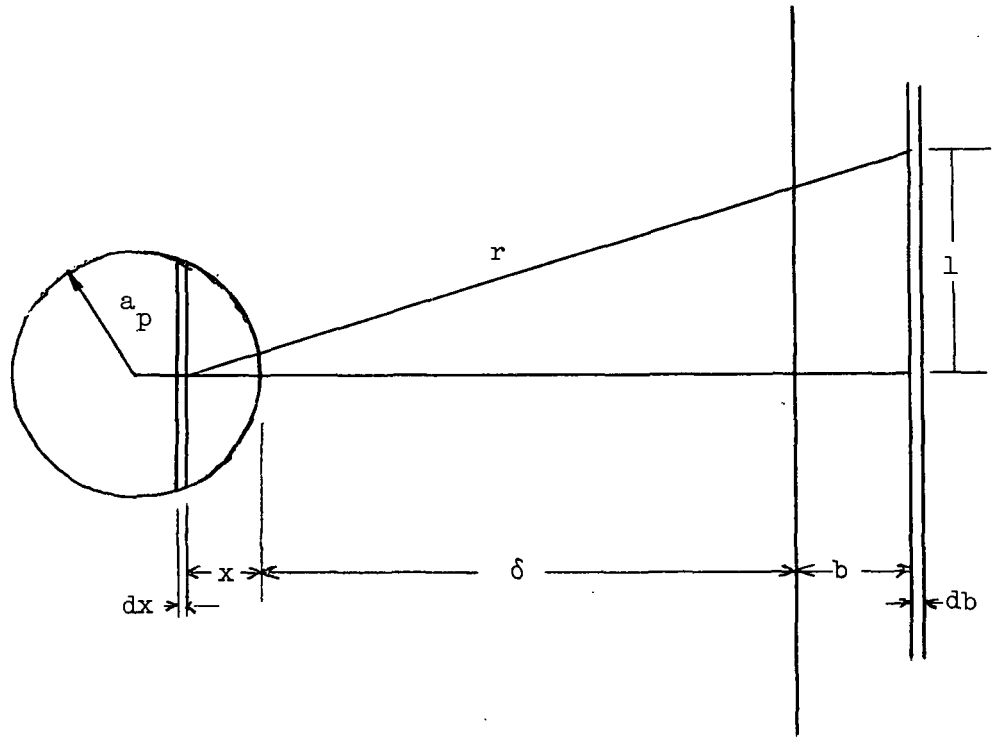

Figure 29. Nomenclature for the Potential Expression Between a Sphere and a Flat Plate

DOUBLE-LAYER FORCE

The force caused by the overlapping of double layers associated with a sphere and a flat plate was given previously:

$$F_{DL} = \varepsilon_d a_p \kappa \left\{ \zeta_1 \zeta_2 \frac{e^{-\kappa\delta}}{(1 + e^{-\kappa\delta})} - \tfrac{1}{2} (\zeta_1 - \zeta_2)^2 \frac{e^{-2\kappa\delta}}{(1 - e^{-2\kappa\delta})} \right\} \qquad (V\text{-}8)$$

Multiplying this expression by (A/mU^2) will make the units of force nondimensional. The final form of the equation is:

$$F_{DL} = \frac{\varepsilon_d a_p \kappa a^2}{(300)^2 mU^2} \left\{ \zeta_1 \zeta_2 \frac{e^{-A\kappa\delta}}{(1 + e^{-A\kappa\delta})} - \tfrac{1}{2} (\zeta_1 - \zeta_2)^2 \frac{e^{-2A\kappa\delta}}{(1 - e^{-2A\kappa\delta})} \right\} \qquad (V\text{-}9)$$

The factor (300) arises from the fact that the zeta potentials represented in this equation are expressed in volts. This had to be converted into units of force. The transition was made by utilizing the statvolt which is equivalent to 300 volts, and is a unit of potential in the cgs electrostatic system.

With the inclusion of the double-layer expression into the radial component equation for particle motion, Equation (34) is obtained. This is the trajectory equation most commonly used in the computer program.

APPENDIX VI

FORTRAN IV LISTING: PARTICLE TRAJECTORY PROGRAM; SOLUTION OF EQUATIONS (34) AND (35)

```
/JOB GO
/FILE TAPE=(1,BLK=2000),RSIZ=20
/FILE DISK=(2,NREC=10000),RSIZ=20
C
C                          PARTICLE TRAJECTORY PROGRAM
C                              DAVID A. DYER   1976
C
C                                  PROGRAM  DAD500
C
C          THIS PROGRAM CALCULATES THE PARTICLE TRAJECTORIES BY TAKING
C          INTO ACCOUNT THE DRAG FORCE EXERTED ON THE PARTICLE.  THE
C          EFFECT OF BOTH UNRETARDED AND RETARDED VAN DER WAALS FORCES
C          AND A DOUBLE LAYER INTERACTION CAN BE APPLIED SEPARATELY TO
C          THESE PARTICLE TRAJECTORIES.  THE INCLUSION OF APPROPRIATE
C          SUBROUTINES WILL ALLOW THE MONITORING OF THE EFFECT CAUSED
C          BROWNIAN MOTION OR DIFFUSION.  THESE SUBROUTINES ARE NOT
C          PROVIDED WITHIN THIS LISTING.
C
C          THE TRAJECTORIES ARE PRODUCED BY THE SOLUTION OF TWO SECOND
C          ORDER DIFFERENTIAL EQUATIONS, ACCOMPLISHED BY EMPLOYING AN
C          APPROPRIATE ALGORITHM OF THE RUNGE-KUTTA METHOD OF NUMERICAL
C          INTEGRATION.
C
C          THIS PROCEDURE PROVIDES INDIVIDUAL COORDINATES OF THE PARTI-
C          CLE TRAJECTORY, WHEN CONNECTED, THEY REPRODUCE THE PREDICTED
C          PATH THAT A PARTICLE ASSUMES AS IT TRAVELS AROUND A FIBER.
C          THIS PROGRAM STORES THESE COORDINATES ON DISK AND THEN
C          TRANSFERS A MAXIMUM OF 2000 INDIVIDUAL POINTS TO TAPE FOR
C          STORAGE AND SUBSEQUENT USE IN PLOTTING.
C
      DOUBLE PRECISION THETA,A,B,D,DT,U,VIS,RHOP,COEFF,C1,C2,C3,C4,FC
      DOUBLE PRECISION R,VELR,VELT,R1,THETA1,VELR1,VELT1,MULT3
      DOUBLE PRECISION P,HAM,XSTOP,YSTOP,AP,VDWC,M,X,Y,KAPPA
      DOUBLE PRECISION OOAP3,XLAMDA,MULT1,MULT2,AP2,AP3,AP4,AP5,MULT4
      DOUBLE PRECISION DTO6,OO6,RI,DIEL,ZETA1,ZETA2
      DOUBLE PRECISION DELTA,ALPHA,XMULT,FDL,CHECK
      COMMON C1,C2,C3,FC,COEFF
      COMMON R,THETA,VELR,VELT,DT
      COMMON R1,VELR1,THETA1,VELT1,KAPPA
      COMMON A,AP,VDWC,DTO6,OO6
      COMMON OOAP3,XLAMDA,MULT1,MULT2,AP2
      COMMON AP3,AP4,AP5,MULT3,MULT4
      COMMON DELTA,ALPHA,XMULT,FDL
C
C          READ THE APPROPRIATE SYSTEM VARIABLES FOR THE PARTICULAR
C          PROBLEM TO BE MODELED.
C               A = FIBER RADIUS
C               B = FLUID ENVELOPE RADIUS
C               D = PARTICLE DIAMETER
C               DT = TIME STEP
C               U = FLUID APPROACH VELOCITY
C               THETA = INITIAL ANGLE
C
    1 READ (5,9017) A, B, D, DT, U
    2 READ (5,9016) THETA
      IF (THETA) 3,15,3
    3 IF (THETA - 5.0) 4,1,1
    4 OO6=1.DO/6.DO
      REWIND 2
```

```
      DT06=DT*006
C
C          DEFINE PHYSICAL PARAMETERS COMMON TO ALL SYSTEMS STUDIED.
C
      VIS = 0.00001
      RHOP = 4.0/980.
      COEFF = (18. * VIS * A)/(D**2 * RHOP * U)
      HAM = 3.22D-13
      M = 3.14159/6.0 * D**3 * RHOP
      AP = D/(A*2.0)
      VDWC = 2.0/(3.0*U*U)*(HAM/M) * AP**3
      OOAP3 = 1.DO/(AP*AP*AP)
      XLAMDA = 0.00159155
      MULT1 = 0.1225 * XLAMDA
      MULT2 = 0.034 * XLAMDA * XLAMDA
      AP2 = 2.DO * AP
      AP3 = 3.DO * AP
      AP4 = 4.DO * AP
      AP5 = 5.DO * AP
      DIEL = 81.
      KAPPA = 4.57D+06
      ZETA1 = -0.025
      ZETA2 = -0.015
      MULT3 = (DIEL * KAPPA * AP * ZETA1 * ZETA2)/(300. * M * U * U)
      MULT4 = (DIEL * KAPPA * AP * (ZETA1 - ZETA2)**2)   /(600. * M * U
     1* U)
      C = (A/B)**2
      C1 = C * C
      C2 = 2. * (1. + C1)
      C3 = (A/B)
      C4 = 1. - C
      FC = C1 - 1. - C2 * DLOG(C3)
      WRITE (6,9019) DT,C4,THETA,COEFF,FC,D
      WRITE (6,9020)
      J = 1
      INC = 100
      K = INC
C
C          THE INITIAL POSITION OF THE PARTICLE IS DEFINED BY RI AND
C          THETA.
C
      R = B/A
      RI = R
      P =  R * 5.00 / RI
      X      = P * DCOS(THETA)
      Y      = P * DSIN(THETA)
      KTR = 1
      WRITE (2,9005) X, Y
C
C           CALCULATE INITIAL RADIAL AND ANGULAR VELOCITY COMPONENTS.
C
      VELR = -U * DCOS(THETA)
      VELT = (3.*C1*R*R + 1./R/R - C2*(DLOG(C3*R)+1.) - FC)
      VELT = -DSIN(THETA)*VELT/(R*FC)
      WRITE (6,9018) J, R, THETA, VELR, VELT
C
C          CALCULATE A NEW PARTICLE POSITION BY SOLVING THE MOTION
C          EQUATIONS IN THE FOLLOWING TWO SUBROUTINES.  NEWR PRODUCES
C          A NEW RADIAL POSITION AND VELOCITY, WHILE NEWTH YIELDS THE
C          THE SAME RESULTS FOR THE ANGULAR COMPONENT.
```

```
C
    6 CONTINUE
      CALL NEWR
      CALL NEWTH
      J = J + 1
      R = R1
      THETA = THETA1
      VELR = VELR1
      VELT = VELT1
      SIG = 1.
      IF (DELTA - 0.005) 111, 111, 112
  111 CHECK = DABS(DELTA - DELTA1)
      IF (CHECK - 1.D-08 ) 110, 110, 17
  110 SIG = -1.
      WRITE (6,9023) DELTA
      GO TO 11
   17 DELTA1 = DELTA
  112 IF (XLAMDA) 11,11,16
   16 IF (J - K) 8,7,8
C
C         CALCULATE THE X AND Y COORDINATES TO BE USED IN PLOTTING.
C
    7 P =  R * 5.00 / RI
      X      = P * DCOS(THETA)
      Y      = P * DSIN(THETA)
      KTR = KTR + 1
      WRITE (2,9005) X, Y
      WRITE (6,9018) J, R, THETA, VELR, VELT
C
C         CHECK THE POSITION OF THE PARTICLE TO INSURE THAT IT IS STILL
C         WITHIN THE UNIT CELL OR HAS IMPACTED ON THE FIBER.  IF IT HAS
C         IMPACTED OR EXITED THE CELL, THE TRAJECTORY IS TERMINATED.
C
      K = K + INC
    8 IF(R-1.D0-AP) 11,11,9
    9 IF(R - RI) 10,10,11
   10 IF(THETA-3.14159D0) 6,6,11
   11 ENDFILE 2
      REWIND 2
C
C         CALCULATE AND TRANSFER APPROPRIATE NUMBER OF POINTS FROM THE
C         DISK TO TAPE.  THE MAXIMUM IS 2000 INDIVIDUAL POINTS.
C
      IN = KTR/2000 + 1
      DO 13 I=1,KTR
      READ (2,9005) X, Y
      IF (I - IN*(I/IN)) 13,12,13
   12 WRITE (1,9005) X, Y
   13 CONTINUE
      X = SIG * 100.
      Y = SIG * 100.
      WRITE (1,9005) X, Y
      WRITE (6,9021)
      WRITE (6,9018) J, R, THETA
      WRITE (6,9022) XLAMDA
      NTAPE = KTR/IN
      WRITE (6,9014) KTR, IN, NTAPE
      GO TO 2
   15 ENDFILE 1
      CALL EXIT
```

```
C
C         ARRANGEMENTS
C
 9005 FORMAT (2A8,4X)
 9014 FORMAT (1HO,'NUMBER POINTS CALCULATED =',I6,2X,'INCREMENT =',I3,
     1    'POINTS ON TAPE FOR PLOTTING =',I5,///)
 9016 FORMAT (F7.4)
 9017 FORMAT (5F10.0)
 9018 FORMAT (1H ,I9,7D17.9)
 9019 FORMAT (1HO,'RESULTS OF PROGRAM DAD500',//,' TIME STEP=',F9.5,
     1/,' POROSITY = ',F9.5,/,' INITIAL ANGLE =',F7.4,//,' COEFF = ',
     2D15.9,/,' F(C) =  ',D15.9,//,' PARTICLE DIAMETER =',F10.6)
 9020 FORMAT (1HO,'POSITION',9X,'R',15X,'THETA',12X,'R VEL',11X,
     1'ANG VEL')
 9021 FORMAT (1HO,'FINAL POSITION')
 9022 FORMAT (1H ,'XLAMDA =',F10.4)
 9023 FORMAT(1H ,'TRAJECTORY LOCKED IN AT DELTA = ',D17.9)
      END
      SUBROUTINE NEWR
C
C           THIS SUBROUTINE EMPLOYS THE RUNGE-KUTTA METHOD OF NUM-
C           ERICAL INTEGRATION TO OBTAIN A NEW RADIAL POSITION AND
C           VELOCTIY OF THE PARTICLE.
C
      DOUBLE PRECISION C1,C2,C3,FC,COEFF,R,THETA,VELR,VELT,DT,MULT3
      DOUBLE PRECISION UR1,UR2,UR3,UR4,M1,M2,M3,M4,R1,VELR1,MULT4
      DOUBLE PRECISION BLANKC,BLANKD,KAPPA, A,AP,VDWC,DCT,VTS
      DOUBLE PRECISION DTVR,DTVR2,DTM22,M22,DM14,DT06,006,F1,G1
      DOUBLE PRECISION 00AP3,XLAMDA,MULT1,MULT2,AP2,AP3,AP4,AP5
      DOUBLE PRECISION DELTA, ALPHA, XMULT, FDL
      COMMON C1,C2,C3,FC,COEFF
      COMMON R,THETA,VELR,VELT,DT
      COMMON R1,VELR1,BLANKC,BLANKD,KAPPA
      COMMON A,AP,VDWC,DT06,006
      COMMON 00AP3,XLAMDA,MULT1,MULT2,AP2
      COMMON AP3,AP4,AP5,MULT3,MULT4
      COMMON DELTA,ALPHA,XMULT,FDL
C
      DCT=DCOS(THETA)/FC
      VTS=VELT*VELT
      DTVR=DT*VELR
      DTVR2=DTVR*.5D0
      UR1 = F1 (R)*DCT
      M1 = DT * G1 (UR1,VTS,VELR,R)
      UR2 = F1 (R+DTVR2)*DCT
      M2 = DT * G1 (UR2,VTS,VELR+M1*.5D0,R+DTVR2)
      M22=M2*.5D0
      DM14=DT*M1*.25D0
      UR3 = F1 (R+DTVR2+DM14)*DCT
      M3 = DT * G1 (UR3,VTS,VELR+M22,R+DTVR2+DM14)
      DTM22=DT*M22
      UR4 = F1 (R+DTVR+DTM22)*DCT
      M4 = DT * G1 (UR4,VTS,VELR+M3,R+DTVR+DTM22)
C        THE NEW RADIAL POSITION AND VELOCITY ARE R1 AND VELR1
C
C
      R1 = R + DTVR     + (DT06 )*(M1 + M2 + M3)
      VELR1 = VELR + (006  ) * (M1 + 2.*M2 + 2.*M3 + M4)
      RETURN
      END
```

```
      DOUBLE PRECISION FUNCTION F1(R)
      DOUBLE PRECISION C1,C2,C3,FC,R,RS
      COMMON C1,C2,C3,FC
C
C          FUNCTION F1 IS USED TO CALCULATE A RADIAL VELOCITY AT ANY
C          POSITION RS AND THETA.
C
      RS=R*R
      F1 = (C1*RS-1.D0/RS-C2*DLOG(R*C3)-FC)
      RETURN
      END
      DOUBLE PRECISION FUNCTION G1(UR,VELT,VELR,R)
      DOUBLE PRECISION COEFF,UR,VELT,VELR,R,OOAP3,XLAMDA,MULT1,MULT2,AP5
      DOUBLE PRECISION AP,VDWC,VDWF,DELTA,DM1(4),DM2( 9),A,AP2,AP3,AP4
      DOUBLE PRECISION ALPHA,FACT1,FACT12,DELTA2,BLANKA,BLANKB,VDWFR
      DOUBLE PRECISION KAPPA,MULT3,MULT4,POWER1,POWER2,FDL,XMULT
      COMMON DM1,   COEFF
      COMMON DM2,KAPPA
      COMMON A,AP,VDWC,BLANKA,BLANKB
      COMMON OOAP3,XLAMDA,MULT1,MULT2,AP2
      COMMON AP3,AP4,AP5,MULT3,MULT4
      COMMON DELTA,ALPHA,XMULT,FDL
C
C          FUNCTION G1 REPRESENTS THE RADIAL MOTION EQUATION AND REFLECTS
C          THE EFFECTS OF ALL FORCES APPLIED TO PARTICLE MOTION.
C
      DELTA = R -1.D0 - AP
      FACT1 = AP2 + DELTA
      FACT12 = FACT1 * FACT1
      DELTA2 = DELTA * DELTA
C
C          CALCULATION OF VAN DER WAALS FORCE.
C
      VDWF = VDWC / (DELTA2 * FACT12)
      ALPHA = OOAP3*(MULT1*((AP2-DELTA)*FACT12/DELTA+ (AP4+DELTA)*
     1    DELTA2/FACT1) - MULT2*((AP3-DELTA)*FACT12/DELTA2 + (AP5+DELTA)
     2    *DELTA2/FACT12))
      IF (ALPHA) 25,26,26
   25 XLAMDA = 0.0
   26 IF (ALPHA - 1.0) 29,28,28
   28 XLAMDA = 0.0
   29 IF (DELTA - 0.001) 27,27,21
   27 XLAMDA = -1.
      GO TO 23
C
C          CALCULATION OF THE DOUBLE LAYER INTERACTION.
C
   21 XMULT = KAPPA *DELTA * A
      IF (XMULT - 100.) 22,22,23
   22 POWER1 = DEXP(-XMULT)
      FDL = MULT3*POWER1/(1.-POWER1)-MULT4*POWER1/((1./POWER1)-POWER1)
      GO TO 24
   23 FDL = 0.
   24 G1 = COEFF * (UR - VELR) + R*VELT - VDWF*ALPHA + FDL
      RETURN
      END
      SUBROUTINE NEWTH
C
C          THIS SUBROUTINE PROVIDES FOR THE NUMERICAL INTEGRATION OF
C          THE ANGULAR COMPONENT EQUATION OF PARTICLE MOTION.  THE
```

```
C           RESULTS ARE A NEW ANGULAR POSITION AND VELOCITY.
C
      DOUBLE PRECISION C1,C2,C3,FC,COEFF,R,THETA,VELR,VELT,DT
      DOUBLE PRECISION UTH1,UTH2,UTH3,UTH4,M1,M2,M3,M4,THETA1,VELT1
      DOUBLE PRECISION BLANKA,BLANKB,BLANKE,BLANKF,BLANKG,BLANKH
      DOUBLE PRECISION FNC,RS,VLOR,DTVT,M22,DT2,DTO6,OO6,F2,G2
      COMMON C1,C2,C3,FC,COEFF
      COMMON R,THETA,VELR,VELT,DT
      COMMON BLANKA,BLANKB,THETA1,VELT1,BLANKE
      COMMON BLANKF,BLANKG,BLANKH,DTO6,OO6
C
      RS=R*R
      VLOR=VELR/R*2.DO
      FNC=(3.DO*C1*RS+1.DO/RS-C2*(DLOG(C3*R)+1.DO)-FC)/FC
      DTVT=DT*VELT
      DT2=DTVT*.5DO
      UTH1 = F2 (THETA)*FNC
      M1 = DT * G2          (VLOR,UTH1,VELT)
      UTH2 = F2 (THETA+DT2)*FNC
      M2 = DT * G2          (VLOR,UTH2,VELT+M1*.5DO)
      M22=M2*.5DO
      UTH3 = F2 (THETA+DT2+DT*M1*.25DO)*FNC
      M3 = DT * G2          (VLOR,UTH3,VELT+M22)
      UTH4 = F2 (THETA+DT*M22+DTVT)*FNC
      M4 = DT * G2          (VLOR,UTH4,VELT+M3)
C
C        THE NEW ANGULAR POSITION AND VELOCITY ARE THETA1 AND VELT1
C
      THETA1 = THETA + DTVT     + (DTO6 ) * (M1 + M2 + M3)
      VELT1 = VELT + (OO6  ) * (M1 + 2.*M2 + 2.*M3 + M4)
      RETURN
      END
      DOUBLE PRECISION FUNCTION F2(THETA)
      DOUBLE PRECISION                 THETA
C
C         FUNCTION F2 REPRESENTS THE EXPRESSION FOR ANGULAR VELOCITY.
C
      F2 = -DSIN(THETA)
      RETURN
      END
      DOUBLE PRECISION FUNCTION G2(VLOR,UTH,VELT)
      DOUBLE PRECISION COEFF,R,VELR,UTH,VELT,DM1(4),DM2,VLOR
      COMMON DM1,COEFF,R
C
C         FUNCTION G2 IS THE EXPRESSION FOR THE ANGULAR MOTION EQUATION.
C
      G2 = COEFF * (UTH/R - VELT) - VLOR*VELT
      RETURN
      END

/END CARD READ, JOB TERMINATED
```

APPENDIX VII

FORTRAN IV LISTING: PROGRAM FOR PLOTTING PARTICLE TRAJECTORIES

```
/JOB GO,TIME=20
/FILE TAPE=(1,BLK=2000),RSIZ=20
C
C                        TRAJECTORY PLOTTING PROGRAM
C                           DAVID A. DYER     1977
C
C         THE FUNCTION OF THIS PROGRAM IS TO PLOT VARIOUS TRAJECTORIES
C         THAT HAVE BEEN STORED ON MAGNETIC TAPE.  THE PARTICULAR
C         SET OF POINTS TO BE PLOTTED IS DETERMINED FROM THE DATA
C         INPUT.  THE TRAJECTORY IS PLOTTED WITHIN A MODIFIED DIAGRAM
C         OF THE UNIT CELL.
C
      DOUBLE PRECISION X(2000),Y(2000)
      DOUBLE PRECISION A, B
      DIMENSION NPLOT(10)
      INTEGER HEAD1(9),HEAD2(9),HEAD3(9),HEAD4(9),HEAD5(6),HEAD6(9)
      INTEGER HEAD7(9),HEAD8(9),HEAD9(9),HEAD10(9),HEAD11(9),HEAD12(9)
      CALL ITLZ
      CALL DPT(1,4)
C
C         THE FOLLOWING STATEMENTS PROVIDE FOR THE CONSTRUCTION OF THE
C         UNIT CELL.
C
      CALL PLOT (0.0,-11.0,2)
      CALL PLOT (0.0,-10.5,-3)
      CALL PLOT (7.5,5.0,-3)
      MOD2 = 1
      CALL DASH (3,MOD2,0.612,5.1,0.0,-5.3,0.0)
      CALL DASH (3,MOD2,0.612,0.0,5.3,0.0,-0.5)
      CALL PLOT (0.0,0.0,3)
      CALL CIRCLE(0.0,0.0,0.0,180.,2.50)
      CALL CIRCLE(0.0,0.0,0.0,180.,5.0)
      READ (5,9001) HEAD1
      CALL SYMBOL (5.5,2.4,0.21,HEAD1,270.,22)
      READ (5,9001) HEAD3
      CALL SYMBOL (4.8,-0.25,0.14,HEAD3,270.,23)
      READ (5,9001) HEAD4
      CALL SYMBOL (2.5,-0.25,0.14,HEAD4,270.,23)
      READ (5,9001) HEAD5
      CALL SYMBOL (-3.0,-0.25,0.14,HEAD5,270.,15)
      READ (5,9001) HEAD6
      CALL SYMBOL (-3.5,-0.25,0.14,HEAD6,270.,24)
      READ (5,9001) HEAD7
      CALL SYMBOL (-4.0,-0.25,0.14,HEAD7,270.,23)
      READ (5,9001) HEAD9
      CALL SYMBOL (-4.5,-0.25,0.14,HEAD9,270.,30)
      READ (5,9001) HEAD10
      CALL SYMBOL (-4.8,-0.25,0.14,HEAD10,270.,30)
C     READ (5,210) HEAD11
C     CALL SYMBOL (-5.3,-0.25,0.14,HEAD11,270.,30)
C     READ (5,210) HEAD12
C     CALL SYMBOL (-2.5,3.5,0.14,HEAD12,270.,15)
C
C         THE TERM  K  REPRESENTS THE TOTAL NUMBER OF TRAJECTORIES TO BE
C         PLOTTED ON A SINGLE DIAGRAM.  THE TERM  KK  REPRESENTS THE
C         LAST TRAJECTORY ON THE STORAGE TAPE TO BE READ.
C
      K =  4
      KK =  4
```

```
      DO 2 J=1,K
    2 READ (5,9003) NPLOT(J)
C
      MM = 193
      J = 1
      KTR = 1
    4 IF (KTR - NPLOT(J)) 5,8,5
    5 READ (1,9009) A, B
      IF (DABS(A) - 100.) 5,6,6
    6 IF (KTR - KK) 7,16,16
    7 KTR = KTR + 1
      GO TO 4
C
    8 NUM = 1
      READ (1,9009) X(NUM),Y(NUM)
      CALL PLOT (X(NUM),Y(NUM),4)
   10 NUM = NUM + 1
      READ (1,9009) X(NUM),Y(NUM)
      IF (DABS(X(NUM)) - 100.) 11,12,12
   11 CALL PLOT (X(NUM),Y(NUM),2)
      GO TO 10
   12 CONTINUE
C     CALL DRAW (X(NUM-1),Y(NUM-1),270.,MM,0.0,-1.0,0.07)
      WRITE (6,9014) J
      WRITE (6,9013) NUM
      MM = MM+1
C
      J = J + 1
      IF (KTR - KK) 15,16,16
   15 KTR = KTR + 1
      GO TO 4
C
   16 CONTINUE
      CALL PLOT (0.0,0.0,3)
      CALL FINAL
      CALL EXIT
C
C        ARRANGEMENTS
C
 9001 FORMAT (9A4)
 9003 FORMAT (I2)
 9009 FORMAT (2A8,4X)
 9013 FORMAT (1H0,'NUMBER OF POINTS PLOTTED = ',I9)
 9014 FORMAT (1H0,'CURVE -- ',I2)
      END
/DATA
FLUID STREAMLINES
FLUID ENVELOPE
FIBER
POROSITY = 0.75
TIME STEP = 0.0001
U = 1.00 CM/SEC
I. A. -- 0.01, 0.10
         0.30 & 0.50
    1
    2
    3
    4
      END
```

APPENDIX VIII

ALTERNATE COLLECTION EFFICIENCY DEFINITIONS

As was stated in the section pertaining to the definition of predicted collection efficiency, the choice of the value employed was arbitrary. The concept behind collection efficiency is that it simplifies the results into a straightforward relationship of system variables. The purpose of this appendix is to present two alternative definitions of efficiency which could be used in a system such as the one modeled.

The first of these is similar to the definition used. In the text, η_p was defined as the ratio of the flow area from which particles are removed to the projected area of the fiber. This can be changed to reflect the porosity of the system, or the open areas in a simulated mat, by alteration of the efficiency equation to read:

$$\eta_p' = \frac{N}{A}(1 - \varepsilon)^{\frac{1}{2}} \qquad \text{(VIII-1)}$$

This equation indicates that as porosity approaches one, efficiency would approach zero. This definition makes the efficiency equal to the ratio of flow area for particle removal to the unit cell area. The effect of this change in definition on efficiency values is shown in Table VI, which represents the efficiencies given in Table I as calculated by this new method. As is evident, all values would be significantly lower for this new definition.

TABLE VI

	Efficiency	
Porosity	Unretarded	Retarded
0.75	0.0175	0.0075
0.80	0.0133	0.0055
0.85	0.0095	0.0039

One additional description of efficiency can be thought of as applying to this system. This would be related to particle concentration in the suspension. The particle flux across the fluid envelope for one quadrant of the unit cell could be calculated. The efficiency would then be the number of particles crossing the envelope which impact on the fiber, compared to the total particle flux across the envelope. The flux across a unit length of the envelope would decrease as θ increases; therefore, the efficiency would be a function of this angle. Also, it is thought that the calculation of this efficiency would depend on the fluid velocity values existing at the fluid envelope.

Once again, the choice of collection efficiency definition used in this thesis was arbitrary. The particular one chosen was thought to be comparable to an efficiency calculated from the experimental data. Even though this was also a somewhat artificial value, it was based on projected fiber area. Experimental data could probably be taken which would compare more favorably with other definitions, such as those presented above.

APPENDIX IX

FORTRAN IV LISTING: SUBROUTINES FOR CALCULATING DIFFUSIONAL MOTION

```
      SUBROUTINE DIFFBM (R1,THETA1,R,THETA,XBAR,IX,J,K)
C
C          THIS SUBROUTINE IS DESIGNED TO BE USED WITH THE PARTICLE
C          TRAJECTORY PROGRAM.  ITS FUNCTION IS TO CALCULATE THE EFFECT
C          OF DIFFUSION ON PARTICLE MOTION.  THE METHOD FOR DOING THIS
C          DEPENDS ON EINSTEIN'S DIFFUSION COEFFICIENT AND RANDOM WALK
C          THEORY.
C
      DOUBLE PRECISION R1,THETA1,R,THETA,X1,Y1,XBAR
      CALL RANDU (IX,IY,YFL)
      IX = IY
      IBR = (100. * YFL)/25. + 1
      GO TO (1,2,3,4),IBR
    1 CALL CALC (R1,THETA1,0.,-XBAR,X1,Y1)
      GO TO 5
    2 CALL CALC (R1,THETA1,-XBAR,0.,X1,Y1)
      GO TO 5
    3 CALL CALC (R1,THETA1,0.,XBAR,X1,Y1)
      GO TO 5
    4 CALL CALC (R1,THETA1,XBAR,0.,X1,Y1)
    5 R = (X1**2 + Y1**2)**0.5
      IF (X1) 7,6,6
    6 THETA = DARSIN(Y1/R)
      GO TO 8
    7 THETA = 3.141592654 - DARSIN(Y1/R)
    8 RETURN
      END
      SUBROUTINE RANDU (IX,IY,YFL)
C
C          THIS SUBROUTINE IS USED TO PRODUCE A RANDOM NUMBER.  THIS
C          NUMBER IS USED TO DENOTE THE DIRECTION A PARTICLE TRAVELS AS
C          IT IS INFLUENCED BY DIFFUSION.
C          (MACLAREN AND MARSAGLIA, JACM 12, 83-9)
C
      IY = IX * 65539
      IF (IY) 1,2,2
    1 IY = IY + 2147433647 + 1
    2 YFL = IY
      YFL = YFL * .4656613E-09
      RETURN
      END
      SUBROUTINE CALC (R1,THETA1,CX,CY,X1,Y1)
C
C          THIS SUBROUTINE CALCULATES A NEW PARTICLE POSITION BASED ON
C          THE DISTANCE AND DIRECTION VALUES PROVIDED BY THE DIFFUSION
C          PARAMETERS.
C
      DOUBLE PRECISION R1,THETA1,CX,CY,X1,Y1
      X1 = DCOS(THETA1) * R1 + CX
      Y1 = DSIN(THETA1) * R1 + CY
      Y1 = DABS(Y1)
      RETURN
      END

/END CARD READ, JOB TERMINATED
```

APPENDIX VII

TABLE VII: LISTING OF ALL TRAJECTORIES CALCULATED WITH THE MODEL

The following table contains a listing of all parameters for which trajectories have been calculated with the mathematical model developed in this thesis. Also, it is stated whether or not the individual particles impacted on the fiber. The detailed trajectories corresponding to these conditions are available on computer tape.

TABLE VII

Trajectory Number	Initial Angle (radians)	Porosity	Velocity (cm/sec)	Particle Diameter (μm)	Remarks
1	0.01	0.75	1.00		Fluid streamlines.
2	0.10				Program DAD100
3	0.30				
4	0.50				
5	0.01	0.75	1.00	0.5	Program for indicating
6	0.10				the effect of drag force
7	0.30				on particle trajectories.
8	0.50				Program DAD200
9*	0.01	0.75	1.00	0.5	Inclusion of Van der Waals unretarded forces.
10*	0.01	0.75	1.00	0.3	Program DAD250
11*	0.005	0.75	1.00	0.5	Program DAD300
12*	0.010				
13*	0.011				
14*	0.012				
15*	0.013				
16*	0.014				
17*	0.015				
18*	0.016				
19*	0.017				
20	0.018				
21	0.019				
22	0.010	0.85	1.00	0.5	
23*	0.009				
24*	0.008				
25*	0.007				
26*	0.006				
27*	0.005				

*Denotes that the particle impacted on the fiber surface.

TABLE VII (Continued)

Trajectory Number	Initial Angle (radians)	Porosity	Velocity (cm/sec)	Particle Diameter (μm)	Remarks
28*	0.004				
29*	0.003				
30*	0.002				
31*	0.001				
32*	0.009	0.85	1.00	1.0	Refined program for the
33*	0.007				inclusion of Van der
34*	0.005				Waals forces.
35*	0.003				Program DAD350
36*	0.001				
37*	0.009	0.80	1.00	0.5	
38*	0.010				
39*	0.011				
40*	0.012				
41*	0.013				
42	0.014				
43	0.015				
44*	0.009	0.85	0.78	0.5	
45*	0.007				
46*	0.005				
47*	0.003				
48*	0.001				
49*	0.009	0.85	1.17	0.5	
50*	0.007				
51*	0.005				
52*	0.003				
53*	0.001				
54	0.009	0.85	1.50	0.5	
55*	0.007				
56*	0.005				
57*	0.003				
58*	0.001				
59*	0.017	0.75	0.78	0.5	
60*	0.015				
61*	0.013				
62*	0.011				
63	0.017	0.75	1.17	0.5	
64*	0.015				
65*	0.013				
66*	0.011				

TABLE VII (Continued)

Trajectory Number	Initial Angle (radians)	Porosity	Velocity (cm/sec)	Particle Diameter (μm)	Remarks
67	0.017	0.75	1.50	0.5	
68*	0.015				
69*	0.013				
70*	0.011				
71	0.013	0.75	1.00	0.3	
72*	0.009	0.80	1.00	0.3	
73*	0.004	0.85	1.00	0.3	
74*	0.018	0.75	1.00	1.0	
75*	0.019				
76*	0.020				
77*	0.021				
78*	0.022				
79*	0.023				
80*	0.013	0.80	1.00	1.0	
81*	0.014				
82*	0.015				
83*	0.016				
84*	0.017				
85*	0.018				
86*	0.019				
87*	0.020				
88*	0.010	0.085	1.00	1.0	
89*	0.011				
90*	0.012				
91*	0.013				
92*	0.014				
93*	0.015				
94*	0.018	0.75	0.78	0.5	
95*	0.019				
96	0.020				
97*	0.016	0.75	1.17	0.5	
98	0.016	0.75	1.50	0.5	
99*	0.010	0.85	0.78	0.5	
100	0.011				
101	0.012				
102	0.010	0.85	1.17	0.5	
103	0.011				
104	0.008	0.85	1.50	0.5	

TABLE VII (Continued)

Trajectory Number	Initial Angle (radians)	Porosity	Velocity (cm/sec)	Particle Diameter (μm)	Remarks
105*	0.010	0.75	1.00	0.5	Hamaker constant = 3.22×10^{-13}
106*	0.001	0.75	1.00	0.5	Hamaker constant +
107*	0.002				3.5×10^{-14}
108*	0.003				
109*	0.004				
110*	0.005				
111*	0.006				
112*	0.007				
113*	0.008				
114	0.009				
115	0.010				
116*	0.010	0.75	1.00	0.5	Hamaker constant =
117*	0.015				3.0×10^{-11}
118*	0.016				
119*	0.017				
120*	0.018				
121*	0.019				
122*	0.020				
123*	0.021				
124*	0.022				
125*	0.023				
126*	0.024				
127*	0.025				
128*	0.005	0.85	1.00	0.5	Hamaker constant = 3.22×10^{-13}
129*	0.001	0.85	1.00	0.5	Hamaker cOnstant =
130*	0.002				3.5×10^{-14}
131*	0.003				
132*	0.004				
133	0.005				
134*	0.005	0.85	1.00	0.5	Hamaker constant =
135*	0.006				3.0×10^{-11}
136*	0.007				
137*	0.008				
138*	0.009				
139*	0.010				
140*	0.002	0.80	1.00	0.5	Inclusion of the retarda-
141*	0.003				factor in Van der Waals
142*	0.004				forces.
143*	0.005				Program DAD400
144	0.006				

TABLE VII (Continued)

Trajectory Number	Initial Angle (radians)	Porosity	Velocity (cm/sec)	Particle Diameter (μm)	Remarks
145*	0.001	0.85	1.00	0.5	
146*	0.002				
147*	0.003				
148	0.004				
149	0.005				
150*	0.071	0.75	1.00	0.5	Hamaker constant = 3.0×10^{-11}
151*	0.072				
152*	0.073				Program DAD350
153*	0.074				
154*	0.075				
155*	0.076				
156	0.077				
157	0.078				
158*	0.051	0.75	1.00	0.5	Hamaker constant = 3.0×10^{-11}
159*	0.052				
160*	0.053				
161*	0.054				
162*	0.055				
163*	0.056				
164*	0.057				
165	0.058				
166	0.059				
167*	0.041	0.80	1.00	0.5	Hamaker constant = 3.0×10^{-11}
168	0.042				
169*	0.004	0.75	1.00	0.5	Program DAD400
170*	0.005				
171*	0.006				
172*	0.007				
173	0.008				
174	0.009				
175	0.010				
176*	0.005	0.75	1.00	1.0	
177*	0.010				
178*	0.011				
179*	0.012				
180*	0.013				
181	0.014				
182	0.015				
183*	0.005	0.75	0.78	0.5	
184*	0.006				
185*	0.007				
186	0.008				
187	0.009				
188	0.010				

TABLE VII (Continued)

Trajectory Number	Initial Angle (radians)	Porosity	Velocity (cm/sec)	Particle Diameter (μm)	Remarks
189*	0.005	0.75	1.17	0.5	
190*	0.006				
191*	0.007				
192	0.008				
193	0.009				
194	0.010				
195*	0.005	0.75	1.50	0.5	
196*	0.006				
197	0.007				
198	0.008				
199	0.009				
200	0.010				
201*	0.010	0.75	1.50	1.0	
202*	0.011				
203*	0.012				
204	0.013				
205	0.014				
206*	0.001	0.85	0.78	0.5	
207*	0.002				
208*	0.003				
209*	0.004				
210	0.005				
211	0.006				
212*	0.001	0.85	1.00	0.5	
213*	0.002				
214*	0.003				
215	0.004				
216	0.005				
217*	0.001	0.85	1.17	0.5	
218*	0.002				
219*	0.003				
220	0.004				
221	0.005				
222*	0.001	0.85	1.50	0.5	
223*	0.002				
224*	0.003				
225	0.004				
226	0.005				
227*	0.005	0.85	1.00	1.0	
228*	0.006				
229	0.007				
230	0.008				

TABLE VII (Continued)

Trajectory Number	Initial Angle (radians)	Porosity	Velocity (cm/sec)	Particle Diameter (μm)	Remarks
231*	0.005	0.85	1.50	1.0	
232*	0.006				
233	0.007				
234	0.008				
235*	0.003	0.80	0.78	0.5	
236*	0.004				
237*	0.005				
238	0.006				
239	0.007				
240*	0.003	0.80	1.00	0.5	
241*	0.004				
242*	0.005				
243	0.006				
244	0.007				
245*	0.003	0.80	1.17	0.5	
246*	0.004				
247*	0.005				
248	0.006				
249	0.007				
250*	0.003	0.80	1.50	0.5	
251*	0.004				
252	0.005				
253	0.006				
254*	0.008	0.80	1.00	1.0	
255*	0.009				
256	0.010				
257	0.011				
258*	0.008	0.80	1.50	1.0	
259*	0.009				
260	0.010				
261	0.011				
262*	0.0071	0.75	0.78	0.5	
263*	0.0072				
264*	0.0073				
265*	0.0074				
266*	0.0075				
267*	0.0076				
268*	0.0077				
269*	0.0078				
270*	0.0079				

TABLE VII (Continued)

Trajectory Number	Initial Angle (radians)	Porosity	Velocity (cm/sec)	Particle Diameter (μm)	Remarks
271*	0.0071	0.75	1.00	0.5	
272*	0.0072				
273*	0.0073				
274*	0.0074				
275	0.0075				
276	0.0076				
277*	0.0071	0.75	1.17	0.5	
278	0.0072				
279	0.0073				
280*	0.0031	0.85	1.00	0.5	
281*	0.0032				
282*	0.0033				
283*	0.0034				
284*	0.0035				
285*	0.0036				
286*	0.0037				
287*	0.0038				
288	0.0039				
289*	0.0031	0.85	1.17	0.5	
290*	0.0032				
291*	0.0033				
292*	0.0034				
293*	0.0035				
294*	0.0036				
295	0.0037				
296	0.0038				
297*	0.0031	0.85	1.50	0.5	
298*	0.0032				
299*	0.0033				
300*	0.0034				
301	0.0035				
302	0.0036				
303*	0.0051	0.80	0.78	0.5	
304*	0.0052				
305*	0.0053				
306*	0.0054				
307*	0.0055				
308*	0.0056				
309*	0.0057				
310*	0.0058				
311	0.0059				

TABLE VII (Continued)

Trajectory Number	Initial Angle (radians)	Porosity	Velocity (cm/sec)	Particle Diameter (μm)	Remarks
312*	0.0051	0.80	1.00	0.5	
313*	0.0052				
314*	0.0053				
315*	0.0054				
316	0.0055				
317	0.0056				
318*	0.0051	0.80	1.17	0.5	
319*	0.0052				
320	0.0053				
321	0.0054				
322*	0.0134	0.75	0.78	1.0	
323*	0.0136				
324*	0.0138				
325*	0.0140				
326*	0.0142				
327	0.0144				
328*	0.0132	0.75	1.00	1.0	
329*	0.0134				
330	0.0136				
331	0.0138				
332*	0.0124	0.75	1.17	1.0	
333*	0.0126				
334*	0.0128				
335*	0.0130				
336	0.0132				
337	0.0134				
338*	0.0122	0.75	1.50	1.0	
339*	0.0124				
340	0.0128				
341*	0.0065	0.85	0.78	1.0	
342*	0.0066				
343*	0.0067				
344*	0.0068				
345*	0.0069				
346*	0.0070				
347*	0.0071				
348*	0.0072				
349	0.0073				
350	0.0074				

TABLE VII (Continued)

Trajectory Number	Initial Angle (radians)	Porosity	Velocity (cm/sec)	Particle Diameter (μm)	Remarks
351*	0.0061	0.85	1.00	1.0	
352*	0.0062				
353*	0.0063				
354*	0.0064				
355*	0.0065				
356*	0.0066				
357*	0.0067				
358*	0.0068				
359	0.0069				
360*	0.0061	0.85	1.17	1.0	
361*	0.0062				
362*	0.0063				
363*	0.0064				
364*	0.0065				
365*	0.0066				
366	0.0067				
367	0.0068				
368*	0.0061	0.85	1.50	1.0	
369*	0.0062				
370	0.0063				
371*	0.0096	0.80	0.78	1.0	
372*	0.0098				
373*	0.0100				
374*	0.0102				
375	0.0104				
376*	0.0094	0.80	1.00	1.0	
377*	0.0095				
378*	0.0096				
379*	0.0097				
380*	0.0098				
381	0.0099				
382*	0.0091	0.80	1.17	1.0	
383*	0.0093				
384*	0.0095				
385	0.0097				
386	0.0099				
387	0.0091	0.80	1.50	1.0	
388	0.0092				
389*	0.0290	0.75	1.00	1.0	Program DAD350
390*	0.0300				
391	0.0310				
392	0.0320				

TABLE VII (Continued)

Trajectory Number	Initial Angle (radians)	Porosity	Velocity (cm/sec)	Particle Diameter (μm)	Remarks
393*	0.0220	0.80	1.00	1.0	
394	0.0230				
395	0.0230				
396*	0.0152	0.85	1.00	1.0	
397*	0.0154				
398*	0.0156				
399*	0.0158				
400*	0.0132	0.80	1.00	0.5	
401	0.0134				
402	0.0136				
403*	0.0130	0.80	0.78	0.5	
404*	0.0132				
405*	0.0134				
406*	0.0136				
407*	0.0138				
408*	0.0140				
409*	0.0122	0.80	1.17	0.5	
410*	0.0124				
411*	0.0126				
412	0.0128				
413	0.0118	0.80	1.50	0.5	
414	0.0120				
415*	0.0154	0.85	0.78	1.0	
416*	0.0156				
417*	0.0158				
418*	0.0160				
419*	0.0162				
420*	0.0164				
421*	0.0146	0.85	1.17	1.0	
422*	0.0148				
423*	0.0150				
424*	0.0152				
425	0.0154				
426	0.0156				
427*	0.0140	0.85	1.50	1.0	
428	0.0142				
429	0.0144				
430	0.0146				
431*	0.0318	0.75	0.78	1.0	
432*	0.0320				

TABLE VII (Continued)

Trajectory Number	Initial Angle (radians)	Porosity	Velocity (cm/sec)	Particle Diameter (μm)	Remarks
433	0.0302	0.75	1.00	1.0	
434	0.0304				
435	0.0290	0.75	1.17	1.0	
436	0.0292				
437*	0.0230	0.80	0.78	1.0	
438*	0.0232				
439*	0.0234				
440*	0.0236				
441*	0.0222	0.80	1.00	1.0	
442	0.0224				
443	0.0226				
444	0.0228				
445*	0.0208	0.80	1.17	1.0	
446*	0.0210				
447*	0.0212				
448	0.0214				
449	0.0216				
450	0.0218				
451	0.0220				
452*	0.0198	0.80	1.50	1.0	
453	0.0200				
454	0.0202				
455	0.0204				
456	0.0206				
457*	0.0142	0.80	0.78	0.5	
458*	0.0144				
459	0.0146				
460	0.0148				
461	0.0150				
462*	0.0110	0.80	1.50	0.5	
463*	0.0112				
464*	0.0114				
465*	0.0116				
466*	0.0322	0.75	0.78	1.0	
467	0.0324				
468	0.0326				
469*	0.0278	0.75	1.17	1.0	
470*	0.0280				
471*	0.0282				
472*	0.0284				

TABLE VII (Continued)

Trajectory Number	Initial Angle (radians)	Porosity	Velocity (cm/sec)	Particle Diameter (μm)	Remarks
473*	0.0286				
474	0.0288				
475*	0.0250	0.75	1.50	1.0	
476*	0.0252				
477*	0.0254				
478*	0.0256				
479*	0.0258				
480*	0.0260				
481*	0.0262				
482*	0.0264				
483	0.0268				
484	0.0270				
485*	0.0238	0.80	0.78	1.0	
486*	0.0240				
487	0.0242				
488	0.0244				
489	0.0246				
490*	0.0166	0.85	0.78	1.0	
491*	0.0168				
492*	0.0170				
493*	0.0172				
494	0.0174				
495	0.0176				
496	0.0178				
497*	0.0092	0.85	1.00	0.5	
498*	0.0094				
499	0.0096				
500	0.0098				
501	0.0092	0.85	1.17	0.5	
502	0.0094				
503*	0.0073	0.75	1.00	0.5	Inclusion of double-layer force — $\kappa = 9 \times 10^6$. Program DAD500
504*	0.0074				
505	0.0075				
506*	0.0078	0.75	0.78	0.5	
507*	0.0079				
508	0.0080				
509*	0.0053	0.80	1.00	0.5	
510*	0.0054				
511	0.0055				

TABLE VII (Continued)

Trajectory Number	Initial Angle (radians)	Porosity	Velocity (cm/sec)	Particle Diameter (μm)	Remarks
512*	0.0051	0.80	1.17	0.5	
513*	0.0052				
514	0.0053				
515*	0.0033	0.85	1.50	0.5	
516*	0.0034				
517	0.0035				
518*	0.0037	0.85	1.00	0.5	
519*	0.0038				
520	0.0039				
521*	0.0128	0.75	1.17	1.0	
522*	0.0130				
523	0.0132				
524*	0.0097	0.85	1.00	1.0	
525*	0.0098				
526	0.0099				
527*	0.0061	0.85	1.50	1.0	
528*	0.0062				
529	0.0063				
530*	0.0070	0.75	1.17	0.5	
531*	0.0071				
532	0.0072				
533*	0.0140	0.75	0.78	1.0	
534*	0.0142				
535	0.0144				
536*	0.0132	0.75	1.00	1.0	
537*	0.0134				
538	0.0136				
539*	0.0057	0.80	0.78	0.5	
540*	0.0058				
541	0.0059				
542*	0.0100	0.80	0.78	1.0	
543*	0.0102				
544	0.0104				
545*	0.0093	0.80	1.17	1.0	
546*	0.0095				
547	0.0097				

TABLE VII (Continued)

Trajectory Number	Initial Angle (radians)	Porosity	Velocity (cm/sec)	Particle Diameter (μm)	Remarks
548*	0.0035	0.85	1.17	0.5	
549*	0.0036				
550	0.0037				
551*	0.0067	0.85	1.00	1.0	
552*	0.0068				
553	0.0069				
554*	0.0065	0.85	1.17	1.0	
555*	0.0066				
556	0.0067				
557*	0.0073	0.75	1.00	0.5	$\kappa = 4.6 \times 10^6$. Program DAD501
558*	0.0074				
559	0.0075				
560*	0.0142	0.75	0.78	1.0	
561	0.0143				
562	0.0144				
563*	0.0065	0.85	1.17	1.0	
564*	0.0066				
565	0.0067				
566*	0.0033	0.85	1.50	0.5	
567*	0.0034				
568	0.0035				
569*	0.0010	0.75	1.00	0.3	$\kappa = 9 \times 10^6$. Program DAD500
570*	0.0030				
571*	0.0050				
572*	0.0010	0.85	1.00	0.3	
573	0.0052	0.75	1.00	0.3	
574	0.0030	0.85	1.00	0.3	
575	0.0035				
576	0.0040				
577*	0.0015				
578*	0.0020				
579*	0.0023				
580	0.0027				
581	0.0028				
582*	0.0023	0.85	1.50	0.3	
583	0.0025				
584	0.0025				

TABLE VII (Continued)

Trajectory Number	Initial Angle (radians)	Porosity	Velocity (cm/sec)	Particle Diameter (μm)	Remarks
585	0.0048	0.75	1.50	0.3	
586	0.0049				
587	0.0050				
588*	0.0040				
589*	0.0045				
590*	0.0046				
591	0.0047				
**********					
The following trajectories were calculated but are not available on tape.					
*	0.0051	0.75	1.00	0.3	
*	0.0025	0.85	1.00	0.3	
*	0.0026				
*	0.0024	0.85	1.50	0.3	
**********					
592	0.0050	0.75	1.00	0.3	$\kappa = 5.75 \times 10^4$. Simulation of no additions to the particle suspension.
593	0.0051				
594	0.0052				
595	0.0050	0.75	1.00	0.3	$\kappa = 9.58 \times 10^3$. (z=1)
596	0.0060				
597	0.0100				
598	0.0150				
599	0.0200				
600	0.0060	0.75	1.00	0.3	$\kappa = 5.75 \times 10^4$. (z=6)
601	0.0100				
602	0.0150				
603	0.0200				
604*	0.0074	0.75	1.00	0.5	Program DAD600. Inclusion of diffusion 23 of 100 trajectories calculated at this value of θ impacted.
•					
•					
•					
•					
703					
704*	0.0073	0.75	1.00	0.5	All 25 impacted.
•					
728*					
729	0.0075	0.75	1.00	0.5	All 25 remained suspended
•					
743					

APPENDIX XI

PROCEDURE FOR DISPERSING TITANIUM DIOXIDE

The material presented in this thesis indicated that it was necessary to employ a particle suspension in which the particles were separate or completely dispersed. The following procedure was used to insure a maximum dispersion within the suspension utilized in the experimental program.

The dispersing agent used was Calgon (sodium hexametaphosphate). A 50% solution of this material was made by dissolving 25 g of Calgon in 50 ml of distilled water. Then 2.4 ml of this solution was combined with 235 ml of distilled water in a laboratory mixer. To this, 550 g Titanox RA50 was mixed in slowly. The entire suspension was agitated for 15 minutes with the mixer. This partially dispersed suspension was transferred to a Waring Blendor and mixed for 2 minutes. The purpose of this was to break up any remaining agglomerations of particles. The suspension then represented a 70% solids solution containing 0.22% Calgon. After the suspension was cooled to room temperature, its viscosity was measured with a Hercules viscometer. The procedure then called for the successive addition of 0.05% Calgon, mixing in a laboratory mixer for 5 minutes, cooling to room temperature, and the measuring of the viscosity. By plotting the percentage of Calgon addition against the viscosity, a minimum in the curve should be observed at the point where maximum dispersion occurs. Figure 30 is presented to indicate the results that were obtained from this procedure. It is evident that maximum dispersion is obtained at a Calgon concentration of 0.25%.

The stock suspension for the experimental program was prepared utilizing this optimum amount of dispersing agent, 550 g TiO_2, and 235 ml distilled water. This 70% solids suspension was diluted to 30% and any agglomerates were allowed

to settle. By continually agitating this suspension, it was kept for a period of time sufficient to serve the entire experimental program.

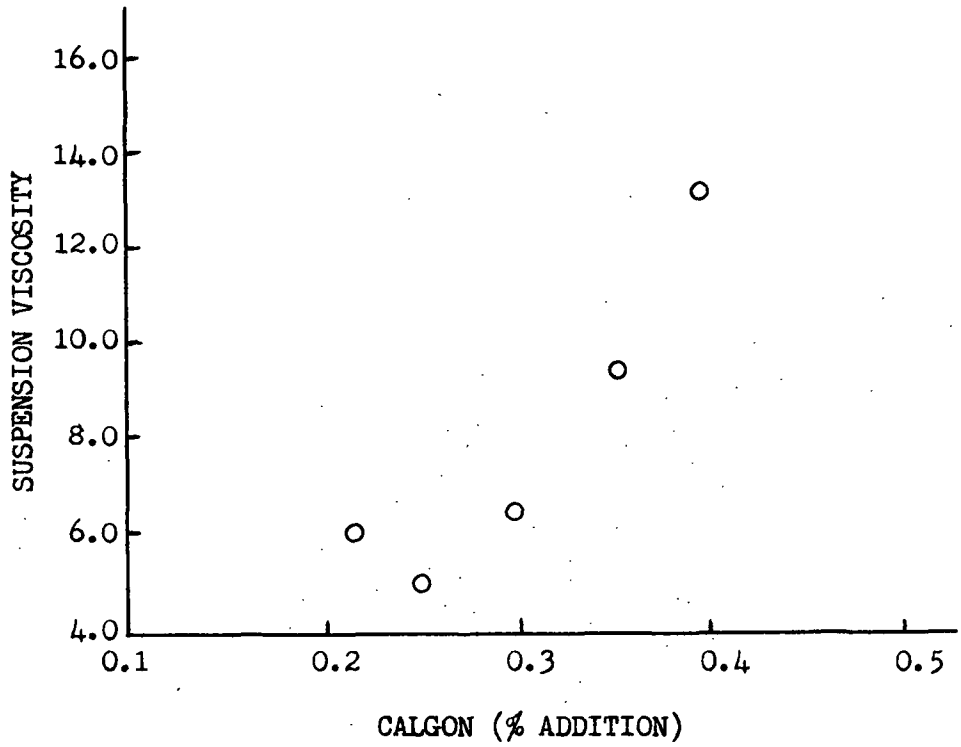

Figure 30. Plot Depicting the Optimum Amount of Dispersing Agent Needed for the Particle Suspension

APPENDIX XII

FORTRAN IV LISTING: PROGRAM FOR THE TABULATION AND PLOTTING OF EXPERIMENTAL RESULTS

```
/JOB GO,TIME=99
C
C                  EXPERIMENTAL DATA SUMMARY PROGRAM
C                       DAVID A. DYER      1977
C
C          THIS PROGRAM IS UTILIZED TO PERFORM VARIOUS CALCULATIONS ON
C          THE EXPERIMENTAL DATA.  ALL OF THE CALCULATED VALUES ARE
C          TABULATED IN A LOGICAL FORM BY THIS PROGRAM.
      DIMENSION TARE(20), WLPT(20),DLPT(20), ASHPT(20), WLAYER(20)
      DIMENSION DLAYER(20), ASH(20), TNYLON(20),XMOIST(20), ASHPC(20)
      DIMENSION ACNYL(20), ACTIO2(20), ACMAT(20), PCTIO2(20), PCNYL(20)
      DIMENSION RETIO2(20)
C
C          READ IN THE SYSTEM VARIABLES--
C               NPAD = RUN NUMBER
C               LAYER = NUMBER OF SECTIONS OBTAINED FROM THE PAD
C               NCARY = NUMBER OF COLORMETRIC RUNS MADE
C               POROS = SYSTEM POROSITY ANTICIPATED
C               WO = GRAMS OF TIO2 IN SUSPENSION
C               FORVEL = FORMING VELOCITY
C               PERVEL = PERMEATING VELOCITY
C               THICK = PAD THICKNESS
C               PH = SUSPENSION PH
      READ (5,9001) NPAD, LAYER, NCARY
      READ (5,9002) POROS, WO, FORVEL, PERVEL, THICK, PH
C
      WRITE (6,9003) NPAD
      WRITE (6,9004) LAYER, POROS, FORVEL, WO, PERVEL, PH
      WRITE (6,9011)
      DO 6 NUM = 1,LAYER
C
C          READ IN RAW DATA--WEIGHT MEASUREMENTS FOR TARE, WET LAYER, DRY
C          LAYER, AND ASH.
C
    6 READ (5,9007) TARE(NUM), WLPT(NUM), DLPT(NUM), ASHPT(NUM)
C
C          CALCULATE WET AND DRY LAYER WEIGHT
C
      DO 8 NUM = 1,LAYER
      WLAYER(NUM) = WLPT(NUM) - TARE(NUM)
      DLAYER(NUM) = DLPT(NUM) - TARE(NUM)
    8 CONTINUE
C
C          CALCULATE ASH, ACCUMULATED NYLON, ACCUMULATED ASH, ACCUMULATED
C          MAT WEIGHT, AND THE PERCENTAGES OF EACH COMPONENT PER LAYER
C
      DO 14 NUM = 1,LAYER
      ASH(NUM) = ASHPT(NUM) - TARE(NUM)
      TNYLON(NUM) = DLAYER(NUM) - ASH(NUM)
      TNYLON(NUM) = TNYLON(NUM) / 0.997
      ASH(NUM) = DLAYER(NUM) - TNYLON(NUM)
      XMOIST(NUM)= (WLAYER(NUM) - DLAYER(NUM))/WLAYER(NUM) * 100.
      ASHPC(NUM) = ASH(NUM)/DLAYER(NUM) * 100.
      IF (NUM - 1) 13,12,13
   12 ACNYL(NUM) = TNYLON(NUM)
      ACTIO2(NUM) = ASH(NUM)
   13 ACNYL(NUM) = ACNYL(NUM-1) + TNYLON(NUM)
      ACTIO2(NUM) = ACTIO2(NUM-1) + ASH(NUM)
   14 CONTINUE
```

```
      POROS = 1. - ( ACNYL(LAYER)/(1.14*45.6*THICK))
      DO 19 NUM = 1,LAYER
      IF (NUM - 1) 18,17,18
   17 ACMAT(NUM) = DLAYER(NUM)
   18 ACMAT(NUM) = ACMAT(NUM-1) + DLAYER(NUM)
      PCTIO2(NUM) = ACTIO2(NUM)/ACMAT(NUM) * 100.
      PCNYL(NUM) = ACNYL(NUM)/ACNYL(LAYER) * 100.
      RETIO2(NUM) = ACTIO2(NUM)/ACTIO2(LAYER) * 100.
C
C           CONSTRUCT A TABLE OF ALL THE CALCULATED VALUES
C
   19 WRITE (6,9020) NUM, WLAYER(NUM), DLAYER(NUM), ASH(NUM),
     1 TNYLON(NUM), ACNYL(NUM), ACTIO2(NUM), ACMAT(NUM), PCTIO2(NUM),
     2 PCNYL(NUM), RETIC2(NUM)
C
C          CALL APPROPRIATE SUBROUTINES FOR DRAWING DIAGRAMS TO REPRE-
C          SENT THE CALCULATED VALUES
C
      CALL DRAW1(NPAD, LAYER, ACMAT, PCNYL, RETIO2)
      CALL DRAW2(NPAD, LAYER, ACMAT, PCTIO2)
C     CALL DRAW3 (LAYER, NCARY, NPAD, POROS, WO, ACMAT)
      CALL DRAW4 (NPAD, LAYER, POROS, WO, ACMAT, ACTIO2, THICK)
C     CALL DRAW5 (NPAD, LAYER, NCARY, POROS, WO, ACMAT)
C
C          ARRANGEMENTS
C
      CALL EXIT
 9001 FORMAT (3I3)
 9002 FORMAT (6F10.0)
 9003 FORMAT (1H1,T50,'******************',/,T50,'*',T66,'*',/,T50,'* PAD
     1 NUMBER ',I2,' *',/,T50,'*',T66,'*',/,T50,'******************',//)
 9004 FORMAT (1H0,39X,'NUMBER OF PAD LAYERS = ',I3,/,40X,'DESIRED POROSI
     1TY = ',F5.2,/,40X,'FORMING VELOCITY (CM/SEC) = ',F5.2,/,40X,'TIO2
     2ADDED TO SUSPENSION (GM) = ',F7.4,/,40X,'PERMEATION VELOCITY (CM/S
     3EC) = ',F5.2,/,40X,'SUSPENSION PH = ',F4.1)
 9007 FORMAT (4F10.0)
C9010 FORMAT (1H0)
 9011 FORMAT(1H0,'  LAYER * WET LAYER* DRY LAYER*    ASH    *   NYLON   *
     1 ACCUM.   *  ACCUM.   *  ACCUM.   *  ACCUM.   *   NYLON   * PCT TOTAL'/
     2 '          *   (GM)    *   (GM)    * PER LAYER* PER LAYER* NYLON WT
     3*  ASH WT  *  PAD WT   * TIO2 PER * DEPOSITED*  RETAINED'/ '
     4  *          *          *   (GM)    *   (GM)    *   (GM)    *   (GM)
     5  *   (GM)   *  ACCUM.  *  IN PAD  *   TIO2'/ '          *
     6 *          *          *          *          *          *
     7 *  PAD WT  *   (PCT)  *  (PCT)'/'          *          *
     8*          *          *          *          *          *   (PCT)
     9*          *'/)
 9020 FORMAT (1H0,3X,I2,'    * ',F8.4,' * ',F8.4,' * ',F8.4,' * ',F8.4,
     1' * ',F8.4,' * ',F8.4,' * ',F8.4,' *  ',F6.2,'  *  ',F6.2,'  *
     2',F6.2)
      END
      SUBROUTINE DRAW1(NPAD, LAYER, ACMAT, PCNYL, RETIO2)
C
C          THIS SUBROUTINE CONSTRUCTS A DIAGRAM WHICH PLOTS THE ACCUMU-
C          LATED PAD WEIGHT AGAINST THE NYLON AND ASH DISTRIBUTIONS.
C
      DIMENSION ACMAT(1), PCNYL(1), RETIO2(1)
      INTEGER HEADX1(10), HEADY1(10), HEAD11(10), HEAC21(10), HEAD31(10)
      CALL ITLZ
      CALL DPT(1,4)
```

```
      CALL PLOT (0.,-11.,2)
      CALL PLOT (0.,-10.5,-3)
      CALL PLOT (2.5,2.,-3)
      READ (5,9001) HEADX1
      READ (5,9001) HEADY1
      READ (5,9001) HEAD11
      CALL SYMBOL (2.0,6.0,0.21,HEAD11,0.0,22)
      CALL SCALE (ACMAT,8.0,LAYER,1)
      CALL AXIS (0.0,0.0,HEADX1,-27,8.0,0.0,0.0,1.0)
      CALL SCALE (PCNYL,5.0,LAYER,1)
      CALL AXIS (0.0,0.0,HEADY1,27,5.0,90.,0.0,20.)
      ACMAT(LAYER+1) = 0.0
      ACMAT(LAYER+2) = 1.0
      PCNYL(LAYER+1) = 0.0
      PCNYL(LAYER+2) = 20.0
      READ (5,9001) HEAD21
      CALL DRAW (1.0,4.80,0.0,170,0.0,1.0,0.35)
      CALL SYMBOL (1.25,4.75,0.14,HEAD21,0.0,10)
      CALL LINE (ACMAT,PCNYL,LAYER,1,-1,1)
      RETIO2(LAYER+1) = 0.0
      RETIO2(LAYER+2) = 20.0
      READ (5,9001) HEAD31
      CALL DRAW (1.0,4.55,0.0,175,0.0,1.0,0.35)
      CALL SYMBOL (1.25,4.5,0.14,HEAD31,0.0,16)
      CALL LINE (ACMAT,RETIO2,LAYER,1,-1,3)
      CALL FINAL
      RETURN
 9001 FORMAT (10A4)
      END
      SUBROUTINE DRAW2 (NPAD, LAYER, ACMAT, PCTIO2)
C
C         THIS SUBROUTINE CONSTRUCTS A DIAGRAM REPRESENTING ACCUMULATED
C         PAD WEIGHT AGAINST ACCUMULATED ASH PERCENT.
C
      DIMENSION ACMAT(1), PCTIO2(1)
      INTEGER HEADX2(10), HEADY2(10), HEAD12(10)
      CALL ITLZ
      CALL DPT(1,4)
      CALL PLOT (0.,-11.,2)
      CALL PLOT (1.,-10.5,-3)
      CALL PLOT (2.5,2.,-3)
      READ (5,9001) HEADX2
      READ (5,9001) HEADY2
      READ (5,9001) HEAD12
      CALL SYMBOL (3.5,6.0,0.21,HEAD12,0.0,11)
      CALL SCALE (ACMAT,8.0,LAYER,1)
      CALL AXIS (0.0,0.0,HEADX2,-27,8.0,0.0,0.0,1.0)
      CALL SCALE (PCTIO2,5.0,LAYER,1)
      CALL AXIS (0.0,0.0,HEADY2,29,5.0,90.,0.0,3.0)
      ACMAT(LAYER+1) = 0.0
      ACMAT(LAYER+2) = 1.0
      PCTIO2(LAYER+1) = 0.0
      PCTIO2(LAYER+2) = 3.0
      CALL LINE (ACMAT,PCTIO2,LAYER,1,-1,3)
      CALL FINAL
 9001 FORMAT (10A4)
      RETURN
      END
      SUBROUTINE DRAW4 (NPAD, LAYER, POROS, WO, ACMAT, ACTIO2, THICK)
C
```

```
C          THIS SUBROUTINE CONSTRUCTS A DIAGRAM USED TO CALCULATE THE
C          EFFICIENCY FOR THE PAD.  ACCUMULATED PAD WEIGHT IS PLOTTED
C          AGAINST A RATIO OF THE TOTAL AMOUNT OF TIO2 TO THE AMOUNT
C          RETAINED.  THE SLOPE OF A REGRESSION LINE THROUGH THE DATA
C          IS PROPORTIONAL TO THE EFFICIENCY
C
      DIMENSION ACMAT(20), ACTIO2(20), RATIO(20)
      INTEGER HEADX4(10), HEADY4(10), HEAD14(10), HEAD24(10), HEAD34(10)
      INTEGER HEAD44(10), HEAD54(10)
      CALL ITLZ
      CALL DPT(1,4)
      CALL PLOT (0.0,-11.0,2)
      CALL PLOT (0.,-10.5,-3)
      CALL PLOT (2.5,1.0,-3)
      READ (5,9002) HEADX4
      READ (5,9002) HEADY4
C     READ (5,9002) HEAD14
      READ (5,9002) HEAD24
      READ (5,9002) HEAD34
      SPACE = 0.15
      CALL SYMBOL (2.6,5.7,0.21,HEAD24,0.0,21)
      CALL SYMBOL (3.5,5.4,0.14,HEAD34,0.0,20)
      CALL SCALE (ACMAT,8.0,LAYER,1)
      CALL AXIS (0.0,0.0,HEADX4,-27,8.0,0.0,0.0,1.0)
      CALL SCALE (RATIO,6.0,LAYER,1)
      CALL AXIS (0.0,0.0,HEADY4,16,6.0,90.,0.0,SPACE)
      ACMAT(LAYER+1) = 0.0
      ACMAT(LAYER+2) = 1.0
      RATIO(LAYER+1) = 0.0
      RATIO(LAYER+2) = SPACE
      SUMX = 0.
      SUMY = 0.
      SUMXY = 0.
      SUMX2 = 0.
      SUMY2 = 0.
      DO 3 NUM = 1,LAYER
      RATIO(NUM) = ALOG(WO/(WO-ACTIO2(NUM)))
C
C          SCHEME FOR OBTAINING THE REGRESSION LINE
C
      SUMX = SUMX + ACMAT(NUM)
      SUMY = SUMY + RATIO(NUM)
      SUMXY = SUMXY + ACMAT(NUM) * RATIO(NUM)
      SUMX2 = SUMX2 + ACMAT(NUM) * ACMAT(NUM)
    3 SUMY2 = SUMY2 + RATIO(NUM) * RATIO(NUM)
      B = (LAYER * SUMXY - SUMX * SUMY)/(LAYER * SUMX2 - SUMX * SUMX)
      A = (SUMY - B * SUMX)/LAYER
C     WRITE (6,9004) B, A
      SX2 = SUMX2 - SUMX * SUMX / LAYER
      SY2 = SUMY2 - SUMY * SUMY / LAYER
      R = (SUMXY - (SUMX * SUMY / LAYER)) / SQRT(SX2 * SY2)
      CALL LINE (ACMAT,RATIO,LAYER,1,-1,3)
      X1 = 0.25
      X2 = 8.0
      Y1 = A + B*X1
      Y2 = A + B*X2
      Y1 = Y1/SPACE
      Y2 = Y2/SPACE
      CALL PLOT (X1,Y1,3)
      CALL PLOT (X2,Y2,2)
```

```
      READ (5,9002) HEAD44
      READ (5,9002) HEAD54
      CALL SYMBOL (5.0,0.7,0.14,HEAD44,0.0,5)
      FACT = 1.14 * 45.6 * (1. - POROS)
C
C          COLLECTION EFFICIENCY CALCULATION
C
      ETA = (3.14159*0.002*FACT *B)/(4.0*(1.-POROS))
      CALL NUMBER (5.7,0.7,0.14,ETA,0.0,4)
      CALL SYMBOL (5.0,0.3,0.14,HEAD54,0.0,3)
      CALL NUMBER (5.4,0.3,0.14,R,0.0,3)
      WRITE (6,9006) THICK, POROS
      WRITE (6,9004) B, A
      WRITE (6,9005) ETA
      WRITE (6,9007)
      CALL FINAL
      RETURN
C
C          ARRANGEMENTS
C
 9002 FORMAT (10A4)
 9004 FORMAT (1H ,T36,'SLOPE OF THE LINE FITTED TO THE DATA --',F10.4,/,
     1T36,'INTERCEPT --',F10.4,/)
 9005 FORMAT(1H ,T31,'**********COLLECTION EFFICIENCY (ETA) = ',F8.5,'**
     1********')
 9006 FORMAT (1HO,/, T36,'COMPRESSED PAD THICKNESS UTILIZED =',F7.3,/,
     1T36,'CALCULATED POROSITY = 'F5.3,/)
 9007 FORMAT (1HO,///,T15,'COMMENTS--')
      END

/END CARD READ, JOB TERMINATED
```

APPENDIX XIII

EXPERIMENTAL DATA AND APPROPRIATE DIAGRAMS

****
* *
* PAD NUMBER 13 *
* *
****

NUMBER OF PAD LAYERS = 10
DESIRED POROSITY = 0.85
FORMING VELOCITY (CM/SEC) = 1.00
TIO2 ADDED TO SUSPENSION (GM) = 1.4117
PERMEATION VELOCITY (CM/SEC) = 1.00
SUSPENSION PH = 5.1

LAYER	WET LAYER (GM)	DRY LAYER (GM)	ASH PER LAYER (GM)	NYLON PER LAYER (GM)	ACCUM. NYLON WT (GM)	ACCUM. ASH WT (GM)	ACCUM. PAD WT (GM)	ACCUM. TIO2 PER ACCUM. PAD WT (PCT)	NYLON DEPOSITED IN PAD (PCT)	PCT TOTAL RETAINED TIO2 (PCT)
1	4.7025	1.2313	0.1519	1.0794	1.0794	0.1519	1.2313	12.33	12.93	20.09
2	6.8989	1.2042	0.1342	1.0700	2.1494	0.2861	2.4355	11.75	25.76	37.83
3	9.4325	1.4698	0.1434	1.3264	3.4758	0.4295	3.9053	11.00	41.65	56.80
4	5.4677	0.8515	0.0710	0.7805	4.2563	0.5004	4.7568	10.52	51.00	66.19
5	4.5323	0.6950	0.0548	0.6402	4.8966	0.5552	5.4518	10.18	58.68	73.43
6	3.8536	0.5858	0.0403	0.5455	5.4421	0.5955	6.0376	9.86	65.21	78.76
7	5.4866	0.7853	0.0504	0.7349	6.1770	0.6459	6.8229	9.47	74.02	85.42
8	5.8794	0.8264	0.0337	0.7927	6.9697	0.6796	7.6493	8.88	83.52	89.88
9	3.2029	0.4663	0.0268	0.4395	7.4092	0.7064	8.1156	8.70	88.78	93.43
10	6.5798	0.9857	0.0497	0.9360	8.3452	0.7561	9.1013	8.31	100.00	100.00

COMPRESSED PAD THICKNESS UTILIZED = 1.087
CALCULATED POROSITY = 0.852

SLOPE OF THE LINE FITTED TO THE DATA -- 0.0828
INTERCEPT -- 0.0319

**********COLLECTION EFFICIENCY (ETA) = 0.00676**********

COMMENTS--

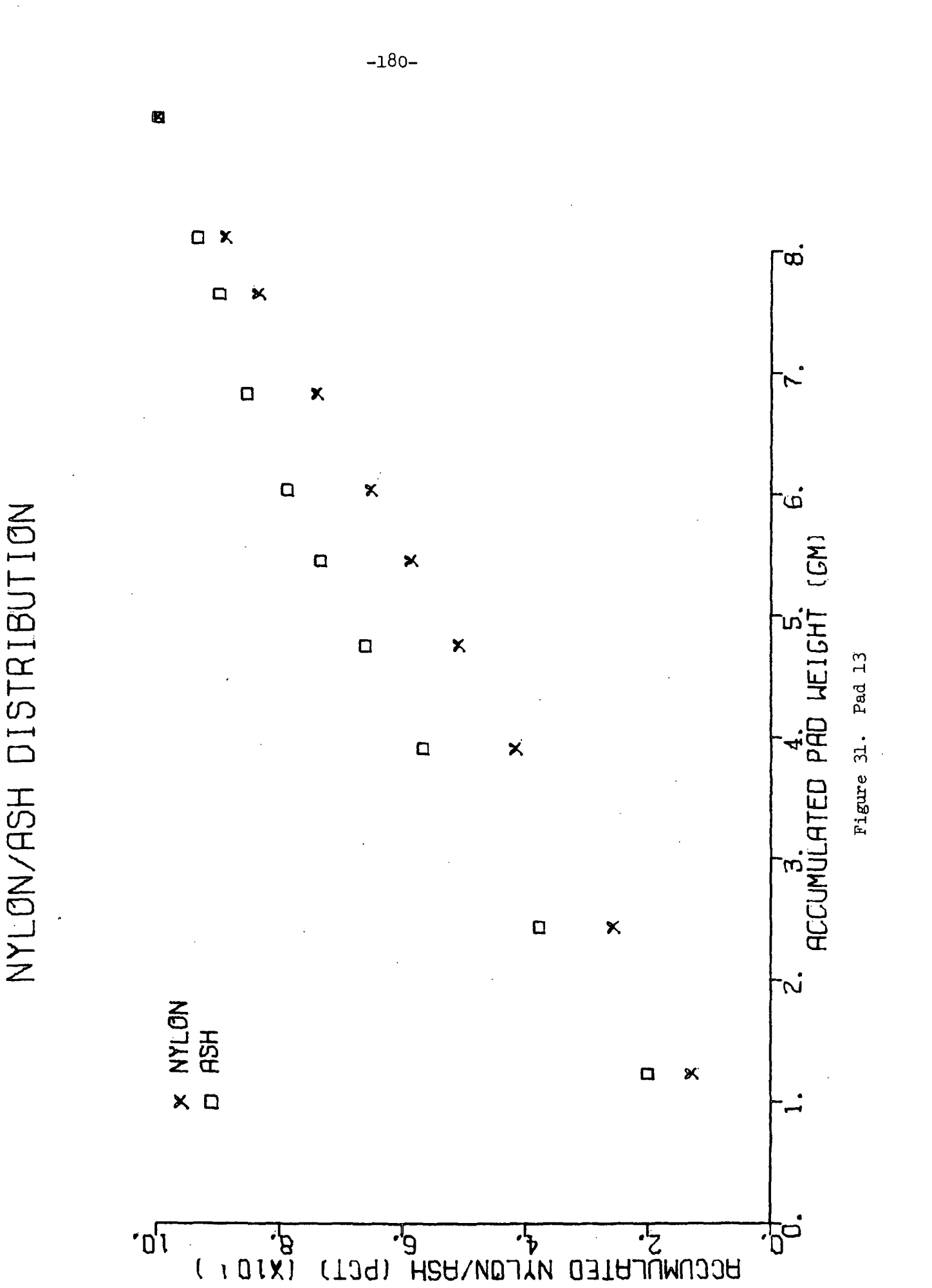

Figure 31. Pad 13

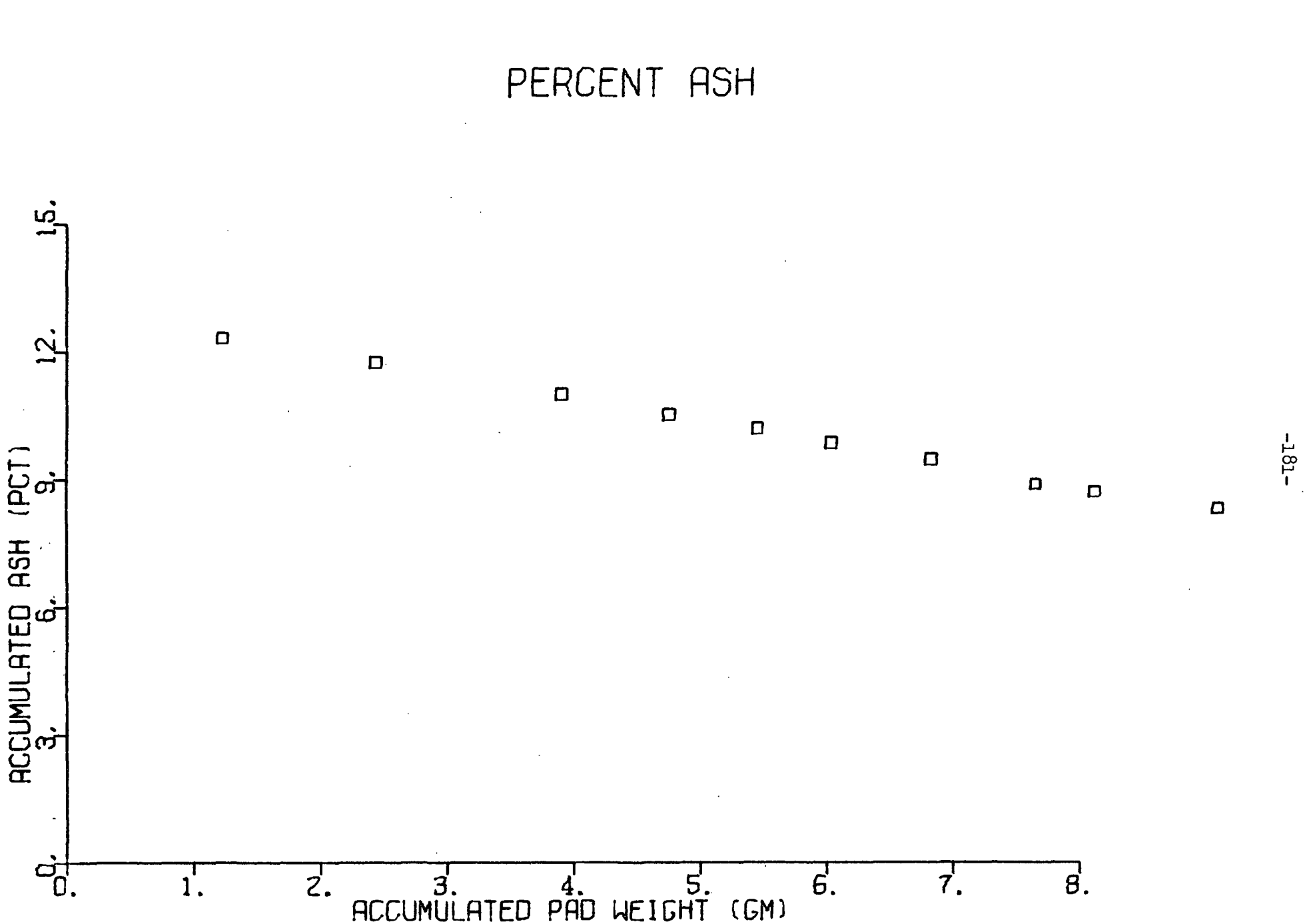

Figure 32. Pad 13

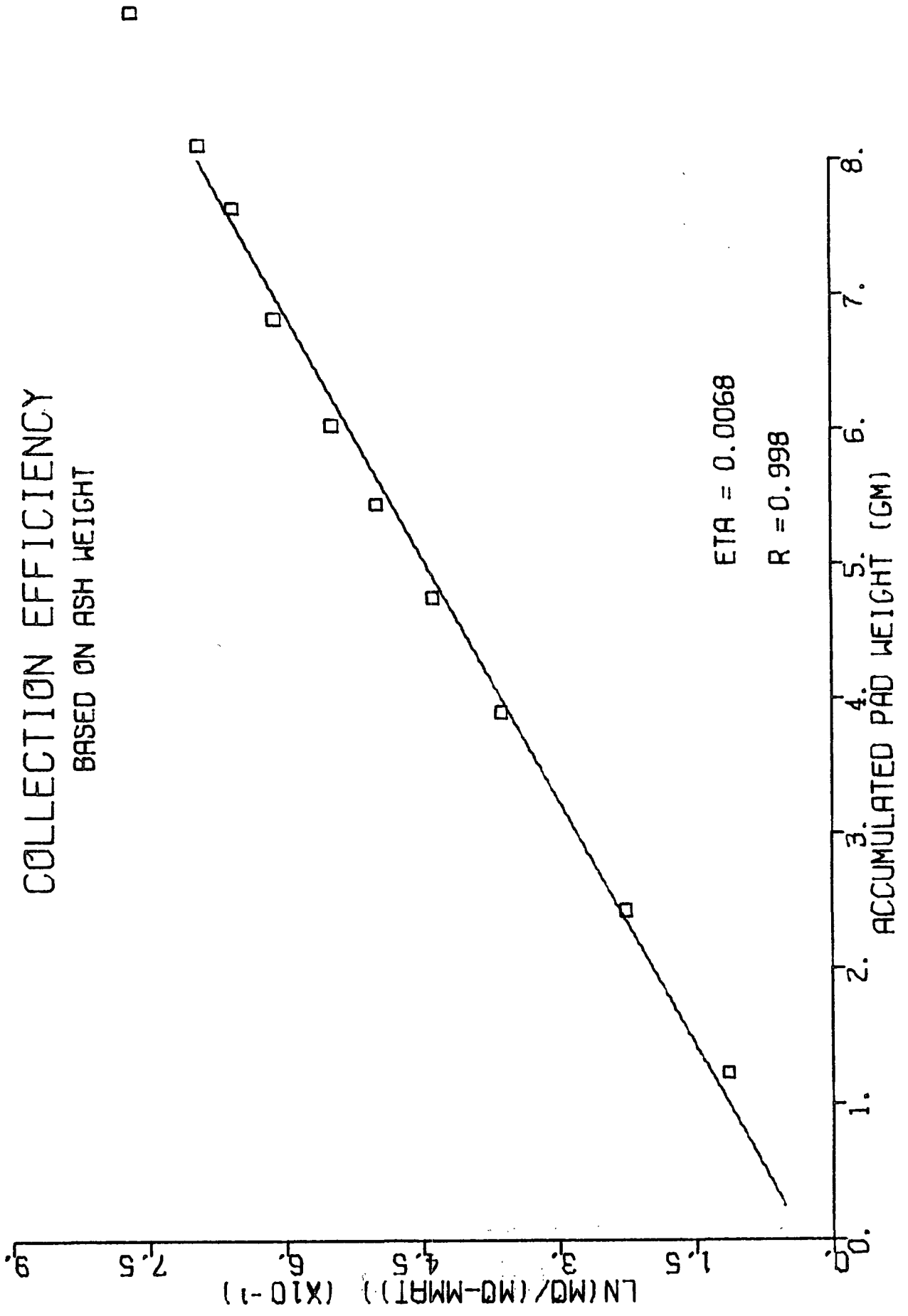

Figure 3.. Pad 13

****
* *
* PAD NUMBER 14 *
* *
****

NUMBER OF PAD LAYERS = 11
DESIRED POROSITY = 0.75
FORMING VELOCITY (CM/SEC) = 1.00
TIO2 ADDED TO SUSPENSION (GM) = 1.4131
PERMEATION VELOCITY (CM/SEC) = 1.00
SUSPENSION PH = 5.1

LAYER	WET LAYER (GM)	DRY LAYER (GM)	ASH PER LAYER (GM)	NYLON PER LAYER (GM)	ACCUM. NYLON WT (GM)	ACCUM. ASH WT (GM)	ACCUM. PAD WT (GM)	ACCUM. TIO2 PER ACCUM. PAD WT (PCT)	NYLON DEPOSITED IN PAD (PCT)	PCT TOTAL RETAINED TIO2 (PCT)
1	1.2364	0.4778	0.0577	0.4201	0.4201	0.0577	0.4778	12.08	5.43	7.99
2	2.0716	0.6857	0.0837	0.6020	1.0221	0.1414	1.1635	12.15	13.22	19.57
3	4.1726	1.0721	0.1222	0.9500	1.9720	0.2636	2.2356	11.79	25.51	36.47
4	5.2439	1.1944	0.1188	1.0756	3.0477	0.3823	3.4300	11.15	39.42	52.90
5	4.8946	1.0055	0.0879	0.9175	3.9652	0.4703	4.4355	10.60	51.29	65.07
6	2.2083	0.4760	0.0355	0.4405	4.4057	0.5058	4.9115	10.30	56.98	69.98
7	3.8481	0.7748	0.0572	0.7177	5.1234	0.5629	5.6863	9.90	66.27	77.89
8	4.3247	0.8938	0.0599	0.8339	5.9573	0.6228	6.5801	9.47	77.05	86.18
9	3.2759	0.7046	0.0417	0.6629	6.6202	0.6645	7.2847	9.12	85.63	91.95
10	2.3251	0.5238	0.0278	0.4960	7.1162	0.6923	7.8085	8.87	92.04	95.80
11	2.1655	0.6456	0.0304	0.6152	7.7314	0.7227	8.4541	8.55	100.00	100.00

COMPRESSED PAD THICKNESS UTILIZED = 0.619
CALCULATED POROSITY = 0.760

SLOPE OF THE LINE FITTED TO THE DATA -- 0.0852
INTERCEPT -- 0.0145

**********COLLECTION EFFICIENCY (ETA) = 0.00696**********

COMMENTS--

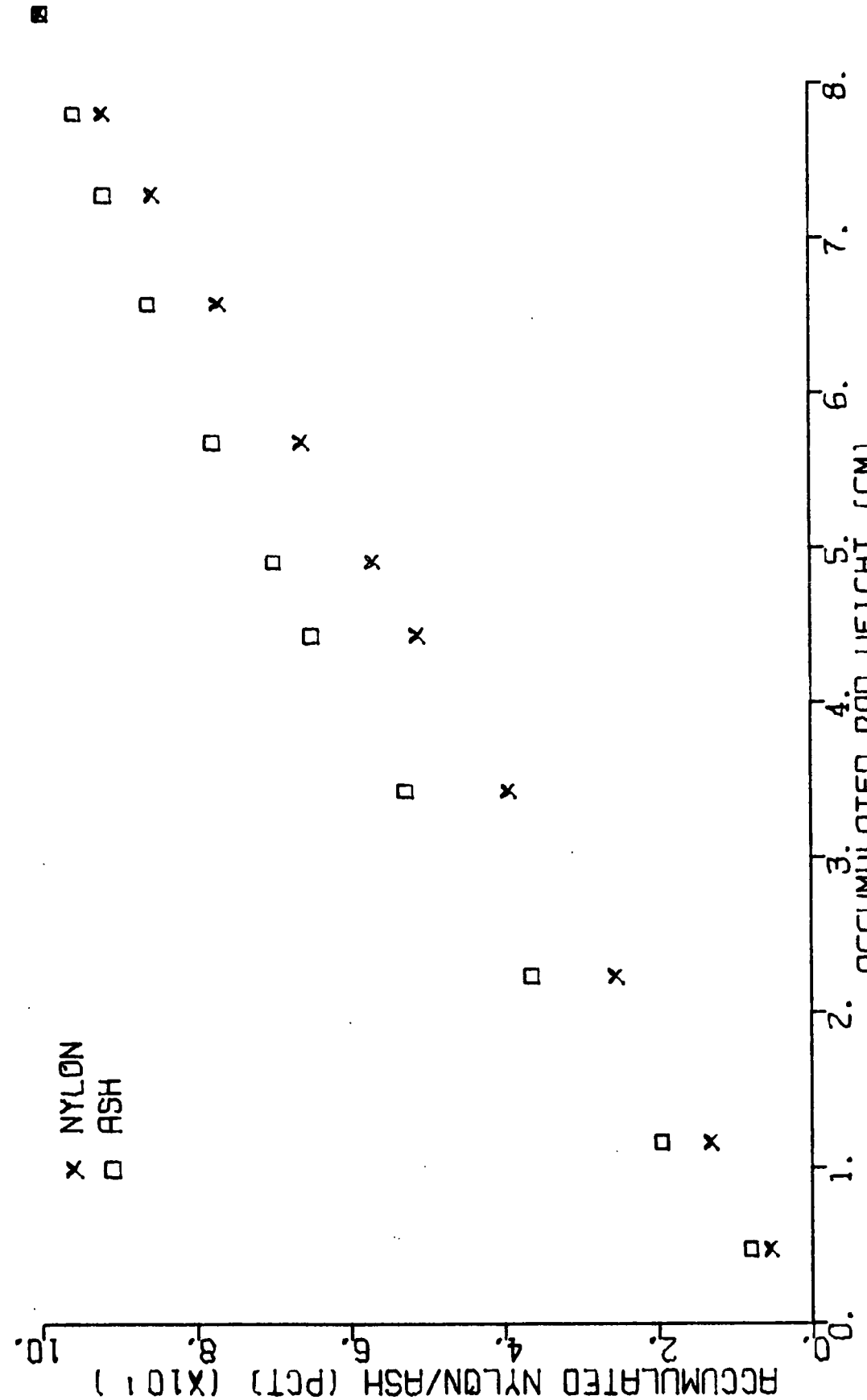

Figure 34. Pad 14

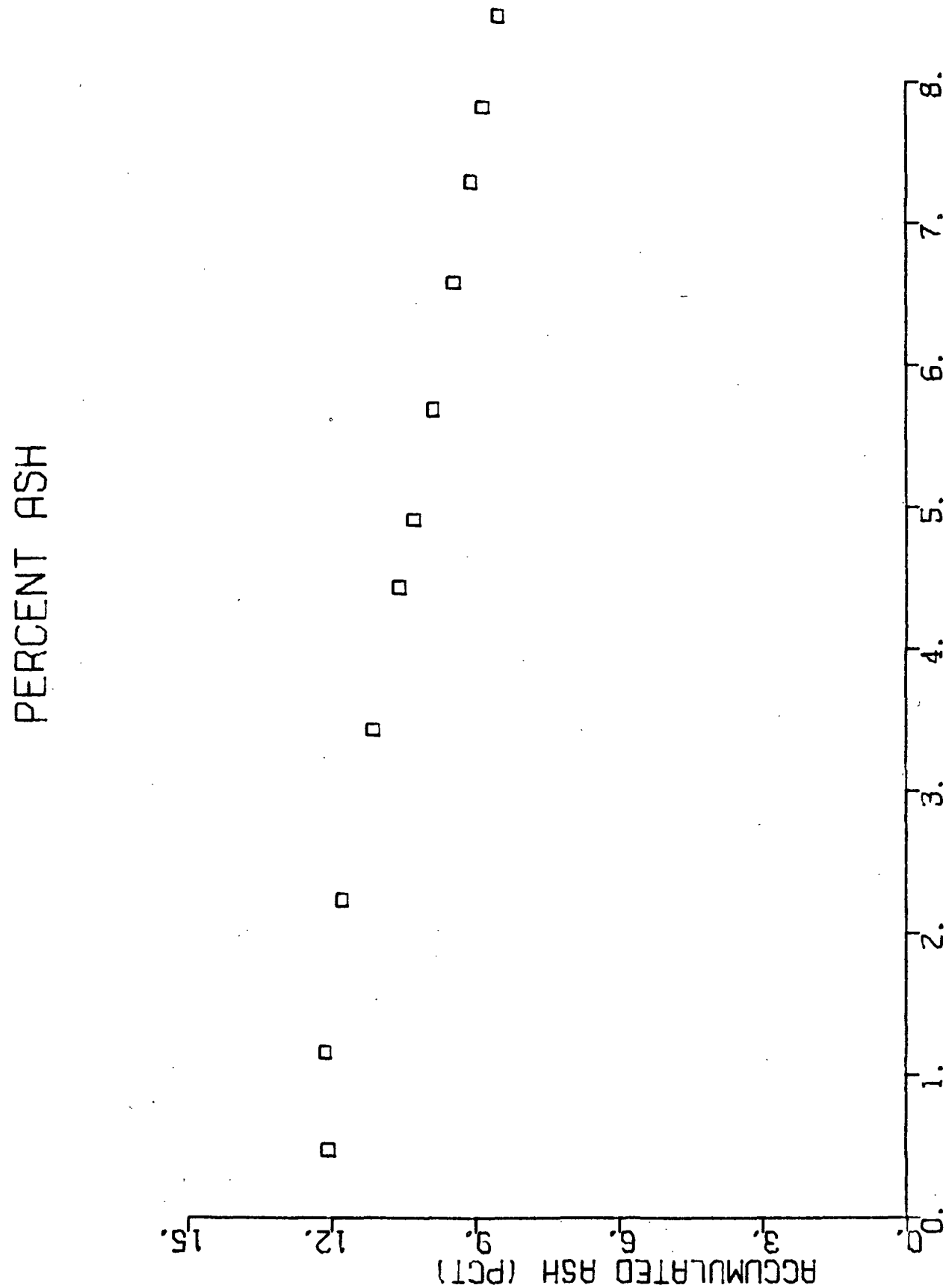

Figure 35. Pad 14

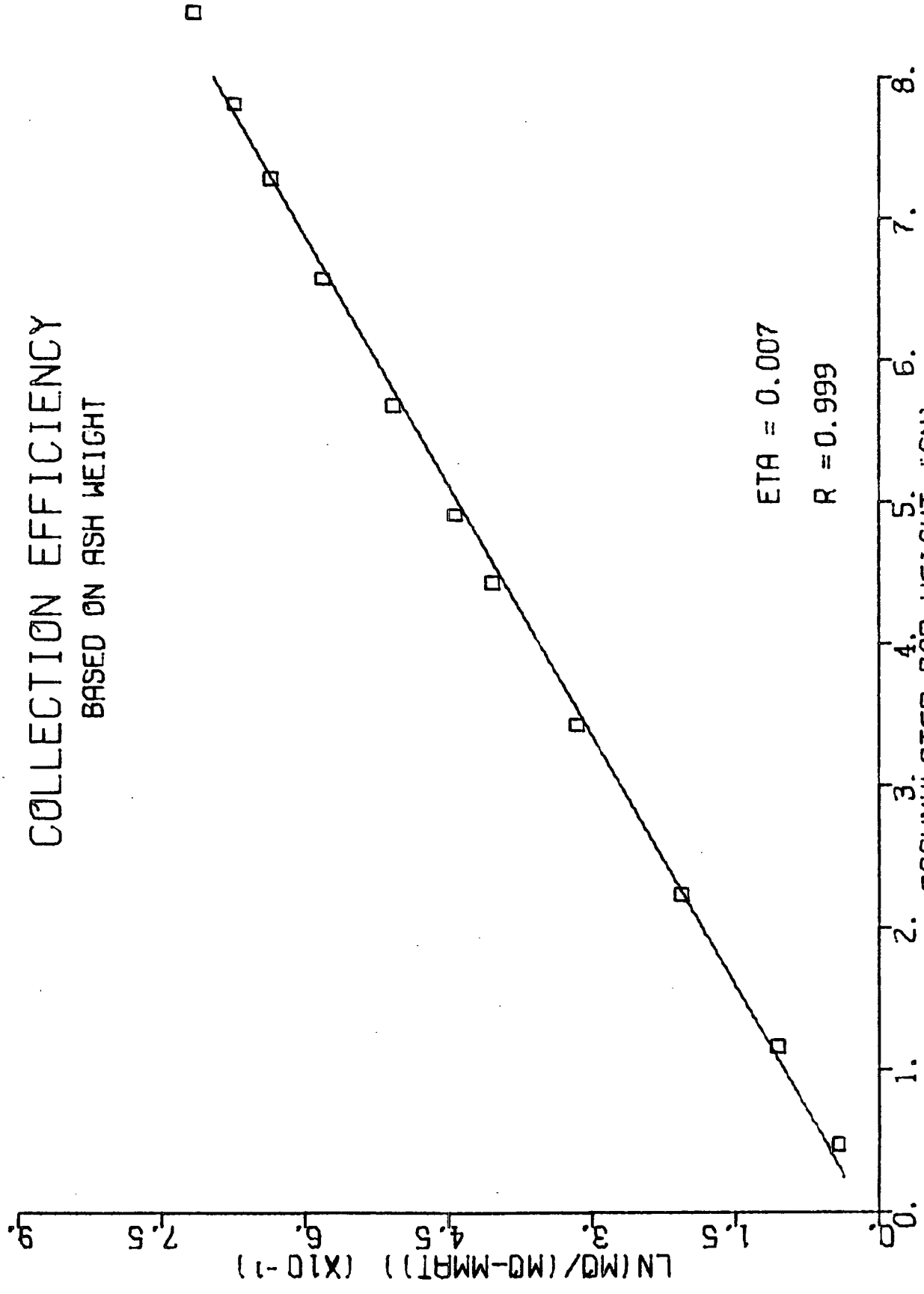

Figure 36. Pad 14

****
*   *
* PAD NUMBER 15 *
*   *
****

NUMBER OF PAD LAYERS = 11
DESIRED POROSITY = 0.75
FORMING VELOCITY (CM/SEC) = 1.00
TIO2 ADDED TO SUSPENSION (GM) = 1.4119
PERMEATION VELOCITY (CM/SEC) = 1.00
SUSPENSION PH = 5.1

LAYER	WET LAYER (GM)	DRY LAYER (GM)	ASH PER LAYER (GM)	NYLON PER LAYER (GM)	ACCUM. NYLON WT (GM)	ACCUM. ASH WT (GM)	ACCUM. PAD WT (GM)	ACCUM. TIO2 PER ACCUM. PAD WT (PCT)	NYLON DEPOSITED IN PAD (PCT)	PCT TOTAL RETAINED TIO2 (PCT)
1	0.4863	0.2585	0.0229	0.2356	0.2356	0.0229	0.2585	8.86	2.94	3.11
2	1.5594	0.5568	0.0715	0.4853	0.7209	0.0943	0.8153	11.57	8.98	12.81
3	3.3590	0.9427	0.1151	0.8276	1.5485	0.2095	1.7580	11.92	19.30	28.43
4	3.5816	0.8652	0.0935	0.7717	2.3202	0.3029	2.6232	11.55	28.91	41.12
5	6.3408	1.2820	0.1239	1.1581	3.4783	0.4269	3.9052	10.93	43.35	57.94
6	3.2608	0.6406	0.0525	0.5881	4.0664	0.4794	4.5458	10.55	50.68	65.07
7	3.5016	0.6692	0.0513	0.6179	4.6842	0.5307	5.2150	10.18	58.38	72.04
8	3.6447	0.7116	0.0489	0.6627	5.3469	0.5796	5.9266	9.78	66.63	78.68
9	5.6174	1.0670	0.0677	0.9993	6.3462	0.6473	6.9936	9.26	79.09	87.87
10	3.3160	0.6602	0.0353	0.6249	6.9711	0.6827	7.6538	8.92	86.87	92.66
11	4.8270	1.1073	0.0540	1.0533	8.0244	0.7367	8.7611	8.41	100.00	100.00

COMPRESSED PAD THICKNESS UTILIZED = 0.642
CALCULATED POROSITY = 0.760

SLOPE OF THE LINE FITTED TO THE DATA -- 0.0858
INTERCEPT -- 0.0106

**********COLLECTION EFFICIENCY (ETA) = 0.00701**********

COMMENTS-- IDENTICAL TO PAD 14, A CHECK OF REPRODUCIBILITY.

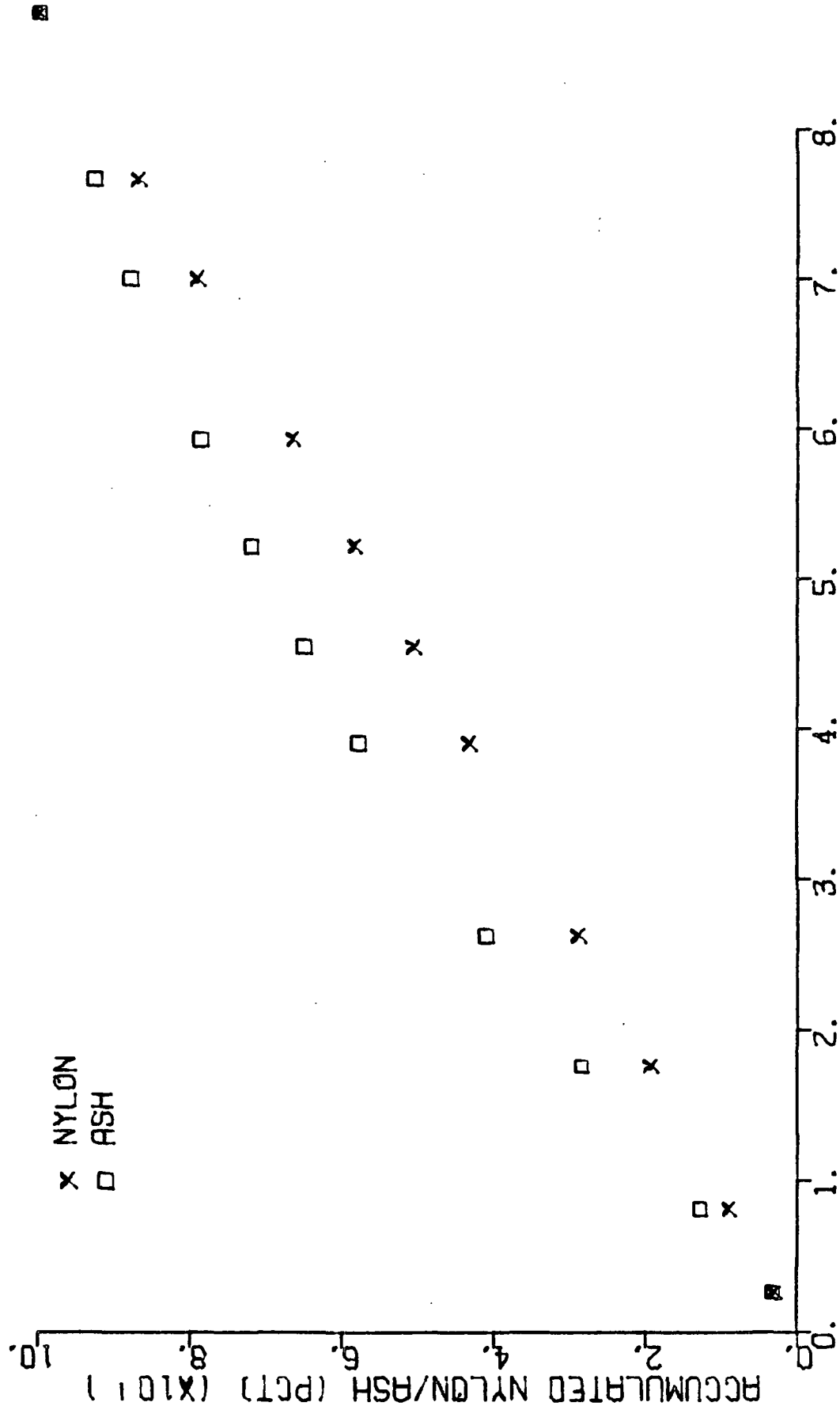

Figure 37. Pad 15

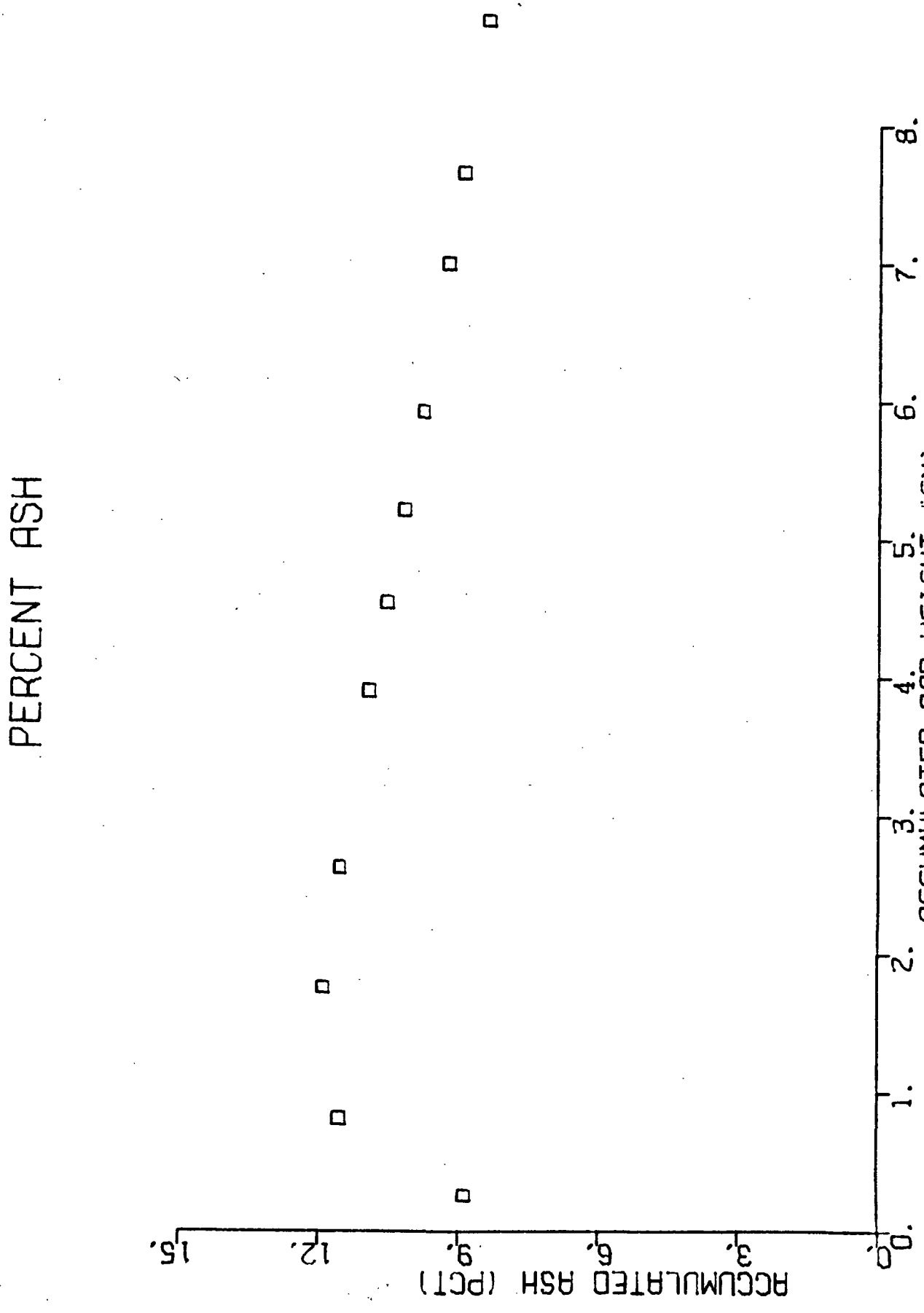

Figure 38. Pad 15

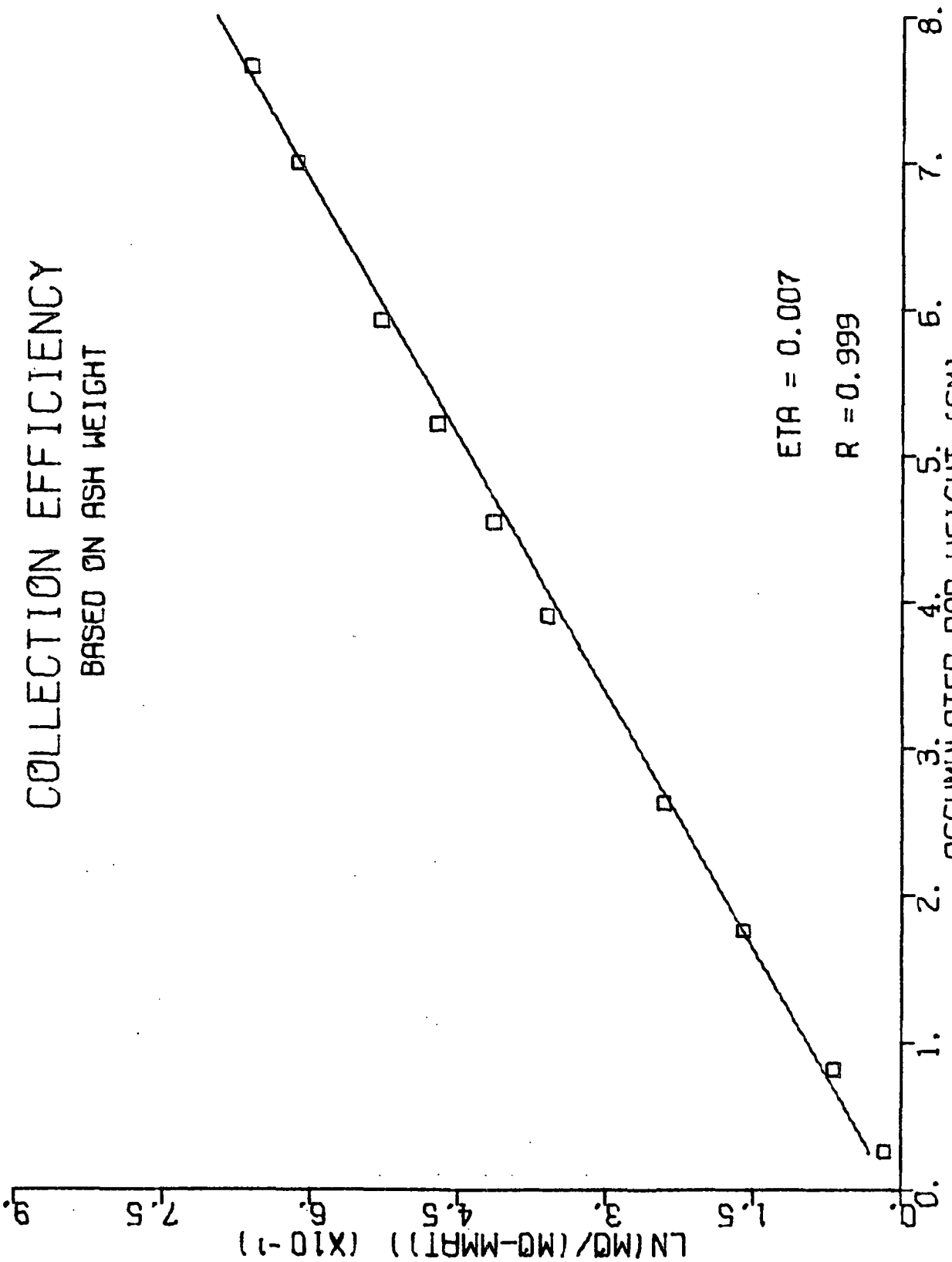

Figure 39. Pad 15

****
* PAD NUMBER 16 *
****

NUMBER OF PAD LAYERS = 10
DESIRED POROSITY = 0.75
FORMING VELOCITY (CM/SEC) = 1.00
TIO2 ADDED TO SUSPENSION (GM) = 1.4050
PERMEATION VELOCITY (CM/SEC) = 1.00
SUSPENSION PH = 5.1

LAYER	WET LAYER (GM)	DRY LAYER (GM)	ASH PER LAYER (GM)	NYLON PER LAYER (GM)	ACCUM. NYLON WT (GM)	ACCUM. ASH WT (GM)	ACCUM. PAD WT (GM)	ACCUM. TIO2 PER ACCUM. PAD WT (PCT)	NYLON DEPOSITED IN PAD (PCT)	PCT TOTAL RETAINED TIO2 (PCT)
1	2.1865	0.7885	0.0733	0.7152	0.7152	0.0733	0.7885	9.29	9.39	11.23
2	4.3755	1.2469	0.1214	1.1255	1.8407	0.1947	2.0354	9.57	24.17	29.85
3	4.9965	1.2386	0.1120	1.1266	2.9673	0.3067	3.2740	9.37	38.97	47.02
4	2.4773	0.6160	0.0497	0.5663	3.5336	0.3564	3.8900	9.16	46.41	54.64
5	2.2540	0.5265	0.0419	0.4847	4.0182	0.3983	4.4165	9.02	52.77	61.06
6	2.7850	0.6139	0.0460	0.5679	4.5862	0.4443	5.0304	8.83	60.23	68.11
7	2.9930	0.6504	0.0460	0.6044	5.1906	0.4902	5.6808	8.63	68.17	75.16
8	3.0096	0.6626	0.0451	0.6175	5.8081	0.5353	6.3434	8.44	76.28	82.06
9	4.8102	1.0480	0.0684	0.9796	6.7878	0.6036	7.3914	8.17	89.14	92.55
10	3.1905	0.8753	0.0486	0.8267	7.6144	0.6523	8.2667	7.89	100.00	100.00

COMPRESSED PAD THICKNESS UTILIZED = 0.604
CALCULATED POROSITY = 0.757

SLOPE OF THE LINE FITTED TO THE DATA -- 0.0765
INTERCEPT -- -0.0055

**********COLLECTION EFFICIENCY (ETA) = 0.00625**********

COMMENTS -- A CHECK OF PARTICLE REMOVAL AFTER PERMEATION.

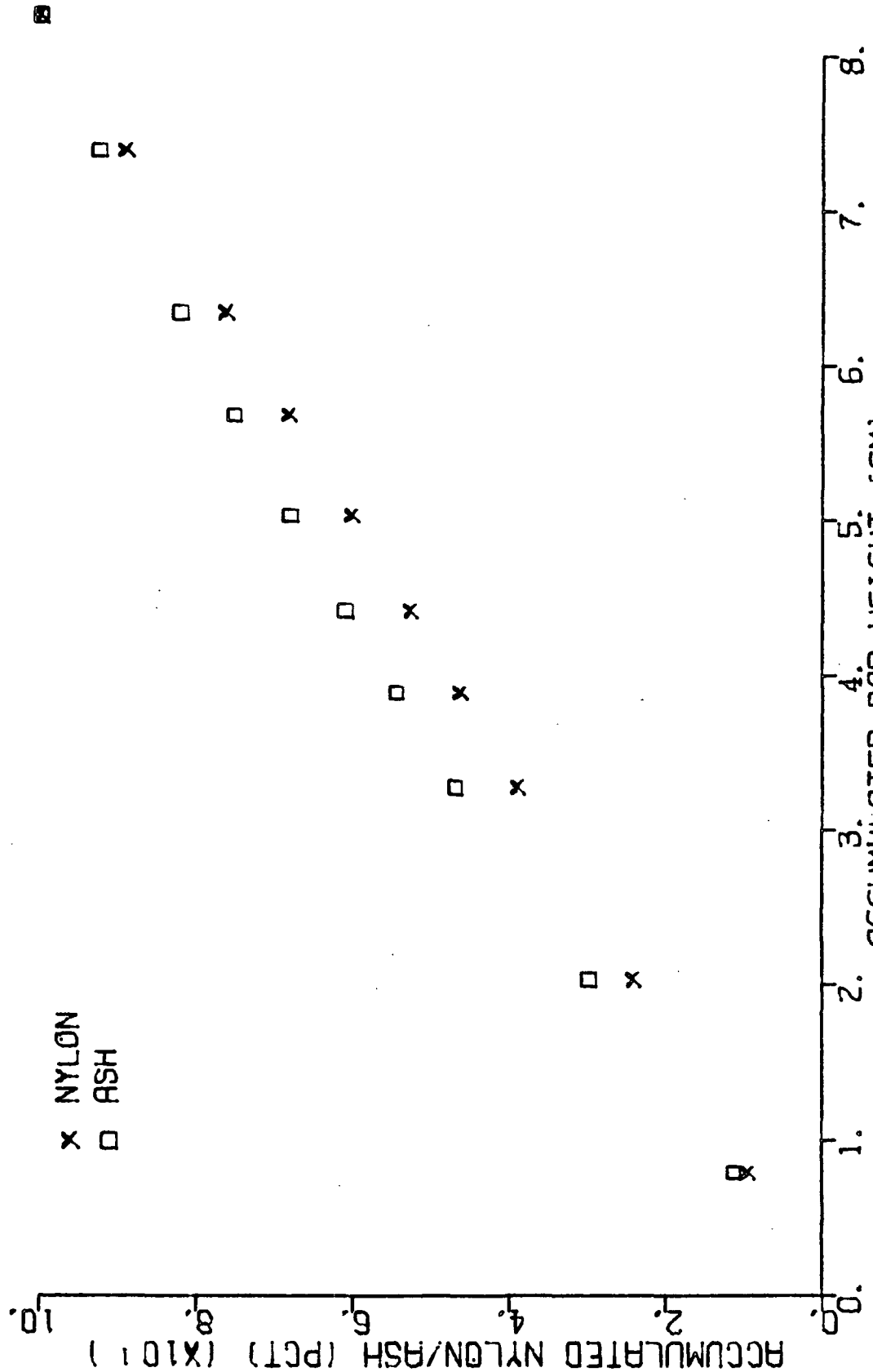

Figure 40: Pad 16

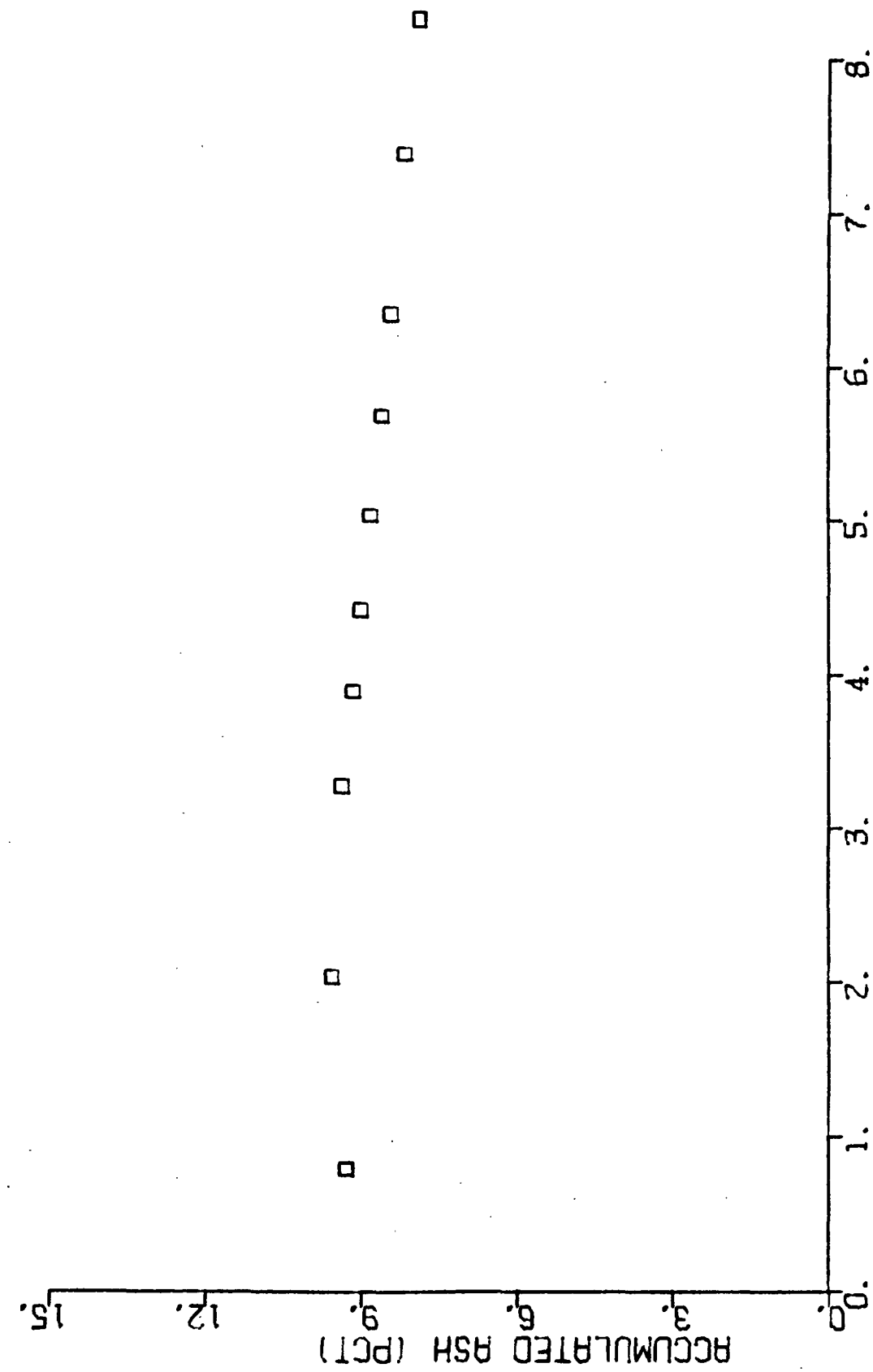

Figure 41. Pad 16

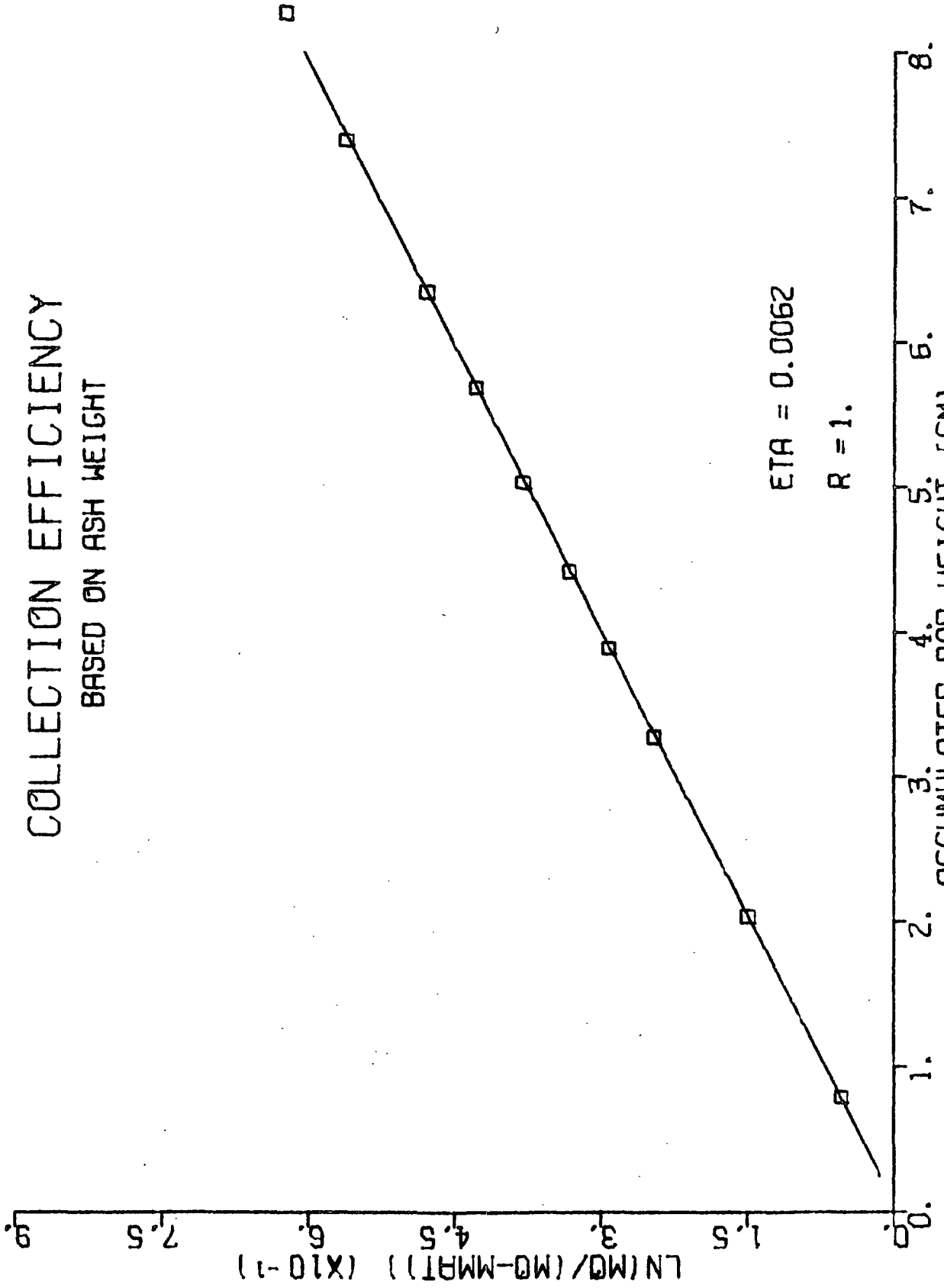

Figure 42. Pad 16

****
*   *
* PAD NUMBER 17 *
*   *
****

NUMBER OF PAD LAYERS = 10
DESIRED POROSITY = 0.75
FORMING VELOCITY (CM/SEC) = 1.00
TIO2 ADDED TO SUSPENSION (GM) = 1.4126
PERMEATION VELOCITY (CM/SEC) = 1.00
SUSPENSION PH = 5.0

LAYER	WET LAYER (GM)	DRY LAYER (GM)	ASH PER LAYER (GM)	NYLON PER LAYER (GM)	ACCUM. NYLON WT (GM)	ACCUM. ASH WT (GM)	ACCUM. PAD WT (GM)	ACCUM. TIO2 PER ACCUM. PAD WT (PCT)	NYLON DEPOSITED IN PAD (PCT)	PCT TOTAL RETAINED TIC2 (PCT)
1	2.8931	1.0370	0.0958	0.9412	0.9412	0.0958	1.0370	9.24	12.04	14.99
2	3.3233	0.9367	0.0905	0.8462	1.7875	0.1862	1.9737	9.44	22.86	29.14
3	6.9816	1.4745	0.1353	1.3392	3.1267	0.3215	3.4482	9.32	39.99	50.31
4	4.7582	0.8933	0.0700	0.8233	3.9499	0.3915	4.3415	9.02	50.53	61.26
5	1.6956	0.3457	0.0224	0.3233	4.2732	0.4140	4.6872	8.83	54.66	64.77
6	3.4645	0.6470	0.0448	0.6022	4.8754	0.4588	5.3342	8.60	62.36	71.78
7	2.9317	0.5487	0.0343	0.5144	5.3899	0.4930	5.8829	8.38	68.94	77.14
8	4.4116	0.8261	0.0511	0.7750	6.1649	0.5441	6.7090	8.11	78.86	85.13
9	3.6259	0.7173	0.0410	0.6763	6.8412	0.5851	7.4263	7.88	87.51	91.54
10	4.3767	1.0306	0.0541	0.9765	7.8177	0.6391	8.4569	7.56	100.00	100.00

COMPRESSED PAD THICKNESS UTILIZED = 0.628
CALCULATED POROSITY = 0.761

SLOPE OF THE LINE FITTED TO THE DATA -- 0.0717
INTERCEPT -- 0.0050

**********COLLECTION EFFICIENCY (ETA) = 0.00586**********

Comments-- NO SALT ADDED TO PARTICLE SUSPENSION

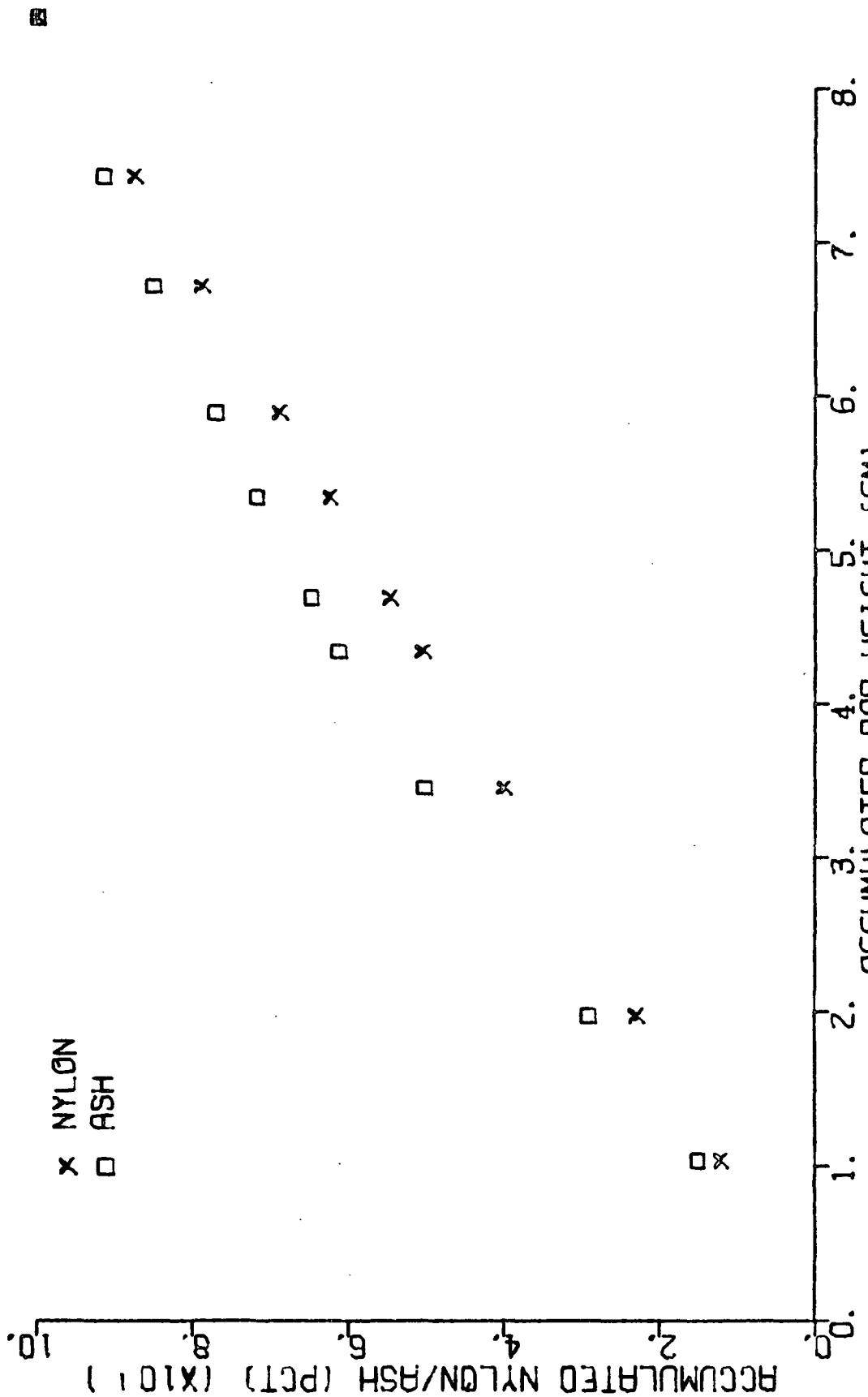

Figure 43. Pad 17

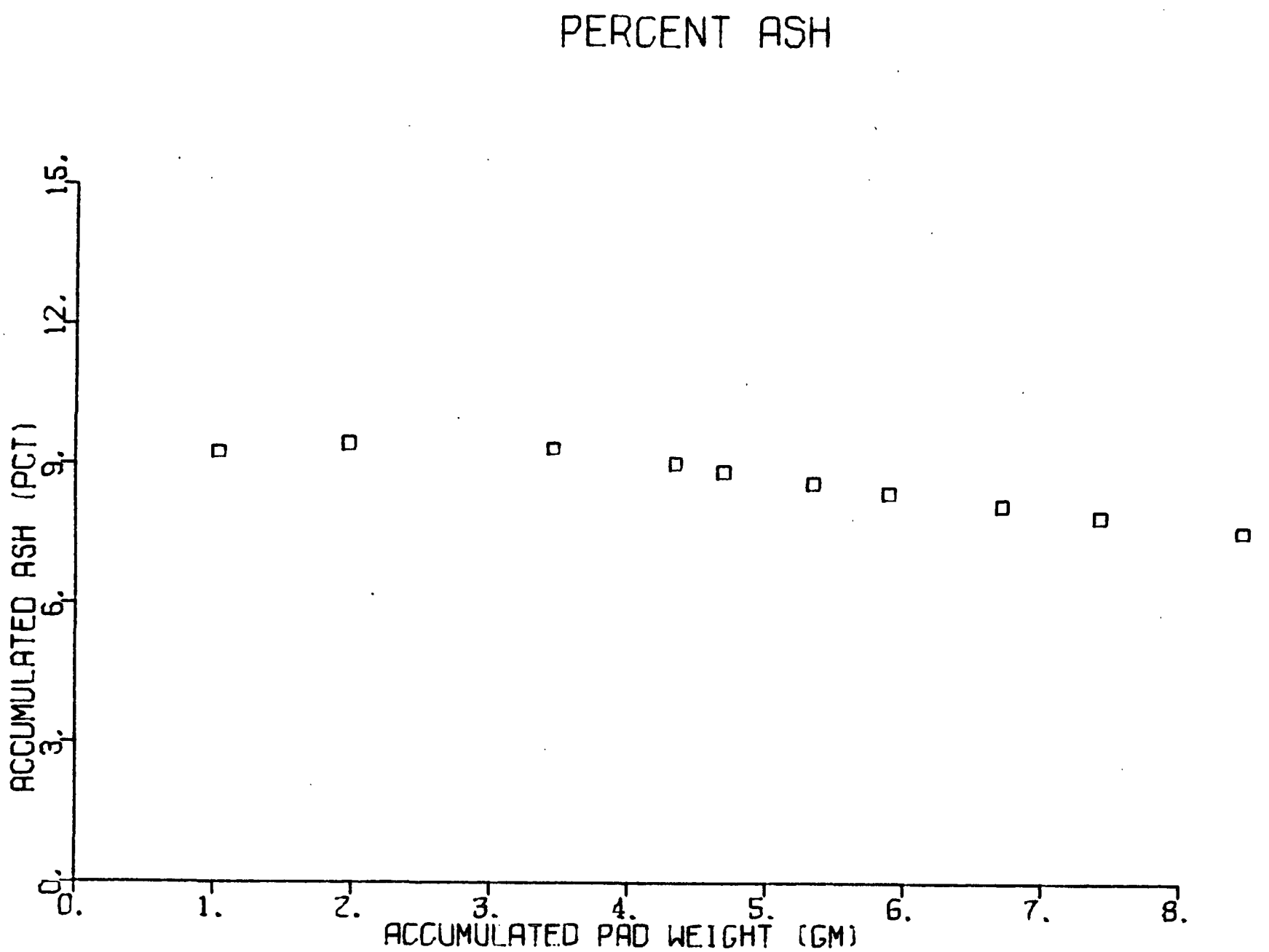

Figure 44. Pad 17

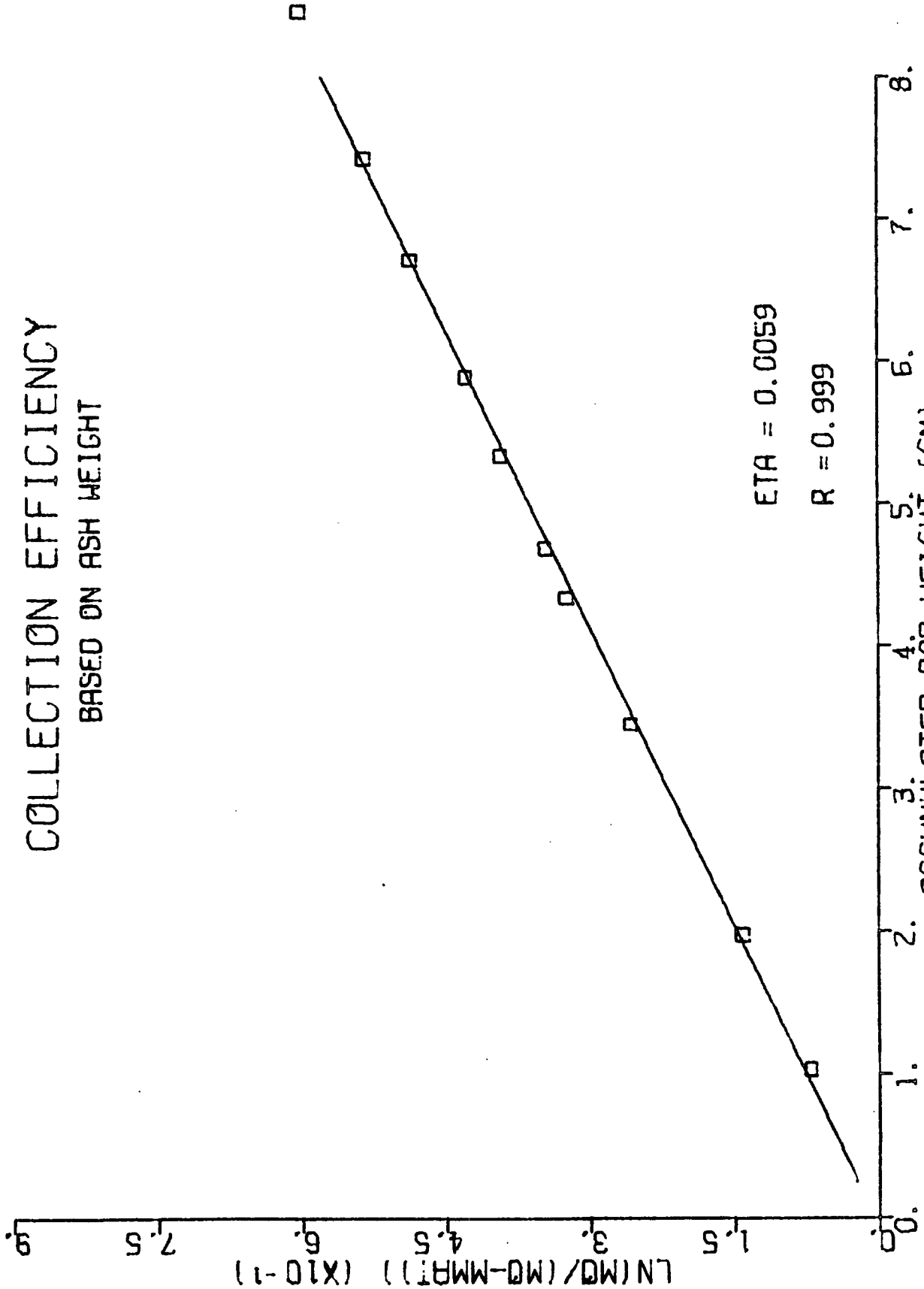

Figure 45. Pad 17

****
* *
* PAD NUMBER 18 *
* *
****

NUMBER OF PAD LAYERS = 10
DESIRED POROSITY = 0.75
FORMING VELOCITY (CM/SEC) = 1.00
TIO2 ADDED TO SUSPENSION (GM) = 1.4143
PERMEATION VELOCITY (CM/SEC) = 1.00
SUSPENSION PH = 7.2

LAYER	WET LAYER (GM)	DRY LAYER (GM)	ASH PER LAYER (GM)	NYLON PER LAYER (GM)	ACCUM. NYLON WT (GM)	ACCUM. ASH WT (GM)	ACCUM. PAD WT (GM)	ACCUM. TIO2 PER ACCUM. PAD WT (PCT)	NYLON DEPOSITED IN PAD (PCT)	PCT TOTAL RETAINED TIO2 (PCT)
1	1.7216	0.5812	0.0068	0.5744	0.5744	0.0068	0.5812	1.17	7.27	6.37
2	2.4427	0.6427	0.0093	0.6334	1.2078	0.0161	1.2239	1.31	15.29	15.12
3	3.1450	0.7509	0.0116	0.7393	1.9471	0.0277	1.9748	1.40	24.65	26.02
4	5.6320	1.1077	0.0172	1.0905	3.0376	0.0449	3.0825	1.46	38.46	42.24
5	5.0571	0.8785	0.0142	0.8643	3.9019	0.0591	3.9610	1.49	49.40	55.60
6	6.5202	1.0838	0.0151	1.0687	4.9706	0.0742	5.0448	1.47	62.94	69.79
7	2.7332	0.4625	0.0036	0.4589	5.4295	0.0778	5.5073	1.41	68.75	73.19
8	6.0456	0.9918	0.0127	0.9791	6.4086	0.0905	6.4991	1.39	81.14	85.10
9	3.9198	0.7008	0.0076	0.6932	7.1018	0.0981	7.1999	1.36	89.92	92.27
10	3.3709	0.8042	0.0082	0.7960	7.8978	0.1063	8.0041	1.33	100.00	100.00

COMPRESSED PAD THICKNESS UTILIZED = 0.624
CALCULATED POROSITY = 0.757

SLOPE OF THE LINE FITTED TO THE DATA -- 0.0100
INTERCEPT -- 0.0005

**********COLLECTION EFFICIENCY (ETA) = 0.00082**********

Comments-- NO CHEMICAL ADDITIONS TO PARTICLE SUSPENSION.

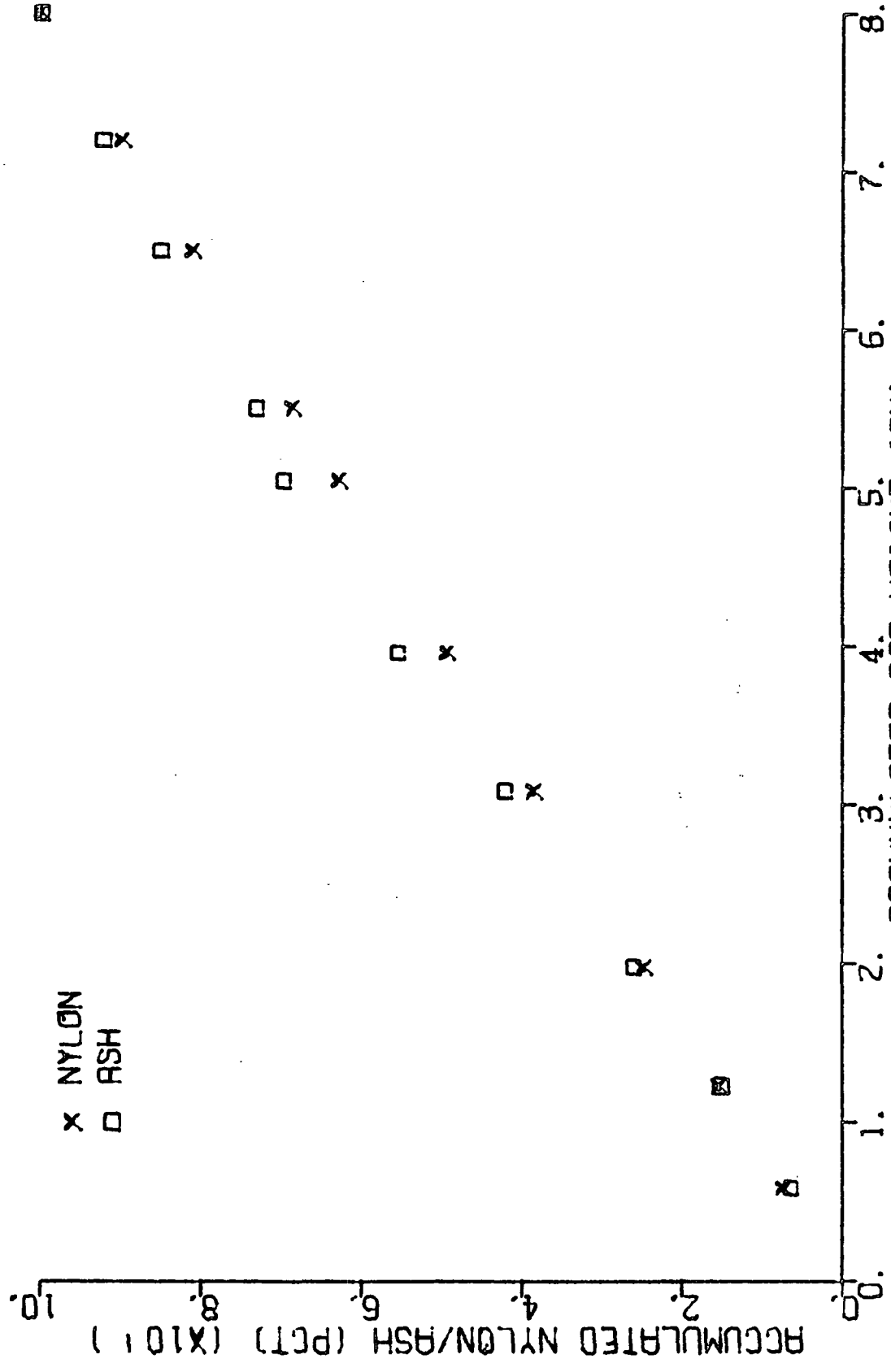

Figure 46. Pad 18

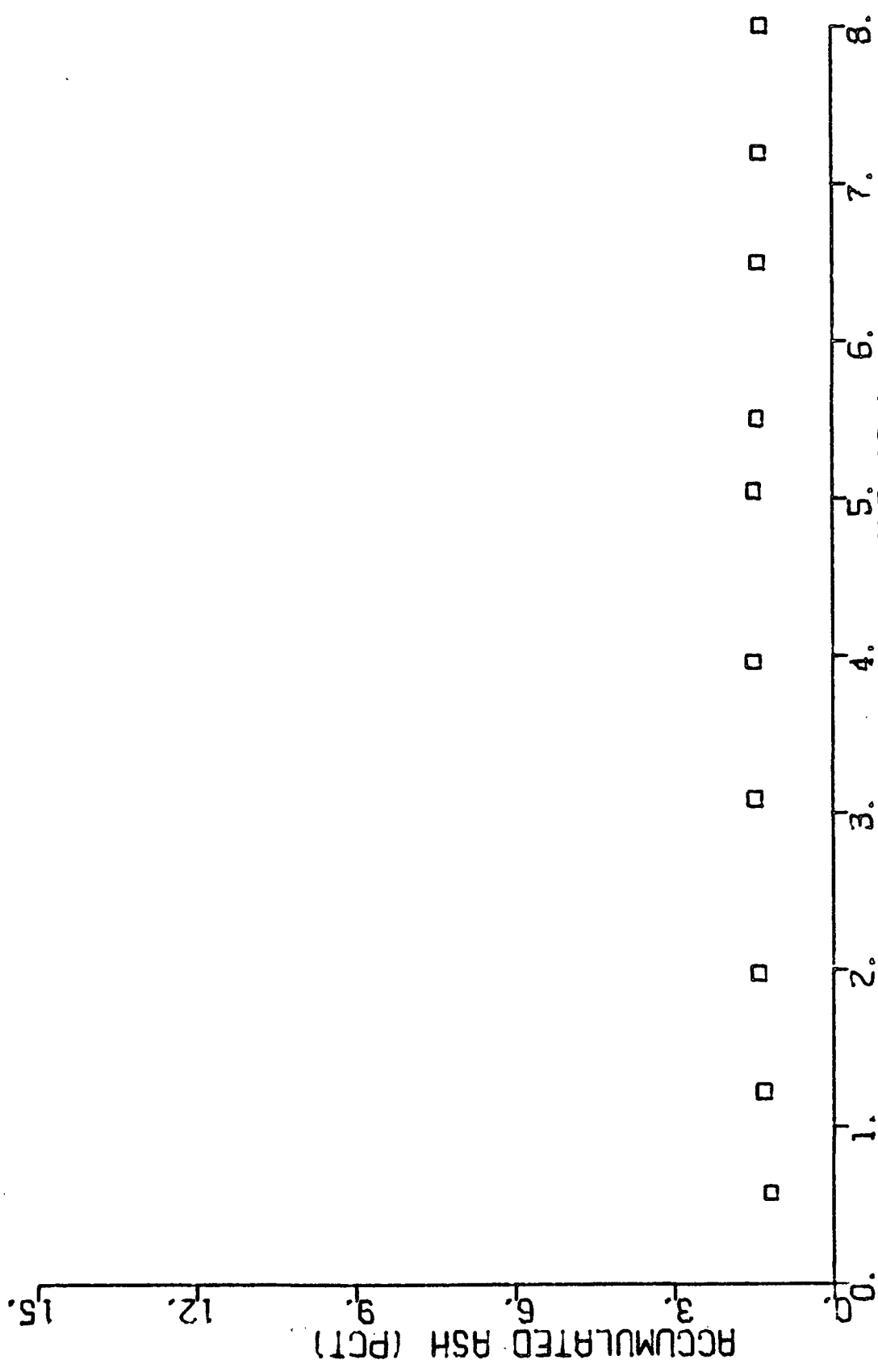

Figure 47. Pad 18

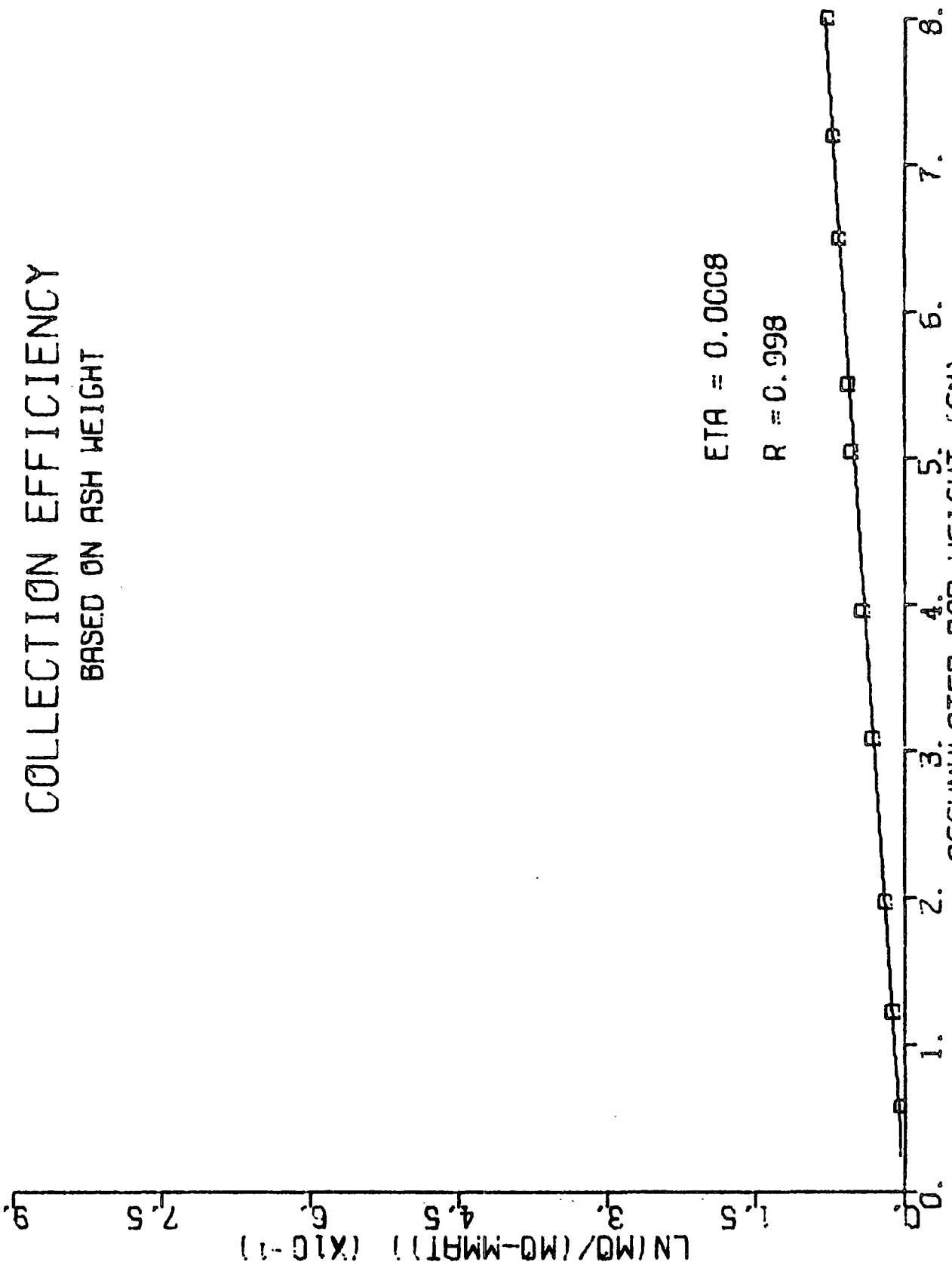

Figure 48. Pad 18

****
*
* PAD NUMBER 19 *
*
****

NUMBER OF PAD LAYERS = 10
DESIRED POROSITY = 0.75
FORMING VELOCITY (CM/SEC) = 1.00
TIO2 ADDED TO SUSPENSION (GM) = 1.0731
PERMEATION VELOCITY (CM/SEC) = 1.50
SUSPENSION PH = 5.1

LAYER	WET LAYER (GM)	DRY LAYER (GM)	ASH PER LAYER (GM)	NYLON PER LAYER (GM)	ACCUM. NYLON WT (GM)	ACCUM. ASH WT (GM)	ACCUM. PAD WT (GM)	ACCUM. TIO2 PER ACCUM. PAD WT (PCT)	NYLON DEPOSITED IN PAD (PCT)	PCT TOTAL RETAINED TIO2 (PCT)
1	3.7139	1.1000	0.0816	1.0184	1.0184	0.0816	1.1000	7.42	13.69	19.21
2	3.0323	0.8003	0.0544	0.7459	1.7643	0.1360	1.9003	7.16	23.72	32.00
3	3.4063	0.7874	0.0480	0.7394	2.5037	0.1840	2.6877	6.84	33.66	43.29
4	3.5014	0.7102	0.0398	0.6704	3.1741	0.2238	3.3979	6.59	42.68	52.66
5	3.8244	0.7367	0.0414	0.6953	3.8694	0.2652	4.1346	6.41	52.02	62.40
6	5.5067	1.0098	0.0491	0.9607	4.8301	0.3143	5.1444	6.11	64.94	73.95
7	3.3095	0.6664	0.0303	0.6361	5.4662	0.3445	5.8108	5.93	73.49	81.08
8	2.5595	0.5490	0.0235	0.5255	5.9917	0.3681	6.3598	5.79	80.56	86.62
9	3.0907	0.6764	0.0273	0.6491	6.6407	0.3954	7.0362	5.62	89.29	93.05
10	3.2411	0.8264	0.0295	0.7969	7.4376	0.4249	7.8626	5.40	100.00	100.00

COMPRESSED PAD THICKNESS UTILIZED = 0.590
CALCULATED POROSITY = 0.757

SLOPE OF THE LINE FITTED TO THE DATA -- 0.0631
INTERCEPT -- 0.0173

**********COLLECTION EFFICIENCY (ETA) = 0.00515**********

Comments-- INCREASED VELOCITY AT POROSITY 0.75

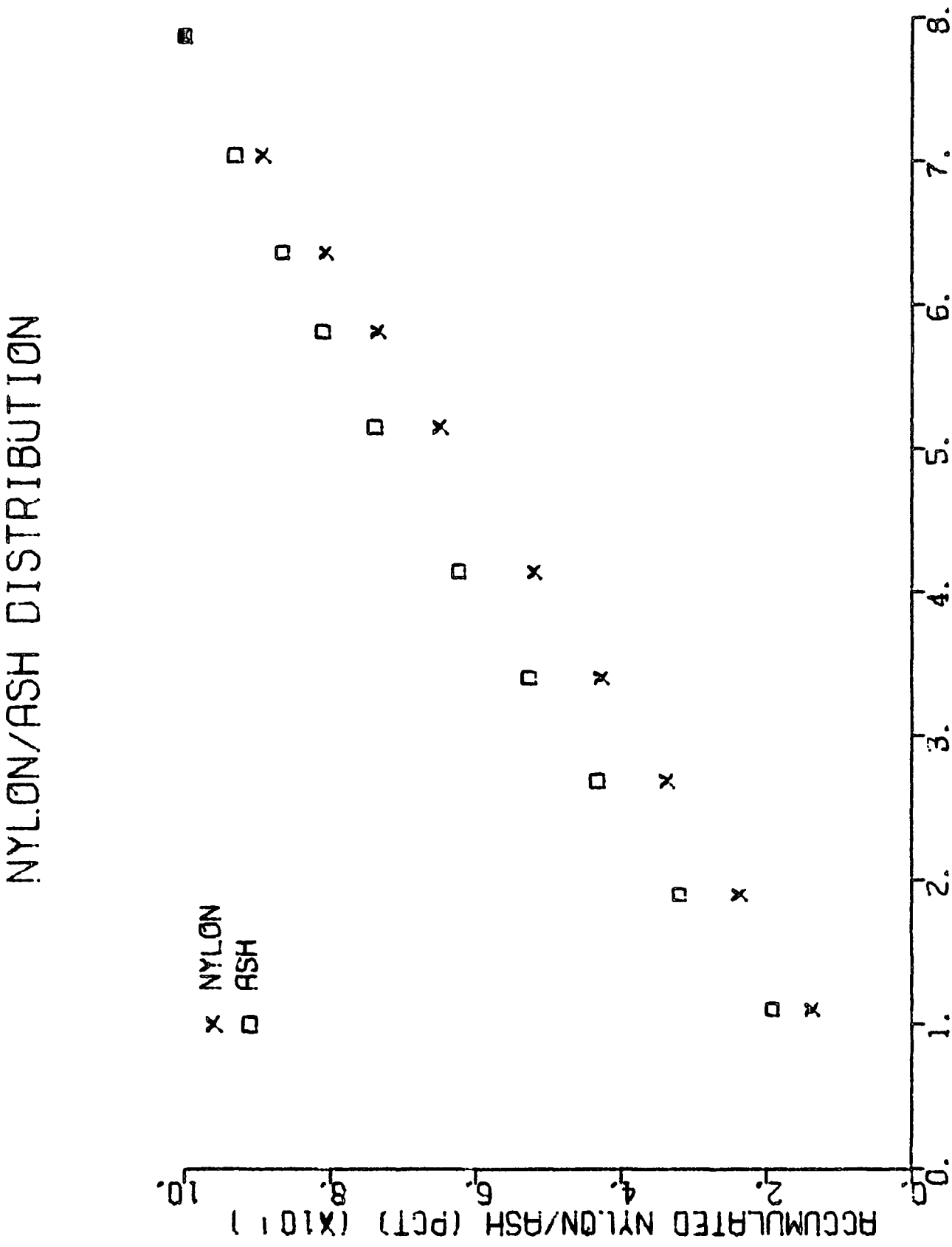

Figure 49. Pad 19

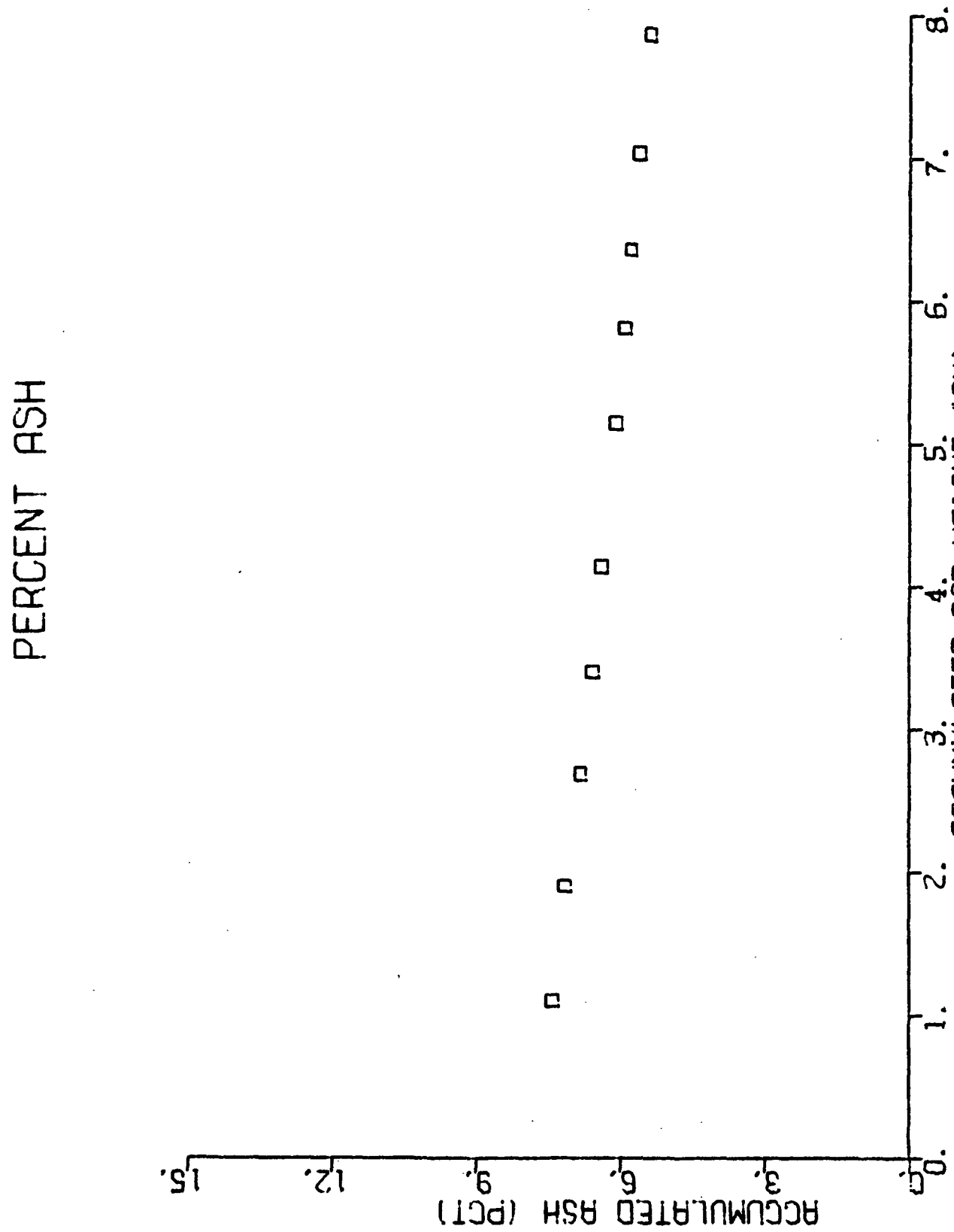

Figure 50. Pad 19

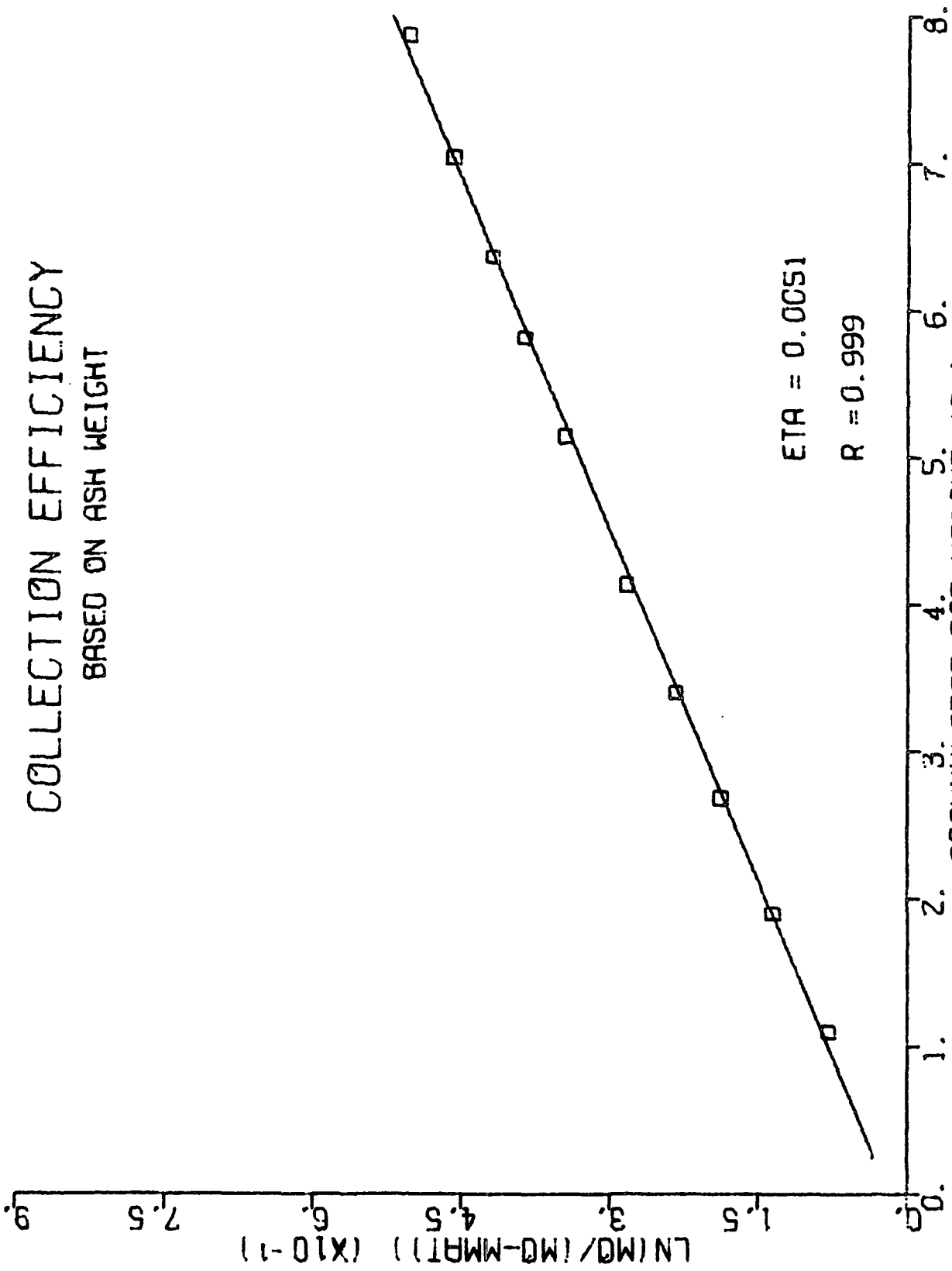

Figure 51. Pad 19

****
* *
* PAD NUMBER 20 *
* *
****

NUMBER OF PAD LAYERS = 10
DESIRED POROSITY = 0.85
FORMING VELOCITY (CM/SEC) = 1.00
TIO2 ADDED TO SUSPENSION (GM) = 1.4561
PERMEATION VELOCITY (CM/SEC) = 1.50
SUSPENSION PH = 5.1

LAYER	WET LAYER (GM)	DRY LAYER (GM)	ASH PER LAYER (GM)	NYLON PER LAYER (GM)	ACCUM. NYLON WT (GM)	ACCUM. ASH WT (GM)	ACCUM. PAD WT (GM)	ACCUM. TIO2 PER ACCUM. PAD WT (PCT)	NYLON DEPOSITED IN PAD (PCT)	PCT TOTAL RETAINED TIO2 (PCT)
1	2.5341	0.6966	0.0593	0.6373	0.6373	0.0593	0.6966	8.51	8.03	10.83
2	4.5140	0.9074	0.0744	0.8330	1.4703	0.1337	1.6040	8.33	18.52	24.43
3	4.2910	0.7702	0.0587	0.7115	2.1818	0.1924	2.3742	8.10	27.48	35.15
4	4.6917	0.7692	0.0532	0.7160	2.8978	0.2456	3.1434	7.81	36.50	44.88
5	5.8320	0.8835	0.0599	0.8236	3.7214	0.3055	4.0269	7.59	46.87	55.83
6	7.6176	1.0903	0.0681	1.0222	4.7435	0.3737	5.1172	7.30	59.75	68.28
7	6.1821	0.8698	0.0493	0.8205	5.5640	0.4230	5.9870	7.07	70.08	77.29
8	8.1295	1.1136	0.0599	1.0537	6.6176	0.4829	7.1006	6.80	83.35	88.24
9	3.4984	0.4929	0.0233	0.4696	7.0873	0.5062	7.5935	6.67	89.27	92.50
10	5.9071	0.8932	0.0411	0.8522	7.9394	0.5473	8.4867	6.45	100.00	100.00

COMPRESSED PAD THICKNESS UTILIZED = 1.045
CALCULATED POROSITY = 0.854

SLOPE OF THE LINE FITTED TO THE DATA -- 0.0553
INTERCEPT -- 0.0092

**********COLLECTION EFFICIENCY (ETA) = 0.00451**********

Comments-- Increased Velocity at Porosity 0.85

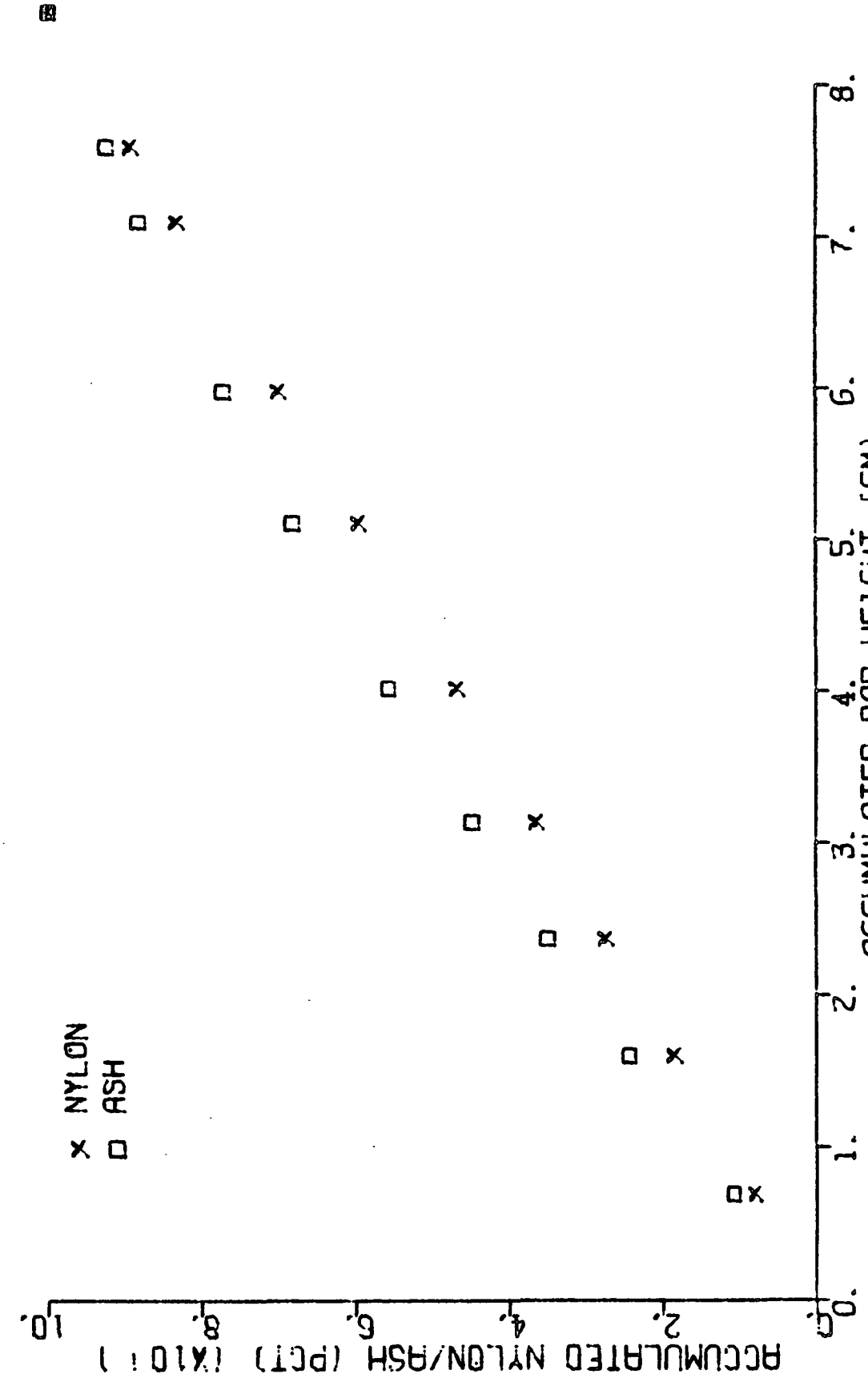

Figure 52. Pad 20

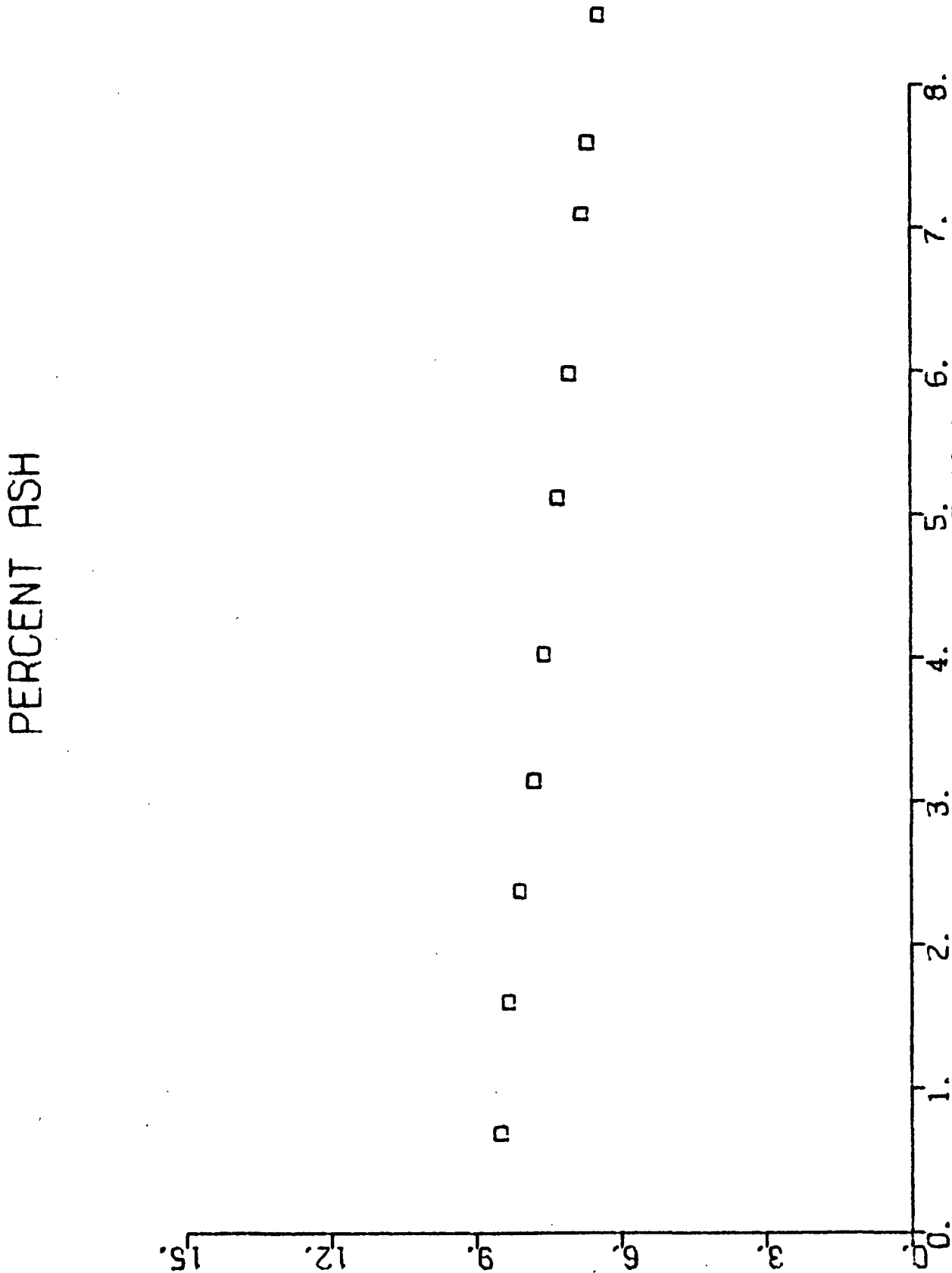

Figure 53. Pad 20

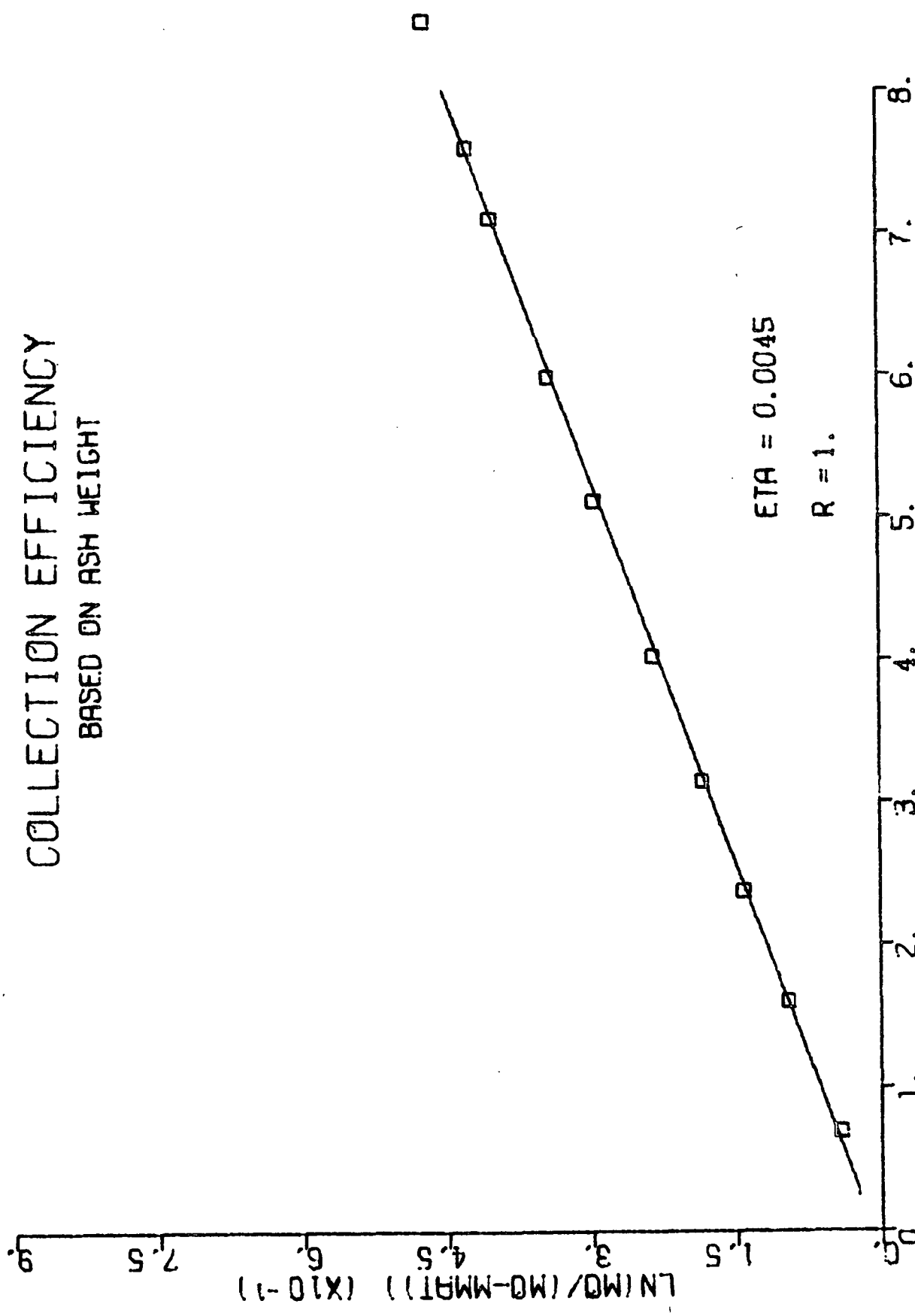

Figure 54. Pad 20